Antigen discovery in immunotherapy-associated myocarditis and blood-based biomarkers for

breast cancer

By

Margaret L. Axelrod

Dissertation
Submitted to the Faculty of the
Graduate School of Vanderbilt University
in partial fulfillment of the requirements
for the degree of

DOCTOR OF PHILOSOPHY
in

Cancer Biology
May 31st, 2022
Nashville, Tennessee

Approved:

Paula J. Hurley, Ph.D. (Chair)

Justin M. Balko, Pharm.D., Ph.D. (Advisor)

Jin Chen, M.D., Ph.D.

Luc Van Kaer, Ph.D.

Jeffery C. Rathmell, Ph.D.

Dedication

For cancer patients and their loved ones

I am grateful and privileged to have the support of my family and friends. Thank you: Howard Axelrod, Janine Begasse, Lauren Begasse, John Axelrod, Daniel Begasse, Aeberli Begasse, Bob Consroe and Leslie Consroe.

I am indebted to the patients and families who donate time, samples and data to research. This is a precious gift.

Finally, thank you to my partner, Andrew Consroe. I am so grateful for the unwavering support for all of my dreams.

Contents

LIST OF TABLES

LIST OF FIGURES

CHAPTER I

Introduction

Cancer is a heterogenous group of diseases with a high morbidity and mortality worldwide. There were an estimated 19.3 million new cancer cases and 9.9 million cancer deaths in 2020, worldwide (Sung et al., 2021). Despite recent advances in the care of patients with cancer, new treatment paradigms are needed. A crucial challenge in the care of cancer patients is the heterogeneity of disease phenotype and response to treatment, even for patients with cancers originating from the same tissue. New strategies are needed to target therapies to cancer patients which maximize benefit and minimize harm. The overarching goals of the projects presented herein are 1) understand the pathogenesis of one of the deadliest side effects of anti-cancer immunotherapy and 2) to develop minimally invasive biomarkers of response to therapy, which could be used to target patients to appropriate treatments and spare patients from unnecessary risks of side effects.

Immunotherapy, toxicities, and myocarditis

Immune checkpoint inhibitors (ICIs) have changed the treatment paradigm for many cancer types (Motzer et al., 2018; Overman et al., 2018; Postow et al., 2015). The first approved ICI, ipilimumab, which targets cytotoxic T lymphocyte antigen 4 (CTLA-4), was approved by the Food and Drug Administration (FDA) for the treatment of melanoma in 2011. Prior to ipilimumab, metastatic melanoma was a universally fatal diagnosis, but with ipilimumab, approximately 20% of patients achieve long-term remissions (Schadendorf et al., 2015). Seven more ICIs have been FDA approved, targeting the programmed cell death protein (PD-1)/programmed cell death ligand 1 (PD-L1) pathways or lymphocyte activating 3 (LAG3; Tawbi et al., 2022). There are 19 different cancer types and two tissue-agnostic indications (high tumor mutational burden or microsatellite instability high tumors) approved for treatment with ICIs

(Twomey & Zhang, 2021). The use of ICIs has transformed the care of cancer patients. The primary mechanism of ICIs is to activate a patient's own immune cells (especially T cells) in order to stimulate immune cell mediated tumor cell killing. In order to more fully discuss the mechanism of action of ICIs, we will first review T cell activation.

In order to become activated T cells need to receive several signals (Tai, Wang, Korner, Zhang, & Wei, 2018). Signal 1 is delivered by signaling through the T cell receptor (TCR) following recognition of the cognate peptide-Major Histocompatibility Complex (MHC; Frauwirth & Thompson, 2004). This interaction is highly diverse, with many possible TCRs, peptides and MHC alleles participating. TCRs are generated by a process known as VDJ recombination, which involves combing V, D, and J genes, with nucleotide additions occurring at the junctions. This process can generate a wide diversity of TCRs, with estimates ranging up to 10^{61} for the possible unique TCRs that can be generated (Mora & Walczak, 2016). There is also a wide diversity in MHC alleles (Migalska, Sebastian, & Radwan, 2019). This high diversity of possible signal 1 interactions controls the specificity of T cell adaptive immune responses. When a TCR recognizes its cognate peptide-MHC, cell signaling through the TCR complex is initiated. However, for T cell activation to occur, this signaling must occur in the correct context. Signal 2 is co-stimulation through coreceptors, such as CD28. CD28 is expressed by T cells and binds to CD80 or CD86 on antigen presenting cells (APCs). This interaction causes further cell signaling to activate a T cell (Hwang, Byeon, Kim, & Park, 2020). Signal 3 for T cell activation is signaling through inflammatory cytokines (Curtsinger & Mescher, 2010). These cytokines can include interleukin-12, and type I interferons (alpha and beta). T cell activation through signals 1, 2, and 3 is shown in **Figure 1.1**.
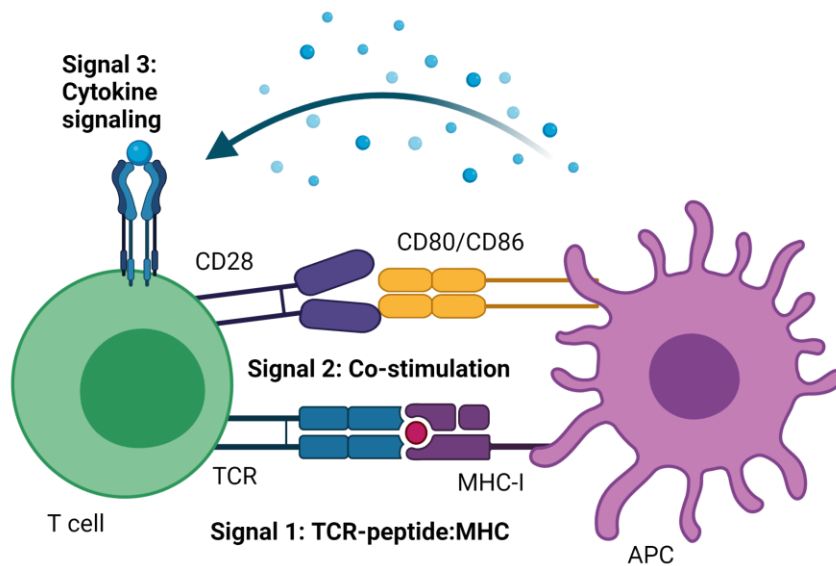
Figure 1.1 T cell activation through multiple signals. This schematic shows the three primary signals needed for T cell activation. Signal 1 is the TCR-peptide:MHC interaction. Signal 2 is co-stimulation through CD28 binding to CD80/CD86. Signal 3 is cytokine support. Figure created with BioRender.com.

In the normal process of T cell activation, T cells upregulate inhibitory receptors, known as immune checkpoints. This is a homeostatic mechanism which functions to prevent autoimmunity and other disease states associated with immune overreaction (i.e., cytokine storm). CTLA-4 and PD-1 are immune checkpoints, expressed by T cells, which act through distinct mechanisms (Parry et al., 2005). Signaling through PD-1 inhibits T cell activation. PD-1 has two ligands: PD-L1 and PD-L2. PD-L1 can be upregulated on many cell types through interferon signaling, and cancer cells often overexpress PD-L1 as a mechanism of immunosuppression (Bardhan, Anagnostou, & Boussiotis, 2016). PD-L2 has a more limited distribution of expression and is thought to play a particularly important role in tolerance in the

lungs and airway epithelia (Akbari et al., 2010). CTLA-4 binds to CD80 and CD86 and prevents

co-stimulatory signaling through CD28. CTLA-4 has much higher affinity for CD80 and CD86

than CD28 does (Buchbinder & Desai, 2016). This prevents the activation of signal 2. Immune

checkpoints are summarized in **Figure 1.2**.
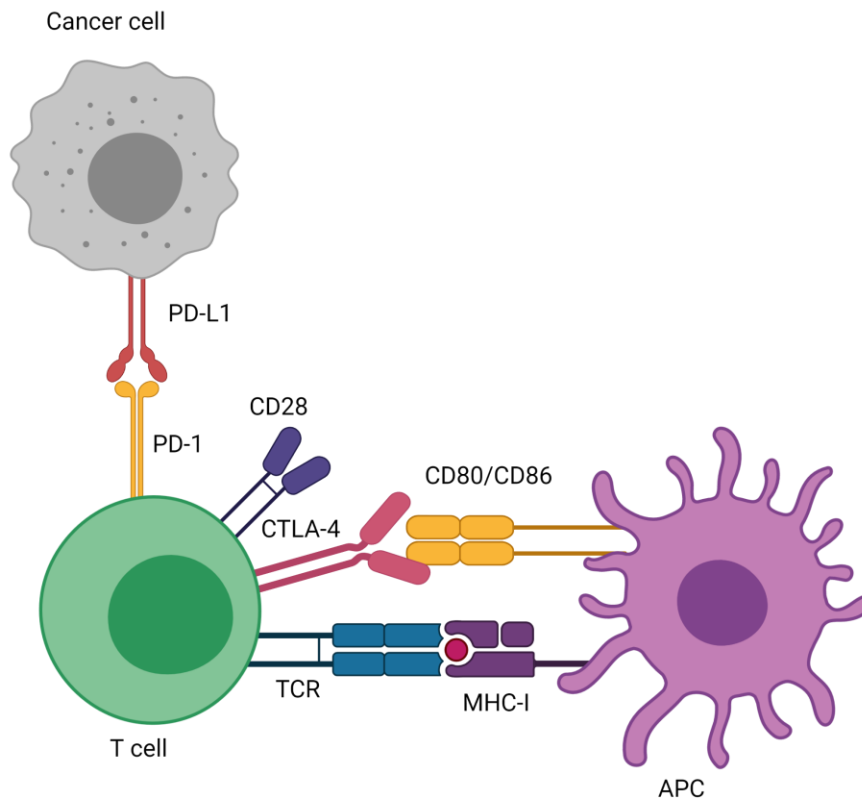
Figure 1.2 Immune checkpoints inhibit T cell activation. This schematic shows the normal homeostatic mechanism of upregulation of immune checkpoints, including PD-1 and CTLA-4. These immune checkpoints prevent further T cell activation. Figure created with BioRender.com.

Generally, ICIs work by blocking the inhibitory interactions of immune checkpoints

expressed on T cells with their ligands on other cell types, enabling prolonged activation of T

cells (Wei et al., 2018a). ICIs are monoclonal antibodies, specific for immune checkpoints or

their ligands. Anti-CTLA-4 is thought to function primarily at the level of initial T cell priming and permit activation of new T cell clones through allowing co-stimulatory signaling and the delivery of signal 2. Anti-CTLA-4 is thought to enhance activation of naïve anti-tumor T cells (Buchbinder & Desai, 2016). Anti-PD-1 is thought to function primarily on "exhausted" T cells, meaning T cells which have already been activated through all three signals and have upregulated PD-1 as part of a homeostatic mechanism to prevent overactivation. Anti-PD-1 is thought to be able to reactive tumor-reactive T cells already present in the tumor microenvironment but which are suppressed in their activation (Bardhan et al., 2016). The action of ICIs is shown in **Figure 1.3**. Though there is some specificity for T cells expressing inhibitory ligands, there is nothing inherently specific about this blocking interaction which should reactivate only cancer specific T cells. Indeed, despite the broad successes of ICI therapy, immune-related adverse events (irAEs) remain major clinical challenges.
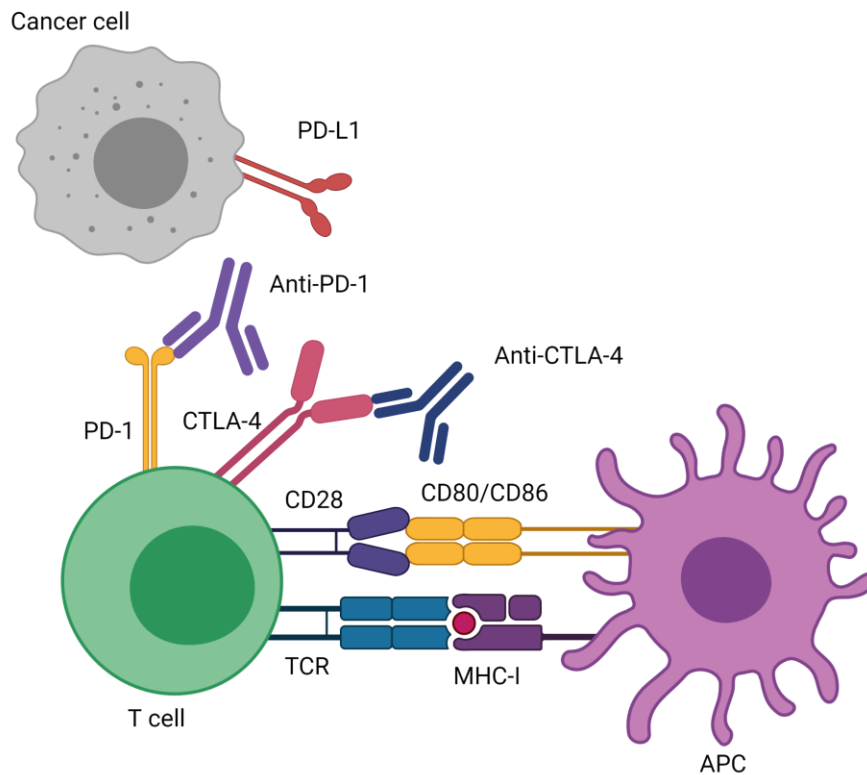
Figure 1.3 Immune checkpoint inhibitors enable T cell activation. This schematic shows how ICIs can block immune checkpoints and allow T cells to become (re)activated. Figure created with BioRender.com.

IrAEs are more common with ipilimumab, compared to anti-PD-1/PD-L1 agents, with approximately 60% of ipilimumab treated patients experiencing an irAE and 10-30% of these being grade 3 or higher as defined by the National Cancer Institute's Common Terminology Criteria for Adverse Events (Martins et al., 2019). This may be due to the mechanism of anti-CTLA-4, as discussed above, which involves priming of new T cell clones. Relatlimab, the first FDA approved ICI targeting LAG3, was recently approved on March 18th, 2022, meaning that limited toxicity data are available outside of clinical trials. Generally, grade $\geq$3 events occur in less than 15-20% of anti-PD-1/PD-L1 treated patients (Martins et al., 2019; Xu et al., 2018).

IrAEs are also broad in scope; nearly any organ can be affected (**Figure 1.4**). Diarrhea, colitis, rash, pneumonitis, and endocrinopathies are some of the most common irAEs (Martins et al., 2019; D. Y. Wang et al., 2018). Though many of these irAEs can be diagnosed and managed symptomatically or with steroids, some irAEs can be serious, even fatal. Fatal irAEs occur in 0.3% to 1.3% of patients (D. Y. Wang et al., 2018). ICI-myocarditis, inflammation of the heart muscle, is the most fatal irAE, with a mortality rate approaching 50% (Moslehi et al., 2018; Wang et al., 2018). ICI-myocarditis also has a higher mortality rate than other forms of drug associated myocarditis (Nguyen et al., 2022). The very serious nature of ICI-myocarditis makes it an important limiting toxicity to ICI use.
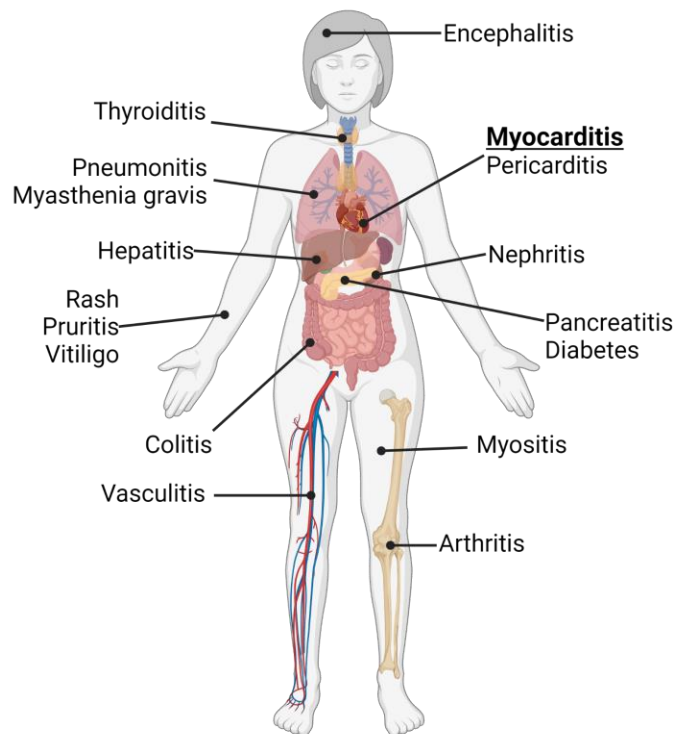
Figure 1.4 Examples of immune-related adverse events. Common or important irAEs are shown in the figure. Myocarditis is highlighted as it is the focus of this research. Figure created with BioRender.com.

ICI-myocarditis was first reported as a possible adverse event of ipilimumab in 2015 (Eggermont et al., 2015). ICI-myocarditis is rare, occurring in approximately 0.27% to 1.14% of patients. ICI-myocarditis tends to occur early, with a median time to onset of 30 days after first ICI treatment (Hu et al., 2019; J. J. Moslehi et al., 2018; J. E. Salem et al., 2018). The most well-established risk factor for the development of ICI-myocarditis is combination ICI therapy (e.g., anti-CTLA-4 therapy with ipilimumab plus an anti-PD1 or anti-PD-L1 agent; Hu et al., 2019; J. J. Moslehi et al., 2018). Concomitant use of cardiovascular or diabetes medications was not associated with increased risk of ICI-myocarditis (J. J. Moslehi et al., 2018). Female sex is associated with a higher risk of ICI-myocarditis, but not other forms of myocarditis (Zamami et al., 2019). This is consistent with female sex as a risk factor for other autoimmune diseases.

Clinical presentation of ICI-myocarditis may be similar to acute heart failure or myocardial infarction, which often makes diagnosis clinically challenging. Presenting symptoms can include chest pain, shortness of breath, palpitations, and syncope. Arrhythmias, including heart block, are common in ICI-myocarditis. Cardiac ejection fraction is often preserved early in the disease course (Hu et al., 2019; Lehmann et al., 2021). Elevated serum biomarkers such as troponin and creatine kinase are common. Due to the similarities with more common cardiac concerns, diagnosis of ICI-myocarditis is a major clinical challenge (Lehmann et al., 2021). Endomyocardial biopsy (EMB) is the gold standard for the diagnosis of myocarditis, with a pathological definition based on immune infiltration and cardiomyocyte cell death. However, inflammation in ICI-myocarditis can often be patchy, which may complicate the diagnostic yield of EMB. Though EMB is generally safe (with high volume centers reporting <1% rates of major complications), it is an invasive procedure and severe, life-threatening complications, such as perforation of the myocardial wall leading to cardiac tamponade, can occur (Chimenti & Frustaci, 2013; Holzmann et al., 2008; Kiamanesh & Toma, 2021; Shah et al., 2018). Early diagnosis is critically important for patients with ICI-myocarditis. Initiation of high dose steroids

within 24 hours of hospital admission is associated with reduced incidence of major cardiac events (Zhang et al., 2020). In general, high clinical suspicion of ICI-myocarditis is sufficient to justify the initiation of steroid treatment and this potentially life-saving intervention should not be delayed for diagnostic confirmation (i.e., with a biopsy).

ICI-myocarditis is characterized histologically by lymphocytic infiltration into the myocardium and destruction of the usual cardiac architecture (Johnson et al., 2016). By immunohistochemistry, the immune infiltrate is primarily composed of CD8+ T cells and CD68+ macrophages (Johnson et al., 2016). TCR sequencing of cardiac tissue shows high clonality, suggesting antigen-directed expansion (Johnson et al., 2016). Interestingly, ICI-myocarditis often co-occurs with myositis and myasthenia gravis-like symptoms (J. E. Salem et al., 2018). Myasthenia gravis is an autoimmune disorder characterized by autoantibody-mediated blockade of neuromuscular junction function which leads to skeletal muscle weakness and rapid fatigue. Myasthenia gravis symptoms following ICI treatment differ from classic myasthenia gravis in several important ways, including predominant respiratory symptoms, higher mortality with ICI-myasthenia gravis and lower prevalence of autoantibodies, indicating a possible difference in disease pathogenesis (Huang et al., 2020). ICI-myasthenia gravis also commonly co-occurs with myositis and myocarditis. This co-occurrence of three muscle-related irAEs suggests the possibility of shared target antigens. This idea is supported by data in a limited number of patients showing overlapping TCR clones between cardiac and skeletal muscle in patients with ICI-myocarditis and myositis (Johnson et al., 2016). Though data are limited, skeletal muscle biopsies in patients with ICI-myasthenia gravis show abundant infiltrating CD8+ T cells (Safa et al., 2019). More work is needed to test the idea that these three irAEs may share a common pathogenesis due to shared target antigens.

Animal models are needed to study disease pathogenesis and treatment for irAEs. Healthy mice treated with ICIs do not reproducibly experience the full spectrum of irAEs seen in

humans. In contrast, mice which are genetically predisposed to autoimmunity are more likely to model irAEs (Adam et al., 2021). The study of ICI-myocarditis in particular is complicated by the rare nature of this toxicity in humans and unclear underlying risk factors. One group used cynomolgus monkeys treated with nivolumab and ipilimumab to model irAEs (Ji et al., 2019). Monkeys treated with combination ICI had mild to moderate inflammation in many organs including the heart, lung, liver, pancreas, bladder, thyroid, and intestines. The cardiac inflammation was mild to moderate in all five treated animals, but mild inflammation was also seen in both control (saline treated) animals. In contrast to ICI-myocarditis in humans, the inflammation seen in the monkeys was milder and tended to have more CD4+ T cells than CD8+ T cells (Ji et al., 2019). This reinforces the notion that pharmacologic models, even in species more closely related to humans than mice, may be insufficient for modeling severe and rare toxicities.

Genetically engineered mouse models provide a useful alternative for studying the most severe consequences of global knockout of checkpoint molecules. Interestingly, the phenotypes associated with knockout depend on the mouse strain used. C57BL/6 mice with knockout of *Pdcd1* develop a lupus-like arthritis and glomerulonephritis (Nishimura et al., 1999). Balb/c mice with knockout of *Pdcd1* develop dilated cardiomyopathy (DCM; Nishimura et al., 2001; Okazaki et al., 2003). In this murine model the diseased heart is characterized by anti-troponin autoantibody immune complexes on the cardiomyocytes, and no apparent signs of active immune cell infiltration (Okazaki et al., 2003). DCM is not a common irAE in humans. Mice with a genetic knockout of both *Pdcd1* and *Lag3* develop fatal myocarditis, which is driven by CD4+ T cells (Okazaki et al., 2011; Woo et al., 2012). It is unknown whether this is similar to myocarditis with anti-LAG3 agents as there is no available clinical data on this toxicity, given the very recent FDA approval of anti-LAG3 therapy.

Chapters II and III describe research on ICI-myocarditis. The goals of the research

described in chapters II and III were: 1) to develop a clinically relevant mouse model of ICI-myocarditis 2) to use this mouse model to test therapeutics 3) to test the hypothesis that ICI-myocarditis may be driven by CD8+ T cells specific for a cardiac self-antigen and 4) to utilize findings from the murine model to advance our understanding of the pathogenesis of ICI-myocarditis in humans.

Rare but severe toxicities associated with anti-cancer therapies highlight the need to target the appropriate treatment to the appropriate patient. Biomarker approaches are one way of doing so.

Immune-related biomarkers in breast cancer

Biomarkers are needed to target the most beneficial treatments to the right patients at the right time. Biomarker approaches can identify patients at higher likelihood of disease recurrence who are likely to benefit from more aggressive therapies. Conversely, biomarkers can also be used to identify patients who are currently being overtreated and spare patients from unnecessary risks of side effects and financial toxicity. An ideal biomarker approach should also be minimally invasive or rely on samples already collected as a part of routine clinical care.

Breast cancer (BC) is a disease where new biomarker strategies are needed. Globally, BC accounts for 24.5% of new cancer cases and 15.5% of cancer deaths in female patients (Sung et al., 2021). BC is commonly stratified based on expression of estrogen receptor (ER), progesterone receptor (PR) and the human epidermal growth factor receptor 2 (HER2). BCs lacking expression of ER, PR and HER2 are classified as triple negative BC (TNBC). Prognosis for BC varies by histologic subtype, with ER+ disease having a better long-term prognosis than TNBC (van Maaren et al., 2019). BC is often treated with neo-adjuvant, which means administered prior to surgery, chemotherapy (NAC). NAC has several advantages over adjuvant (administered after surgery) chemotherapy, including often shrinking the tumor and increasing

the likelihood of breast-conserving surgery as a viable option and also providing important

prognostic information. If no residual tumor cells are identified microscopically in the surgical

resection specimen, that is classified as a pathological complete response (pCR). For patients

with residual disease (RD) in the breast, the size of the RD can be measured and given a

residual cancer burden score (RCB). This information is prognostic of long-term outcomes

across breast cancer histologic subtypes (Yau et al., 2021). Another important and well-

validated prognostic factor is the number of tumor-infiltrating lymphocytes (TILs). Stromal TILs

(sTILs) are particularly prognostic of good outcomes in TNBC (Luen et al., 2019; Salgado et al.,

2015). The prognostic value of TILs is independent of therapy, suggesting an immune-related

component to good outcomes across therapies in BC. The general treatment paradigm for

breast cancer is summarized in **Figure 1.5**.
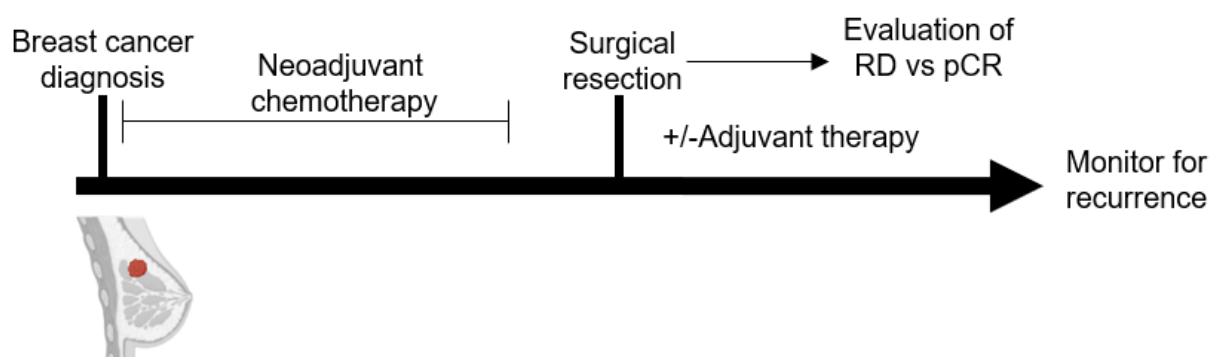
Figure 1.5 General paradigm of breast cancer treatment. This timeline schematic shows the
general paradigm for breast cancer treatment with NAC and surgery. Figure created with
BioRender.com.

Some patients with BC have durable responses with NAC and surgery alone and will not

experience a cancer recurrence in their lifetime. For other patients, their cancer may return,

sometimes many years following surgery (van Maaren et al., 2019). Biomarkers are needed to

distinguish these groups of patients. This is becoming increasing important as ICIs are being

used in earlier settings in BC (Schmid et al., 2022). As noted above, though ICIs can improve

outcomes for some patients, there is a risk of life-threatening adverse events. It is important to identify which patients with BC will or will not benefit from additional therapies like ICIs. Additionally, the use of ICI in combination with chemotherapy to treat BC, increases the importance of understanding the effects of chemotherapy on the immune system. Chemotherapy can have both immunosuppressive and immunostimulatory effects which may affect the overall efficacy of combination chemo- and immune-therapy (Zitvogel et al., 2008).

Blood is an intriguing site for biomarker development because of the relative ease of longitudinal sampling and the ability to sample circulating immune cells. Blood is generally already sampled clinically to monitor the patient throughout treatment and is easier to access than tumor biopsies. Most therapies also have systemic, not just local, effects and systemic responses may be heterogenous across patients. In chapters IV and V, we examine the local and systemic effects of NAC on breast cancer patients of different histologic subtypes. We further focus on blood to examine differences by long-term outcome. We aim to determine whether changes in peripheral blood gene expression or cell type abundance following NAC may differentiate BC outcomes.

Overview and significance of research

Chapters II and III focus on the pathogenesis of ICI-myocarditis. The major goals and questions addressed in chapters II and III are summarized in **Figure 1.6**. Chapters IV and V focus on the effects of NAC on the immune system in BC patients and how these are associated with outcome. The major goals and questions addressed in chapters IV and V are summarized in **Figure 1.7**. These distinct projects are united by the idea of improving the safety and efficacy of therapy for cancer patients.
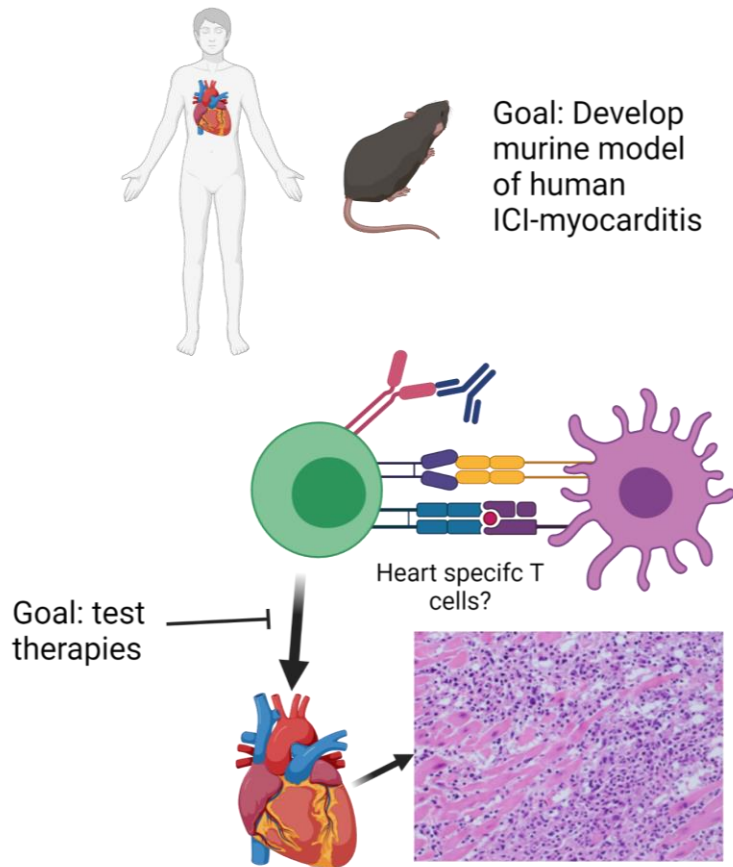
Figure 1.6 Goals of chapters II and III. Chapters II and III describe research on ICI-myocarditis. The goals of the research described in chapters II and III were: 1) to develop a clinically relevant mouse model of ICI-myocarditis 2) to use this mouse model to test therapeutics 3) to test the hypothesis that ICI-myocarditis may be driven by CD8+ T cells specific for a cardiac self-antigen and 4) to utilize findings from the murine model to advance our understanding of the pathogenesis of ICI-myocarditis in humans. Figure created with BioRender.com.
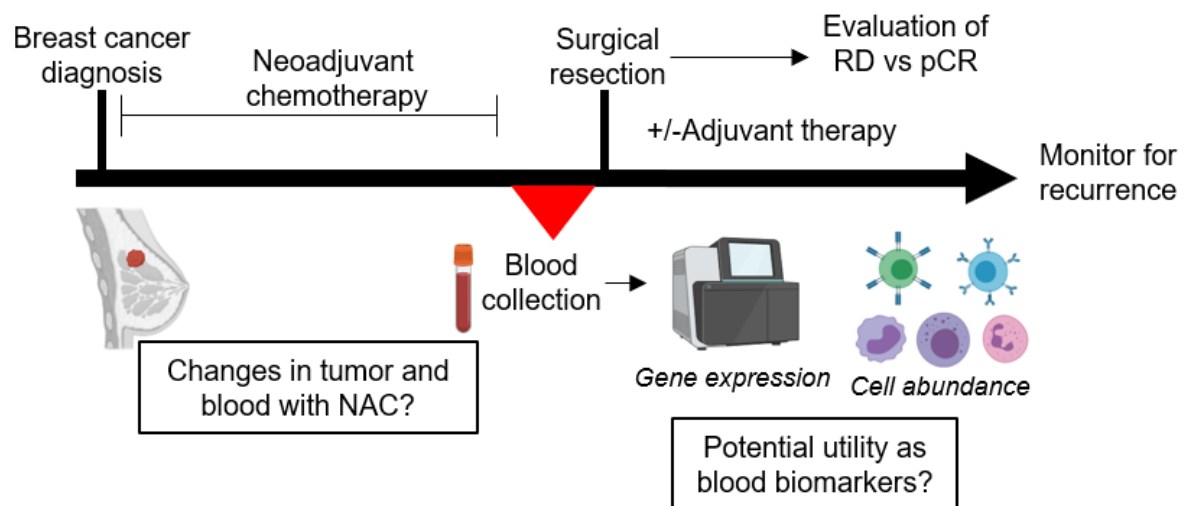
Figure 1.7 Goals of chapters IV and V. In chapters IV and V, we examine the local (tumor) and systemic (blood) effects of NAC on breast cancer patients. We further focus on blood to examine differences by long-term outcome. We aim to determine whether changes in peripheral blood gene expression or cell type abundance following NAC may differentiate BC outcomes. Figure created with BioRender.com.

CHAPTER II

A genetic mouse model recapitulates immune checkpoint inhibitor-associated myocarditis and

supports a mechanism-based therapeutic intervention. [1]

Abstract

Immune checkpoint inhibitors (ICI) targeting CTLA-4 or PD-1/PD-L1 have transformed cancer

therapy but are associated with immune-related adverse events, including myocarditis. Here, we

report a robust preclinical mouse model of ICI-associated myocarditis in which monoallelic loss

of *Ctla4* in the context of complete genetic absence of *Pdcd1* leads to premature death in

approximately half of mice. Premature death results from myocardial infiltration by T cells and

macrophages and severe ECG abnormalities, closely recapitulating the clinical and pathologic

hallmarks of ICI-associated myocarditis observed in patients. Using this model, we show

that *Ctla4* and *Pdcd1* functionally interact in a gene dosage–dependent manner, providing a

mechanism by which myocarditis arises with increased frequency in the setting of combination

ICI therapy. We provide a preclinical model of ICI-associated myocarditis which recapitulates

this clinical syndrome. Using this model, we demonstrate that CTLA-4 and PD-1 (ICI targets)

functionally interact for myocarditis development and that intervention with CTLA4–Ig

(abatacept) attenuates myocarditis, providing mechanistic rationale and preclinical support for

therapeutic clinical studies.

Introduction

Immune checkpoint inhibitors (ICI), including combination therapies such as ipilimumab (anti-CTLA-4) plus nivolumab (anti-PD-1), have shown remarkable efficacy across multiple tumor types (Larkin et al., 2015; Motzer et al., 2018; Postow et al., 2015; Wolchok et al., 2013) but are associated with immune-related adverse events (irAE) including myocarditis (Hu et al., 2019; Johnson et al., 2016; J. Moslehi et al., 2021; J. J. Moslehi et al., 2018; Sznol et al., 2017). ICI-myocarditis is characterized by myocardial T-cell and macrophage infiltration and significant ECG disturbances, with preliminary data suggesting a female predominance, clinically distinguishing it from other forms of myocarditis (Johnson et al., 2016; Valpione et al., 2018; Zamami et al., 2019). ICI-myocarditis is also often fulminant and fatal, despite corticosteroid therapy. Therefore, mechanism-based treatment strategies are needed to mitigate serious irAEs such as myocarditis. One major obstacle to improving our understanding of irAEs is the lack of preclinical animal models that recapitulate the clinical course. Herein, we report a murine model that phenotypically recapitulates the clinical pathology of ICI-myocarditis and provides mechanistic support for the inhibition of T-cell costimulation by CTLA4–Ig as a treatment for ICI-myocarditis.

Methods

Mice. *Ctla4*[tm1All] mice were bred to *Pdcd1*-knockout mice (*Pdcd1*[tm1.1Shr]), which were purchased from The Jackson Laboratory (021157). *Pdcd1*-knockout mice were backcrossed once to C57BL/6J, prior to breeding crosses with *Ctla4* mice. We first used a heterozygous intercross-breeding scheme using *Ctla4-* and *Pdcd1*-knockout transgenic mice to allow for the generation of all possible permutations of mutant alleles from a single cross and for estimation of the observed recombination frequency between *Ctla4* and *Pdcd1*. To verify findings from the first breeding scheme, a second related breeding scheme was utilized. Importantly, this breeding

approach utilized different genotypes; the mutant alleles could be either in *cis* or in *trans* and would generate *Ctla4*$^{+/-}$ *Pdcd1*$^{-/-}$ (experimental) and *Ctla4*$^{+/+}$ *Pdcd1*$^{-/-}$ (control littermates) in a 1:1 ratio. This allows for the generation of many more *Ctla4*$^{+/-}$ *Pdcd1*$^{-/-}$ mice than in the initial breeding approach. Specifically, male *Ctla4*$^{+/-}$ *Pdcd1*$^{-/-}$ and female *Ctla4*$^{+/+}$ *Pdcd1*$^{-/-}$ were bred. Female *Ctla4*$^{+/+}$ *Pdcd1*$^{-/-}$ were used to eliminate the possibility that the autoimmunity or other phenotypes observed in *Ctla4*$^{-/+}$ *Pdcd1*$^{-/-}$ might affect fetal-maternal tolerance or the ability to produce viable litters. For the generation of survival curves, events were defined as either death (i.e., mice found dead) or identification of mice by veterinary staff as requiring euthanasia (e.g., due to lethargy, moribund, dyspnea). Mice utilized for breeding or other analyses (e.g., histologic examination) were included in survival analyses in addition to initial cohorts primarily dedicated to assessing survival. Mice were censored from survival analyses at the time they were utilized for alternative purposes or analyses. Survival analyses of *Ctla4*$^{+/-}$ *Pdcd1*$^{-/-}$ *Rag1*$^{-/-}$ and littermate *Rag1* competent mice were described as above. Notably as a caveat of these specific analyses, because *Ctla4*$^{+/-}$ *Pdcd1*$^{-/-}$ *Rag1*$^{-/-}$ mice are the only immunodeficient genotype within the groups expected to develop fatal myocarditis (i.e., *Ctla4*$^{+/-}$ *Pdcd1*$^{-/-}$ groups), premature deaths in this genotype can be attributed to either causes associated solely with immunodeficiency (e.g., infection) or incomplete rescue of autoimmune phenotypes (e.g., myocarditis) by loss of adaptive immunity. Analysis of female mice in which the premature death is more penetrant provided further support for the former possibility. All mice were housed at The University of Texas MD Anderson Cancer Center South Campus Vivarium, an Association for Assessment and Accreditation of Laboratory Animal Care International (AAALAC)– accredited, specific pathogen-free (SPF) animal facility, or at the Vanderbilt University Medical Center, also an AAALAC-accredited, SPF animal facility. All experiments were performed in accordance with The University of Texas MD Anderson Cancer Center Institutional Animal Care and Use Committee (IACUC) guidelines or the Vanderbilt University Medical Center IACUC guidelines.

Genotyping. Genomic DNA was isolated using DirectPCR Lysis Reagent (Viagen Biotech, 101-T) supplemented with Proteinase K. PCR-based genotyping using crude lysate was performed for *Ctla4-* and *Pdcd1*-knockout mice. *Ctla4*[tm1All] mice were genotyped as previously described (Chambers et al., 1997). The expected band sizes for the *Ctla4* wild-type and mutant alleles are approximately 75 and 150 bp, respectively. *Pdcd1*-knockout mice were genotyped as previously described (Keir et al., 2007). The expected band sizes for the *Pdcd1* wild-type and mutant alleles are 418 and 350 bp, respectively. *Ctla4* primers: 5′ AAACAACCCCAAGCTAACTGCGACAAGG 3′, 5′ CCAGAACCATGCCCGGATTCTGACTTC 3′, 5′ CCAAGTGCCCAGCGGGGCTGCTAAA 3′. *Pdcd1* primers: PD1 KO common 24743 (5′ CACTATCCCACTGACCCTTCA), PD1 KO WT rev (5′ AGAAGGTGAGGGACCTCCAG), and PD1 KO Mut rev (5′ CACAGGGTAGGCATGTAGCA).

Pathology. Formalin-fixed tissues were routinely processed, cut at 4 to 5 μm, and stained with H&E by standard protocols in Vanderbilt University Medical Center's Translational Pathology Shared Resource (TPSR) core laboratory. To further characterize the mononuclear cardiac infiltrates detected by light microscopy, a panel of IHC markers was employed. IHC staining was performed in the TPSR using standard, validated protocols for chromogenic IHC. All steps besides dehydration, clearing, and coverslipping were performed on the Leica Bond-Max IHC autostainer (Leica Biosystems Inc.). Slides were deparaffinized. Antigen retrieval was performed using EDTA (CD markers) or proteinase K (F4/80). Slides were incubated with primary antibodies as indicated below. Secondary antibody labeling was performed for all markers except CD3 by incubating in rabbit anti-rat antibody (BA-4001, Vector Laboratories, Inc.) for 15 minutes at a 1:650 dilution. Immunolabeling by rabbit antibody was visualized using the Bond polymer refine detection system (#DS9800, Leica Biosystems, Inc.). Slides were then dehydrated, cleared, and coverslipped. For primary antibodies, anti-CD45R (BD Biosciences, RA3–6B2) was used at 1:20,000 dilution as a B-cell marker, anti-CD3 (Abcam, Ab16669) was

used at 1:250 dilution as a pan–T-cell marker, anti-CD4 (eBioscience, 14–9766–82) was used at 1:1,000 dilution as a Th cell marker, anti-CD8 (eBioscience, 14–0808–82) was used at 1:1,000 dilution as Tc cell marker, and anti-F4/80 (Novus Biologicals, NB600–404) was used at 1:900 dilution as macrophage marker.

Histologic Scoring. Microscopic analysis and semiquantitative scoring of morphologic lesions were conducted by two board-certified veterinary anatomic pathologists, one of whom was blinded to the mouse genotypes/treatments. Semiquantitative scoring was performed to characterize the magnitude of myocardial infiltrates in six distinct cardiac regions: ventricular endocardium, ventricular myocardium and perivascular adventitia, ventricular epicardium, atria, aorta, and pericardium. The sum of scores assigned for all regions was calculated for each mouse for a composite score, and group means of the composite scores are presented. Scores were performed as follows: 0, within normal limits; 1, minimal (<10% affected); 2, mild (10%–20% affected); 3, moderate (20%–50% affected); and 4, marked (>50% affected). I

Cardiac Dissociation and Flow Cytometry. Single-cell suspensions were obtained from hearts of 3- to 6-week-old female wild-type, $Ctla4^{+/+} Pdcd1^{-/-}$ or $Ctla4^{+/-} Pdcd1^{-/-}$ mice by mincing followed by enzymatic digestion with 125 U/mL DNase I (Worthington; cat no. LS002138) and 250 U/mL Collagenase 3 (Worthington; cat no. LS004182). Dissociated hearts were filtered through a 70μm filter. Red blood cells were lysed using ACK lysing buffer (KD Medical/MediaTech; cat no. NC0274127). Cells were washed with PBS and stained for flow cytometry. Cells were first stained with Zombie Violet fixable viability dye for 20 minutes at room temperature, followed by Fc block [TruStain FcX (anti-mouse CD16/32) Antibody; BioLegend; cat no. 101320] for 5 minutes at 4°C. Cells were washed and stained with surface stain for 20 minutes at 4°C, as indicated below. Cells were then fixed with either eBioscience Fix/Perm (Thermo Fisher Scientific; cat no. 88–8824–00) kit for cytoplasmic antigens (i.e., CD68) or True-Nuclear Transcription Factor Buffer Set (BioLegend; cat no. 424401) for nuclear antigens (i.e.,

FoxP3). Samples were run on an Attune NxT Acoustic Focusing Cytometer. Analysis was performed in FlowJo, using two different panels of antibodies on the same sample. Gating was first done on forward scatter (FSC) and side scatter to exclude debris. Doublets were excluded by gating on FSC area versus FSC height. Given massive cell death in the cardiomyocytes, percentages were calculated out of total cardiac single cells. Next, viable (zombie violet negative) immune cells (CD45$^+$) were gated and used for all downstream immune cell gates. T cells were defined as CD3$^+$ and gated into CD3$^+$CD4$^+$CD8$^-$ or CD3$^+$CD8$^+$CD4$^-$. Tregs were defined as CD3$^+$CD4$^+$CD8$^-$FoxP3$^+$. Macrophages were defined as CD68$^+$. Natural killer/NK-T cells were defined as CD68-NK1.1$^+$. B cells were defined as CD68$^-$CD19$^+$. CD68$^-$CD11c$^+$ cells are also enumerated, which are primarily comprised of dendritic cells. Zombie Violet (cat no. 423114), PerCP/Cy5.5 anti-mouse CD45 (clone 30-F11; cat no. 103132), Alexa Flour 488 anti-mouse CD3 (clone 17A2; cat no. 100210), APC anti-mouse CD4 (clone GK1.5; cat no. 100412), PE/Cy7 anti-mouse CD8a (clone 53–6.7; cat no. 100722), APC/Cy7 anti-mouse CD19 (clone 6D5; cat no. 115530), Alexa Flour 488 anti-mouse CD11c (clone N418; cat no. 117311), PE/Cy7 anti-mouse IA/IE (clone M5/114.15.2; cat no. 107630), PE anti-mouse CD68 (clone FA-11; cat no. 137013), APC anti-mouse NK1.1 (clone PK136; cat no. 108710), and APC/Cy7 anti-mouse CD11b (clone M1/70; cat no. 101225) were purchased from BioLegend. PE anti-mouse FoxP3 (clone FJK-16s; cat no. 101225) was purchased from Thermo Fisher Scientific.

Abatacept Injection. Mice were injected i.p. with either 100 µL PBS with 200 µg CTLA4 Ig (Abatacept, purchased from Vanderbilt pharmacy) or vehicle, 3 times a week, for up to 80 days, starting at 21 days of age. Although abatacept is a human CTLA-4-Ig fusion, it also functions in mouse models due to the high similarity between human and mouse CTLA4 (Kallikourdis et al., 2017).

ECG in Anesthetized Mice. ECG records were created in the different genetic models to assess presence of arrhythmogenic disturbances. Once mice were anesthetized with 3% isoflurane

inhalation, needle electrodes were placed s.c. into all four limbs. Isoflurane was then lowered to 1% to maintain stable sedation, and ECG recording was started. ECG traces were recorded for 4 to 5 minutes. ECG analysis was conducted in LabChart 8 by two observers blinded to the genotype and then compared for precision. Conduction disturbances were quantified as the number of mice in each group as percentage. ECG records were reviewed and ventricular ectopic beats identified based on standard criteria (i.e., wide QRS complex, AV dissociation).

Echocardiography. Before sacrifice, *in vivo* cardiac dimensions were assessed with M-mode and two-dimensional transthoracic echocardiography (Vevo 2100; Fujifilm VisualSonics). Mice were not anesthetized during echocardiography. Parasternal long axis views were used to record M-mode tracings at left ventricular midpapillary level to measure left ventricular dimensions (interventricular septum, left ventricular posterior wall, left ventricular internal diameter, and % ejection fraction).

Results

Lethal Haploinsufficiency of Ctla4 in the Genetic Absence of Pdcd1

CTLA4 and PD-1 attenuate T-cell activation, but do so through distinct cellular and molecular mechanisms (Chen & Flies, 2013; Parry et al., 2005; Wei et al., 2018b). We crossed transgenic mouse strains harboring loss-of-function alleles of *Ctla4* (encoding CTLA4) and *Pdcd1* (encoding PD-1) to understand how compound loss of CTLA4 and PD-1 would affect T-cell function and the manifestation of autoimmune pathologies. Consistent with prior findings, mice with homozygous loss of *Ctla4* succumbed to fatal lymphoproliferative disease with complete penetrance (**Figure 2.1A**) (Chambers et al., 1997; Tivol et al., 1995; Waterhouse et al., 1995). Approximately 50% of $Ctla4^{+/-}$ $Pdcd1^{-/-}$ mice died by 3 months of age, whereas littermate controls, including $Ctla4^{+/+}$ $Pdcd1^{-/-}$ mice, remained healthy. This dramatic effect of single copy loss of *Ctla4* in the absence of PD-1 is surprising, given that no haploinsufficiency

22

phenotypes have been previously reported in *Ctla4*^{+/-} mice with homozygous wild-type *Pdcd1* alleles at either the organismal or cellular level (Wei et al., 2019), suggesting that negative regulation by PD-1 is sufficient to buffer against perturbations in T-cell signaling caused by heterozygous loss of *Ctla4*. To confirm the mortality observed in *Ctla4*^{+/-} *Pdcd1*^{-/-} mice, we used a second breeding scheme that yields only *Ctla4*^{+/-} *Pdcd1*^{-/-} and *Ctla4*^{+/+} *Pdcd1*^{-/-} littermate mice, which yielded similar findings with mortality of approximately 50% of *Ctla4*^{+/-} *Pdcd1*^{-/-} mice (**Figure 2.1B**). Comprehensive histologic analysis revealed prominent lymphocytic infiltration in the heart and pancreas of *Ctla4*^{+/-} *Pdcd1*^{-/-} mice (**Supplementary Table S2.1**). The frequency of mortality was partially sex-dependent, with female mice dying at higher frequency than male mice, consistent with the characteristics of ICI-myocarditis in patients (**Figure 2.1C**; Valpione et al., 2018; Zamami et al., 2019).

Because *Ctla4*-null mice die due to systemic lymphoproliferative disease and *Pdcd1*-knockout mice develop mild autoimmunity in specific strains of mice, we explored the possibility that *Ctla4*^{+/-} *Pdcd1*^{-/-} mice develop systemic autoimmunity. No differences in morphology of lymphoid tissues between genotypes were detected in *Ctla4*^{+/-} *Pdcd1*^{-/-} mice (**Supplementary Fig. S2.1**). Furthermore, in contrast to *Ctla4*-null mice, *Ctla4*^{+/-} *Pdcd1*^{-/-} mice do not die from uncontrolled lymphoproliferation or a major defect in central tolerance. There was no evidence of systemic organ immune infiltration or elevations in levels of serum cytokines or antibodies (**Supplementary Fig. S2.2A, B**). This indicates that *Ctla4*^{+/-} *Pdcd1*^{-/-} mice do not die due to cytokine storm or systemic autoimmunity. However, *Ctla4*^{+/-} *Pdcd1*^{-/-} mice had elevations in serum troponin, a marker of cardiac damage, raising the possibility that cardiac involvement underlies the premature death of *Ctla4*^{+/-} *Pdcd1*^{-/-} mice (**Supplementary Fig. S2.2C**). In a subset of mice where matched flow cytometry data were also available, elevated troponin was associated with increased cardiac CD45^{+} immune cell infiltration (**Supplementary Fig. S2.2D**). Interestingly, histopathologic analysis of other tissues, such as skeletal muscle, colon, and lung,

showed minor or no increased immune infiltration in *Ctla4*$^{+/-}$ *Pdcd1*$^{-/-}$ mice compared with

Ctla4$^{+/+}$ *Pdcd1*$^{-/-}$ mice (**Supplementary Fig. S2.3**), which did not generally result in overt tissue

death and was assessed as unlikely to be pathophysiologically relevant. These infiltrations were

substantially less pronounced in comparison with the pathologies observed in the heart and

pancreas. Together, these data suggested that *Ctla4*$^{+/-}$ *Pdcd1*$^{-/-}$ mice die due to a breach in

peripheral tolerance manifesting in organ-specific autoimmunity.
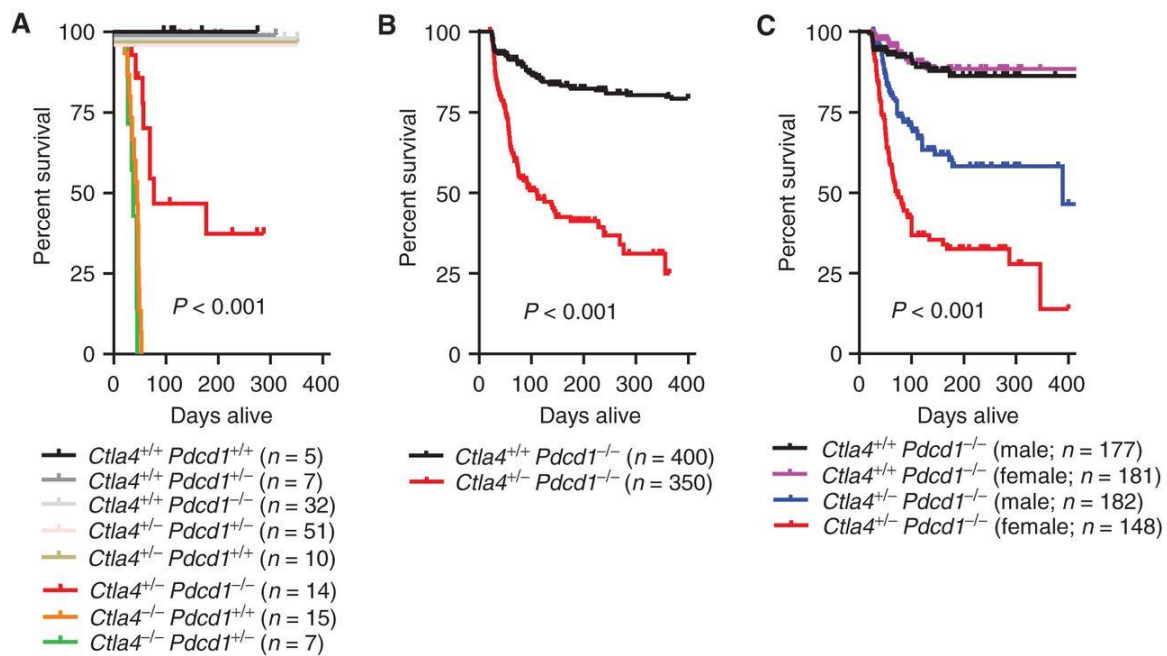
Figure 2.1. Lethal haploinsufficiency of *Ctla4* in the genetic absence of *Pdcd1*.
A, Kaplan–Meier survival curve of transgenic C57BL6/J mice harboring *Ctla4*- and *Pdcd1*-knockout alleles. Mice were derived from an intercross of *Ctla4*$^{+/-}$ *Pdcd1*$^{+/-}$ mice in which *Pdcd1* and *Ctla4* loss-of-function alleles are in *trans*. Individual mice were censored if used for breeding or alive at the time of data analysis. Death events were defined as mice found dead or identified by veterinary staff as requiring euthanasia. *P* value represents the result of the Mantel–Cox log-rank test. **B,** Kaplan–Meier survival curve of *Ctla4*$^{+/-}$ *Pdcd1*$^{-/-}$ (*n* = 350) and littermate *Ctla4*$^{+/+}$ *Pdcd1*$^{-/-}$ (*n* = 400) mice derived from a *Ctla4*$^{+/-}$ *Pdcd1*$^{-/-}$ by *Ctla4*$^{+/+}$ *Pdcd1*$^{-/-}$ breeding cross performed at the Vanderbilt University Medical Center (VUMC) vivarium. *P* value represents the result of the Mantel–Cox log-rank test. **C,** Kaplan–Meier survival curve of *Ctla4*$^{+/-}$ *Pdcd1*$^{-/-}$ and littermate *Ctla4*$^{+/+}$ *Pdcd1*$^{-/-}$ mice stratified by sex. Data are pooled from studies performed at MD Anderson Cancer Center and VUMC. *P* value represents the result of the Mantel–Cox log-rank test.

Myocarditis Manifests Due to Ctla4 Haploinsufficiency in the Absence of Pdcd1

Histologic examination of the heart tissue indicated dense cellular infiltrates with associated cardiomyocyte necrosis, consistent with myocarditis, in *Ctla4$^{+/-}$ Pdcd1$^{-/-}$* mice. Although myocarditis was generally widespread among atrial and ventricular sites, the infiltrates were mostly epicardial and endocardial, consistent with fulminant myocarditis observed in ICI-treated patients (Johnson et al., 2016). Lymphocytic infiltration into the myocardial tissue and myocyte destruction demonstrated patterns similar to those observed in human patients with ICI-myocarditis (**Figure 2.2A**). Interestingly, the other site of dramatic lymphocytic inflammation occurred in the exocrine pancreas, with sparing of the islet cells (**Supplementary Fig. S2.4**). The intensity of the inflammation in *Ctla4$^{+/-}$ Pdcd1$^{-/-}$* mice varied, consistent with the incomplete penetrance of mortality. These pathologic abnormalities were not observed in *Ctla4$^{+/+}$ Pdcd1$^{-/-}$* mice, underscoring the critical importance of *Ctla4* in disease pathogenesis. Lymphocytic infiltration consisted of CD3^{+} CD8^{+} T cells, and CD4^{+} T cells to a lesser abundance in *Ctla4$^{+/-}$ Pdcd1$^{-/-}$* mice, mirroring observations in patients (**Figure 2.2B-E**). In agreement with phenotypic observations, histopathology scores of cardiac hematoxylin and eosin (H&E) sections in *Ctla4$^{+/-}$ Pdcd1$^{-/-}$* mice demonstrated increased prevalence of myocarditis with high CD3^{+} lymphocytic infiltrate, high F4/80^{+} macrophage infiltrate, and low FOXP3^{+} regulatory T-cell abundance (**Figure 2.2D**). We further characterized cellular infiltrates in female 3- to 6-week-old *Ctla4$^{+/-}$ Pdcd1$^{-/-}$* and *Ctla4$^{+/+}$ Pdcd1$^{-/-}$* mice by flow cytometry. Increased frequencies of total CD45^{+} immune cells, CD8^{+} T cells, and CD68^{+} macrophages were observed in *Ctla4$^{+/-}$ Pdcd1$^{-/-}$* mice compared with littermate *Ctla4$^{+/+}$ Pdcd1$^{-/-}$* mice (**Figure 2.2E; Supplementary Fig. S2.5, S 2.6A**). In contrast, no difference was observed in matched splenic populations (**Supplementary Fig. S2.6B**). Mice were highly heterogeneous in levels of infiltrate, consistent with the heterogeneity and incomplete penetrance observed at the phenotypic level. Given

these observations, we then tested whether the disease pathogenesis of $Ctla4^{+/-}$ $Pdcd1^{-/-}$ mice is immune-mediated. Premature mortality appeared to be attenuated in $Ctla4^{+/-}$ $Pdcd1^{-/-}$ $Rag1^{-/-}$ mice compared with littermate $Ctla4^{+/-}$ $Pdcd1^{-/-}$ $Rag1$ competent mice (**Figure 2.2F**). Although this comparison did not meet statistical significance (potentially due to the impact of $Rag1^{-/-}$ immunodeficiency independent of myocarditis, evidenced by premature deaths observed in $Ctla4^{+/-}$ $Pdcd1^{+/-}$ $Rag1^{-/-}$ mice), it is consistent with a role for adaptive immunity in disease pathogenesis.
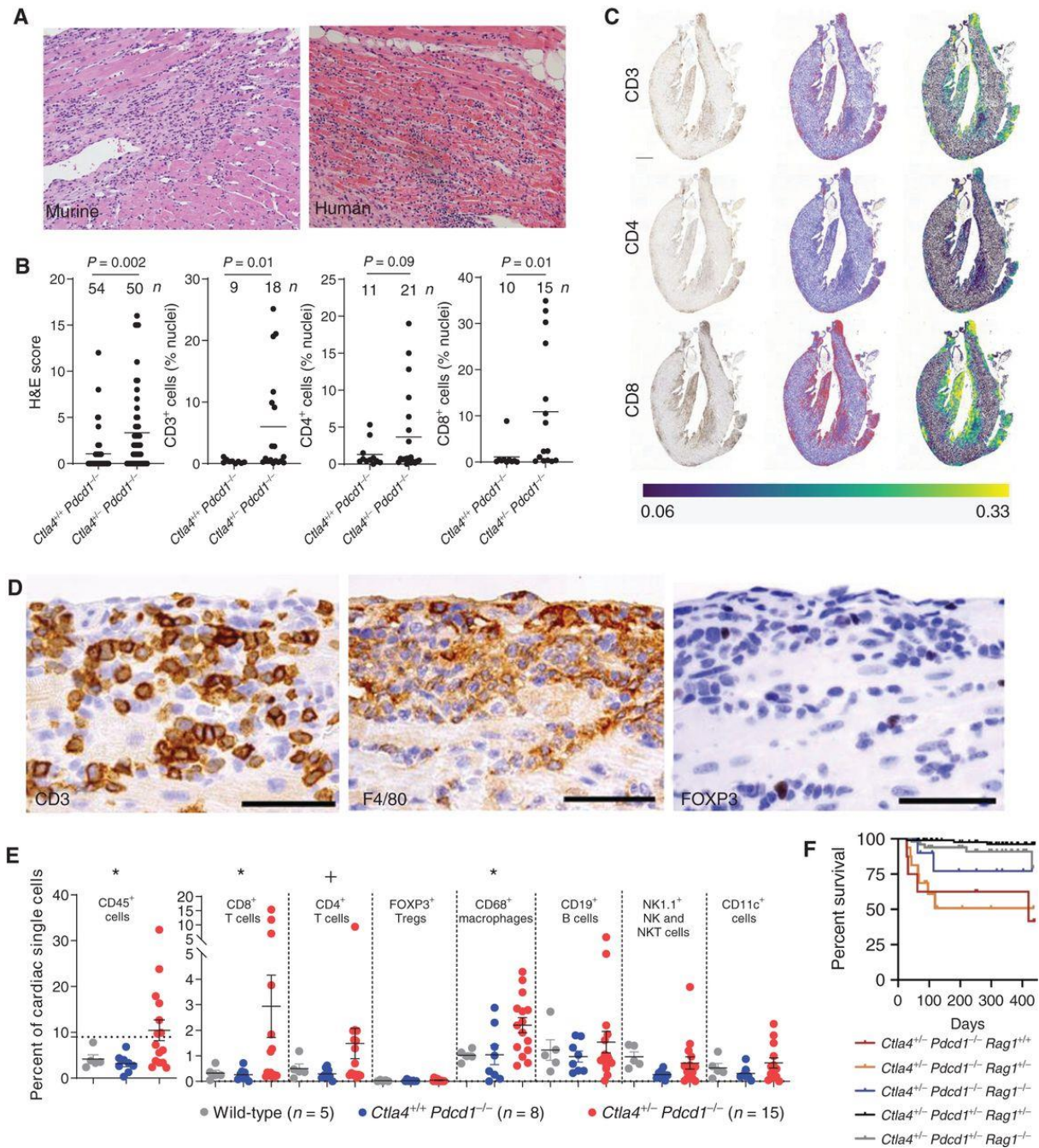
Figure 2.2. *Ctla4*^{+/−} *Pdcd1*^{−/−} **mice present with cardiac immune infiltration**. **A,** H&E images (20X) of lymphocytic infiltration in *Ctla4*^{+/−} *Pdcd1*^{−/−} mouse (left) and human (right; autopsy sample from myocardium of a patient that had complete heart block and ventricular tachycardia following ICI treatment). **B,** Quantification of lymphoid infiltrate scores from H&E-stained heart tissue (see Methods) and frequency of CD3, CD4, and CD8^{+} cells (IHC) as a fraction of total nucleated cells. *P* value represents result of unpaired Student *t* test with Welch correction. **C,** Representative images of CD3, CD4, and CD8 IHC (right) stained heart tissue sections from female *Ctla4*^{+/−} *Pdcd1*^{−/−} mice. Left plots: IHC; middle plots: segmentation (red = positive and blue = negative cells); right plots: positive cell density (blue = low, green = intermediate, and yellow = high). Heat-map values represent arbitrary density units. **D,** Representative images of additional IHC (CD3, F4/80[+] macrophages, and

27

FOXP3$^+$ Tregs) stained heart tissue from *Ctla4*$^{+/-}$ *Pdcd1*$^{-/-}$ mice. Scale bars, 50 μm. **E,** Flow cytometry analysis of immune populations in murine cardiac tissue. * (ANOVA) $P < 0.05$; + (ANOVA) $P < 0.10$. Dashed line at 9% CD45$^+$ cells was used as a stratification factor for "high" versus "low" infiltrated samples. **F,** Kaplan–Meier survival curve of *Ctla4*$^{+/-}$ *Pdcd1*$^{-/-}$ *Rag1*$^{-/-}$ ($n = 10$) and littermate *Ctla4*$^{+/-}$ *Pdcd1*$^{-/-}$ *Rag1*$^{+/+}$ and *Ctla4*$^{+/-}$ *Pdcd1*$^{-/-}$ *Rag1*$^{+/-}$ mice ($n = 8$ and 16, respectively). Littermate *Ctla4*$^{+/-}$ *Pdcd1*$^{+/-}$ *Rag1*$^{+/-}$ and *Ctla4*$^{+/-}$ *Pdcd1*$^{+/-}$ *Rag1*$^{-/-}$ mice are also displayed ($n = 99$ and 51, respectively). Treg, regulatory T cell.

Cardiac Alterations in Ctla4+/− Pdcd1−/− Mice Reflect the Clinical Course of Checkpoint

Blockade–Associated Autoimmune Myocarditis

To further characterize clinical cardiac disease, we performed extensive cardiovascular and physiologic examination in all *Ctla4*$^{+/-}$ *Pdcd1*$^{-/-}$ and littermate *Ctla4*$^{+/+}$ *Pdcd1*$^{-/-}$ mice. Considerable heterogeneity was observed in echocardiographic parameters of *Ctla4*$^{+/-}$ *Pdcd1*$^{-/-}$ mice compared with *Ctla4*$^{+/+}$ *Pdcd1*$^{-/-}$ mice such that no statistically significant differences were observed. However, stratification of mice based on immune infiltrates revealed an association between increased immune infiltration and cardiomegaly as manifested by increased heart-weight to body-weight ratio and ventricular wall thickening on echocardiography without systolic cardiac dysfunction (**Figure 2.3A, B**). Detailed ECG examination revealed significant arrhythmogenic disturbances, including sinus node dysfunction, sinus arrest, and atrioventricular conduction block, and severe bradycardia in *Ctla4*$^{+/-}$ *Pdcd1*$^{-/-}$ mice, but not *Ctla4*$^{+/+}$ *Pdcd1*$^{-/-}$ mice (**Figure 2.3 C-E**), consistent with the arrhythmogenic nature of ICI myocarditis in patients (**Figure 2.3F**). The pattern of myocarditis and ECG instability observed in these mice is consistent with clinical observations from patients with ICI-myocarditis (Escudier et al., 2017; Johnson et al., 2016; Mahmood et al., 2018).
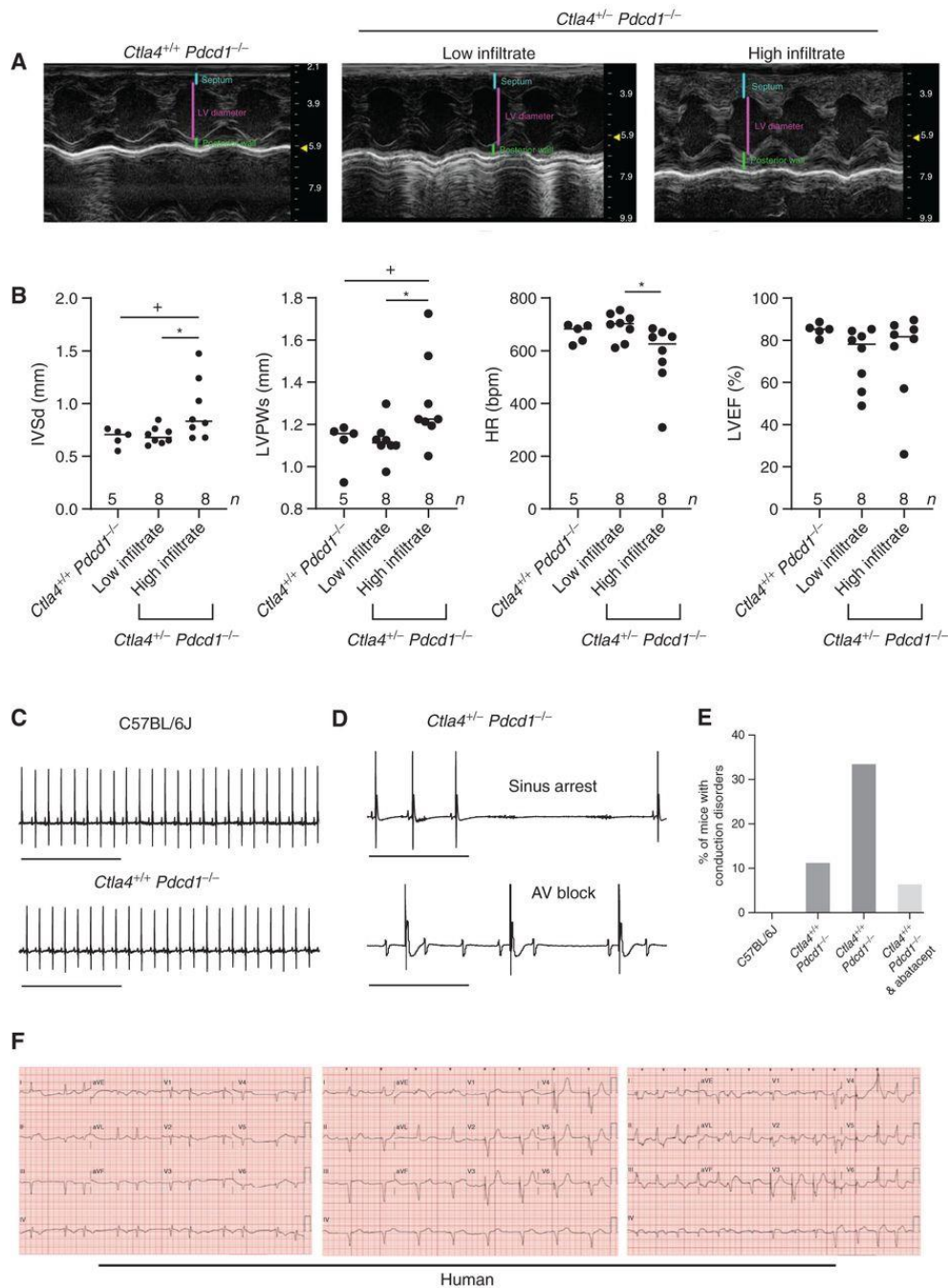
Figure 2.3. Functional cardiologic manifestations of autoimmune myocarditis in *Ctla4*^{+/−} *Pdcd1*^{−/−} mice are similar to those occurring in patients. A, Representative echocardiograms from *Ctla4*^{+/+} *Pdcd1*^{−/−}, low immune infiltrate (<9% CD45^{+} cells) *Ctla4*^{+/−} *Pdcd1*^{−/−}, and high immune infiltrate (≥9% CD45^{+} cells) *Ctla4*^{+/−} *Pdcd1*^{−/−} mice. **B,** Quantification of cardiac properties and output in *Ctla4*^{+/+} *Pdcd1*^{−/−}, low immune infiltrate (<9%) *Ctla4*^{+/−} *Pdcd1*^{−/−}, and high immune infiltrate (≥9%) *Ctla4*^{+/−} *Pdcd1*^{−/−} mice. HR, heart rate; IVSd, interventricular septum (diastole); LVEF, left ventricular ejection fraction; LVPWs, left ventricular posterior wall (systole). *, $P < 0.05$; +, $P < 0.10$ Kruskal–Wallis test with Dunn multiple comparison. **C,** Representative ECG records from wild-type C57BL/6J (left) and *Ctla4*^{+/+} *Pdcd1*^{−/−} mice demonstrating normal sinus rhythm. **D,** Representative ECG records from *Ctla4*^{+/−} *Pdcd1*^{−/−} mice demonstrating sinus arrest

and AV block. **E,** Percentage of mice in wild-type C57BL/6J, *Ctla4$^{+/+}$ Pdcd1$^{-/-}$*, and *Ctla4$^{+/-}$ Pdcd1$^{-/-}$* genotypes or *Ctla4$^{+/-}$ Pdcd1$^{-/-}$* treated with abatacept demonstrating observed conduction disorders. **F,** Representative ECG from 3 patients with ICI-associated myocarditis. All patients were treated with ipilimumab and nivolumab with clinical presentation within 2 weeks of dose with ECG on admission. There is 3:2 conduction block and QRS widening (left), third-degree heart block with ventricular pacing (middle), and ventricular pacing competing with an accelerated ventricular rhythm (right).

Therapeutic Intervention with CTLA4–Ig Rescues the Fatal Myocarditis That Arises

in Ctla4+/− Pdcd1−/− Mice

The development of a robust mouse model of ICI-associated myocarditis enables the testing of therapeutic regimens. Our finding that the development of myocarditis is gene dosage–dependent raises the hypothesis that restoration of CTLA4 and/or PD-1 signaling would be sufficient to prevent disease progression. To test this hypothesis, 3-week-old *Ctla4$^{+/-}$ Pdcd1$^{-/-}$* mice were treated with vehicle or abatacept (recombinant CTLA4–Ig) to block T-cell costimulation by binding to B7 ligands, prior to the development of any overt clinical signs. Abatacept treatment significantly reduced mortality of *Ctla4$^{+/-}$ Pdcd1$^{-/-}$* mice (**Figure 2.4A**). At a cellular level, abatacept did not decrease myocardial immune infiltrates at 2 weeks; however, after 14 weeks, immune infiltrates in the heart returned to near-baseline levels (**Figure 2.4B**). No statistically significant difference was observed in heart weight–body weight ratios between genotypes; however, decreased cardiomegaly was observed following abatacept treatment (**Figure 2.4C**). These observations provide preclinical rationale for further investigation of CTLA4–Ig as a treatment for autoimmune irAEs associated with ICI therapy. Clinically, we have previously published a case report of a corticosteroid-refractory ICI myocarditis successfully treated with abatacept (J.-E. Salem et al., 2019). Thus, preliminary evidence exists that response to CTLA4–Ig in this model seems to replicate that observed in clinical patients, though more investigation is clearly needed. Nonetheless, these data further support the mechanistic basis for the ability of CTLA4–Ig intervention to attenuate autoimmunity caused by either anti–PD-1 monotherapy or combination anti-CTLA4 plus anti–PD-1 treatment.
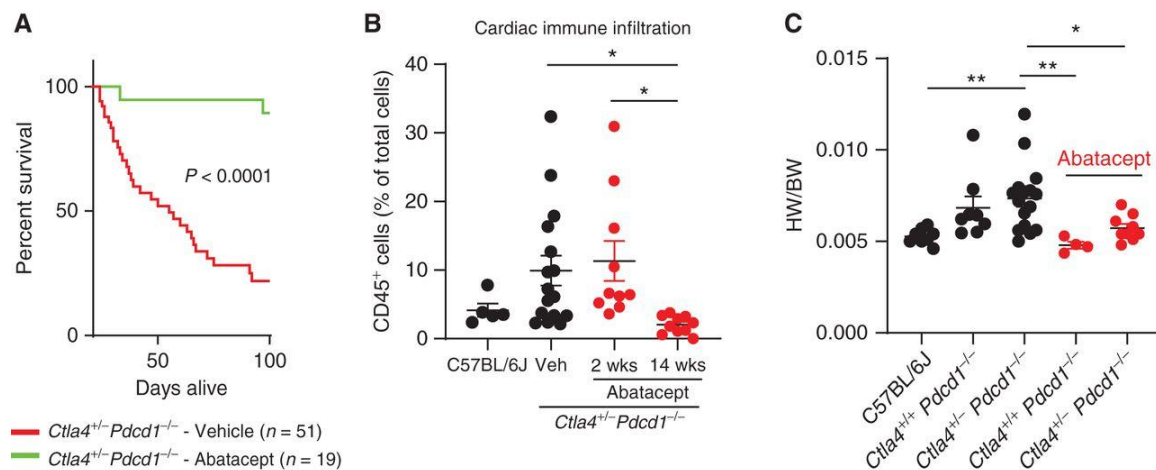
Figure 2.4. Modulation of CTLA4 and PD-1 T cell–negative costimulation leads to functional changes in cardiac pathology. A, Kaplan–Meier survival curve of female *Ctla4*^+/− *Pdcd1*^−/− mice treated with either vehicle (*n* = 51) or abatacept (*n* = 19). *P* value represents the outcome of the log-rank test.**B,** Infiltration of CD45^+ immune cells assessed by flow cytometry analysis of heart tissue from female *Ctla4*^+/+ *Pdcd1*^−/− and *Ctla4*^+/− *Pdcd1*^−/− mice with and without abatacept treatment. *, *P* < 0.05 ANOVA with Tukey multiple testing correction. **C,** Heart weight/body weight (HW/BW) ratio of female *Ctla4*^+/+ *Pdcd1*^−/− and *Ctla4*^+/− *Pdcd1*^−/− mice with and without abatacept treatment. *, *P* < 0.05; **, *P* < 0.01 ANOVA with Dunn multiple testing correction comparing all groups with *Ctla4*^+/− *Pdcd1*^−/− control mice.

Discussion

Here, we identify gene dosage–dependent genetic and functional interaction between the T cell–negative costimulatory genes *Ctla4* and *Pdcd1*, which manifests as fatal myocarditis in *Ctla4*^+/− *Pdcd1*^−/− mice, providing a robust genetic mouse model for myocarditis and other cardiovascular toxicities associated with CTLA-4 and PD-1 ICI therapy. This model addresses a key limitation in the field and enables mechanistic investigation of ICI-induced irAEs. Importantly, this mouse strain models myocarditis associated with monotherapy and combination ICI therapy, which are both fundamentally driven by aberrant T-cell activation. In patients, most T cells are antigen experienced, whereas most T cells in laboratory mice are naïve, which may explain why PD-1 blockade can lead to myocarditis in humans, but additional perturbations are required in mice. Specifically, naïve T cells require CD28 costimulation to

activate (which will not normally be provided for self-antigens), whereas in contrast, the activity of antigen-experienced cells can be enhanced by PD-1 blockade alone. Dual PD-1 and CTLA-4 blockade enhances both of these processes, providing a mechanistic rationale for the association with a higher frequency of myocarditis. Fundamentally, these data support a threshold model of T-cell activation in which CTLA-4 and PD-1 regulatory signals functionally integrate to provide a critical buffering system to restrain T-cell activation. Gene dosages of *Ctla4* and *Pdcd1* together define the functional threshold of T-cell self-recognition. These findings are consistent with the understanding that CTLA-4 and PD-1 attenuate T-cell activation through distinct cellular and molecular mechanisms (Chen & Flies, 2013; Wei et al., 2018b), provide mechanistic insights into how ICI-associated myocarditis arises, and present a preclinical model to test therapeutic interventions to mitigate irAEs.

Based on the functional interaction between CTLA-4 and PD-1, intervention with CTLA4–Ig, which blocks T-cell costimulation, may be an effective therapeutic intervention for myocarditis associated with monotherapy and combination ICI therapy—a provocative possibility that is supported by preliminary clinical reports and warrants future prospective clinical testing (Salem et al., 2019). However, the effect of CTLA4–Ig treatment on tumor growth must be fully understood, particularly given that CD28 signaling is required for T-cell priming and for responses to checkpoint blockade (Kamphorst et al., 2017). It is tempting to speculate that CTLA4–Ig could be administered after the initial priming of tumor-reactive T cells, allowing antitumor responses to be maintained; however, this possibility requires investigation.

Critical open questions remain, including how ICI efficacy and irAEs are related, how irAEs may be mitigated, and in what contexts ICI therapy is warranted. Our results reveal a functional interaction between CTLA-4 and PD-1, with particular relevance to cardiovascular homeostasis. Although mice heterozygous for *Ctla4* appear normal, complete loss of CTLA-4 leads to unrestrained fatal lymphoproliferation; however, the inflammation is not specific to the

cardiovascular system in these models. On the other hand, the phenotype of $Pdcd1^{-/-}$ mice is dependent on genetic background. Although PD-1 loss in a C57BL/6 strain does not result in significant cardiovascular toxicity, BALB/c mice deficient for PD-1 display autoantibody-mediated cardiomyopathy upon aging (Nishimura et al., 1999, 2001; Okazaki et al., 2003). However, this model does not recapitulate ICI-myocarditis in humans clinically or pathologically. On the other hand, the disease etiology of $Ctla4^{+/-} Pdcd1^{-/-}$ mice closely recapitulates ICI-myocarditis. The sex imbalance seen in our mice is consistent with emerging data from patients where female sex is associated with increased risk of irAEs and myocarditis specifically (Valpione et al., 2018; Zamami et al., 2019). These early observations in ICI myocarditis are in contrast with general myocarditis which appears to occur with higher frequency in men (Elamm et al., 2012).

From a perspective of basic T-cell biology, the precise molecular and cellular mechanism by which CTLA-4 and PD-1 functionally interact remains unclear. These data further support a threshold model of T-cell costimulation, in which loss of PD-1 and CTLA-4 leads to a decreased threshold for T-cell activation and enables aberrant activation of self-reactive T cells. The manifestation of severe autoimmunity in specific tissues in this model and individual patients receiving ICIs may reflect one or more potential mechanisms, including the predisposition of particular antigens to autoimmune recognition in the absence of negative costimulation, functional differences between tissue-specific regulatory T-cell (Treg) populations, or environmental factors.

Our findings also raise the possibility that subtle changes in gene dosage of *CTLA4* and *PDCD1* may predispose some patients to the development of cardiovascular irAEs. Heterozygous germline loss of function alleles of *CTLA4* in humans leads to immune dysregulation with highly variable clinical presentation and incomplete penetrance (Kuehn et al., 2014; Schubert et al., 2014; Schwab et al., 2018). Our preclinical data provide biological

rationale and support further investigation of CTLA4–Ig as a potential therapy for ICI-induced autoimmune irAEs. Our results are further supported by preliminary patient data whereby treatment with abatacept attenuated cases of steroid-refractory ICI-myocarditis (J.-E. Salem et al., 2019; Wei et al., 2020). Further data are needed to understand the effects of abatacept on tumor growth in preclinical and clinical settings. These clinical data are provocative but preliminary, but they support the pivotal importance of manipulating T-cell costimulation for the treatment of ICI-myocarditis and the need for prospective interventional trials with abatacept for ICI-myocarditis, where both cardiovascular endpoints as well as cancer endpoints would be assessed.

Chapter III will focus on further dissecting the mechanism of ICI-myocarditis, using the murine model introduced in this chapter. In particular, chapter III will focus on the role of CD8+ T cells, the TCR repertoires, and antigen discovery.

CHAPTER III

Cytotoxic T cells specific for alpha-myosin drive immunotherapy related myocarditis[2]

Abstract

Immune-related adverse events, particularly severe toxicities such as myocarditis, are major
challenges to immune checkpoint inhibitor (ICI) utility in anti-cancer therapy (D. Y. Wang et al.,
2018). The pathogenesis of ICI-myocarditis is poorly understood. *Pdcd1-/-Ctla4+/-* mice
recapitulate clinicopathologic features of ICI-myocarditis, including myocardial T cell infiltration
(Chapter II; Wei et al., 2020). Single cell RNA/T cell receptor (TCR) sequencing on the cardiac
immune infiltrate of *Pdcd1-/-Ctla4+/-* mice identified activated, clonal CD8+ T cells as the
dominant cell population. Treatment with anti-CD8, but not anti-CD4, depleting antibodies
rescued survival of *Pdcd1-/-Ctla4+/-* mice. Adoptive transfer of immune cells from mice with
myocarditis induced fatal myocarditis in recipients which required CD8+ T cells. Alpha-myosin, a
cardiac specific protein not expressed in the thymus (Gabrielsen et al., 2019; Lv et al., 2011),
was identified as the cognate antigen source for three MHC-I restricted TCRs derived from mice
with fulminant myocarditis. Peripheral blood T cells from two patients with ICI-myocarditis were
expanded by alpha-myosin peptides, and these alpha-myosin expanded T cells shared TCR
clonotypes with diseased heart and skeletal muscles, indicating that alpha-myosin may be a
clinically important autoantigen in ICI-myocarditis. These studies underscore the critical role for
cytotoxic CD8+ T cells, are the first to identify a candidate autoantigen in ICI-myocarditis and
yield new insights into ICI toxicity pathogenesis.

Introduction

Immune checkpoint inhibitors (ICIs) have drastically altered the treatment landscape and prognosis for many cancers. However, not all patients respond to treatment and many patients experience immune-related adverse events (irAEs), especially when ICIs are used in combination. With increasing use of ICIs, preventing, diagnosing, and treating irAEs are urgent clinical challenges. Currently, clinically actionable biomarkers of response and toxicity are limited. Furthermore, the mechanistic basis of irAEs is poorly defined.

Myocarditis is an uncommon irAE, affecting < 1% of ICI-treated patients, but has a mortality rate of nearly 50% (Johnson et al., 2016; D. Y. Wang et al., 2018). Combination ICI therapy (with anti-PD-1 and anti-CTLA4) is the most well-established risk factor for ICI-myocarditis (Hu et al., 2019; J. Moslehi et al., 2021; J. E. Salem et al., 2018; Zamami et al., 2019). ICI-myocarditis is pathologically characterized by predominance of T lymphocytes and macrophages in the heart and often co-occurs with myositis, with early studies suggesting common clonotypes of T lymphocytes in both tissues (Johnson et al., 2016). These data suggest the possibility of shared target antigens driving T lymphocyte expansion and activation, which would be critical for pathogenesis; however, experimental data have been lacking.

Generally, mice treated with ICIs do not replicate the full spectrum of irAEs seen in patients, limiting research on mechanisms of toxicity. In chapter II, we described a mouse model of ICI-myocarditis in which C57BL6/J mice with homozygous knockout of *Pdcd1* and heterozygous deletion of *Ctla4* die prematurely and specifically due to myocarditis, recapitulating clinical and pathological features of ICI-myocarditis. Severe inflammation is specific to the heart in these mice. By flow cytometry, the myocardial immune infiltrate is primarily composed of CD8+ T cells, similar to patients with ICI-myocarditis. Furthermore, treatment with abatacept, a CTLA-4 fusion protein, attenuates myocarditis and increases survival in the mice, consistent with early clinical data from patients with ICI-myocarditis treated

with abatacept (J.-E. Salem et al., 2019; Wei et al., 2020). Here we utilize this mouse model of ICI-myocarditis to characterize the immune infiltrates, establish CD8+ T cells as necessary for disease, and identify alpha-myosin as a cognate antigen for the most abundant TCRs in myocarditis. Furthermore, we extend some of these findings into human disease and find that alpha-myosin expanded TCRs are present in inflamed cardiac and skeletal muscles in patients with ICI-myocarditis.

Methods

Mice. Pdcd1-/-Ctla4+/- mice were maintained as previously described in chapter II (Wei et al., 2020). Female mice were used in these studies due to their higher incidence of myocarditis. *Rag1-/-* mice were purchased from The Jackson Laboratory (#002216; Mombaerts et al., 1992). For the generation of survival curves, events were defined as either death (i.e., mice found dead) or identification of mice requiring euthanasia (e.g., due to lethargy, moribund, dyspnea, weight loss). All mice were housed at Vanderbilt University Medical Center vivarium, an Association for Assessment and Accreditation of Laboratory Animal Care International (AAALAC)–accredited, specific pathogen-free (SPF) animal facility. All experiments were performed in accordance with Vanderbilt University Medical Center Institutional Animal Care and Use Committee (IACUC) guidelines.

Preparation of cardiac dissociates for single-cell RNA/TCR sequencing. Single-cell suspensions were obtained from murine hearts by mincing followed by enzymatic digestion with 125 U/mL DNase I (Worthington; cat no. LS002138) and 250 U/mL Collagenase 3 (Worthington; cat no. LS004182). Dissociated hearts were filtered through a 30µm filter. Red blood cells were lysed using ACK lysing buffer (KD Medical/MediaTech; cat no. NC0274127). Single-cell suspensions were either used fresh or cryopreserved in 10% DMSO 90% FBS. Prior to sorting, cells were stained with Alex Flour 488 anti-mouse CD45 (BioLegend; clone 30-F11; cat no. 103122) for 20 minutes at 4°C. Following staining and washing with PBS, cells were resuspended in PBS with

DAPI. Live CD45+ immune cells were sorted by fluorescence-activated cell sorting on AF488-positive DAPI-negative events. The wildtype control sample consisted of pooled, without hashing, cardiac immune infiltrates from six female animals, in order to obtain sufficient cells as the healthy heart has a low frequency of cardiac immune cells. The myocarditis sample consisted of four inflamed hearts from female *Pdcd1-/-Ctla4+/-* mice. Inflammation was confirmed by flow cytometry for CD45. Only mice with CD45+ cells comprising greater than ten percent of the total single cells were included. Mice ranged from three to six weeks in age. One inflamed heart was run as an individual sample on the 10X Genomics chromium platform. The additional three inflamed hearts were hashed together using Total Seq C reagents according to the manufacturer's instructions (BioLegend: TotalSeq™-C0301 cat# 155861, TotalSeq™-C0302 cat# 155863, TotalSeq™-C0303 cat# 155865).

Single-cell RNA/TCR sequencing. Each sample (targeting 5,000 – 15,000 cells/sample) was processed for single cell 5' RNA and TCR sequencing utilizing the 10X Chromium system. Libraries were prepared following the manufacturer's protocol. The libraries were sequenced using the NovaSeq 6000 with 150 bp paired end reads. RTA (version 2.4.11; Illumina) was used for base calling and analysis was completed using 10X Genomics Cell Ranger software. Data were analyzed in R using the filtered h5 gene matrices in the Seurat package (Butler et al., 2018; Satija et al., 2015; Stuart et al., 2019). Briefly, samples were subset to include cells with greater than 200 but less than 3000 unique transcripts to exclude likely non-cellular RNA reads and doublets. Cells with greater than 15% of reads coming from mitochondrial transcripts were also excluded as likely dying cells. For murine hearts, hash tag oligos were deconvoluted using HTODemux with positive quantile set at 0.85. Samples were downsized so that equivalent numbers of cells originating from healthy wild type or myocarditis *Pdcd1-/-Ctla4+/-* cardiac infiltrating immune cells were included (2509 cells per genotype of origin). Ten clusters were identified using a resolution of 0.4. UMAP was used for dimensionality reduction with 15 nearest

neighbors and minimum distance of 0.5. Clonal is defined as more than two cells with the same TCR clonotype (defined by unique combinations of CDR3 regions).

T cell receptor sequencing. TCR sequencing and clonality quantification was assessed in formalin-fixed paraffin embedded (FFPE) or snap frozen samples of murine hearts or spleens. All human samples were derived from FFPE or isolated PBMC. For FFPE, RNA was extracted from 10µm sections using the Promega Maxwell 16 FFPE RNA kits and the manufacturer's protocol. TCRs were sequenced using the TCR Immunoverse all chain assay following the manufacturer's protocol (Invitae/ArcherDX). Sequencing results were evaluated using the Archer Immunoverse analyzer. CDR3 sequences and frequency tables were extracted from the manufacturers' analysis platform and imported into R for analysis using the Immunarch package (https://immunarch.com) in R.

Antibody-mediated depletion. Female *Pdcd1-/-Ctla4+/-* mice were randomly assigned to control, anti-CD8a, or anti-CD4 injections at 21 days of age. Mice were injected intraperitoneally three times a week with 200µg of anti-CD4 (BioXCell, Cat# BE0003-1, clone GK1.5) or anti-CD8 (BioXCell, Cat# BE0061, clone 2.43) depleting antibodies or vehicle, all in a maximum volume of 100µL. Treatment lasted until 90 days of age. Peripheral blood was sampled via tail prick for assessment of depletion efficiency at week 3.

Adoptive transfer. Splenocytes were isolated from *Pdcd1-/-Ctla4+/-* mice with myocarditis by manual dissociation, filtering, and red blood cell lysis. Myocarditis of the donor mice was confirmed by either H&E or dissociation of the heart and flow cytometry for CD45+ immune cells. A portion of each spleen underwent CD8 depletion using magnetic bead isolation (Miltenyi CD8 (TIL) MicroBeads, Mouse, Cat# 130-116-478). One million whole or CD8 depleted splenocytes were injected into each *Rag1-/-* recipient mouse in 100µL PBS via tail vein injection. Mice were monitored for death or signs of distress. At death or euthanasia, hearts, spleens, livers, lungs, and kidneys were stained by H&E and evaluated microscopically.

Histology and pathology. Formalin-fixed tissues were processed routinely into paraffin blocks, sectioned at 5μm, and stained with H&E by standard protocols in Vanderbilt University Medical Center's Translational Pathology Shared Resource (TPSR) core laboratory. To further characterize the mononuclear cardiac infiltrates detected by light microscopy, a panel of IHC markers was employed. IHC staining was performed in the TPSR using standard, validated protocols for chromogenic IHC. All steps besides dehydration, clearing, and coverslipping were performed on the Leica Bond-Max IHC autostainer (Leica Biosystems Inc.). Slides were deparaffinized. Antigen retrieval was performed using EDTA (CD markers) or proteinase K (F4/80). Slides were incubated with primary antibodies as indicated below. Secondary antibody labeling was performed for all markers except CD3 by incubating in rabbit anti-rat antibody (BA-4001, Vector Laboratories, Inc.) for 15 minutes at a 1:650 dilution. Immunolabeling by rabbit antibody was visualized using the Bond polymer refine detection system (#DS9800, Leica Biosystems, Inc.). Slides were then dehydrated, cleared, and coverslipped. For primary antibodies, anti-CD3 (Abcam, Ab16669) was used at 1:250 dilution, anti-CD4 (eBioscience, 14–9766–82) was used at 1:1,000 dilution, anti-CD8 (eBioscience, 14–0808–82) was used at 1:1,000 dilution, and anti-F4/80 (Novus Biologicals, NB600–404) was used at 1:900 dilution.

Flow cytometry. Samples were run on an Attune NxT Acoustic Focusing Cytometer (Life Technologies). Analysis was performed in FlowJo. Gating was first done on forward scatter and side scatter to exclude debris. Doublets were excluded by gating on FSC area versus FSC height. DAPI was used to exclude dead cells from analyses. Antibodies used: CD45-PerCP/Cy5.5 (BioLegend, cat# 103132, clone 30-F11), CD3-AF488 (BioLegend, cat# 100210, clone 17A2), CD4-APC (BioLegend, cat# 100412, clone GK1.5), CD8a-PE/Cy7 (BioLegend, cat# 100722, clone 53-6.7), Thy1.1 (BioLegend, cat# 202506, Clone OX-7) and TCR-beta chain (BioLegend, cat# 109208, Clone H57-597).

TCR sequences and cloning. TCR sequences were generated from CDR3 regions, V genes and

J genes using Stitchr (Heather et al., 2021). Alpha genes and beta genes were separated using a T2A sequence. Restriction digest sites were added to either end. Full TCR gene blocks were synthesized as custom orders from Genewiz. Full TCR block sequences can be found in supplemental material in Appendix III. TCR sequences were cloned into MSCV-IRES-Thy1.1 DEST vector. MSCV-IRES-Thy1.1 DEST was a gift from Dr. Anjana Rao (Addgene plasmid # 17442; http://n2t.net/addgene:17442 ; RRID:Addgene_17442)(Wu et al., 2006). Retrovirus was made using the platA retroviral packaging cell line (Cell BioLabs RV-102). Jurkat-TCR-ko-CD8+-NFAT-GFP reporter cells were a gift from Dr. Peter Steinberger. Reporter cells were retrovirally transduced with TCRs of interest. TCR expression was confirmed via flow cytometry for Thy1.1 and TCR-beta chain. Retrovirally transduced cells were sorted on the WOLF cell sorter (NanoCellect) for Thy1.1-AF488. Cells were confirmed to be >90% Thy1.1 positive post-sort prior to use in downstream assays.

Antigen discovery. Jurkat-NFAT-GFP cell lines with reconstructed TCRs were used for antigen screening. Syngeneic (derived from C57BL6 mice) bone marrow derived dendritic cells (BMDCs) were used as APCs. BMDCs were generated by flushing femurs and tibias from mice with PBS, filtering the cells though a 70μM filter, lysing RBCs, and plating in RMPI + 10% FBS + 1% HEPES + 20ng/mL GM-CSF (ProSpec Cat# CYT-222). BMDCs were polarized in GM-CSF containing media for 9 days (replacing the media at days 3 and 6) prior to harvesting the adherent fraction via mechanical dissociation using a cell scrapper and cryopreservation for future experiments. For antigen discovery, BMDCs were thawed into GM-CSF containing media in flat bottom plates the day before adding TCR cell lines and peptides. Cells were plated at a ratio of 1 TCR cell to 3 BMDCs. The alpha myosin peptide library was generated as 20aa peptides with 5aa overlaps from GenScript. Due to insolubility in aqueous solution, two 20aa peptides were replaced by three 10aa peptides each. Peptides were added at a concentration of 10μg/mL and co-cultures were incubated overnight. TCR cell lines were stained with DAPI to

41

assess viability and analyzed via flow cytometry for NFAT-GFP reporter activity.

MHC blocking. Jurkat TCR cell lines were co-cultured with EL-4 cells as APCs with or without 10µg/mL cognate peptide overnight. EL-4 cells were a gift from Dr. Simon Mallal. Blocking antibodies (anti-Db clone 28-14-8S or anti-Kb clone B8-24-3) were added to cells at a concentration of 10µg/mL for 1 hour prior to adding peptides. Blocking antibodies were generously provided by Dr. John Sidney. TCR cell lines were stained with Thy1.1-APC/Cy7 (BioLegend, cat# 202506, Clone OX-7) to differentiate from EL-4s and with DAPI to assess viability and analyzed via flow cytometry for NFAT-GFP reporter activity.

Patients. Healthy donors provided informed consent under an institutionally approved protocol (IRB# 030062). Myocarditis patients and families provided informed consent for research use of biospecimens and clinical data (IRB# 191213).

Generation of LCLs from PBMC. EBV-transformed lymphoblastoid B cell lines were generated from cryopreserved donor PBMCs by infection with EBV virus stock (Granato et al., 2014; Oh et al., 2003). Approximately, 1-3 × 10^6 PBMCs in RPMI-1640 media supplemented with non-heat inactivated 20% fetal bovine serum (FBS), 1 µg/mL cyclosporin A (CSA; Sigma-Aldrich C1832), and 2.5 µg/mL CpG (Invitrogen ODN2006) were infected with filtered EBV stock and cultured for 2-3 weeks, until clusters of cells were visible by light microscopy.

PBMC expansion. PBMCs were isolated from EDTA collection tubes and processed using a Ficoll gradient. Antigen-specific PBMC expansion was adapted from previously described protocols (Eberhardt et al., 2021; Wölfl & Greenberg, 2014). Fresh or cryopreserved PBMCs were stimulated with 130 pooled alpha-myosin peptides at a final concentration of 400ng/mL of each peptide or a pool of control CMV, EBV, and flu (CEF) peptides (AnaSpec, AS-61036-003). PBMCs were cultured in CTS OpTmizer medium (CTS OpTmizer T Cell Expansion SFM with CTS supplement A1048501, substituted with 2mM L-glutamine, and 2% human serum, Sigma-Aldrich, H3667) with cytokine supplementation (25ng/mL each of rhIL-2, rhIL-7 and rhIL-15,

Peprotech). For myocarditis patients 1 and 2, expansion cultures were also supplemented with autologous LCLs to serve as antigen presenting cells at a ratio of 1 APC per 10 PBMC. For healthy donors, expansion was done directly from fresh, not cryopreserved, blood. Peptides were only added on the first day of culture. On day 3, additional media with cytokines was added. On day 7, cells were transferred to a new culture dish with fresh media with cytokines. Cells were analyzed or cryopreserved on day 14.

Single cell sequencing of exPBMC. Expanded PBMCs (exPBMC) from patient 1 were prepared for single cell sequencing as follows. exPBMC were incubated with Human TruStain FcX™ (Fc Receptor Blocking Solution; BioLegend cat# 422302) for 5 minutes on ice, then washed and incubated with human anti-CD3-AF488 (BioLegend, cat# 300319, clone HIT3a) for 30 minutes on ice, and then washed and resuspended to a concentration of $5x10^5$ cells/mL. SYTOX AADvanced™ Ready Flow™ Reagent (Invitrogen, cat# R37173) was used following the manufacturer's instructions to exclude dead cells. CD3+ live cells were sorted on the WOLF cell sorter (Nanocellect). Cells were sequenced and data were analyzed as described above. Data were analyzed in R using the filtered h5 gene matrices in the Seurat package(Butler et al., 2018; Satija et al., 2015; Stuart et al., 2019). Briefly, samples were subset to include cells with greater than 200 but less than 4000 unique transcripts to exclude likely non-cellular RNA reads and doublets. Cells with greater than 15% of reads coming from mitochondrial transcripts were also excluded as likely dying cells. Clonal is defined as more than two cells with the same TCR clonotype (defined by unique combinations of CDR3 regions). For exPBMC, 5,816 cells with TCR reads were analyzed. To identify TCRs overlapping with the cardiac repertoire, beta CDR3 sequences were used.

Statistical analysis. All statistical analyses were performed in R. All single-cell statistical analyses were calculated in R using the Seurat package (Butler et al., 2018; Satija et al., 2015; Stuart et al., 2019). Visualization and graph generation was performed in R. Shannon diversity

was calculated using the R package vegan (Oksanen et al., 2020). The R package immunarch was used for evaluating TCR repertoires (Nazarov et al., 2020). P-value cut-offs displayed on plots correspond to "ns" equals $p > 0.05$, * equals $0.01 < p < 0.05$, ** equals $0.001 < p < 0.01$, *** equals $0.0001 < p < 0.001$, **** equals $p < 0.0001$.

Results

Clonal CD8+ T cells are abundant in ICI-myocarditis

As described in Chapter II, fulminant myocarditis affects 50% of *Pdcd1-/-Ctla4+/-* mice and is characterized by histologic destruction of the myocardial architecture (**Figure 3.1A, B**; Wei et al., 2020). We used single cell RNA and TCR sequencing to characterize sorted CD45+ infiltrating immune cells from six healthy wild type mouse hearts and four hearts from *Pdcd1-/-Ctla4+/-* mice affected by myocarditis. Dimensionality reduction with uniform manifold approximation and projection (UMAP) and cell type annotation assisted by SingleR reveals distinct clustering by genotype (**Figure 3.1C**; **Supplementary Fig. S3.1A**)(Aran et al., 2019). Activated T lymphocytes and myeloid cells comprise the majority of the immune cells in myocarditis. The largest difference is seen in the activated T cell cluster, which makes up 34% of the myocarditis immune cells, and only 2% of the control immune cells. Markers of activation such as *Ccl5, Ccl4, Tigit, Nkg7,* and *Gzmb* are upregulated in the T cell clusters in myocarditis compared to control T cell clusters (**Figure 3.1D**). Conversely, markers of naïve status such as *Ccr7, Lef1* and *Sell* are upregulated in control T cells. Activation markers are also upregulated in other clusters, including myeloid cell subsets, in the myocarditis samples (**Supplementary Fig. S3.1B**). *Aw112010*, a long noncoding RNA essential for the orchestration of mucosal immunity during infections and in colitis, is strongly upregulated in several clusters in the myocarditis samples (Jackson et al., 2018; Yang et al., 2020). In contrast, B lymphocytes make up most of the immune cells in the control heart, consistent with previous studies (Adamo et al., 2020;

Bönner et al., 2012; Martini et al., 2019).
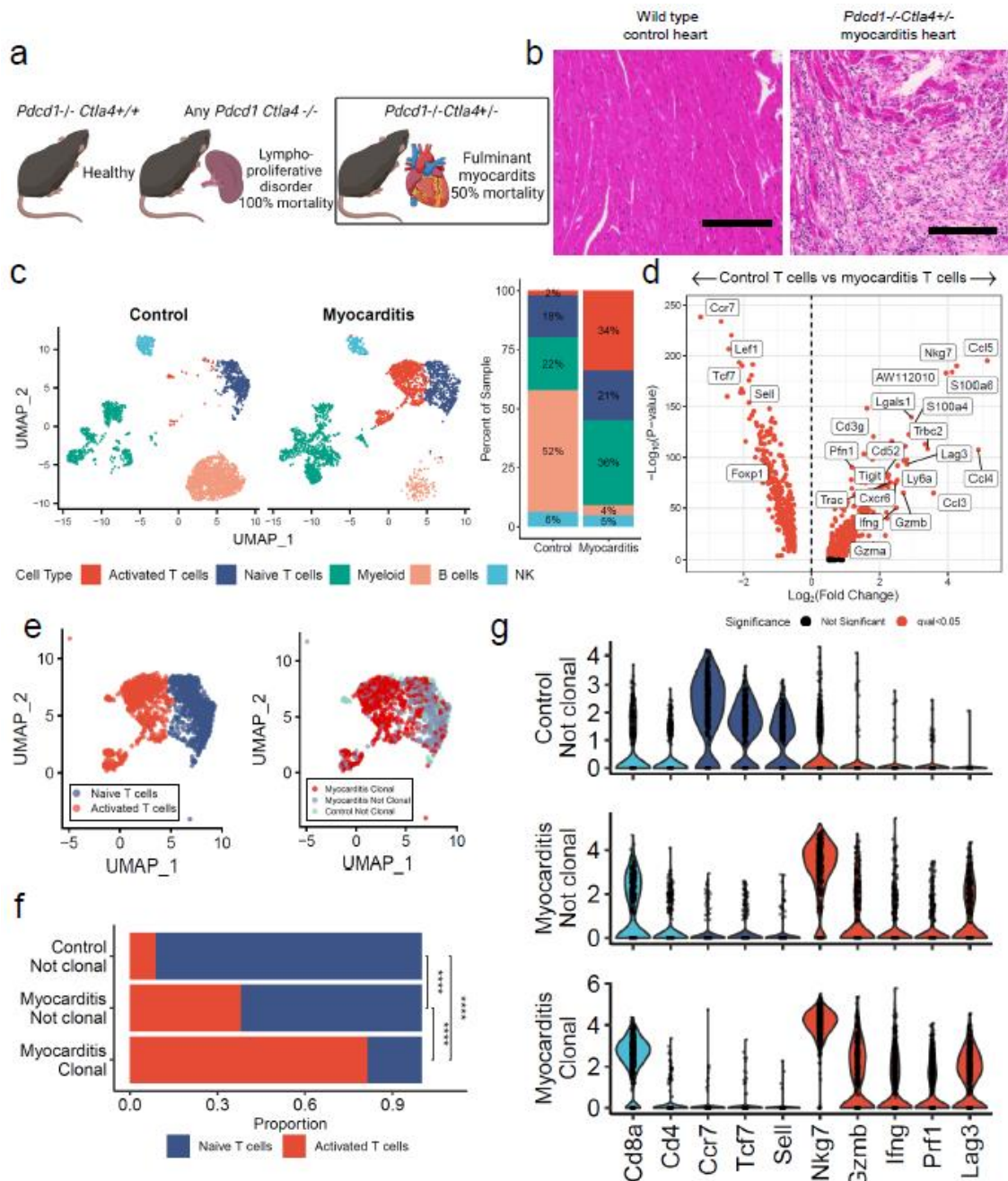
Figure 3.1 Single Cell RNA/TCR sequencing reveals abundant highly activated, clonal CD8+ T cells in ICI-myocarditis. a) Phenotypic summary of mice with different combinations of *Pdcd1* and *Ctla4* genetic loss. *Pdcd1-/-Ctla4+/+* mice do not have an overt phenotype. Mice with complete loss of *Ctla4* have a fatal lymphoproliferative disorder, regardless of *Pdcd1* genotype. *Pdcd1-/-Ctla4+/-* mice develop fulminant myocarditis and are the focus of this study. b) H&E of cardiac tissue from a healthy wild type mouse and a *Pdcd1-/-Ctla4+/-* mouse with myocarditis. Scale bar represents 200µm. c) Dimensionality reduction with UMAP of single cell RNA sequencing on sorted CD45+ immune cells from control wild type mouse hearts (n=6) compared to hearts (n=4) of *Pdcd1-/-Ctla4+/-* mice with myocarditis (n= 2509 cells per genotype of origin).

Cell type annotations were assisted by singleR and are quantified on the right. d) Differential gene expression between control and myocarditis T cells (both activated and naïve T cell clusters are included). Higher expression in myocarditis T cells is indicated by positive fold change. Red indicates FDR-corrected p-value (q-value) <0.05. Black indicates not significant. e) UMAP is subset on only T cells with TCR reads. Clonal is defined as >2 cells with the same TCR clonotype. No clonal cells are seen in the control sample (n=1495 cells). f) The proportion of cells in the naïve or activated T cell clusters are shown stratified by sample and clonality. P-values represent multiple fisher's exact tests. g) Violin plots shown expression of key genes by clonality and sample. Identity genes are shown in light blue. Genes associated with naïve T cells are shown in dark blue. Genes associated with T cell activation are shown in red.

Given the high infiltration of activated T cells, we next sought to assess the clonality of TCRs in the myocarditis samples using both bulk and single cell TCR sequencing. Cardiac tissue from affected *Pdcd1-/-Ctla4+/-* mice had lower Shannon diversity compared to splenic tissue (whether derived from healthy wild type mice or mice with myocarditis), indicating a higher degree of clonal TCRs (**Supplementary Fig. S3.1C**). In single cell TCR data, clonal was defined as more than two cells with the same TCR clonotype (same TCR alpha and beta CDR3 regions). No clonal cells were identified by single cell TCR sequencing of the healthy cardiac immune infiltrate. In contrast, 63% of cells with TCR reads in the myocarditis sample had clonal TCRs and clonal cells were identified in all four myocarditis samples (**Supplementary Fig. S3.1D**). Dimensionality reduction of only T cells with TCR reads showed that clonal cells overlap with the activated T cell cluster whereas not clonal cells overlap with naïve T cells (**Figure 3.1E**). A significantly higher proportion of the clonal cells in myocarditis are activated T cells relative to not clonal cells in either control or myocarditis samples (**Figure 3.1F**). Comparing gene expression by clonality shows that not clonal cells from control samples express *Cd8a*, *Cd4*, and markers associated with naïve status, but not genes associated with activation. In contrast, clonal cells from myocarditis samples express *Cd8a* and cytotoxicity genes such as *Nkg7* and *Gzmb,* but do not express *Cd4* or markers of naïve status (**Figure 3.1G**). These data show that there is a large population of highly activated, clonally expanded CD8+ T cells in murine ICI-myocarditis.

CD8+ T cells are necessary for myocarditis

Using anti-CD8 and anti-CD4 depleting antibodies we tested whether depletion of these cell subsets would attenuate myocarditis and affect survival of *Pdcd1-/-Ctla4+/-* mice. Depletion of target cells was confirmed by flow cytometry on peripheral blood (**Supplementary Fig. S3.2A**). Depletion of CD8+ cells, but not CD4+ cells, significantly rescued survival in these mice (**Figure 3.2A**). Conversely, we tested whether transfer of immune cells could recapitulate disease. Adoptive transfer of whole splenocytes, but not splenocytes from which CD8+ cells were depleted, from *Pdcd1-/-Ctla4+/-* mice with myocarditis to *Rag1-/-* recipients was sufficient to induce fatal myocarditis (**Figure 3.2B**). CD8 depletion was confirmed by flow cytometry on transferred splenocytes (**Supplementary Fig. S3.2B**). Myocarditis was confirmed histologically on necropsy tissue (**Figure 3.2C**). The single fatality in the CD8 depleted arm was due to a bowel obstruction and there was no evidence of myocarditis histologically. Immunohistochemistry for CD3, CD4, CD8 and F4/80 showed abundant cardiac infiltration of CD3+ and CD8+ cells in the whole splenocyte recipients but not the CD8 depleted recipients. Some CD4+ cells and limited F4/80+ cells were also found in the hearts of whole splenocyte recipients (**Figure 3.2D**; **Supplementary Fig. S3.3A**). We performed TCR sequencing on the cardiac tissue of one donor mouse (Donor) and four whole splenocyte recipients (Rec1, Rec2, Rec3, and Rec4; Fig. 2e). High numbers (>2000) of TCR reads were seen in all sequenced hearts, indicating significant T cell infiltration, as expected from histology (**Supplementary Fig. S3.3B**). In all four recipient mice the single most clonal TCR beta chain occupied greater than 65% of the total cardiac TCR repertoire, indicating massive expansion of a single TCR clonotype. The most clonal TCR beta chain (CDR3: CASSLRRGEQYF) in the donor heart (which comprised 37% of the donor cardiac repertoire) was expanded in three of four recipients (Rec1, 3, 4). Interestingly, in one recipient mouse (Rec2), a low frequency TCR from the donor

was expanded and occupied the majority of the TCR repertoire (CDR3:

CASSLGGTVQDTQYF). This high degree of expansion from donor to recipient cardiac tissue

suggests a single TCR clonotype may drive myocarditis in the recipient animals. Together,

these results strongly indicated that CD8+ T lymphocytes are necessary for the development of
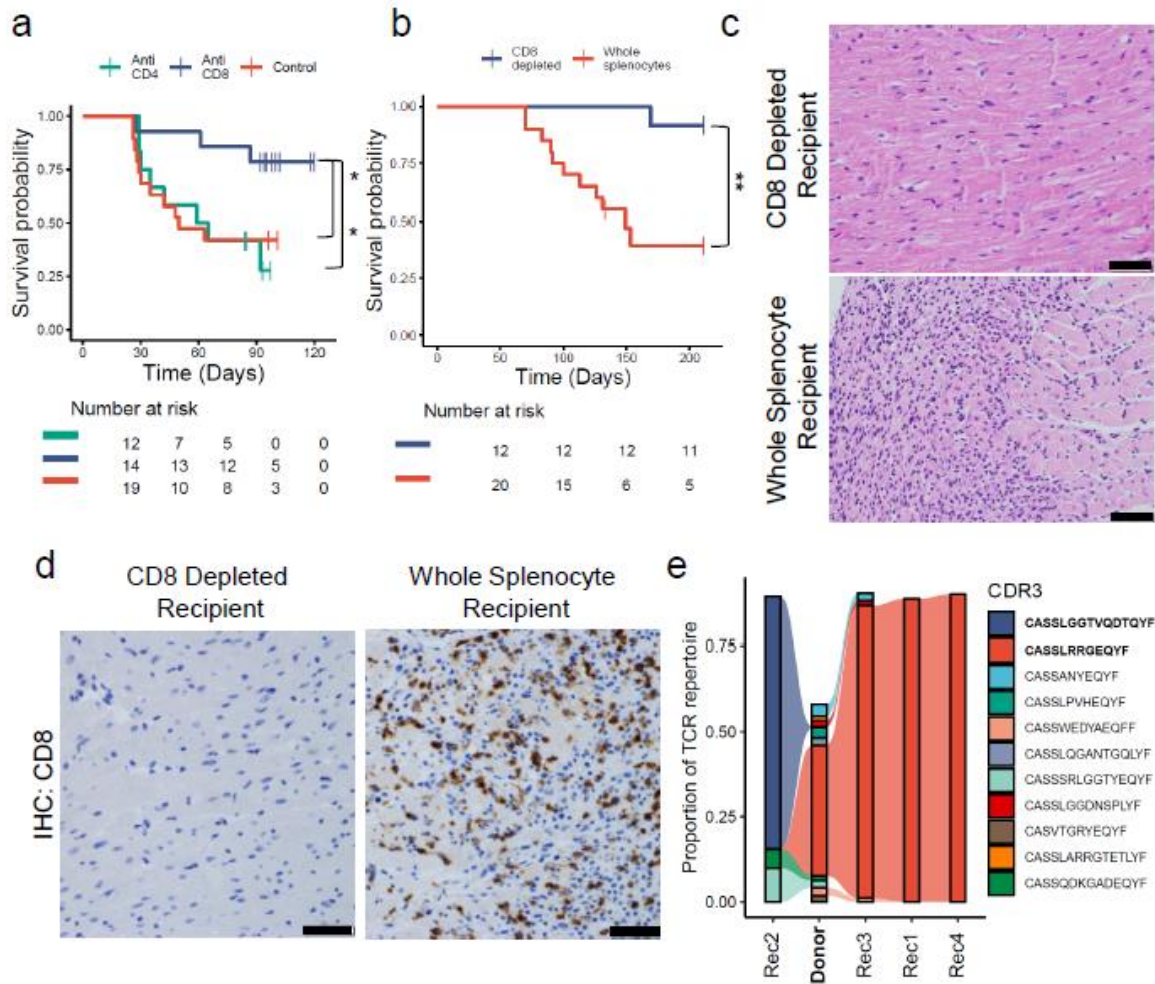
myocarditis.

Figure 3.2. CD8+ T cells are necessary for myocarditis. a) *Pdcd1-/-Ctla4+/-* mice were treated with anti-CD4, anti-CD8 or control antibodies. P-values represent cox proportional hazard tests. Risk tables show size of groups. b) Whole splenocytes or splenocytes from which CD8 cells were depleted from *Pdcd1-/-Ctla4+/-* mice with myocarditis were transferred to *Rag1-/-* recipient mice. P-value represents cox proportional hazard test. Risk tables show size of groups. c) Representative H&E from CD8 depleted splenocyte recipients compared to whole splenocyte recipients. Only cardiac sections are shown. Scale bars show 50µm. d)

Representative IHC for CD8 on cardiac sections from CD8 depleted splenocyte recipients compared to whole splenocyte recipients. Scale bars show 50µm. e) TCR beta chain sequencing on cardiac tissue from a donor *Pdcd1-/-Ctla4+/-* mouse (Donor, in bold) and *Rag1-/-* whole splenocyte recipients (Rec1-4). The top ten most abundant TCRs from the donor plus the most abundant TCR from Rec2 are shown. Flow between samples indicates shared TCRs. Bolded CDR3s indicate most clonal TCRs.

Myocarditis-derived TCRs are specific for alpha-myosin

Next, we aimed to identify the cognate antigen for clonal murine TCRs. TCR-A was derived from the single cell RNA/TCR sequencing and was associated with the activated T cell cluster (**Figure 3.3A**). TCRs B and C were derived from the adoptive transfer of whole splenocytes. TCR-B was the most abundant TCR in the heart of the donor and three recipients (Beta CDR3: CASSLRRGEQYF). TCR-C was the most abundant TCR in the heart of recipient 2 (Beta CDR3: CASSLGGTVQDTQYF; **Figure 3.2E**). CDR3 amino acid sequences, V genes, and J genes are shown in Table 3.1. These TCRs were reconstructed using Stitchr, cloned and retrovirally transduced into Jurkat nuclear factor of activated T cells (NFAT)-GFP reporter cells (Heather et al., 2021; Jutz et al., 2016; Rosskopf et al., 2018). Syngeneic bone marrow derived dendritic cells were used as antigen presenting cells (APCs).

Table 3.1. Summary of TCR CDR3, V and J genes for murine TCRs used in antigen discovery experiments.

TCR ID	TCR Source	Beta CDR3	TRBV	TRBJ	Alpha CDR3	TRAV	TRAJ	Antigen
A	Single Cell Sequencing	CSAAWGGSAETLYF	TRBV1	TRBJ2-3	CAVSDRGSALGRLHF	TRAV7-3*04	TRAJ18	MYH6$_{191-198}$ (VIQYFASI)
B	Adoptive transfer (Donor, Rec1,3,4)	CASSLRRGEQYF	TRBV15	TRBJ2-7	CALERASGSWQLIF	TRAV13-1	TRAJ22	MYH6$_{191-198}$ (VIQYFASI)
C	Adoptive Transfer (Rec2)	CASSLGGTVQDTQYF	TRBV12-2	TRBJ2-5	CALGDRNNAGAKLTF	TRAV6D-6	TRAJ39	MYH6$_{418-425}$ (VQQVYYSI)

We used a candidate autoantigen approach for TCR screening. Analysis of published RNA sequencing data on thymic APCs (including thymic epithelial cells) showed four cardiac enriched genes (genes where expression in the heart was significantly enriched relative to other tissues) with no detectable expression in the thymus (**Figure 3.3B**; Gabrielsen et al., 2019). Lack of thymic expression would be predicted to enable self-reactive T cells to escape negative selection, an important mechanism of tolerance. Of these four genes, *MYH6* (alpha-myosin) has been confirmed by other groups to not be expressed in the thymus in mice or humans and has been shown to be an MHC-II restricted autoantigen in mouse models (Gil-Cruz et al., 2019; Lv et al., 2011; Massilamany et al., 2011). We used a library of 130 overlapping peptides, covering all of alpha-myosin protein. All three TCR cell lines had NFAT activity in response to alpha-myosin peptides. TCRs A and B activated NFAT reporters in response to the same alpha-myosin peptide ($MYH6_{181-200}$), whereas TCR-C had NFAT activity against a distinct alpha-myosin peptide ($MYH6_{406-425}$; **Figure 3.3C**). From these 20 amino acid peptides, we used TepiTool to narrow down the most likely immunogenic epitopes (Paul et al., 2016). TCRs A and B recognize the epitope $MYH6_{191-198}$ (VIQYFASI). TCR-C recognizes the epitope $MYH6_{418-425}$ (VQQVYYSI; **Figure 3.3D**). VIQYFASI and VQQVYYSI both have strong predicted binding to H2-Kb using TepiTool. The tyrosine and phenylalanine residues at position five of the peptides are known to be key binding epitopes for H2-Kb (Falk et al., 1991). In line with these predictions, blocking H2-Kb, but not H2-Db, with an antibody abrogates NFAT reporter activity for all three cell lines (**Figure 3.3E**). All three clonal TCRs derived from independent murine cardiac TCR repertoires recognized alpha-myosin epitopes. Therefore, this strongly suggests that alpha-myosin is an important MHC-I restricted autoantigen in murine ICI-myocarditis.
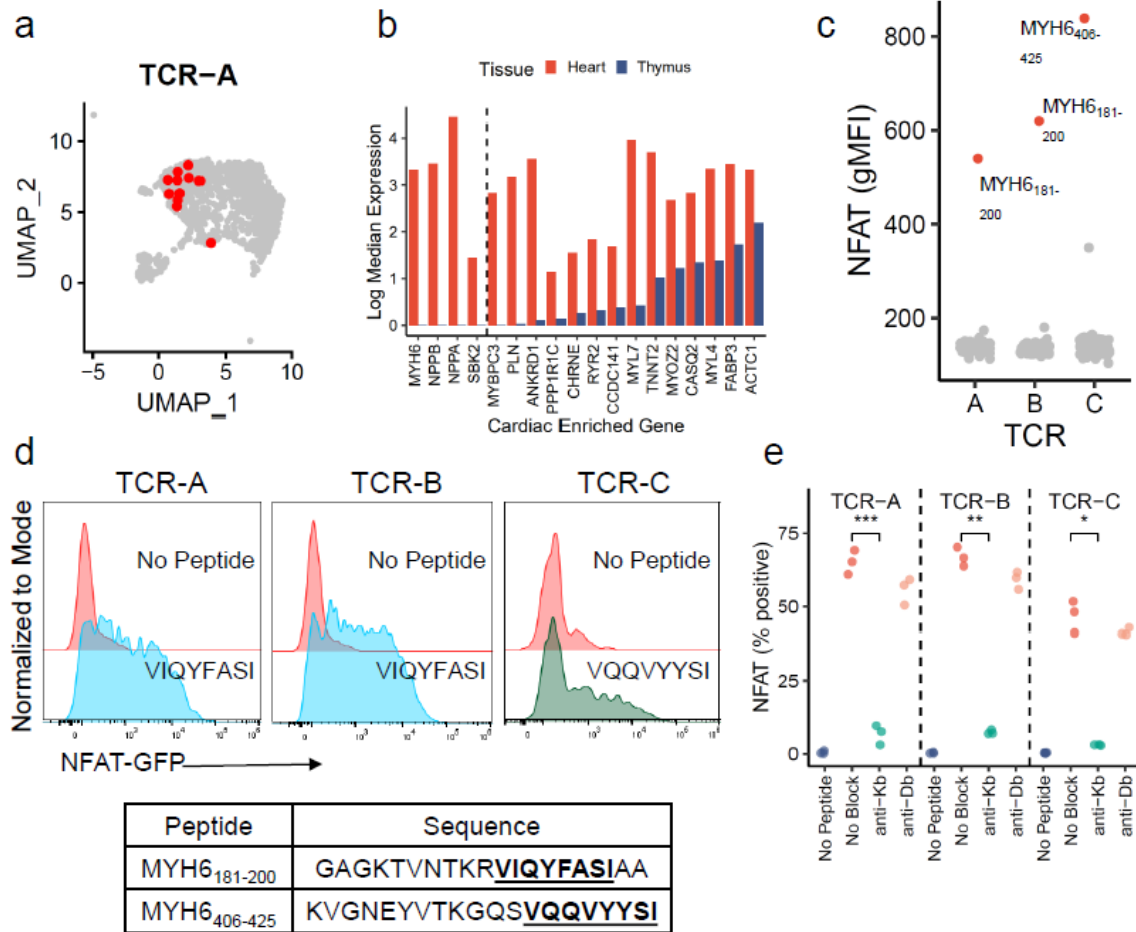
Figure 3.3. Alpha-myosin is an MHC-I restricted autoantigen in murine myocarditis. a) TCR-A, a TCR used for antigen discovery, is shown on the same UMAP plot as shown in Fig. 1e. Red cells indicate cells expressing TCR-A. b) Log median expression of 18 cardiac enriched genes in the heart (red) and thymus (blue). Genes are sorted by thymic expression. Genes to the left of the dashed line have no detectable expression in thymic APCs. c) NFAT-GFP reporter activity, measured by flow cytometry and shown as geometric mean fluorescence intensity, of three TCR cell lines stimulated independently with 130, 10-20aa alpha-myosin peptides. Top peptide hits are colored in red and labeled. d) Representative flow cytometry histograms of each TCR cell line co-cultured with BMDCs and stimulated with 10µg/mL predicted cognate peptide relative to no peptide. Peptide sequences are shown in the table. e) Each TCR cell line was co-cultured with EL-4 APCs and 10µg/mL cognate peptide (VIQYFASI for TCRs A and B; VQQVYSI for TCR C; except for no peptide controls) with or without 10µg/mL of anti-Kb or anti-Db blocking antibody. NFAT-GFP reporter activity is shown as percent of live cells. n=3 biological replicates. P-values represent t-tests.

Alpha-myosin expanded TCRs are present in fulminant myocarditis in patients

We next aimed to test the relevance of alpha-myosin as a potential autoantigen in

humans, using three healthy donors and two patients with ICI-myocarditis. ICI-myocarditis

patient information is summarized in Table 3.2. First, we tested whether it was possible to

expand alpha-myosin specific T cells from peripheral blood mononuclear cells (PBMCs).

PBMCs were stimulated with alpha-myosin peptides or control cytomegalovirus, Epstein-Barr

virus and influenza (CEF) peptides (for healthy donors only) for 14 days to generate expanded

PBMCs (exPBMC). Shannon diversity decreased significantly from pre-expansion PBMC to

alpha-myosin exPBMC for healthy donors and myocarditis patients, indicating clonal expansion

of alpha-myosin specific T cells. Interestingly, Shannon diversity did not significantly change

from baseline to CEF peptide expansion, suggesting that alpha-myosin is a strong stimulus for

clonal T cell expansion (**Figure 3.4A**). For all donors, both alpha-myosin and CEF stimulation

resulted in expansion of some individual TCR clonotypes (**Supplementary Fig. S3.4A, B**).

These data suggest that both healthy donors and ICI-myocarditis patients have alpha-myosin

specific T cells in the periphery that may be expanded.

Table 3.2. Summary of myocarditis patient information.

Patient	Age	Sex	ICI history	Primary Tumor	Disease tissue TCR sequencing
1	75	M	Ipilimumab + Nivolumab	Renal cell carcinoma	Cardiac biopsy; Autopsy: diaphragm, psoas
2	64	M	Nivolumab	Small cell lung cancer	Autopsy: RV, LV, IVS, deltoid, diaphragm
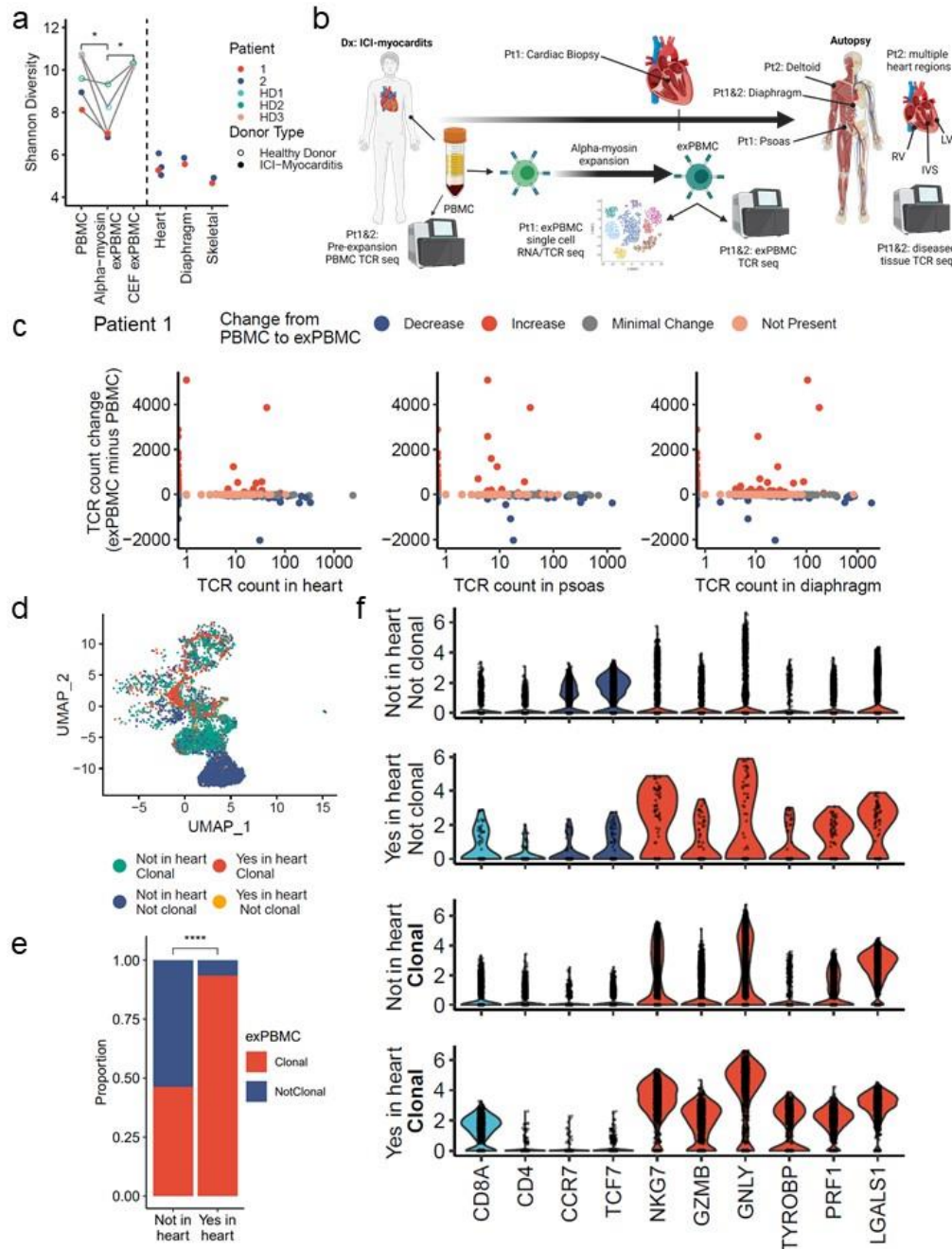
Figure 3.4. Alpha-myosin expanded TCRs are present in cardiac and skeletal muscle of patients with ICI-myocarditis. a) Shannon diversity of indicated TCR repertoires. Healthy donors are shown in open circles, while myocarditis donors are shown in closed circles. Lines connect the pre-expansion PBMC to the same donor's expanded PBMC (exPBMC). Dashed line separates PBMC and exPBMC from diseased heart and skeletal muscles in myocarditis patients. Skeletal refers to psoas muscle for patient 1 and deltoid muscle for patient 2. P-values represent t-tests. b) Schematic describing patient tissues and process of expanding PBMCs. RV= right ventricle. LV = left ventricle. IVS = interventricular septum. c) Change in TCR counts from PBMC to alpha-myosin expanded PBMC (exPBMC) plotted by abundance in indicated tissues for patient 1. Minimal change is less than a 50 read count change. Not present means

not found in either PBMC or exPBMC, but present in indicated tissue. d) Dimensionality reduction with UMAP on single cell RNA/TCR sequencing of CD3+ sorted patient 1 exPBMC. Only cells with TCR expression are shown. Groups are divided by whether the TCR expressed by that cell is also found in the patient's heart and whether that TCR is clonal (expressed by >2 cells in exPBMC single cell TCR sequencing). d) Proportion of single cell sequenced exPBMCs that are clonal, stratified by whether that TCR is also found in the heart. P<0.0001 by Fisher's Exact test. f) Violin plots of key gene expression by presence or absence in cardiac TCR repertoire and clonality in exPBMC. Identity genes are shown in light blue. Genes associated with naïve T cells are shown in dark blue. Genes associated with T cell activation are shown in red.

To assess whether alpha-myosin expanded TCR clones might be involved in cardiac and skeletal muscle toxicity, we compared TCR repertoires in the heart and inflamed muscle to those overrepresented in alpha-myosin exPBMC relative to unexpanded PBMC. We performed bulk TCR sequencing on formalin-fixed paraffin embedded tissues from endomyocardial biopsy (patient 1 only) and autopsy material (patients 1 and 2). Tissue samples from each myocarditis patient are summarized in **Figure 3.4B**. High numbers of total TCR reads (>1500) were seen in each sequenced sample, consistent with high T cell infiltration (**Supplementary Fig. S3.4C**). Shannon diversity was low in heart, diaphragm, and other skeletal muscle samples, indicating clonal TCR repertoires at the sites of toxicity (**Figure 3.4A**). Alpha-myosin expanded TCRs (shown in red; count in alpha-myosin exPBMC minus count in pre-expansion PBMC) were present in inflamed tissues from both patients (**Figure 3.4C**; **Supplementary Fig. S3.5A, B**). Some alpha-myosin expanded TCRs were present at high frequencies in the inflamed heart and skeletal muscles. This overlap suggests that alpha-myosin may be a relevant disease antigen for ICI-myocarditis and myositis. We performed single cell RNA/TCR sequencing on the sorted CD3+ exPBMC from patient 1 and filtered on only cells with expression of a TCR. Gene expression analysis shows expression of *CD3E* in all cells, presence of both *CD8A* and *CD4* expressing cells, and a very small population of residual *CD79A* expressing B cells (**Supplementary Fig. S3.5C**). Clonal cells in the exPBMC are expected to be enriched for alpha-myosin specificity. We further separated cells based on whether their TCR was shared with the cardiac TCR repertoire. Shared TCR clonotypes with the heart would be expected to be

enriched for disease relevant TCRs. Following dimensionality reduction with UMAP, the cells

cluster distinctly by group (**Figure 3.4D**). Of the cells with TCR clonotypes shared with the heart,

a significantly higher proportion were clonal in the exPBMC relative to cells with TCRs not

present in the heart (**Figure 3.4E**). Clonal cells with TCRs shared with the diseased heart have

high expression of *CD8A* relative to clonal cells with TCRs not present in the heart (**Figure**

3.4F). These data suggest that CD8+ alpha-myosin specific T cells are present at the site of

toxicity, in line with results from our mouse model. Clonal cells with TCRs present in the heart

also have high expression of markers of activation such as *NKG7*, *GZMB*, and *GNLY* (**Figure**

3.4F). Expression of activation genes in the exPBMC is not expected to reflect *in vivo* cell state,

given the two-week *in vitro* expansion period. Rather, higher expression of activation associated

genes following stimulation and expansion with alpha-myosin peptides would be expected to

further enrich for alpha-myosin specific TCRs and suggest cytotoxic capability of progenitor

cells. Taken together, these data suggest that CD8+ cytotoxic T cells specific for alpha-myosin

are present in the diseased hearts of patients with fulminant ICI-myocarditis.
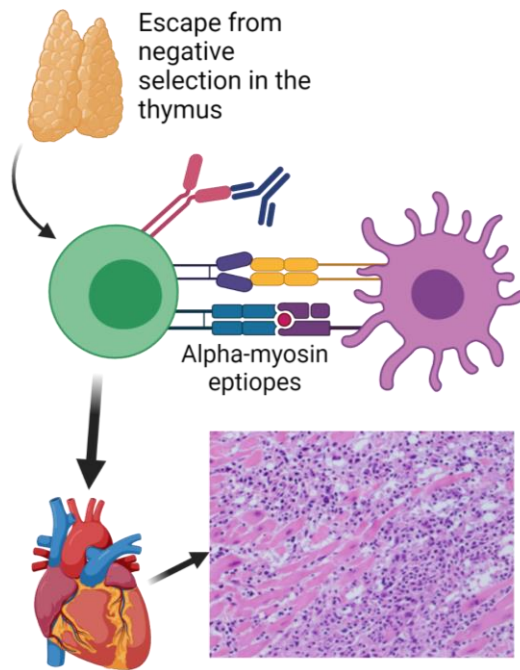
Figure 3.5. Proposed mechanism for ICI-myocarditis. Schematic showing self-reactive T cells escape from negative selection in the thymus. Some of these T cells then go on to be aberrantly reactivated by ICIs. Those specific for alpha-myosin can traffic to the heart and cause cardiac destruction.

Discussion

Immunotherapy toxicities are important limitations to the expanding indications for ICIs. Here we present a new perspective on ICI-myocarditis as an antigen-driven, T cell mediated toxicity. Our proposed mechanism is summarized in **Figure 3.5**. We show in our mouse model (initially discussed in chapter II) that myocarditis is characterized by cytotoxic CD8+ T cells with highly clonal TCRs, and that CD8+ cells are necessary for the development of myocarditis. Three of the most clonal TCRs, derived from independent mice, recognize alpha-myosin epitopes. Two of these TCRs, though derived from independent experiments, recognize the same alpha-myosin epitope. Strikingly, alpha-myosin specific TCRs expanded when transferred to recipient mice and occupied greater than 65% of the highly inflamed cardiac TCR repertoire

at the time of death from myocarditis. Lack of thymic expression increases the likelihood that alpha-myosin specific T cells may escape central tolerance mechanisms (Lv et al., 2011). Alpha-myosin specific T cells can be expanded from the blood of healthy donors and patients with ICI-myocarditis. Alpha-myosin expanded TCRs overlap with TCR repertoires in the diseased hearts and skeletal muscle of two patients with fatal ICI-myocarditis. Although presence of shared clones is insufficient to assess whether alpha-myosin specific T cells play a causal role in the initiation of myocarditis, these data suggest that alpha-myosin may be an important autoantigen in ICI-myocarditis. The presence of other high frequency TCRs in the hearts that were not enriched in the alpha-myosin expanded repertoires suggests that there are likely to be other relevant antigens, particularly by the time myocarditis has become severe. Knowledge of the most relevant disease antigens may allow for antigen-directed approaches to suppressing inflammation without sacrificing anti-tumor efficacy such as tolerogenic vaccines. Identification of alpha-myosin as an autoantigen may also permit identification of biomarkers to predict which patients are at higher risk for myocarditis.

Chapters IV and V will focus further on the idea of immune-related biomarkers of response and toxicity. Chapter IV will focus on how chemotherapy can alter both local (site of tumor) and peripheral (blood) immunity. Chapter V will focus on blood-based biomarkers to predict breast cancer patient outcomes.

CHAPTER IV

Changes in peripheral and local tumor immunity after neoadjuvant chemotherapy reshape

clinical outcomes [3]

Abstract

The recent approval of anti-PD-L1 immunotherapy in combination with nab-paclitaxel for

metastatic triple-negative breast cancer (TNBC) highlights the need to understand the role of

chemotherapy in modulating the tumor-immune microenvironment (TIME). We examined

immune-related gene expression patterns before and after neoadjuvant chemotherapy (NAC) in

a series of 83 breast tumors, including 44 TNBCs, from patients with residual disease (RD).

Changes in gene expression patterns in the TIME were tested for association with recurrence-

free (RFS) and overall survival (OS). Additionally, we sought to characterize the systemic

effects of NAC through single cell analysis (RNAseq and cytokine secretion) of PD-1[HI] CD8+

peripheral T cells and examination of a cytolytic gene signature in whole blood. In non-TNBC,

no change in expression of any single gene was associated with RFS or OS, while in TNBC

upregulation of multiple immune-related genes and gene sets were associated with improved

long-term outcome. High cytotoxic T cell signatures present in the peripheral blood of patients

with breast cancer at surgery were associated with persistent disease and recurrence,

suggesting active anti-tumor immunity that may indicate ongoing disease burden. We have

characterized the effects of NAC on the TIME, finding that TNBC is uniquely sensitive to the

immunologic effects of NAC, and local increases in immune genes/sets are associated with

improved outcomes. However, expression of cytotoxic genes in the peripheral blood, as opposed to the TIME, may be a minimally invasive biomarker of persistent micrometastatic disease ultimately leading to recurrence.

Translational Relevance: Indications for immunotherapy, alone or in combination, are expanding, including in breast cancer. However, the immunologic landscape of breast cancer and how chemotherapy, the current standard of care for triple negative breast cancer (TNBC), influences local and systemic immune responses are incompletely characterized. Herein, we show that increases in expression of immune-related genes and gene sets in the tumor over the course of chemotherapy are associated with improved prognosis in TNBC, but not other subtypes of breast cancer. Conversely, a gene expression signature of immune activation and cytotoxicity in the peripheral blood was associated with persistent disease following chemotherapy and disease recurrence following surgery. Examining immune-related signatures locally and systemically may serve as biomarkers of patients likely to benefit from additional immunotherapeutic approaches.

Introduction

Combination of conventional chemotherapy with an immunotherapeutic targeting programmed death-ligand 1 (PD-L1), atezolizumab, was recently approved for the treatment of patients with metastatic triple-negative breast cancer (TNBC) based on results from a Phase III clinical trial (Schmid et al., 2018). Furthermore, addition of the anti-programmed death-1 (PD-1) monoclonal antibody pembrolizumab to neoadjuvant chemotherapy (NAC) can significantly improve TNBC pathological complete response (pCR) rates (Schmid et al., 2019). Thus, existing clinical data indicate that chemotherapy combinations with immunotherapy demonstrate enhanced efficacy compared to chemotherapy alone. However, these results suggest a growing need to better understand how chemotherapy modulates the tumor-immune microenvironment (TIME).

High levels of stromal tumor-infiltrating lymphocytes (sTILs) in the pre-treatment biopsy are predictive of pCR in TNBC patients treated with NAC (Denkert et al., 2015). In NAC-treated TNBC patients with residual disease (RD) at surgery or in untreated primary TNBC tumors, higher sTILs in the resected tumor also confer improved prognosis (Dieci et al., 2014; Loi et al., 2016, 2019; Luen et al., 2019). However, the immunomodulatory effect of chemotherapy on sTILs in patients and how chemotherapy influences the TIME are poorly understood. In a study of patients with non-small cell lung carcinoma, tumors treated with NAC had higher expression of PD-L1 and higher density of CD3+ T cells, suggesting NAC may be immunomodulatory in some tumor types (Parra et al., 2018). Additionally, in a small breast cancer study, post-NAC natural killer cells and IL-6 expression were associated with better response. However, this study was limited by inclusion of only a small number of TNBCs (n=4; Kim et al., 2020). Intriguingly, a larger study of breast cancer patients (n=60) showed that pre-NAC sTILs and higher pre-NAC expression of cytotoxic T cell markers and cytokines were associated with higher pCR rate. However, this study did not examine long term outcomes in patients with RD,

for whom prognosis is worse than those with pCR and only included a limited number of TNBC samples (n=13; Li et al., 2019). Furthermore, whether immunomodulatory effects of NAC are loco-regional or systemic (*i.e.,* able to be detected in the peripheral blood) is unknown.

In order to address this gap in knowledge, we examined expression patterns of immune-related genes before and after NAC in a series of 83 breast tumors, including 44 TNBCs, from patients with RD. As patients with pCR generally experience excellent outcomes, we chose to focus on patients with RD, who may benefit from additional therapies. Changes in gene expression patterns in the TIME were tested for association with recurrence-free (RFS) and overall survival (OS). T cell receptor sequencing (TCRseq) was performed on a subset (n=15) of tumors. Additionally, in four patients undergoing NAC, PD-1-high and PD-1-negative CD3+CD8+ peripheral blood mononuclear cells (PBMCs) were profiled using single-cell RNA sequencing (scRNAseq) and multiplexed cytokine secretion assays. Finally, we used a scRNAseq-derived signature of activated cytolytic cells to measure immune activation in the peripheral blood of two cohorts of patients: a Vanderbilt cohort consisting of 34 patients after NAC (collected within 2 weeks prior to surgery) and 24 untreated patients, and a cohort from the Dana Farber Cancer Institute (DFCI) consisting of 30 hormone receptor positive, HER2 negative patients treated with NAC (including bevacizumab) as part of a clinical trial (Tolaney et al., 2015). We then tested the association of this signature with surgical outcome (pCR or residual disease burden) and post-surgical cancer recurrence.

Intriguingly, higher expression of the gene signature at the time of surgery was associated with higher disease burden (*i.e.,* in those with RD who experienced disease recurrence within three years following surgery or those with the highest residual cancer burden [RCB]). Thus, peripheral cytotoxic activity, guarded by immune checkpoints, may reflect ongoing micrometastatic and primary disease burden, and could be a useful biomarker for disease recurrence and possibly immune checkpoint inhibitor benefit.

61

Materials and Methods

Patients. Three cohorts of patients were combined for the tumor profiling study. All included patients received neoadjuvant therapy and had residual disease and matched pre-treatment tissue was required for inclusion. All but 2 (ER+) patients received cytotoxic chemotherapy as part of their regimen. Four patients (ER+) received courses of hormone therapy as part of their neoadjuvant regimen, two of which were in conjunction with cytotoxic chemotherapy. Five patients (HER2+) received HER2-directed therapy as part of their neoadjuvant regimen. For the 'Peru' cohort, clinical characteristics and molecular analysis of the patients (n=48 with matched pre-treatment tissue) were previously described at the Instituto Nacional de Enfermedades Neoplásicas (Balko et al., 2014). Clinical and pathologic data were retrieved from medical records under an institutionally approved protocol (INEN IRB 10-018). For the 'VICC' cohort, which included PBMC and whole blood analyses, clinical and pathologic data were retrieved from medical records under an institutionally approved protocol (VICC IRB 030747). For the DARTMOUTH cohort patient samples were collected under a protocol approved by the Dartmouth College Institutional Review Board and the waiver of the subject consent process was IRB-approved. (IRB 28888). For the peripheral blood study, two cohorts of patients were used. For the Vanderbilt cohort, all blood was collected within 14 days preceding definitive surgery. For the DFCI cohort (Tolaney et al., 2015), all blood was collected in the interlude between completion of NAC and definitive surgery.

Tumor-infiltrating lymphocytes quantification. Stromal tumor-infiltrating lymphocytes were analyzed using full face H&E sections from pre-NAC diagnostic biopsies or post-NAC RD surgical specimens. Samples were scored according to the International TILs Working Group Guidelines (Hendry et al., 2017a, 2017b; Salgado et al., 2015). The pre-defined cut point of 30% was used for all survival analyses (Loi et al., 2019).

NanoString nCounter analysis. Gene expression and gene set analysis on pre- and post-NAC formalin-fixed tissues were performed using the nanoString Pan-Cancer Immunology panel (770 genes) according to the manufacturers' standard protocol. Data were normalized according to positive and negative spike-in controls, then endogenous housekeeper controls, and transcript counts were log transformed for downstream analyses. Gene sets were calculated by summing the $\log_2$-transformed normalized NanoString counts for all genes contained in a given gene set. Samples were simultaneously assayed for PAM50 molecular subtyping using a custom-designed 60-gene Elements panel. Briefly, 10µm sections of diagnostic biopsies or residual tumors were used for RNA preparation (Promega Maxwell 16 RNA FFPE) and 50ng of total RNA >300nt (assayed on a Agilent Tapestation 2200 Bioanalyzer) was used for input into nCounter hybridizations for Pan-Cancer Immunology panels or 500-1000ng RNA for PAM50 analysis. Data were normalized according to positive and negative spike-in controls, then endogenous housekeeper controls, and transcript counts were log transformed for downstream analyses. Subtype prediction was performed in R using the genefu package. For the 8 gene signature analysis in whole blood, a custom NanoString Elements was constructed to measure the gene expression levels of *PDCD1, NKG7, LAG3, GZMH, GZMB, GNLY, FGFBP2, HLA-DRB5*, and *HLA-G*, as well as 3 normalization control genes (*PTPRC, RPL13a, TBP*). RNA was isolated from whole blood (Promega Maxwell 16 Simply RNA Blood) and 100-200ng was used for input into the nCounter analysis. Data were normalized as above.

Isoplexis (single-cell cytokine profiling). On day 1, cryopreserved PBMCs were thawed and resuspended in complete RPMI media with IL-2 (10 ng/ml) at a density of 1-5 x 10^6 cells/ml. Cells were recovered at 37°C, 5% CO2, overnight. Plates were prepared by coating with anti-human CD3 (10 µg/ml in PBS, 200-300 µl/well) in a 96-well flat-bottom plate at 4°C, O/N. On day 2, non-adherent cells for each sample were collected and viability was confirmed, with dead cell depletion by Ficoll. For each sample, where sufficient, volume was split in half for each of

the following negative isolations: with one half of cells from each sample, CD4 T cells were isolated with CD4+ negative isolation kit following Miltenyi protocol (130-096-533); with the other half of cells from each sample, CD8 T cells were isolated with CD8+ negative isolation kit following Miltenyi protocol (130-096-495). The PD-1+ and PD-1- subsets were from isolated CD4 or CD8 T cells by staining with PE-conjugated anti-PD-1 antibody using the manufacturer's protocol (Miltenyi, 130-096-164) as follows: 1) stain each subset with 10µl stain :100µl Robosep buffer for every $1x10^7$ total cells; 2) incubate at 4°C for 10 mins; 3) rinse cells by adding 1-2 mL of Robosep and C/F at 300xg for 10 mins; 4) aspirate supernatant and resuspend cells pellets in 80ul buffer per $1x10^7$ total cells. PD-1+ cells were then isolated with anti-PE microbeads following the manufacturer's protocol (Miltenyi, 130-097-054). Cells were resuspended in complete RPMI media at a density of 1×10^6/ml and seeded into wells of the CD3-coated 96-well flat-bottom plate with soluble anti-human CD28 (5 µg/ml). Plates were incubated at 37°C, 5% CO2 for 24 hrs. On day 3, supernatants (100 µl per well) were collected from all wells and stored at -80°C for population assays. T cells were collected and stained with Brilliant Violet cell membrane stain and AlexaFluor-647-conjugated anti-CD8 at RT for 20 min, rinsed with PBS and resuspended in complete RPMI media at a density of 1×10^6/mL Approximately 30 µl of cell suspension was loaded into the IsoCode Chip and incubated at 37°C, 5% CO_2 for additional 16 hours. Protein secretions from ~1000 single cells were captured by the 32-plex antibody barcoded chip and analyzed by fluorescence ELISA-based assay (Lu et al., 2015; Ma et al., 2011, 2013; Parisi et al., 2020; Rossi et al., 2018; Xue et al., 2017). Polyfunctional T cells that co-secreted 2+ cytokines per cell were evaluated by the IsoSpeak software across the five functional groups: Effector: Granzyme B, TNFα, IFN-γ, MIP1α, Perforin, TNFβ; Stimulatory: GM-CSF, IL-2, IL-5, IL-7, IL-8, IL-9, IL-12, IL-15, IL-21;

Chemoattractive: CCL11, IP-10, MIP-1β, RANTES; Regulatory: IL-4, IL-10, IL-13, IL-22, sCD137, sCD40L, TGFβ1; Inflammatory: IL-6, IL-17A, IL-17F, MCP-1, MCP-4, IL-1β.

TP53 sequencing. TP53 gene sequencing was performed using either the Foundation Medicine assay as previously reported (Balko et al., 2014) or using the SureMASTR TP53 sequencing assay (Agilent). For the later, purified DNA from FFPE breast tumor sections were amplified and sequenced according to the manufacturer's standard protocol. Samples were sequenced to a depth of ~10,000 and mutations were called using the SureCall software (Agilent). Mutation allele frequency was set at 5% and only likely functional (early stops, frameshift deletions and known recurrent hotspot single-nucleotide variation mutations) were selected for sample annotation.

T cell receptor sequencing. TCR sequencing and clonality quantification was assessed in FFPE samples of breast cancer specimens or PBMCs. For FFPE tissue, DNA or RNA was extracted from 10µm sections using the Promega Maxwell 16 FFPE DNA or FFPE RNA kits and the manufacturer's protocol. For PBMCs, PD-1^{HI} and PD-1^{NEG} CD8+ T cells sorted by fluorescence-activated cell sorting from samples isolated from EDTA collection tubes and processed using a Ficoll gradient. At least 100K cells were collected, centrifuged, and utilized for RNA purification. TCRs were sequenced using survey level immunoSEQ^{TM} (DNA; Adaptive Biotechnologies) and the Immunoverse^{TM} assay (RNA; ArcherDX). Sequencing results were evaluated using the immunoSEQ analyzer version 3.0 or Archer Immunoverse analyzer. CDR3 sequences and frequency tables were extracted from the manufacturers' analysis platforms and imported into R for analysis using the Immunarch package (https://immunarch.com) in R (Nazarov et al., 2020). Shannon entropy, a measure of sample diversity, was calculated on the clonal abundance of all productive TCR sequences in the data set. Shannon entropy was normalized by dividing Shannon entropy by the logarithm of the number of unique productive TCR sequences. This normalized entropy value was then inverted (1 − normalized entropy) to produce the 'clonality' metric.

Single-cell RNA sequencing. Peripheral blood mononuclear cells were isolated from EDTA

collection tubes, processed using a Ficoll gradient, and cryopreserved in 10% DMSO 90% FBS.

Upon thaw, whole live PBMCs were prepared by depleting dead cells using a dead cell removal

kit (Miltenyi, cat no: 130-090-101). PD-1^{HI} and PD-1^{NEG} CD8+ T cells were sorted by

fluorescence-activated cell sorting from peripheral blood mononuclear cells. Each sample

(targeting 5,000 – 10,000 cells/sample) was processed for single cell 5' RNA sequencing

utilizing the 10X Chromium system. Libraries were prepared using P/N 1000006, 1000080, and

1000020 following the manufacturer's protocol. The libraries were sequenced using the

NovaSeq 6000 with 150 bp paired end reads. RTA (version 2.4.11; Illumina) was used for base

calling and analysis was completed using 10X Genomics Cell Ranger software v2.1.1. Data

were analyzed in R using the filtered h5 gene matrices in the Seurat package (Butler et al.,

2018; Satija et al., 2015; Stuart et al., 2019). Briefly, samples were merged, and all cells were

scored for mitochondrial gene expression (a marker of dying cells) and cell cycle genes to

determine phase. Data were transformed using SCTransform, regressing against mitochondrial

gene expression and cell cycle phase. Dimensional reduction was performed using Harmony

(Korsunsky et al., 2019). Missing values were imputed using the RunALRA function in the

SeuratWrappers package (Linderman et al., 2018). For the whole PBMC single cell data, cell

types were assigned to individual cells using SingleR (Aran et al., 2019). BlueprintEncodeData

was used as a reference (Dunham et al., 2012; J. H. A. Martens & Stunnenberg, 2013).

Statistical analysis. All statistical analyses were performed in R or Graphpad. For survival

curves (RFS and OS), the log-rank statistic was reported (or trend-test for >2 groupings). For

gene-level analysis, nominal p-values were calculated using a cox proportional hazards model,

and then a adjusted p-value (q-value) was calculated based on the FDR (Benjamini & Hochberg,

1995). All single-cell statistical analyses were calculated in R using the Seurat package (Butler

et al., 2018; Satija et al., 2015). Shared Nearest Neighbors were calculated using the Harmony

reduction, and clusters were identified at a resolution of 0.3, defining 5 total clusters. UMAP was

performed for visualization, and missing values were imputed using ALRA (Linderman et al., 2018). Visualization and graph generation was performed in R. Some heatmaps were made using the complex heatmap package in R (Gu et al., 2016). P-value cut-offs displayed on plots correspond to "ns" equals $p > 0.05$, * equals $0.01 < p \leq 0.05$, ** equals $0.001 < p \leq 0.01$, *** equals $0.0001 < p \leq 0.001$, **** equals $p \leq 0.0001$. Code used to generate figures can be accessed at: https://github.com/MLAxelrod/Immunologic_changes_with_chemotherapy_inTNBC

Results

Stromal tumor-infiltrating lymphocytes (sTILs) in residual disease prognosticate improved outcomes in TNBC patients with incomplete response to neoadjuvant chemotherapy (NAC)

We procured matched archived pre-treatment (diagnostic biopsy) and post-treatment (residual disease surgical specimen) tumor specimens from a series of 83 patients, including 44 TNBC patients. Importantly, we refined our study to include only patients who had residual disease at surgery for analysis, thereby excluding patients who achieved pCR. This was a purposeful selection strategy, as patients with pCR usually experience good outcomes, and we instead chose to focus on patients with RD for whom additional risk stratification could identify those who are most likely to benefit from additional therapies. Metadata for the patients, including treating institution, molecular subtype (PAM50), recurrence-free and overall survival (RFS and OS, respectively), *TP53* mutation status, and other molecular and clinical data are summarized in **Table 4.1**.

Table 4.1: Demographic information for tumor cohort

	DART	EA1311	PERU	Entire Cohort
	n (%)	n (%)	n (%)	n (%)
Total	24	11	48	83
PAM50 Subtype				
Basal	7 (29.17%)	4 (36.36%)	31 (64.58%)	42 (50.60%)
Her2 enriched	2 (8.33%)	3 (27.27%)	10 (20.83%)	15 (18.07%)
Luminal A	6 (25%)	1 (9.09%)	1 (2.08%)	8 (9.64%)
Luminal B	8 (33.33%)	3 (27.27%)	1 (2.08%)	12 (14.46%)
Normal	1 (4.17%)	0 (0%)	4 (8.33%)	5 (6.02%)
NA	0 (0%)	0 (0%)	1 (2.08%)	1 (1.20%)
IHC Subtype				
ER+	20 (83.33%)	5 (45.45%)	1 (2.08%)	26 (31.33%)
PR+	13 (54.17%)	4 (36.36%)	1 (2.08%)	18 (21.69%)
HER2+	6 (25%)	2 (18.18%)	12 (25%)	20 (24.10%)
TNBC	4 (16.67%)	5 (45.45%)	35 (72.92%)	44 (53.01%)
Neoadjuvant Chemotherapy				
Taxane	21 (87.50%)	7 (63.64%)	21 (43.75%)	49 (59.04%)
No Taxane	3 (12.5%)	4 (36.36%	27 (56.25%)	34 (40.96%)

As sTILs have been described and rigorously validated in breast cancer as both a prognostic factor (in surgical specimens for post-surgical outcomes, particularly in TNBC and HER2+ cancers), and a predictive factor (in diagnostic biopsies for benefit from NAC), we first asked whether these findings were consistent with our study cohort. Using the published cutoff (30%) of sTILs (Loi et al., 2019), we found that higher abundance of sTILs in the post-NAC residual disease in TNBC patients (n=44) was significantly prognostic for both RFS (log-rank p=0.019) and OS (p=0.05; **Figure 4.1A**). Representative histology of high (>30%) and low (<30%) sTILs are shown in **Supplementary Figure S4.1.** Interestingly, pre-NAC sTILs in the

diagnostic biopsy were not prognostic for outcomes in TNBC patients (**Supplementary Figure S4.2A**), presumably due to the selection strategy of including only patients who lacked pCR. Consistent with prior literature that the prognostic and predictive effect of sTILs differs by breast cancer subtype (Denkert et al., 2018), neither pre-NAC nor post-NAC sTILs were prognostic for OS when considering our entire cohort (n=83).
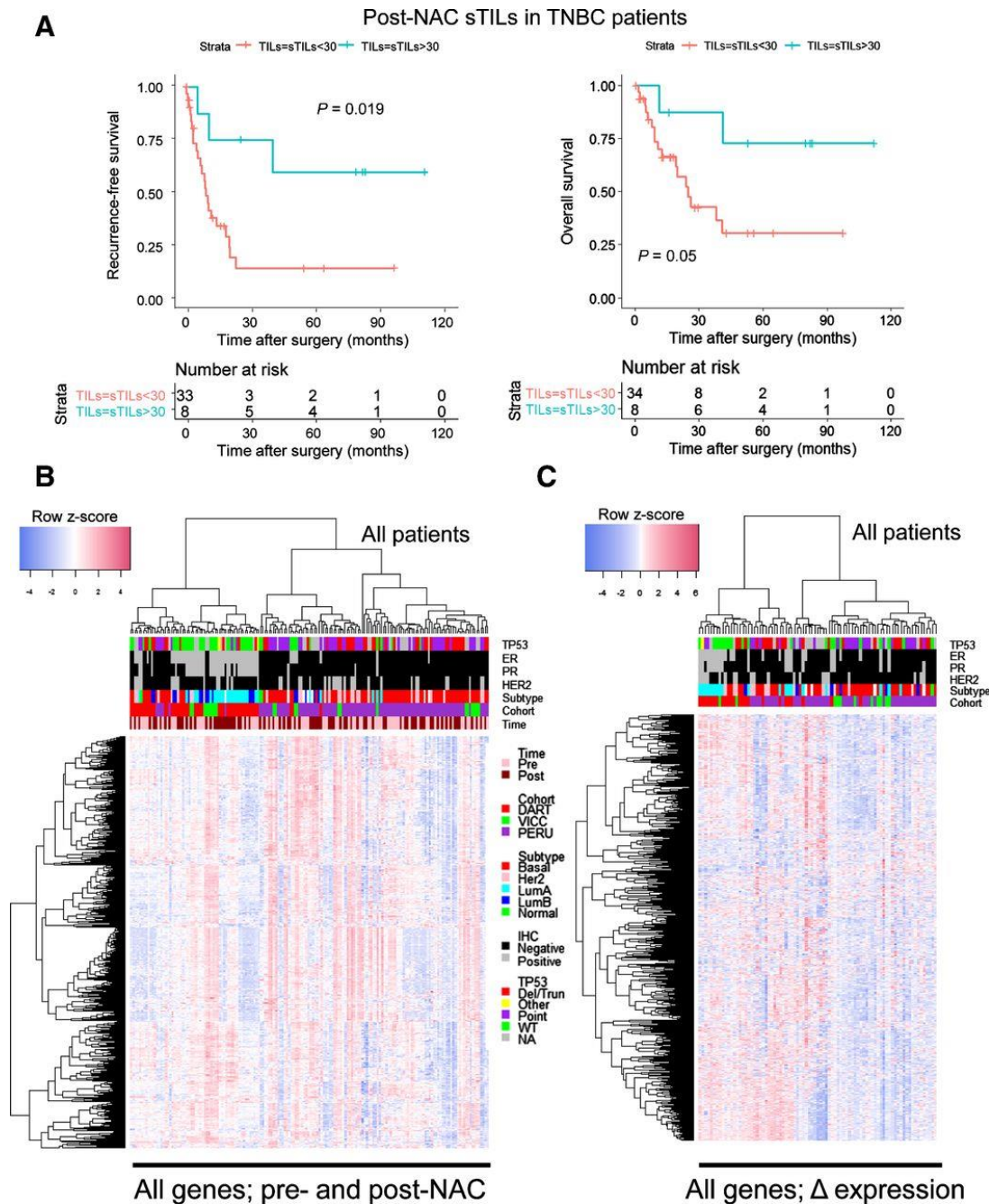
Figure 4.1. Immunologic changes in breast tumors after NAC. A, High levels of sTILs are associated with RFS (left; n = 41) and OS (right; n = 42) after surgery in TNBC. Patients are stratified on the basis of post-NAC sTILs ≤ 30% or > 30%, scored as recommended by the International TILs Working Group, according to the predefined cut point. B, Heatmap demonstrating gene expression patterns for 770 immune-related genes (NanoString Pan-Cancer Immunology panel) across all patients (TNBC and non-TNBC; n = 83 total patients, 166 samples). C, Heatmap of gene expression patterns as detailed in B, instead depicting the change in expression of each gene in matched paired (pre- and post-NAC; n = 83) samples. Red data points represent an upregulation, while blue data points represent a downregulation in the post-NAC RD compared with the pretreatment diagnostic biopsy.

However, post-NAC sTILs were prognostic for RFS (p=0.031) in the whole cohort (**Supplementary Figure S4.2B, S4.3A**). This effect seems primarily driven by TNBC tumors as post-NAC sTILs are not prognostic of either RFS or OS in non-TNBCs (**Supplementary Figure S4.3B**). Neither pre-NAC nor post-NAC sTILs were prognostic in either ER+ or HER2+ patients only (data not shown). This may be limited by our sample size as sTILs have been previously shown to be associated with longer RFS in HER2+ cancer patients and shorter overall survival in luminal/HER2- cancer patients (Denkert et al., 2018). Stratifying TNBC patients by whether sTILs were qualitatively increased or decreased/equivocal in the surgical resection compared to the diagnostic biopsy did not provide any prognostic capability in this cohort (**Supplementary Figure S4.4A**). Interestingly, most patients, regardless of clinical subtype, had a decrease in sTILs over the course of NAC (**Supplementary Figure S4.4B**)**.** Importantly, our cohort includes only patients with RD, and there is currently not a validated method for quantifying sTILs in pCR where, by definition, a tumor is no longer present. Thus, in our cohort, abundance of sTILs has the strongest prognostic effect for the post-NAC surgical resection specimen in TNBC tumors with an incomplete response to NAC. These findings, consistent with both retrospective studies and analyses from randomized controlled trials, prompted us to perform more detailed molecular studies aimed at understanding how NAC influences the TIME.

Suppression of immunologic gene expression with NAC in TNBC

To measure transcriptional changes occurring in the tumor-immune microenvironment (TIME) induced by NAC, we performed gene expression profiling for a series of 770 immune-related genes using nanoString (Pan-Cancer Immune Panel), before and after NAC in the entire cohort (n=83). Transcriptional patterns and hierarchical clustering for all data primarily segregated tumors based on receptor status (ER/PR/HER2) and/or molecular subtype, with

most luminal/hormone receptor-positive tumors appearing in the first cluster, most HER2-positive tumors in the second cluster, and most basal-like/TNBC tumors in the third cluster (**Figure 4.1B**). Examining the data as the change in gene expression for each gene after NAC in a patient-matched fashion (Δ expression; post-NAC minus pre-NAC) yielded similar patterns, with a trend of most TNBC patients having generalized decreased immune gene expression patterns after NAC (**Figure 4.1C**). In order to test for effects driven by differences in sampling (i.e., pre-NAC samples are biopsies whereas post-NAC samples are surgical resection samples) or treating institution, we performed principal component analyses. We did not detect significant clustering by time of sampling or cohort (**Supplementary Figure S4.5**).

NAC-induced immunologic gene expression is a positive predictor of outcome in TNBC

While the TIME change in sTIL abundance did not prognosticate outcome in TNBC patients, we asked if changes in individual immune-related genes are associated with outcome. We performed iterative Cox proportional hazards models, using the delta (Δ) of each gene (post-NAC minus pre-NAC) in an independent univariate analysis, for both RFS and OS. All analyses are reported using a nominal p-value as well as a false discovery rate (FDR; Benjamini-Hochberg method) q-value for association with RFS or OS. After correction for FDR (q <0.10), upregulation of 11 genes were associated with improved RFS, while upregulation of only one gene was significantly associated with worse RFS (*CDH1*, which encodes e-cadherin) in our TNBC cohort. Interestingly, e-cadherin is known to interact with killer cell lectin-like receptor G1 (KLRG1), an inhibitory receptor expressed by memory T cells and NK cells (Rosshart et al., 2008). In contrast, upregulation of a larger number of genes was associated with improved OS (n=189) or reduced OS (n=15) at FDR q<0.10 (**Figure 4.2A**). Kaplan-Meier visualization examples of strongly prognostic genes (negative prognostic: *CDH1*; positive prognostic: *CD70*) reinforced the prominent association of TNBC disease outcomes with

changes in immune gene expression during NAC (**Figure 4.2B**). Conversely, no changes in

immune-related gene expression were significantly associated with RFS or OS in non-TNBC

patients at q<0.10 (**Supplementary Figure S4.6A**).
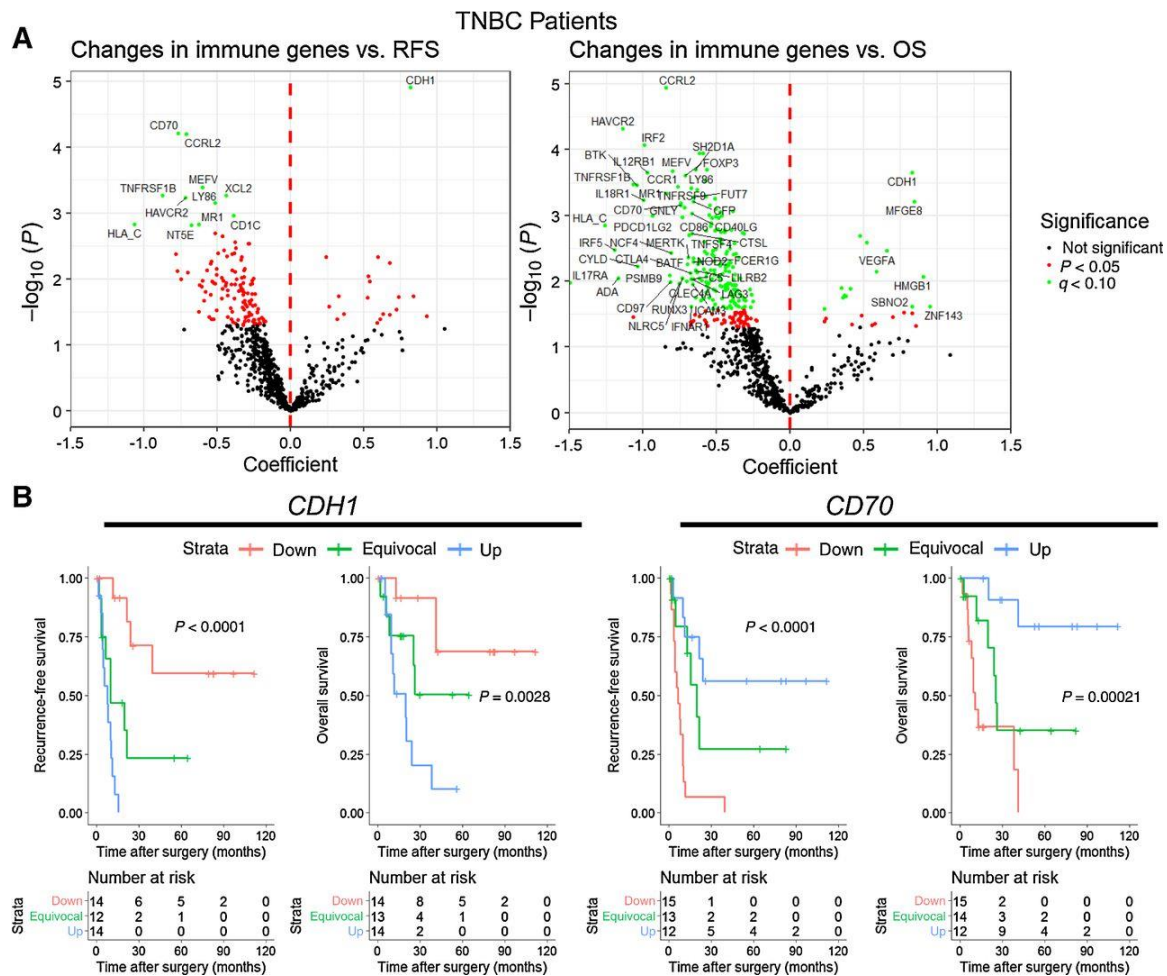
Figure 4.2. Identification of immune-associated genes associated with RFS and OS in TNBC after chemotherapy. A, Individual genes (changes pre- to post-NAC) were tested iteratively in a univariate Cox proportional hazards model for their association with RFS (left) or OS (right) after chemotherapy and surgery. Individual genes are colored for their statistical significance (red: nominal P value <0.05; green: q value (FDR) < 0.10; black: not significant). Selected top genes are labeled but are limited in number for clarity. Genes with negative coefficients (left of the center line) are associated with better outcome, while genes with positive coefficients (right of the center line) are associated with worse outcome. B, Representative Kaplan–Meier plots for selected detrimental (CDH1; e-cadherin) and beneficial (CD70) genes are shown. Strata are defined by tertiles, and generally represent upregulation during NAC (blue), no change/equivocal (green), and downregulation (red). P values represent the log-rank test for trend.

Dimensional reduction through collapsing individual genes into pathways or defined functions can improve interpretation of high-dimensional data. Thus, we collapsed the gene expression data into bioinformatically-categorized immune signatures (sum-scores, defined as the summation of the $\log_2$ expression values for all genes in a category). Organization of the data in this manner and testing the signatures (n=70) for association with RFS and OS yielded a surprising finding - all significant (q<0.10) gene sets (n=40 for RFS and n= 60 for OS) identified in this analysis were associated with good outcome (**Figure 4.3A**). Many of the top-scoring gene sets were associated with T cells, including "T cell polarization", "T cell immunity", "T cell activation", among others. Although manual inspection revealed some overlap in these gene sets, they were largely composed of signature-exclusive genes. Kaplan-Meier visualization examples of strongly prognostic gene sets ("NK cell functions" and "T cell activation") reinforced the considerable association of changes in immune gene sets during NAC with outcomes (**Figure 4.3B**). Interestingly, no gene or gene set was significantly associated with RFS or OS in non-TNBC patients at q<0.10 (**Supplementary Figure S4.6A-B**). When the non-TNBC group is separated into ER+ and HER2+ groups, no gene or gene set was significantly associated with outcome (data not shown). Thus, these data suggest that NAC, exclusively in TNBC, could promote immunologic activity leading to improved outcomes in a subset of patients. However, these effects may be related to factors beyond TNBC biology, as hormone-receptor-positive and HER-2 positive patients receive additional endocrine or HER-2 directed therapy in the adjuvant setting, complicating associations with RFS and possibly OS. Nonetheless, immune-related signatures, particularly those derived from T cells, appeared to be strongly associated with improved outcomes in TNBC.
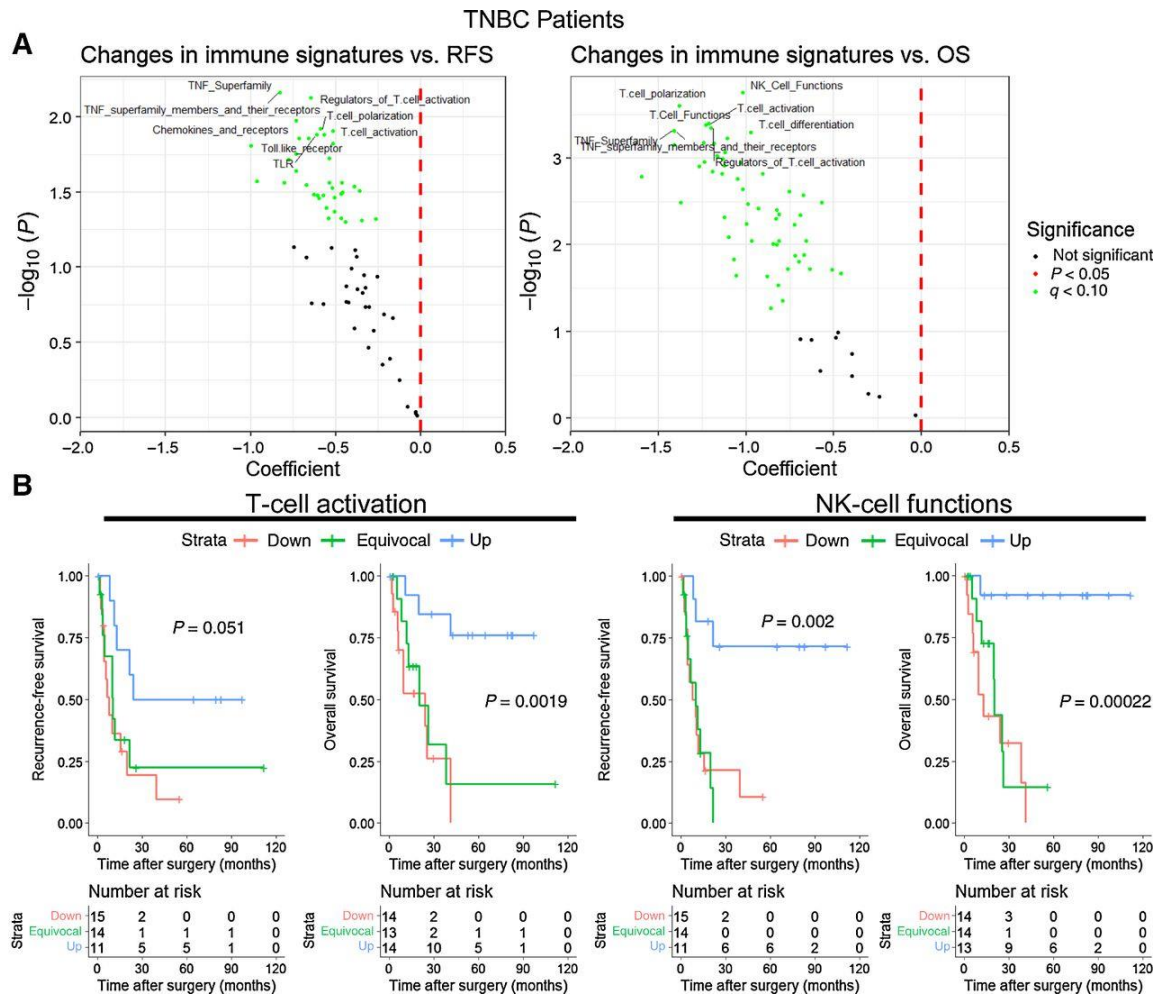
Figure 4.3. Upregulation of immune-associated gene sets after chemotherapy are associated with improved RFS and OS in TNBC. A, Gene set scores were calculated by summing expression levels of all gene set member genes across each candidate gene set (n = 70). Changes pre- to post-NAC was then calculated for each patient with TNBC (n = 44) and each gene set score was tested iteratively in a univariate Cox proportional hazards model for association with RFS (left) or OS (right) after chemotherapy and surgery. Individual gene sets are colored for their statistical significance [red: nominal P value < 0.05; green: q value (FDR) < 0.10; black: not significant]. Selected top gene sets are labeled but are limited for clarity. Gene sets with negative coefficients are associated with better outcome, while gene sets with positive coefficients are associated with worse outcome. B, Representative Kaplan–Meier plots for selected gene set changes with beneficial associations are shown (left: T-cell activation; right: NK-cell functions). Strata are defined by tertiles, and generally represent upregulation during NAC (blue), no change/equivocal (green), and downregulated (red). P values represent the log-rank test for trend.

Changes in T cell clonality and function in tumors and peripheral blood induced by NAC

A robust T cell response is characterized by oligoclonal expansion of antigen-specific T cells. Therefore, we next asked whether clonality of T cells in the TIME was altered during NAC. In a subset of samples (n=15; 8 TNBC, 7 non-TNBC), we performed T cell receptor (TCR) β chain sequencing using the ImmunoSeq assay to estimate the number of unique T cell clones (diversity), and the presence of expanded T cell clones in the TIME before and after NAC. Given the breadth of sTILs fractions observed among breast tumors as well as caveats associated with comparison of samples derived from diagnostic core needle biopsies vs. surgical resections, we first verified that the number of productive T cells was associated with estimation of sTILs determined on adjacent sections. We detected a strong association between these parameters (R^2=0.6; p<0.0001; **Supplementary Figure S4.7A**), raising confidence in the assay results. In this sample set, NAC did not universally alter productive clonality (**Supplementary Figure S4.7B**), a measurement of the number of times the same (productive) TCRβ sequence is represented in the sample, which is a descriptor of T cell clonal expansion. When stratified by breast cancer subtype, there was no significant change in productive clonality with NAC (one-sample t-test). However, TNBC tumors demonstrated a qualitative trend toward decreased clonality after NAC, while non-TNBC tumors trended toward increased clonality after NAC. The difference between these two subgroups approached significance (p=0.054; two-sample t-test; **Supplementary Figure S4.7C**). There was no association of change in clonality with change in sTILs, suggesting that changes in sTIL abundance after NAC are not necessarily due to expansion of existing clones (**Supplementary Figure S4.7D)**.

To further explore changes in T cell clonality and function in response to chemotherapy, we prospectively collected PBMCs from four breast cancer patients (including two TNBCs) before and after NAC (**Figure 4.4A**). In addition, the post-NAC residual disease (or in one case, pCR residual scar) was analyzed in tandem. Based on previous findings demonstrating that

76

tumor-reactive T cells are enriched in the CD8+ PD-1^{HI} population of peripheral T cells(Gros et al., 2016), we purified CD4+ and CD8+ cells from each sample by fluorescence-activated cell sorting (FACS), further stratifying by PD-1-negative (PD-1^{NEG}) and PD-1^{HI} (top 20% expressers of CD8+ or CD4+ cells) status (gating scheme shown in **Supplementary Figure S4.8**). Using a functional fluorescence ELISA-based assay of cytokine (32-plex antibody barcoded chip, **Supplementary Figure S4.9A**) secretion following CD3/CD28 stimulation, we determined that PD-1^{HI} peripheral T cells had functional capacity, secreting multiple cytokines following activation, and these effects were particularly pronounced in CD8+ T cells (**Supplementary Figure S4.9B**). In 2/2 TNBC patients, the percentage of 'polyfunctional' PD-1^{HI} CD8+ T cells – those capable of expressing multiple cytokines after TCR stimulation – were increased following NAC (**Figure 4.4B**). In contrast, 2/2 ER+ breast cancer patients experienced a drop or stasis in the functionality of the PD-1^{HI} CD8+ population of cells following NAC (**Figure 4.4B**). Of note, the patient with ER+HER2+ disease has a near complete loss of T cell functionality after NAC. Cytokines produced by individual PD-1^{HI} CD8+ cells in TNBC patients were primarily effector (*e.g.,* Granzyme B, IFN-γ, MIP-1α, TNF-α, and TNF-β) and chemo-attractive (MIP-1β) cytokines (**Figure 4.4C**). PD-1^{HI} CD4+ T cells also produced primarily effector cytokines including IFN-γ and TNF-α (**Supplementary Figure S4.9C**).
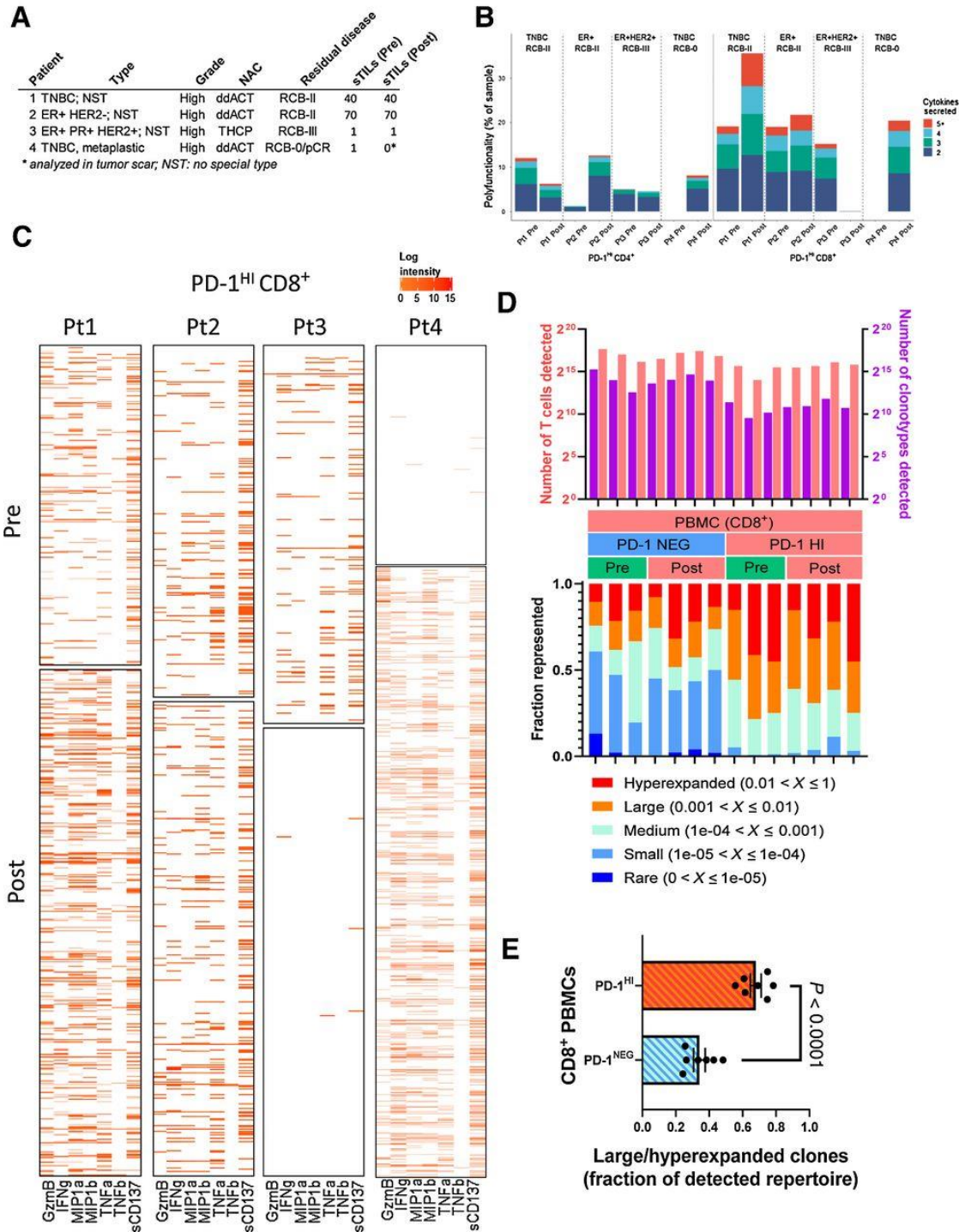
Figure 4.4. Evidence of enhanced T-cell functionality in the CD8+ PD-1^{HI} peripheral compartment. A, Clinical details of 4 patients analyzed prospectively for changes in peripheral blood T-cell functionality. NST indicates no special type. B, Polyfunctionality of PD-1HICD4+ and PD-1HI CD8+ T cells isolated from PBMCs in 4 patients prior and after NAC (>1,000 individual cells/sample/timepoint) was determined by Isoplexis single-cell cytokine profiling. Polyfunctionality is defined as the percentage of cells capable of producing ≥ 2 cytokines following CD3/CD28 stimulation. The percentage of cells in each sample capable of

78

secreting 2, 3, 4, or 5+ cytokines are depicted in stacked bars. Characteristics of each of the 4 patients are shown above the bars. Patients with TNBC (Pt. 1 and Pt. 4) had greater increases in polyfunctionality in the CD8+ compartment with NAC. C, Heatmap representation of log cytokine signal intensity of each cell in each patient sample, pre- and post-NAC. Each row represents one PD-1Hi CD8+ T cell. White indicates no cytokine secreted. D, TCRβ chain repertoire analysis in CD8+ peripheral blood T cells. Upper plots indicate the number of individual T cells sequenced plotted by sample on the left y axis; number of clonotypes (unique CDR3 amino acid sequences) plotted by sample on the right y axis. In the lower graph, each sample is divided into the number of clonotypes comprising expanded (hyperexpanded, large, medium, small, and rare) compositions of the detected repertoire (categories divided by orders of magnitude of fraction of total repertoire). E, The fraction of repertoire clonotypes identified in PD-1HI versus PD-1NEG CD8+ T cells (before or after NAC) classified as "hyperexpanded" or "large" (comprising > 0.1% of repertoire). P value represents a two-sample two-tailed t test.

PD-1^{HI} CD8+ and PD-1^{NEG} CD8+ T cells from pre-NAC and post-NAC blood (except patient 4, for whom a sufficient pre-NAC sample was not available) were also analyzed by TCR sequencing. While the number of detected T cells was consistent among all samples, the clonotypes detected (unique TCRs) were considerably lower in PD-1^{HI} CD8+ T cells (**Figure 4.4D**). This suggests that there are more repetitive sequences detected in the PD-1^{HI} population, indicating clonal expansion. Consistent with this observation, the proportion of the overall TCR repertoire occupied by expanded clonotypes (large or hyperexpanded clonotypes consisting of greater than 0.1% or 1% of the total repertoire, respectively) was substantially higher in the PD-1^{HI} than in PD-1^{NEG} CD8+ T cell fractions (**Figure 4.4E**). We additionally sequenced the TCR repertoire in the post-NAC residual disease, although the number of T cells sequenced in these samples were limited due to fixation of tissue and small T cell abundance as a function of total RNA in the bulk samples, and thus should be interpreted with caution. Nonetheless, we found that the similarity (Jaccard index, normalized to size of repertoire detected) of tumor-infiltrating TCRs in the post-NAC sample was universally more similar to the PD-1^{HI} CD8+ peripheral TCR repertoires, compared to the PD-1^{NEG} CD8+ repertories (**Supplementary Figure S4.10**). This suggests that the PD-1^{HI} peripheral compartment is enriched for similarity to TILs relative to the PD-1^{NEG} peripheral compartment.

Single-Cell RNAseq of peripheral PD-1^{HI} CD8+ T cells identifies a unique population of cytolytic effector cells

Next, we utilized scRNAseq to describe the post-NAC peripheral PD-1^{HI} CD8+ T cell populations at the time of surgery in the blood of two TNBC patients: one with residual disease (Pt. 1) and one with matrix-producing metaplastic TNBC who experienced pCR (Pt. 4). Uniform Manifold Approximation and Projection (UMAP) analysis was performed on Harmony-normalized samples to adjust for inter-sample technical variation, and we stratified cells based on 5 clusters identified through the Louvain algorithm (**Figure 4.5A-B**). A heatmap of the top 10 most differentially expressed genes by cluster is presented in **Figure 4.5C**. Although the composition of the cells was largely similar, we identified one cluster ('cluster 0') which was enriched in Pt. 4. Examination of genes differentially expressed in this cluster of cells suggested a cellular identity concordant with that of highly cytotoxic memory (*TBX21*-expressing) T cells, which had an abundance of MHC-I (*HLA-A*/*B*/*C*) and MHC-II (*e.g., HLA-DRA, HLA-DRB5*) family member expression as well as expression of cytolytic and immune checkpoint genes (*e.g., LAG3*, *FCRL6* (Johnson et al., 2018), and higher transcriptional expression of *PDCD1;* **Figure 5C-D**). Verification of the pattern of expression of key cytolytic and killer-identity genes [*GNLY* (granulysin)*, GZMB* (granzyme B)*,* and *FGFBP2* (killer-secreted protein 37)] showed that these genes were almost exclusively expressed in cluster 0 (**Supplementary Figure S4.11A**). This analysis also demonstrated purity-of-sort in that all clusters expressed *CD8A* and *PDCD1*, but not *CD4* (**Supplementary Figure S4.11B**).
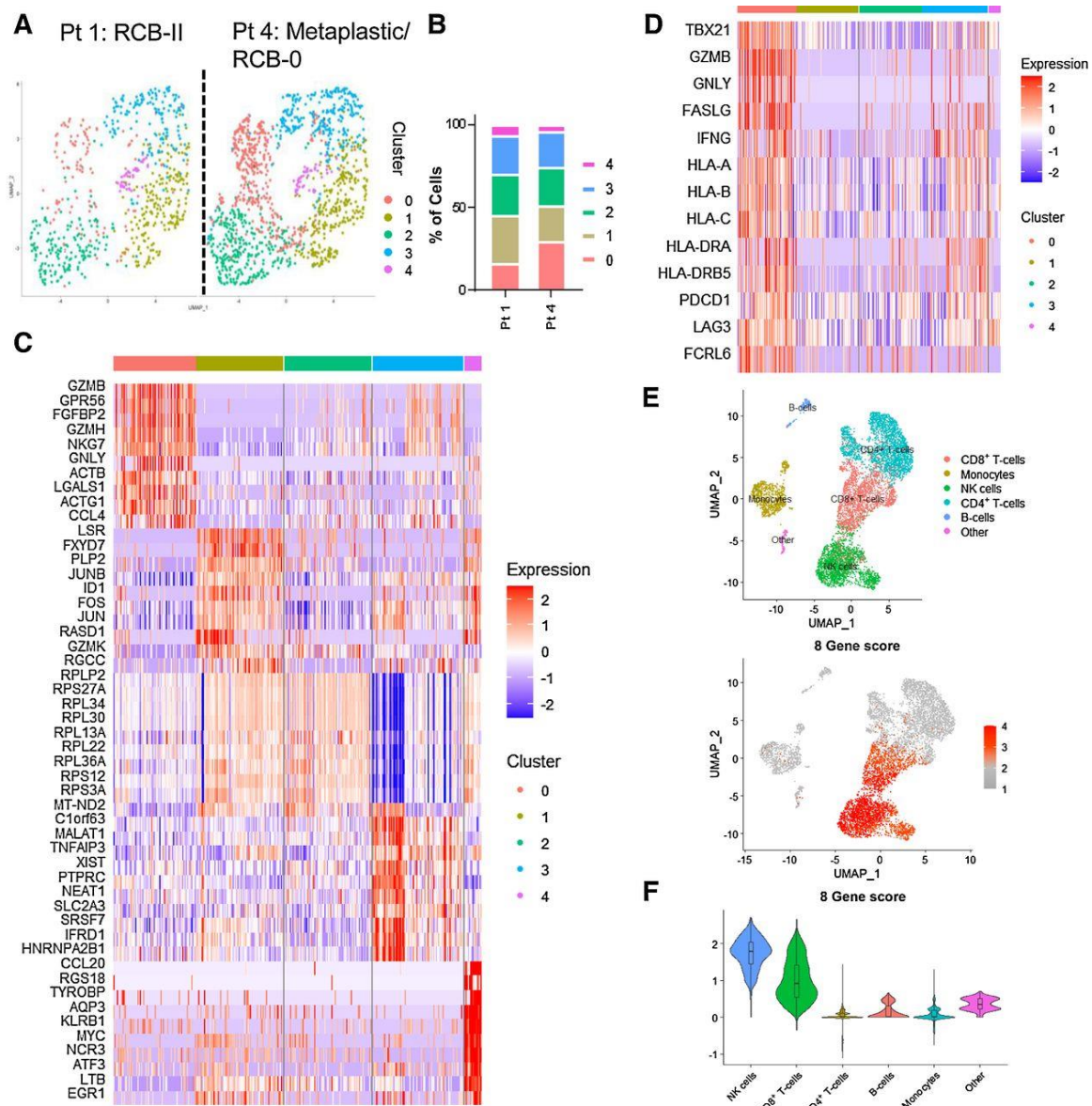
Figure 4.5. scRNAseq of CD8+ PD-1HI peripheral T cells from 2 patients with TNBC after NAC demonstrate high expression of cytolytic markers. A, UMAP plots of 1,964 PD-1HI CD8+ peripheral T cells across 2 patients (672 and 1,292 respectively) are shown. Five clusters (0–4) were defined. **B,** Percent of cells sequenced comprising each cluster are plotted. **C,** Heatmap identifying top 10 most differentially expressed transcripts across clusters. **D,** A selection of genes defining cluster 0 are highlighted. Data depicted include combined cells from both Pt. 1 and Pt. 4. **E,** UMAP plots of 7,062 PBMCs from 2 patients with TNBC (3,525 cells from Pt. 4 and 3,537 cells from Pt. 5). Cell type annotations are defined by SingleR. The 8-gene score is defined by expression of *FGFBP2 + GNLY + GZMB + GZMH + NKG7 + LAG3 + PDCD1 – HLA-G*. **F,** Violin plots showing expression of the 8-gene score by cell type. Overlaid box plots show mean and interquartile range for each cell type.

These data led us to propose two competing hypotheses: 1) Cluster 0 genes, reflective of cytolytic CD8+ T cells, are a positive prognostic factor reflective of robust anti-tumor immunity as evidenced by their enrichment in the metaplastic TNBC patient with pCR; or 2) Cluster 0 genes are reflective of ongoing disease including the micrometastatic component that cannot be sampled from the primary tumor. The second hypothesis is supported by the observations that pCR is less prognostic of RFS and OS in metaplastic disease (Han et al., 2019; Kaminsky, 2012) and that rates of recurrence following chemotherapy are higher for metaplastic disease than non-metaplastic TNBC (Aydiner et al., 2015; Bae et al., 2011; Han et al., 2019). Interestingly, matrix-producing metaplastic breast cancer (Pt. 4) has been shown to be associated with pCR to NAC, but often can still recur despite pCR (Al-Hilli et al., 2019; Han et al., 2019). Follow-up for this individual patient was immature at the time of reporting, and thus recurrence, and therefore presence of micrometastatic disease at the time of sampling, cannot be ruled out.

To gain a deeper understanding of cluster 0 genes, we performed additional single cell RNA sequencing on post-NAC whole PBMCs from two TNBCs patients with pCR (patient 4, described above, and patient 5, not used in any prior analysis). UMAP was used for dimensionality reduction on Harmony-normalized samples. SingleR was used to computationally assign cell type annotations (**Figure 4.5E**). Low confidence cell type annotations were collapsed into the category "other" and make up a minor fraction of cells (**Supplementary Figure S4.12C**). Seven genes enriched in cluster 0 (*PDCD1, NKG7, LAG3, GZMH, GZMB, GNLY, FGFBP2*) and one gene strongly de-enriched in patient 4 (*HLA-G*) were chosen as an 8 gene signature for downstream applications, including validation in a larger cohort of patients (**Supplementary Figure S4.12A-B**). Expression of this 8 gene score (*PDCD1 + NKG7 + LAG3+ GZMH + GZMB + GNLY + FGFBP2 – HLA-G*) was the highest in CD8+ T cells (as expected, given the derivation from PD-1^{HI}C8+T cells) and natural killer cells (**Figure**

4.5F). This finding was similar in both patients (**Supplementary Figure S4.12D**). Strong expression of this signature in post-NAC whole PBMCs led us to test whether this signature was predictive of response in archived whole blood samples from breast cancer patients.

Cytolytic gene expression signatures are present in blood and associated with increased likelihood of recurrence

To determine whether cytolytic signatures representative of cluster 0 genes were associated with disease outcome, we evaluated archived whole blood from a series of 58 breast cancer patients. All samples were collected within 14 days preceding surgical resection for primary breast cancer, with 34 samples having received NAC, in addition to 24 samples from untreated patients. As described above, a series of eight genes enriched in cluster 0 (*PDCD1, NKG7, LAG3, GZMH, GZMB, GNLY, FGFBP2, HLA-DRB5*), one gene enriched in Pt 1 (RCB-II) over Pt 4 (pCR; *HLA-G*; **Supplementary Figure S4.12**), and three normalization control genes (*PTPRC, RPL13a, TBP*; Ledderose et al., 2011) were selected for a 12-gene custom NanoString gene expression analysis. HLA-G has been described as an immune checkpoint which can dampen anti-tumor immune responses (Carosella et al., 2015; Dumont et al., 2019; Lin & Yan, 2018), and thus we expected *HLA-G* expression to be inversely correlated with the other selected genes, as is the case in our scRNAseq dataset. One of these genes performed poorly (*HLA-DRB5*), likely due to frequent polymorphisms in the gene leading to highly variable probe binding and was therefore omitted from further analysis. Information on the presence of pCR/RD at surgery, ER/PR/HER2 status, and clinical follow-up (recurrence at 1000 days after surgery for RD patients) was collected (**Table 4.2**).

Table 4.2: Demographic information for peripheral blood cohorts

Blood Cohort, n (%)		
	Vanderbilt	**DFCI**
Total	58	30
IHC Subtype		
ER+	27 (46.55%)	27 (90%)
PR+	26 (44.82%)	27 (90%)
HER2+	17 (29/31%)	0 (0%)
TNBC	21 (36.21%)	0 (0%)
Response		
No NAC	24 (41.38%)	0 (0%)
pCR	10 (17.24%)	1 (3.33%)
RD	24 (41.38%)	29 (96.67%)
RCB I not recur		3 (10%)
RCB I recur		2 (6.67%)
RCB II not recur		7 (23.33%)
RCB II recur		4 (13.33%)
RCB III		13 (43.33%)
NAC		
No Taxane	7 (12.07%)	0 (0%)
Taxane	27 (46.55%)	30 (100%)
No NAC	24 (41.38%)	0 (0%)

Nearly all tested genes demonstrated a pattern supporting the hypothesis that gene expression in whole blood is associated with ongoing disease, being highest (or lowest in the case of HLA-G) in untreated patients (who have ongoing tumor burden by virtue of not having received therapy prior to surgery) and those with RD compared to those with pCR. However, it is important to note that there is a high degree of heterogeneity in the untreated patients, possibly reflecting heterogeneity in tumor size, strength of anti-tumor immune response at

baseline, or anti-tumor response following systemic therapy. Furthermore, among patients with RD, higher expression (or lower in the case of HLA-G) tended to be observed in patients who had early recurrences in the first 3 years following surgery (and thus may have had micrometastatic disease at the time of surgery). Several of these genes (FGFBP2, GNLY, PDCD1, LAG3, and NKG7) were also significantly differentially expressed or approached statistical significance across the outcome groups (Kruskal-Wallis test). Comparisons were particularly striking between the group of patients with RD who experienced early disease recurrence and the group with pCR following NAC (post-hoc Dunn test; **Figure 4.6A**). A composite score of PDCD1 + NKG7 + LAG3+ GZMH + GZMB + GNLY + FGFBP2 – HLA-G also demonstrated statistically significant associations with presence of ongoing disease (**Figure 4.6B**). Interestingly, expression levels of these genes did not always correlate with one another, indicating heterogeneity in their expression patterns and some degree of independence (**Figure 4.6C**). Trends in gene expression were similar for TNBC and non-TNBC patients, but in-depth subgroup analyses were limited by sample size. Thus, peripheral anti-tumor immunity in blood may be a useful measure of persistent residual primary or micrometastatic disease and could identify patients likely to benefit from additional therapy.
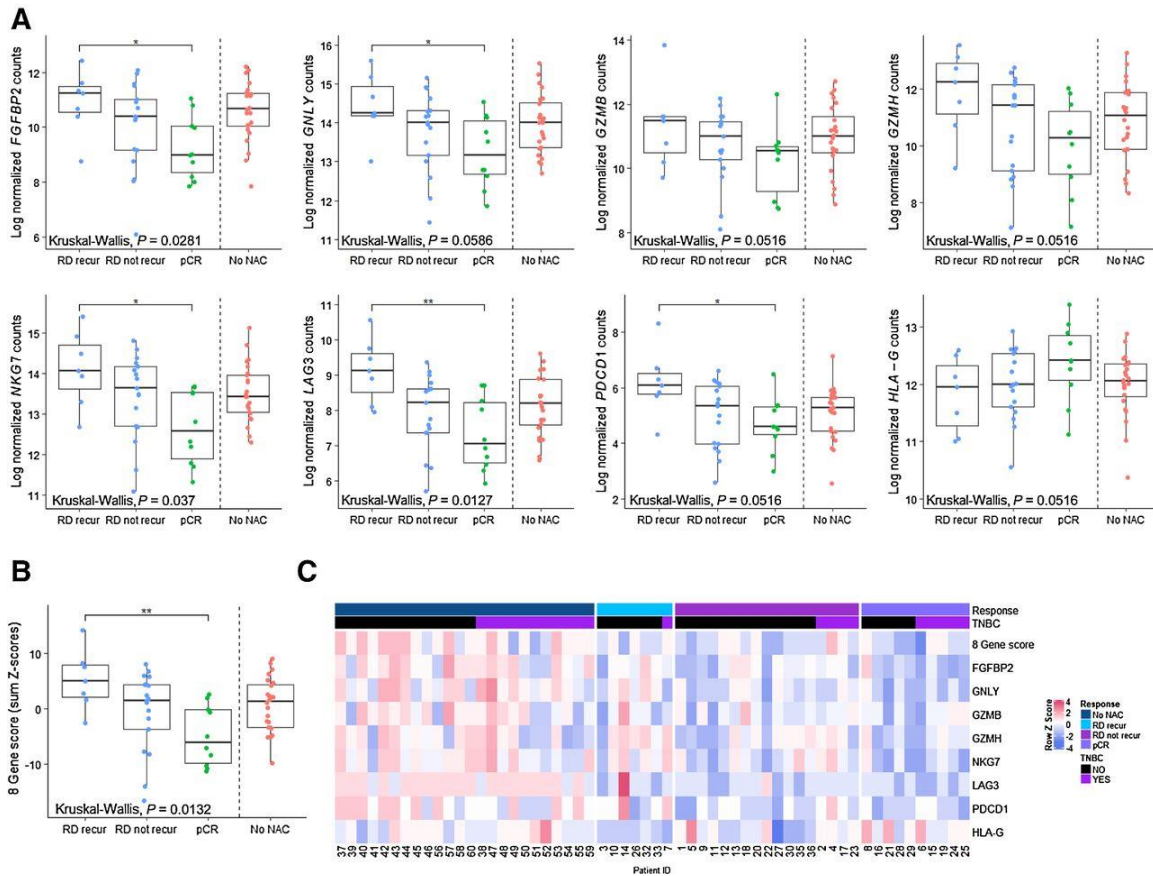
Figure 4.6. An 8-gene activated T-cell signature derived from whole blood at surgery is associated with pCR and prognosticates recurrence in patients with RD. A, Individual gene plots of 8 analyzed genes by nanoString from RNA derived from whole blood sampled within 14 days leading up to definitive surgery. Datapoints are stratified by untreated patients (No NAC), those experiencing pCR (pCR), those with RD that did not recur (RD not recur), and those with RD that recurred (RD recur) within 3 years after surgery. Box plots represent the interquartile range. *P* values represent Kruskal–Wallis tests. *, *P* < 0.05 by *post hoc* Dunn test. **B,** A composite gene signature derived as *PDCD1 + NKG7 + LAG3 + GZMH + GZMB + GNLY + FGFBP2 – HLA-G* (sum of Z-scores), stratified by outcome, as in **A**. **C,** Heatmap showing row standardized (Z-score) gene expression for genes assayed across all patients.

To extend these findings, we evaluated gene expression in a second cohort of archival blood from breast cancer patients treated at DFCI (n=30), with blood collected in the interlude between completing NAC and definitive surgery. Notably, this cohort had differing baseline characteristics (summarized in **Table 4.2**). All of the patients were hormone receptor positive (a subtype known to have a lower pCR rate than TNBC patients), HER2 negative, and all were treated with bevacizumab. Intriguingly, expression of the 8 gene composite score was also correlated with enhanced disease burden in this cohort, being highest in patients with RCB III (regardless of recurrence) and lowest in patients with RCB 0/I/II who did not have a breast cancer recurrence within 3 years (**Supplementary Figure S4.13**). These findings suggest that peripheral blood gene expression may be predictive of response in diverse groups of breast cancer patients.

Discussion

With the recent approval of immunotherapy in combination with chemotherapy in mTNBC, and promising early results in the neoadjuvant setting, an improved understanding of how chemotherapy re-shapes anti-tumor immunity, both in the tumor and in the peripheral compartment, is needed. Perhaps the most widely studied marker to approximate anti-tumor immunity is sTILs, which are predictive of improved NAC response when measured in the primary untreated tumor and are prognostic of good outcomes in the residual disease of patients lacking pCR. Moreover, sTILs have primarily been a useful biomarker in TNBC as opposed to hormone receptor-positive cancers, but this inference is complicated by the routine use of endocrine-targeted agents in the adjuvant setting, that can impact post-surgical outcomes. However, this likely confounder leaves space for a biological contribution, as numerous differences between molecular and clinical subtypes exist. Even when considering

only TNBC, quantification of sTILs is an imperfect biomarker, which does not precisely inform on the immuno-biology of the tumor.

In this study, we present a molecular analysis of the TIME in response to NAC in 83 breast cancer patients, specifically focusing on patients lacking a pCR, as these patients have worse outcomes. We found that changes in tumor immunity seem to be most prevalent in TNBC, often resulting in decreases in expression of immune-related genes. However, an upregulation of immune-related gene expression in tumors following NAC was associated with a strikingly improved outcome after surgery, specifically in TNBC. Of these genes, those involved in cytotoxic effector cells were among the most robustly associated with outcome. Furthermore, we found that cytokines expressed by PD-1^{HI} CD8+ T cells in the peripheral blood were increased dramatically in TNBC patients following NAC.

Analysis of TCR clonotypes infiltrating into tumors suggested that chemotherapy may preferentially increase the recruitment of new T cell clones into the tumor, rather than expanding the T cells already present. This effect was consistent with that observed in the peripheral blood, where PD-1^{HI} CD8+ T cells, while highly clonal compared to PD-1^{NEG} cells, did not substantially change in clonality during NAC; these observations reflect a lack of clonal expansion in response to NAC, as we found in the TIME.

Assessment of peripheral blood represents a unique opportunity to monitor anti-tumor immunity through minimally invasive means. Using scRNAseq, we identified a population of cytolytic effector T cells in blood that expressed elevated levels of exhaustion/checkpoint genes. A gene expression signature derived from this population was used to test the hypothesis that these highly cytolytic, but potentially exhausted cells may be reflective of an ongoing disease process, and therefore a peripheral approximation of disease burden. This hypothesis was confirmed in two validation sets totaling 88 breast cancer patients and serves as a proof-of-principle for the use of this signature as a possible biomarker of outcome.

Importantly, there has been a paucity of studies looking at the effect of chemotherapy on peripheral blood, with little data on disease outcomes (Foulds et al., 2018). This study provides a novel assessment and framework for an improved understanding of how chemotherapy alters anti-tumor immunity both in the TIME and the peripheral compartment. These data represent a unique opportunity to better understand patient populations most likely to benefit from the addition of immunotherapy to chemotherapy, particularly in the neoadjuvant setting. Furthermore, our findings demonstrating the association of expression of key cytolytic and immune-activation genes in the peripheral blood with presence of residual disease and recurrence represent a possible biomarker platform. Peripheral gene expression signatures may identify high-risk populations with potentially exhausted T cells and either primary or micrometastatic disease who may benefit from additional immunotherapeutic strategies.

Chapter V will build on the ideas introduced here with a focus on changes in blood gene expression and cell type abundance over the course of NAC. Chapter V will also explore that idea of using blood as a site of biomarker development for predicting breast cancer patient outcomes.

CHAPTER V

Peripheral blood monocyte abundance predicts outcomes in breast cancer patients[4]

Abstract

Biomarkers of response are needed in breast cancer to stratify patients to appropriate therapies and avoid unnecessary toxicity. We used peripheral blood gene expression and cell type abundance to identify biomarkers of response and recurrence in neoadjuvant chemotherapy treated breast cancer patients. We identified a signature of interferon and complement response that was higher in the blood of patients with pathologic complete response. This signature was preferentially expressed by monocytes in single cell RNA sequencing. Monocytes are routinely measured clinically, enabling examination of clinically measured monocytes in multiple independent cohorts. We found that peripheral monocytes were higher in patients with good outcomes in four cohorts of breast cancer patients. Blood gene expression and cell type abundance biomarkers may be useful for prognostication in breast cancer.

Significance: Biomarkers are needed in breast cancer to identify patients at risk for recurrence. Blood is an attractive site for biomarker identification due to the relative ease of longitudinal sampling. Our study suggests that blood-based gene expression and cell type abundance biomarkers may have clinical utility in breast cancer.

Introduction

Neoadjuvant chemotherapy (NAC), the standard of care for many breast cancer patients, is known to have systemic immunologic effects and is increasingly being used in clinical trials in combination with immunotherapeutics. Currently, there are few biomarkers to predict NAC or immunotherapy response, although response to NAC is known to be associated with long term outcome in breast cancer (Liedtke et al., 2008). Thus, biomarkers are needed to identify patients who will benefit from combination therapy compared to those who are likely to respond to NAC alone, and thereby avoid the added risk of toxicity and financial burden. Peripheral blood is an attractive site of biomarker development due to the relative ease of longitudinal sampling. In chapter IV, we show that high expression of a cytotoxicity gene signature in the blood following NAC is associated with the presence of residual disease (RD) and future breast cancer recurrence, demonstrating the feasibility of using blood-based transcriptional biomarkers (Axelrod et al., 2020). Herein, we use peripheral blood collected following NAC (if received) and prior to surgery as a tool for biomarker development, using both gene expression and cell type abundance analyses in multiple independent cohorts of breast cancer patients (**Figure 5.1A; Table 5.1**).

Materials and Methods

Patients. For all cohorts, data use was approved by the relevant ethics committee, institutional review board, and national competent authority and adheres to the ethical principles of the Declaration of Helsinki. For the VICC-1 cohort, clinical and pathologic data were retrieved from medical records under an institutionally approved protocol (VICC IRB 030747). For the VICC-SD cohort, clinical and pathologic data were retrieved from the deidentified synthetic derivative medical record under and institutionally approved protocol (VICC IRB 202207). First, all female patients with International Classification of Diseases, 9th/10th Revision, Clinical Modification (ICD-9/10-CM) billing codes for malignant neoplasm of breast were identified. Next, from this

cohort, patients with at least one breast cancer surgical procedure using Current Procedural

Terminology (CPT) codes and exposure to cyclophosphamide and doxorubicin within 12 months

preceding the surgery date were automatically selected. Finally, the electronic health records of

the selected patients were manually reviewed to extract the VICC-SD cohort used in this study.

To guide the manual chart review process, additional clinical information was automatically

extracted from the SD. This includes breast cancer surgery dates, dates when patients received

cyclophosphamide and doxorubicin, laboratory measurements, other chemotherapy or cytokine-

related medications and date of administration, pathology reports and operative notes. The

GeparNuevo cohort consisted of patients from the placebo arm of the GeparNuevo trial

(registration number NCT02685059)(Massa et al., 2020). The Instituto Valenciano de Oncología

cohort consisted of HR+HER2- patients treated with neoadjuvant chemotherapy. All data use

was approved by the relevant ethics committees.

RNA Sequencing. RNA was extracted from 0.5-2mL of whole blood or processed PBMCs using

the Promega Maxwell RSC simplyRNA Blood kit (AS1380, Promega). Total RNA quality was

assessed using the 2200 TapeStation (Agilent). Library preparation was done with a ribo-

depletion total RNA library preparation kit and 150 bp paired-end sequencing was performed on

the Illumina NovaSeq 6000 targeting an average of 10M reads per sample. Quality control was

evaluated at different levels, including RNA quality, raw read data, alignment, and gene

expression. Raw RNA-seq paired-ends were mapped to the human reference genome hg19

using STAR 2.7.3. Raw reads count matrix was calculated by featureCounts and used for

downstream analysis. 25 genes were removed from the RNA sequencing analysis and

transcripts-per-million (TPM) calculation due to over representation. These genes represent red

blood cell contamination of the PBMC. The removed genes are: "RN7SL1", "RN7SL2","HBA1",

"HBA2", "HBB", "HBQ1", "HBZ", "HBD", "HBG2", "HBE1", "HBG1", "HBM", "MIR3648-1",

"MIR3648-2", "AC104389.6","AC010507.1", "SLC25A37", "SLC4A1", "NRGN", "SNCA",

"BNIP3L", "EPB42", "ALAS2", "BPGM", "OSBP2". DESeq2 was used to identify differentially

expressed genes and apeglm was used for log fold change reduction (Anders & Huber, 2010; Zhu et al., 2019). GSEA was used to identify pathways using the Molecular Signatures Database hallmark gene sets (Korotkevich et al., 2016; Liberzon et al., 2015). CIBERSORTx was used in relative mode with 500 permutations and the LM22 reference matrix(Newman et al., 2019). Simplified cell type categories were collapsed as follows: CD4 T cells = Memory activated CD4 T cells + memory resting CD4 T cells + naïve CD4 T cells + T regulatory cells. B cells = Naïve B cells + Memory B cells + plasma cells. NK cells = activated NK cells + resting NK cells. Other Myeloid = M0 macrophages + M1 macrophages + M2 macrophages + activated dendritic cells + resting dendritic cells. Notably, these populations were very low as these are all cell types not commonly seen in the peripheral blood. Granulocytes = activated mast cells + resting mast cells + eosinophils+ neutrophils.

NanoString nCounter Analysis. Gene expression was assessed on the GeparNuevo cohort using a custom NanoString Elements panel to measure PIRS genes according to the manufacturer's standard protocol. Briefly, RNA was extracted from processed PBMC pellets using the Promega Maxwell RSC simplyRNA Blood kit and 50 ng of total RNA was used for input into nCounter hybridizations. Data were normalized according to positive and negative spike-in controls, then endogenous housekeeper controls, and transcript counts were log transformed for downstream analyses. PIRS was calculated as described for RNA sequencing data, using Z-scores.

Statistical analysis. All statistical analyses were performed in R. Single-cell statistical analyses were calculated in R using the Seurat package (Butler et al., 2018; Satija et al., 2015). Shared Nearest Neighbors were calculated using the Harmony reduction, and clusters were identified at a resolution of 0.3. UMAP was performed for visualization, and missing values were imputed using ALRA (Linderman et al., 2018). Cell types were assigned to individual cells using SingleR (Aran et al., 2019). BlueprintEncodeData was used as a reference(Dunham et al., 2012; J. H. A.

Martens & Stunnenberg, 2013). Some heatmaps were generated using the R package Complex Heatmap (Gu et al., 2016). ROC analyses were done in R using the package precrec (Saito & Rehmsmeier, 2017). P-value cut-offs displayed on plots correspond to "ns" equals p>0.05, * equals 0.01<p< 0.05, ** equals 0.001<p<0.01, *** equals 0.0001<p<0.001, **** equals p<0.0001.

Data Availability. The datasets generated during and analyzed during the current study have been deposited in NCBI's Gene Expression Omnibus (GEO) and are accessible through GEO Series accession number GSE201085 (https://www.ncbi.nlm.nih.gov/geo/query/acc.cgi?acc=GSE201085). Code used to generate figures can be found at: https://github.com/MLAxelrod/BC_Blood_Monocytes

Results

Expression of immune related genes in the peripheral blood is associated with good outcome following NAC.

RNA sequencing was performed on whole blood of 53 breast cancer patients after completion of NAC (if received) and prior to definitive surgery (**Figure 5.1A**; n=23 RD, 9 pathologic complete response (pCR), 21 no NAC; Table 5.1). We stratified patients with RD by whether they experienced a breast cancer recurrence (RD-R) or remained free of recurrence for at least three years (RD-nR). Follow-up time was at least three-years for all patients (mean 8.9 years, max 14.5 years), which covers the time period at highest risk for recurrence (Pogoda et al., 2013; Ribelles et al., 2013; van Maaren et al., 2019). Using DeSeq, we identified 1,238 (FDR corrected q-value <0.1) differentially expressed genes between pCR and RD samples (Anders & Huber, 2010). Using gene set enrichment analysis (GSEA), we collapsed differentially expressed genes into pathways using the Molecular Signatures Database hallmark gene sets (Korotkevich et al., 2016; Liberzon et al., 2015). Hallmark Interferon (IFN) Gamma

Response (q-value <0.0001; normalized enrichment score (NES)=3.32), Hallmark Interferon

Alpha Response (q-value <0.0001; NES=3.14), and Hallmark Complement (q-value=0.000111;

NES=2.29) pathways were significantly enriched in the blood of patients experiencing pCR

compared to those with RD (**Figure 5.1B**). No pathways were statistically significantly

upregulated in RD samples relative to pCR samples. To evaluate the genes involved in these

pathways, we identified the leading-edge genes from each pathway (IFN gamma = 49 genes;

IFN alpha = 26 genes; complement = 15 genes) and selected only the unique genes (n=60

genes). There is strong, uniform upregulation of many of these genes in many of the pCR

samples, regardless of TNBC status (**Supplementary Fig. S5.1A**). We combined expression of

these genes into an IFN/complement score, calculated as sum of z-scores divided by number of

genes in the signature (n=60 genes). We compared expression of the IFN/complement score to

the 8 gene cytotoxic score described in chapter IV (*FGFBP2 + GNLY + GZMB + GZMH + NKG7

+ LAG3 + PDCD1 – HLA-G*; Axelrod et al., 2020). No genes overlapped between the two

signatures. Samples with the highest expression of the IFN/complement had low expression of

the cytotoxic score and tended to be pCR samples. Conversely, those with highest expression

of the cytotoxic score tended to have low expression of the IFN/complement score and be RD

samples (**Figure 5.1C**). A combination peripheral immunologic response score (PIRS) of

IFN/complement score minus cytotoxic score had improved predictive power compared to either

signature alone (p= 0.006 for pCR vs RD-R, p = 0.01 for pCR vs RD-nR, Wilcoxon tests with

FDR corrections; **Figure 5.1D**). The same trends were observed when examining TNBC, ER+

or HER2+ only patients (**Supplementary Fig. S5.1B**). To examine which cell types

predominately express each signature, we used single cell RNA sequencing data from whole

peripheral blood mononuclear cells (PBMCs) from two breast cancer patients post-NAC, prior to

surgery (Axelrod et al., 2020). These two patients were not included in any other analyses.

Expression of the cytotoxic score was the highest in CD8+ T cells and natural killer cells, while

the IFN/complement score was the highest in a subset of monocytes. There was very little co-

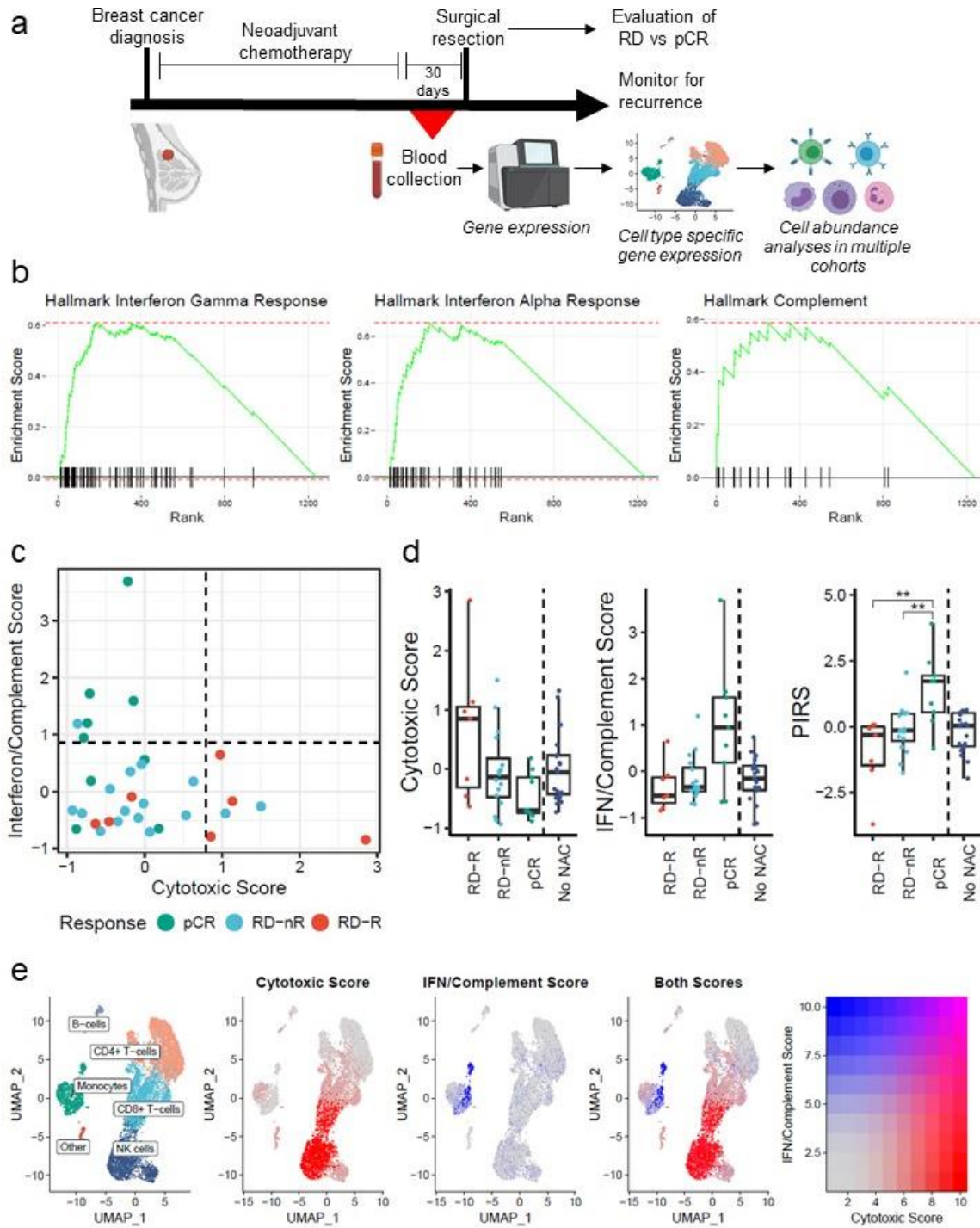expression of the signatures across cells (**Figure 5.1E; Supplementary Fig. S5.1C**).

Figure 5.1: Expression of immune related genes in the peripheral blood is associated with good outcome following NAC. A) Schematic describing blood collection timing and downstream analyses. B) GSEA plots for gene sets enriched in blood of patients with pCR

relative to RD. C) Expression of IFN/Complement and cytotoxicity scores is shown for each sample. D) Cytotoxic, IFN/complement, and combined peripheral immunologic response scores (PIRS; IFN/Complement score minus cytotoxic score) are shown for each sample, stratified by outcome. Box plots show the median, first and third quartiles. P-values represent FDR corrected Wilcox tests. E) Single cell sequencing of PBMCs shows cell type specific expression of each score. Cytotoxic score is shown in red. IFN/Complement score is shown in blue. Co-expression would be shown in pink.

Table 5.1: Cohort Descriptions

| VICC-1	
Response	
No NAC	21
pCR	9
RD-nR	16
RD-R	7
Receptor Status	
TNBC	17
HR+HER2+	9
HR+HER2-	19
HR-HER2+	8
GeparNuevo	
Response	
RD	18
pCR	23
TNBC	
Yes	41
No	0
Instituto Valenciano	
Metastasis	
Yes	5
No	9
Hormone Receptor +	
Yes	14
No	0
VICC-SD	
Response	
RD	75
pCR	35
Receptor Status	
TNBC	50
HR+HER2+	6
HR+HER2-	44
HR-HER2+	10

Monocytes are most abundant in blood of patients with good outcomes following NAC.

Given the partitioning of the gene expression scores into cell types, we next aimed to identify whether there were differences in cell type abundances between the outcome groups. CIBERSORTx was used to deconvolute relative cell type abundance from the RNA sequencing data (Newman et al., 2019; **Figure 5.2A**). Relative mode normalizes all cell fractions of the cell types in the signature matrix to 100%. Relative monocyte abundance was highest in samples with pCR, intermediate in those with RD, and lowest in samples not receiving NAC (p=0.003 for No NAC vs. pCR, p=0.028 for No NAC vs. RD, p=0.028 for pCR vs. RD, Wilcox tests with FDR corrections for multiple comparisons; **Figure 5.2B**). Naïve B cells were also statistically significantly different across groups, being highest in no NAC samples and lowest in pCR samples (p=0.0009 for No NAC vs. pCR, p=0.0008 for No NAC vs. RD, p=0.043 for pCR vs. RD, Wilcox tests with FDR corrections for multiple comparisons; **Supplementary Fig. S5.2A**). However, only monocytes followed the trend of increases from no NAC to RD-R to RD-nR to pCR (**Supplementary Fig. S5.2B**). The trend of higher monocytes in patients with pCR relative to RD was also observed when examining TNBC, ER+ or HER2+ only patients (**Supplementary Fig. S5.2C**).

Monocytes comprise a heterogenous population and associations of differing monocyte subpopulations have been associated with both good and poor outcomes in cancer (Canè et al., 2019; Liu et al., 2018; A. Martens et al., 2016; Olingy et al., 2019; Valdés-Ferrada et al., 2020; L. Wang et al., 2020; Wong et al., 2012). The majority of circulating monocytes have a classical phenotype, characterized by CD14 expression and lack of CD16 expression (Wong et al., 2012). We found that gene expression of classical monocyte associated genes (i.e., *CD14* p=0.05 *CCR2* p=0.013, for pCR vs RD-nR two-tailed Wilcox tests with FDR corrections for multiple comparisons) was significantly higher in the blood of patients with pCR, whereas there was no significant difference in expression of genes associated with non-classical monocytes

(i.e., *FCGR3A*, *FCGR3B* which are the genes encoding CD16; **Figure 5.2C**).

The routine nature of clinically measuring total monocytes made monocyte values an intriguing metric for further study. We reviewed electronic medical records and extracted monocyte values from complete blood counts for patients receiving NAC in this cohort. 23 out of 32 (72%) of NAC-treated patients (n=7 pCR, 12 RD-nR, 4 RD-R) had a complete blood count with differential (which includes monocyte values) in the 30-day interval prior to surgery (following completion of NAC), indicating the commonality of collecting this information clinically. Clinically measured relative monocyte values are reported as percent of circulating leukocytes. Clinically measured monocyte values were significantly positively correlated with monocyte values inferred by CIBERSORTx (R=0.51, p=0.012; **Supplementary Fig. S5.2D**), even though monocyte values were not always collected on the same day as the blood for RNA sequencing (though in the same 30-day window). Post-NAC, but not pre-NAC, clinically measured monocytes were significantly higher in patients with pCR compared to those with RD (p=0.0197, one-tailed Wilcoxon for RD vs pCR; **Figure 5.2D**; p=0.018 one-tailed Wilcoxon with FDR correction for RD-R vs pCR; **Supplementary Fig. S5.2E**). The change in monocytes from pre- to post-NAC was not statistically significantly different for patients with RD or pCR, though the monocytes increased from pre- to post- NAC for most patients with pCR (**Supplementary Fig. S5.2F)**.
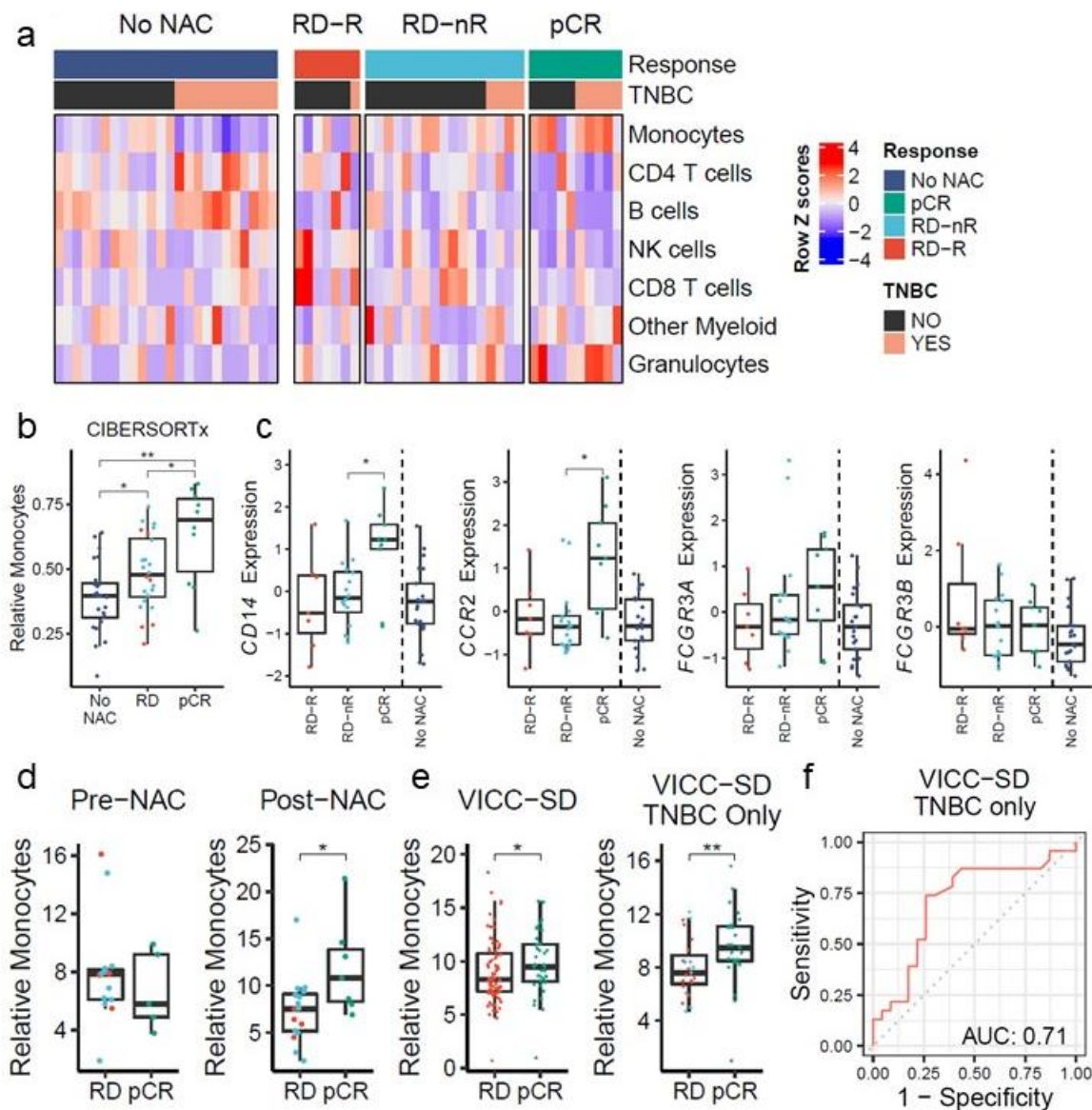
Figure 5.2: Monocytes are most abundant in blood of patients with good outcomes following NAC. A) Heatmap showing row standardized (z-score) of CIBERSORTx inferred cell type abundance. Most abundant cell types are listed first. B) CIBERSORTx monocyte values, stratified by outcome. C) Row standardized (z-score) expression of key monocyte related genes in VICC-1 RNA sequencing cohort. D) Clinical lab values for relative monocytes pre- and post-NAC. E) Relative monocytes in full and TNBC only synthetic derivative cohort. Box plots show the median, first and third quartiles. P-values represent one-tailed Wilcox tests (FDR corrected where applicable). F) Receiver operating characteristic curve for differentiating pCR vs RD in the VICC-SD TNBC only cohort.

Next, we sought to assess whether monocyte abundance was associated with outcome

in independent cohorts. Higher monocytes were also seen with pCR in an additional cohort of

41 TNBC patients (n=18 RD, 23 pCR; placebo arm of the GeparNuevo study; Table 5.1),

though this association was not statistically significant (p=0.0638 for absolute monocyte counts,

p=0.186 for relative monocyte frequencies, one-tailed Wilcoxon; **Supplementary Fig. S5.3A**;

Massa et al., 2020). In this TNBC only dataset PIRS, measured by NanoString, was not

associated with outcome, indicating independence of monocytes and PIRS measurements

(**Supplementary Fig. S5.3B**). In an additional independent cohort of 14 hormone receptor

positive (HR+) HER2- breast cancer patients from the Instituto Valenciano de Oncología,

monocytes tended to be higher in patients without metastatic recurrence, with at least four years

of follow-up time for each patient (p=0.0949, one-tailed Wilcoxon; n= 5 with metastasis, 9

without metastasis; **Supplementary Fig. S5.3C**; Table 5.1). Using a de-identified medical

record database called the synthetic derivative (SD), we identified 110 breast cancer patients

(VICC-SD; n=35 pCR, 75 RD; Table 5.1) who had been treated with NAC, had a breast surgery,

and had a monocyte value within 30 days prior to surgery. In the VICC-SD cohort, relative

frequencies of monocytes were statistically significantly higher in patients with pCR compared to

those with RD (p=0.037 one-tailed Wilcoxon; **Figure 5.2E**). This effect was more pronounced

when considering only the TNBC patients (p=0.0074, one-tailed Wilcoxon; n=50), which may be

reflective of underlying TNBC-specific biology, or the more uniform treatment options for TNBC

(chemotherapy rather than targeted therapy agents; p=0.046 for RD-R vs pCR, one-tailed

Wilcoxon with FDR correction; **Supplementary Fig. S5.3D**). In all cohorts, patients who had

received cytokine-support products (i.e., granulocyte colony-stimulating factor) in the 30-day

window prior to surgery were excluded from analysis as this may affect monocyte counts. To

summarize our findings, we performed receiver operating characteristic (ROC) analyses on all

key findings. Area under the curve (AUC) for ROC analyses are summarized in table 5.2. Where

possible, we calculated the AUC for differentiating pCR vs. RD as well as overall good outcome

(pCR and RD-nR) with poor outcome (RD-R), which may be more clinically useful. A

representative ROC curve for using monocytes to differentiate pCR vs RD in the VICC-SD

TNBC only cohort is shown in **Figure 5.2F**. Taken together, these data suggest that higher

blood monocyte levels post-NAC may be indicative of superior outcomes in breast cancer

patients.

Table 5.2: AUC Analyses

Metric	Method	Cohort	AUC (pCR vs RD)	AUC (no recurrence vs recurrence)
PIRS	RNA Sequencing	VICC-1	0.86	0.75
PIRS	NanoString	GeparNuevo	0.41	NA
Monocytes	CIBERSORTx (RNA sequencing)	VICC-1	0.74	0.70
Monocytes	Clinical	VICC-1	0.65	0.68
Monocytes	Clinical	VICC-SD	0.61	NA
Monocytes	Clinical	VICC-SD TNBC only	0.71	0.66
Monocytes	Clinical	Instituto Valenciano	NA	0.73 * (metastasis vs no)
Monocytes	Clinical	GeparNuevo	0.64 (absolute); 0.58 (relative)	NA

Discussion

Peripheral blood gene expression scores and cell type abundance may be useful

biomarkers of NAC response and outcomes in breast cancer. We identified an immunologic

gene signature (PIRS) that was highest in patients with the best outcomes (pCR) and lowest in those with the worst outcome (RD with recurrence). However, PIRS was not associated with outcome in a separate cohort of TNBC only patients. There are several possible reasons for this difference including that the GeparNuevo cohort consisted of the control arm of a clinical trial and these patients received a more uniform chemotherapy regimen (nanoparticle albumin-bound paclitaxel followed by epirubicin and cyclophosphamide). Ten patients from this cohort were excluded from our analyses due to proximal treatment with cytokine-support products (i.e., granulocyte colony-stimulating factor), relative to only one excluded in the VICC-1 cohort. The VICC-1 patients were treated as routine clinical standard of care and included patients of all histologic subtypes. Additional studies are needed to test whether PIRS or other gene expression scores may be useful biomarkers in breast cancer patients. Additional studies will also be needed to identify and standardize appropriate cutoffs for gene expression scores.

Higher peripheral monocytes, a standard clinical assay performed on most breast cancer patients, was associated with improved patient outcomes (pCR or lack of recurrence). The association of higher monocytes with improved outcomes was observed in four independent breast cancer patient cohorts, though this difference was only statistically significant ($p < 0.05$) in two of four cohorts. Circulating monocyte subpopulations have previously been associated with both good and poor outcomes in several cancer types (A. Martens et al., 2016; Meyer et al., 2014; Olingy et al., 2019; Schauer et al., 2016). Interestingly, a prior study in breast cancer patients showed that a stronger interferon gamma response in monocytes was associated with lack of relapse, in line with our results (L. Wang et al., 2020). Several studies have also seen an increase in circulating monocytes following chemotherapy in breast and other cancer types, and this increase has variably been statistically or numerically associated with better outcomes (Liu et al., 2018; Schauer et al., 2016; Valdés-Ferrada et al., 2020). Given that blood monocytes may increase following chemotherapy in multiple tumor types and in our data higher monocytes

are associated with better outcomes regardless of breast cancer histologic subtype, we hypothesize that the increase in monocytes may represent post-chemotherapy hematopoietic regeneration, which is likely to be more reflective of the patient's immune and hematopoietic system than tumor-intrinsic biology. However, this idea remains to be tested. Additional efforts are needed to explore whether there might be a causal link between chemotherapy induced monocyte mobilization and improved response. As blood is sampled following completion of NAC, it is unknown how stage of disease, nodal status, or other clinicopathologic variables may affect gene expression or cell type abundances. Taken together, these results suggest that peripheral blood biomarkers following NAC may be useful in predicting long-term outcome. Future work will explore the utility of peripheral blood biomarkers in predicting immunotherapy response.

Chapter VI

Conclusions and Future Directions

Pathogenesis of ICI-myocarditis

In chapters II and III above, I describe our work on the pathogenesis of ICI-myocarditis. First, we characterized a novel murine model of ICI-myocarditis. *Pdcd1-/-Ctla4+/-* mice on the C57BL/6 background develop fulminant myocarditis which is characterized by infiltration of CD8+ T cells, cardiomyocyte death, arrythmias, and preserved ejection fraction, similar to what is seen in patients with ICI-myocarditis. Treatment of the mice with abatacept, an FDA approved recombinant CTLA-4-Ig protein, abrogated myocarditis and rescued survival. Early clinical data, in the form of case reports, suggests that abatacept may be a promising treatment for patients (J.-E. Salem et al., 2019; Wei et al., 2020).

Next, I aimed to further characterize the T cells infiltrating the myocardium in our murine model. Using single cell RNA/TCR sequencing, I found that CD8+ T cells are highly activated and have highly clonal TCRs. CD8+ T cells are required for disease pathogenesis. Treatment with anti-CD8, but not anti-CD4, depleting antibodies rescues survival in the mice. Adoptive transfer of splenocytes from mice with myocarditis, but not splenocytes from which CD8 cells were depleted, recapitulates myocarditis in immunodeficient recipient mice. I next aimed to discover what antigen the clonal CD8+ T cells were recognizing. I found that three clonal TCRs, derived from independent mice, recognize epitopes on alpha-myosin, a heart-specific protein not expressed during T cell development in the thymus.

Aiming to test the relevance of alpha-myosin as an autoantigen in humans, I found that PBMCs from healthy donors or patients with ICI-myocarditis expanded in the presence of alpha-myosin peptides. TCR sequencing showed overlapping TCRs between the alpha-myosin expanded blood and the diseased hearts in patients with ICI-myocarditis. This suggests that alpha-myosin may be a relevant disease antigen in ICI-myocarditis, though additional studies

are needed. This study was limited by the paucity of available samples from human patients with ICI-myocarditis.

There are many possible future directions which follow from the identification of alpha-myosin as an autoantigen in myocarditis. The question still remains why some patients develop ICI-myocarditis and others do not. An interesting possibility is that some tumors may aberrantly express alpha-myosin, leading to the development of tumor-reactive T cells against alpha-myosin, which then may also target the heart. This idea is supported by preliminary data from one of the earliest identified patients with ICI-myocarditis where RNA sequencing showed muscle-specific transcripts, including alpha-myosin, in the tumor (Johnson et al., 2016). One way of partially investigating this hypothesis would be to overexpress alpha-myosin in a murine cancer model, treat the mice with ICIs and monitor for myocarditis or increased frequencies of alpha-myosin specific T cells (i.e., using a tetramer).

Another possible risk factor for ICI-myocarditis, which may be related to alpha-myosin expression, is what HLA alleles a patient carries. It is possible that some HLA alleles have higher affinity for alpha-myosin peptides than others and that this may modify disease risk. HLA types have previously been associated with response and toxicity to ICIs (Chowell et al., 2018; Hasan Ali et al., 2019; Naranbhai et al., 2021). Larger patient cohorts will be needed in order to have sufficient statistical power to test this hypothesis.

Another future direction would be to identify more exact TCR-epitope-MHC combinations in patients with ICI-myocarditis. This would permit the development of tetramers and the characterization of the frequency of alpha-myosin specific T cells in the blood, and ideally, also diseased tissues (where fresh samples are available). It is unknown whether patients susceptible to ICI-myocarditis might have increased frequencies of alpha-myosin specific T cells in the peripheral blood. As we were able to easily expand blood from all three healthy donors with alpha-myosin peptides, this suggests that the presence of alpha-myosin specific T cells in

106

the periphery is likely to be quite common.

An interesting approach to determining what tolerance mechanisms are critical to protect cardiomyocytes would be to develop a human *in vitro* system. Alpha-myosin specific T cells could be expanded as described in chapter III. Autologous cardiomyocytes could be generated using induced pluripotent stem cell approaches from skin fibroblasts. It could then be tested what stimuli are needed in order for the alpha-myosin specific T cells to attack and destroy the autologous cultured cardiomyocytes. Different stimuli could include ICIs, cytokines, and other drugs. Immuno-inhibitory drugs could also be tested in this system. Though an *in vitro* system cannot fully recapitulate what happens *in vivo*, this system would have the advantage of being fully human in order to model the human toxicity.

Another possible risk factor for ICI-myocarditis may be mutations in genes associated with immune tolerance, such as immune checkpoint genes. Genetic loss of *CTLA4* in humans has a variable clinical presentation which can include immune dysregulation (Kuehn et al., 2014; Schubert et al., 2014; Schwab et al., 2018). It is unknown whether mutations in checkpoint genes may contribute to risk of ICI-myocarditis or other irAEs. This could be addressed using whole exome sequencing on tissues from patients with ICI-myocarditis (and potentially other irAEs) compared to patients treated with ICIs who did not develop myocarditis (or other toxicities).

Another intriguing area of future study is the question of why *Pdcd1-/-Ctla4+/-* mice specifically develop myocarditis. It also remains to be studied whether this phenotype is unique to the C57BL/6 background or whether *Pdcd1-/-Ctla4+/-* mice of other strains would also develop myocarditis. The answer to this query may provide insights into why myocarditis develops (i.e., is there something unique about C57BL/6 mice or is this phenomenon common to all *Pdcd1-/-Ctla4+/-* mice, regardless of strain?). It appears that peripheral tolerance may be particularly important for antigens where central tolerance is impaired (i.e., lack of expression in

107

the thymus). An interesting approach to further determine which tolerance associated genes are crucial would be to use a CRISPR screening approach. T cells specific for alpha-myosin could be transduced with a tolerance (or immune checkpoint) CRISPR library and transferred into host mice. T cells could be retrieved and sequenced from any hosts which develop myocarditis. This approach could be adapted to study other toxicities or autoimmune diseases as well.

Alpha-myosin may also be a relevant antigen in other forms of myocarditis. Some other forms of myocarditis are also known to have clonal TCRs (Amancherla et al., 2021). A similar antigen discovery process of cloning TCRs and using autologous LCLs as APCs could be applied to other patients with myocarditis where samples are available. This antigen discovery process, described in chapter III, could be relatively easily adapted for any model system in which a TCR, candidate antigen, and possible MHC molecules are known. Less antigen directed approaches, such as T-scan, could also be applied in this and other disease settings (Kula et al., 2019). A significant limitation to T-scan is the requirement of knowing the HLA type which the cognate antigen is presented on.

The identification of alpha-myosin through lack of expression in the thymus also raises the possibility that other autoantigens may not be expressed in the thymus. It would be interesting to identify other proteins not expressed during thymic selection and determine if they may be autoantigens for relevant disease contexts, possibly in other forms of irAEs, where mechanisms of peripheral tolerance are impaired. However, it should be noted that lack of thymic gene expression does not exclude the possibility of direct antigen capture by APCs which may traffic to the thymus and engage in negative selection.

The very recent FDA approval of the anti-LAG3 antibody relatlimab, also raises the question of whether myocarditis will be seen with wider clinical use of anti-LAG-3 agents. Myocarditis was reported in 1.7% of relatlimab-nivolumab treated patients compared to 0.6% of nivolumab treated patients in a key clinical trial (Tawbi et al., 2022). All myocarditis events

resolved in the relatlimab-nivolumab group, raising the possibility that anti-LAG-3 myocarditis may be less severe than anti-CTLA-4 myocarditis. It would be interesting to further characterize anti-LAG-3 related myocarditis in humans to determine if there are significant differences relative to anti-CTLA-4 myocarditis. *Pdcd1-/-Lag3-/-* mice develop a CD4+ predominant myocarditis, in contrast to the CD8+ predominant disease seen in *Pdcd1-/-Ctla4+/-* mice (Okazaki et al., 2011).

Another possible future direction arises from the difficulties with breeding *Pdcd1-/-* mice. We noticed that often litters would be much smaller than expected. This is in line with the recent publication by McNew et. al. showing that in pregnant female NOD mice (mice which are prone to autoimmune diabetes), fetuses are reabsorbed at a higher rate relative to wild type pregnancies (McNew et al., 2022). The PD-1/PD-L1 pathway is known to play a role in pregnancy tolerance (Meggyes et al., 2020; Zeng et al., 2020). Our murine model could be an interesting model for further investigating the mechanistic role of PD-1. This work would be important in both the understanding of normal pregnancy and in understanding the possible consequences of ICI use during pregnancy for pregnant people with cancer (Andrikopoulou et al., 2021).

Blood-based biomarkers in breast cancer

In chapters IV and V, we have investigated the local and peripheral effects of chemotherapy in breast cancer, with the aim of differentiating chemotherapy responders from non-responders. We found that upregulation of immune-related genes and gene signatures in the TIME following NAC was associated with good outcomes in TNBC. We next aimed to focus on blood, as a site of monitoring systemic immune response, and a potentially less-invasive mechanism of disease monitoring. We found that TCR repertoires from PD-1^{Hi} CD8+ T cells in the blood were more similar to tumor infiltrating T cell TCR repertoires relative to their PD-1 non-

expressing counterparts. We also found that a signature of T cell cytotoxicity, derived from genes expressed by PD-1^{Hi} CD8+ T cells, was highest in the whole blood of patients with worse outcomes, suggesting the possibility of ongoing anti-tumor immunity. We next aimed to further investigate peripheral blood changes. Using RNA-sequencing, we found that interferon response and complement pathways were highest in the blood of patients with good response. We found that these pathways were expressed primarily by monocytes, which are routinely measured clinically in patients receiving cytotoxic chemotherapy. In several independent cohorts of breast cancer patients, we found that blood monocytes, measured following NAC, were highest in patients with better outcomes. Our studies were retrospective in nature and limited by the samples and data available. No pre-treatment blood samples were available to study changes in gene expression over the course of treatment. We were also limited by size of the available cohorts matching our inclusion criteria, leading some of our analyses to be underpowered.

Overall, we hypothesize that the association of higher monocytes with good outcomes reflects robust hematopoietic regeneration following chemotherapy and indicates good overall health which may be independently related to good outcomes. However, further studies are needed to test this hypothesis and determine whether or not monocytes may play any mechanistic role in anti-tumor immunity in this setting. Taken together, these results suggest that peripheral blood biomarkers following NAC may be useful in predicting long-term outcome. Future work will explore the utility of peripheral blood biomarkers in predicting immunotherapy response.

An important future direction which would allow more direct mechanistic investigation, would be the development of a murine model in which peripheral changes could be monitored over the course of therapy. This could be done by using a murine model of breast cancer and longitudinally sampling blood pre and post treatment with chemotherapy. RNA sequencing could

110

be used to investigate changes in blood gene expression over time. Changes in blood gene expression may lead to new candidate biomarkers or drug targets to improve response rates. These could also be tested in a murine system. Flow cytometry could be used to easily and quickly monitor changes in cell type abundances in the blood over the course of therapy. These methods of studying blood in response to therapy in a mouse could be applied to multiple different types of therapy and to multiple cancer models. Cell type abundances could be artificially manipulated (i.e., through adoptive transfer of cells, antibody mediated depletion or genetic manipulation of the murine model system) to determine if different cell types (especially monocytes) may play a causal role in response.

Additionally, this work could be further expanded to encompass response to ICIs in addition to chemotherapy. ICIs are increasingly used in breast cancer, but acquired and intrinsic resistance, through multiple possible mechanisms, is an important limitation (Hanna & Balko, 2021; Taylor & Balko, 2022). Biomarkers for ICI response in BC are especially important given that many patients have very good long-term outcomes with chemotherapy alone. These patients are unlikely to derive additional benefit from exposure to ICI and may face risk of significant harm, both from a risk of irAEs and from potential added financial and treatment burden.

Furthermore, there is a need to identify which patients will experience resistance to ICI therapy and devise new therapeutic strategies to improve outcomes for these patients. Studying peripheral blood changes in response to ICI could be done in both longitudinal patient samples (which may be available from clinical trials) and in murine models. This type of work could also examine blood markers of toxicity, as has been recently shown in melanoma (Lozano et al., 2022).

Final thoughts

This work encompasses two distinct projects. First, we developed a useful murine model to characterize one of the deadliest toxicities associated with anti-cancer immunotherapy. We used this model to learn more about disease pathogenesis. We found that CD8+ T cells are key drivers of myocarditis and that the most clonal T cells recognize alpha-myosin. We found in humans that alpha-myosin expanded T cells overlap with T cells found in the inflamed heart, suggesting alpha-myosin may be an important autoantigen in humans.

Second, we aimed to understand the effects of chemotherapy on local and systemic immunity in breast cancer, with an aim of developing blood-based biomarkers. We found differences in gene expression and cell type abundance in the blood, following treatment with NAC, predicted response to NAC and breast cancer recurrence.

These projects have used different methods and addressed distinct biological questions relating to anti-cancer therapy. The overarching goals of these projects were to provide insights which may help optimize the care of cancer patients. We have provided mechanistic insight into a deadly toxicity and helped further the goal of minimally-invasive biomarker development. Future work will be needed to translate the work described herein into tangible benefits for cancer patients.

References

Adam, K., Iuga, A., Tocheva, A. S., & Mor, A. (2021). A novel mouse model for checkpoint inhibitor-induced adverse events. *PLOS ONE*, *16*(2), e0246168. https://doi.org/10.1371/JOURNAL.PONE.0246168

Adamo, L., Rocha-Resende, C., Lin, C. Y., Evans, S., Williams, J., Dun, H., Li, W., Mpoy, C., Andhey, P. S., Rogers, B. E., Lavine, K., Kreisel, D., Artyomov, M., Randolph, G. J., & Mann, D. L. (2020). Myocardial B cells are a subset of circulating lymphocytes with delayed transit through the heart. *JCI Insight*, *5*(3). https://doi.org/10.1172/JCI.INSIGHT.134700

Al-Hilli, Z., Choong, G., Keeney, M. G., Visscher, D. W., Ingle, J. N., Goetz, M. P., & Jakub, J. W. (2019). Metaplastic breast cancer has a poor response to neoadjuvant systemic therapy. *Breast Cancer Research and Treatment*, *176*(3), 709–716. https://doi.org/10.1007/S10549-019-05264-2/TABLES/2

Amancherla, K., Qin, J., Wang, Y., Axelrod, M. L., Balko, J. M., Schlendorf, K. H., Hoffman, R. D., Xu, Y., Lindenfeld, J., & Moslehi, J. (2021). RNA-Sequencing Reveals a Distinct Transcriptomic Signature for Giant Cell Myocarditis and Identifies Novel Druggable Targets. *Circulation Research*, 451–453. https://doi.org/10.1161/CIRCRESAHA.121.319317

Anders, S., & Huber, W. (2010). Differential expression analysis for sequence count data. *Genome Biology*, *11*(10), R106. https://doi.org/10.1186/gb-2010-11-10-r106

Andrikopoulou, A., Korakiti, A. M., Apostolidou, K., Dimopoulos, M. A., & Zagouri, F. (2021). Immune checkpoint inhibitor administration during pregnancy: a case series. *ESMO Open*, *6*(5). https://doi.org/10.1016/J.ESMOOP.2021.100262

Aran, D., Looney, A. P., Liu, L., Wu, E., Fong, V., Hsu, A., Chak, S., Naikawadi, R. P., Wolters, P. J., Abate, A. R., Butte, A. J., & Bhattacharya, M. (2019). *Reference-based analysis of lung single-cell sequencing reveals a transitional profibrotic macrophage*. *20*(2), 163–172. https://doi.org/10.1038/s41590-018-0276-y

Axelrod, M. L., Nixon, M. J., Gonzalez-Ericsson, P. I., Bergman, R. E., Pilkinton, M. A., McDonnell, W. J., Sanchez, V., Opalenik, S. R., Loi, S., Zhou, J., Mackay, S., Rexer, B. N., Abramson, V. G., Jansen, V. M., Mallal, S., Donaldson, J., Tolaney, S. M., Krop, I. E., Garrido-Castro, A. C., … Balko, J. M. (2020). Changes in Peripheral and Local Tumor Immunity after Neoadjuvant Chemotherapy Reshape Clinical Outcomes in Patients with Breast Cancer. *Clinical Cancer Research*, *26*(21), 5668–5681. https://doi.org/10.1158/1078-0432.ccr-19-3685

Aydiner, A., Sen, F., Tambas, M., Ciftci, R., Eralp, Y., Saip, P., Karanlik, H., Fayda, M., Kucucuk, S., Onder, S., Yavuz, E., Muslumanoglu, M., & Igci, A. (2015). Metaplastic Breast Carcinoma Versus Triple-Negative Breast Cancer: Survival and Response to Treatment. *Medicine*, *94*(52). https://doi.org/10.1097/MD.0000000000002341

Bae, S. Y., Lee, S. K., Koo, M. Y., Hur, S. M., Choi, M. Y., Cho, D. H., Kim, S., Choe, J. H., Lee, J. E., Kim, J. H., Kim, J. S., Nam, S. J., & Yang, J. H. (2011). The prognoses of metaplastic breast cancer patients compared to those of triple-negative breast cancer patients. *Breast Cancer Research and Treatment*, *126*(2), 471–478. https://doi.org/10.1007/S10549-011-1359-8/FIGURES/4

Balko, J. M., Giltnane, J. M., Wang, K., Schwarz, L. J., Young, C. D., Cook, R. S., Owens, P., Sanders, M. E., Kuba, M. G., Sánchez, V., Kurupi, R., Moore, P. D., Pinto, J. A., Doimi, F. D., Gómez, H., Horiuchi, D., Goga, A., Lehmann, B. D., Bauer, J. A., … Arteaga, C. L. (2014). Molecular Profiling of the Residual Disease of Triple-Negative Breast Cancers after Neoadjuvant Chemotherapy Identifies Actionable Therapeutic

Targets. *Cancer Discovery, 4*(2), 232–245. https://doi.org/10.1158/2159-8290.CD-13-0286

Benjamini, Y., & Hochberg, Y. (1995). Controlling the False Discovery Rate: A Practical and Powerful Approach to Multiple Testing. *Journal of the Royal Statistical Society: Series B (Methodological), 57*(1), 289–300. https://doi.org/10.1111/J.2517-6161.1995.TB02031.X

Bönner, F., Borg, N., Burghoff, S., & Schrader, J. (2012). Resident cardiac immune cells and expression of the ectonucleotidase enzymes CD39 and CD73 after ischemic injury. *PloS One, 7*(4). https://doi.org/10.1371/JOURNAL.PONE.0034730

Butler, A., Hoffman, P., Smibert, P., Papalexi, E., & Satija, R. (2018). Integrating single-cell transcriptomic data across different conditions, technologies, and species. *Nature Biotechnology, 36*(5), 411–420. https://doi.org/10.1038/nbt.4096

Canè, S., Ugel, S., Trovato, R., Marigo, I., de Sanctis, F., Sartoris, S., & Bronte, V. (2019). The endless saga of monocyte diversity. *Frontiers in Immunology, 10*, 1786. https://doi.org/10.3389/FIMMU.2019.01786/BIBTEX

Carosella, E. D., Rouas-Freiss, N., Roux, D. T. le, Moreau, P., & LeMaoult, J. (2015). HLA-G: An Immune Checkpoint Molecule. *Advances in Immunology, 127*, 33–144. https://doi.org/10.1016/BS.AI.2015.04.001

Chambers, C. A., Cado, D., Truong, T., & Allison, J. P. (1997). Thymocyte development is normal in CTLA-4-deficient mice. *Proceedings of the National Academy of Sciences of the United States of America, 94*(17), 9296–9301. https://doi.org/10.1073/PNAS.94.17.9296

Chen, L., & Flies, D. B. (2013). Molecular mechanisms of T cell co-stimulation and co-inhibition. *Nature Reviews Immunology 2013 13:4, 13*(4), 227–242. https://doi.org/10.1038/nri3405

Chimenti, C., & Frustaci, A. (2013). Contribution and risks of left ventricular endomyocardial biopsy in patients with cardiomyopathies: A retrospective study over a 28-year period. *Circulation, 128*(14), 1531–1541. https://doi.org/10.1161/CIRCULATIONAHA.13.001414

Denkert, C., von Minckwitz, G., Brase, J. C., Sinn, B. v., Gade, S., Kronenwett, R., Pfitzner, B. M., Salat, C., Loi, S., Schmitt, W. D., Schem, C., Fisch, K., Darb-Esfahan, S., Mehta, K., Sotiriou, C., Wienert, S., Klare, P., André, F., Klauschen, F., … Loibl, S. (2015). *Tumor-infiltrating lymphocytes and response to neoadjuvant chemotherapy with or without carboplatin in human epidermal growth factor receptor 2-positive and triple-negative primary breast cancers. 33*(9), 983–991. https://doi.org/10.1200/JCO.2014.58.1967

Denkert, C., von Minckwitz, G., Darb-Esfahani, S., Lederer, B., Heppner, B. I., Weber, K. E., Budczies, J., Huober, J., Klauschen, F., Furlanetto, J., Schmitt, W. D., Blohmer, J. U., Karn, T., Pfitzner, B. M., Kümmel, S., Engels, K., Schneeweiss, A., Hartmann, A., Noske, A., … Loibl, S. (2018). Tumour-infiltrating lymphocytes and prognosis in different subtypes of breast cancer: a pooled analysis of 3771 patients treated with neoadjuvant therapy. *The Lancet Oncology, 19*(1), 40–50. https://doi.org/10.1016/S1470-2045(17)30904-X

Dieci, M. v., Criscitiello, C., Goubar, A., Viale, G., Conte, P., Guarneri, V., Ficarra, G., Mathieu, M. C., Delaloge, S., Curigliano, G., & Andre, F. (2014). Prognostic value of tumor-infiltrating lymphocytes on residual disease after primary chemotherapy for triple-negative breast cancer: a retrospective multicenter study. *Annals of Oncology, 25*(3), 611–618. https://doi.org/10.1093/ANNONC/MDT556

Dumont, C., Jacquier, A., Verine, J., Noel, F., Goujon, A., Wu, C. L., Hung, T. M., Desgrandchamps, F., Culine, S., Carosella, E. D., Rouas-Freiss, N., & LeMaoult, J. (2019). CD8+PD-1–ILT2+ T Cells Are an Intratumoral Cytotoxic Population Selectively

Inhibited by the Immune-Checkpoint HLA-G. *Cancer Immunology Research*, *7*(10), 1619–1632. https://doi.org/10.1158/2326-6066.CIR-18-0764

Dunham, I., Kundaje, A., Aldred, S. F., Collins, P. J., Davis, C. A., Doyle, F., Epstein, C. B., Frietze, S., Harrow, J., Kaul, R., Khatun, J., Lajoie, B. R., Landt, S. G., Lee, B. K., Pauli, F., Rosenbloom, K. R., Sabo, P., Safi, A., Sanyal, A., … Lochovsky, L. (2012). An integrated encyclopedia of DNA elements in the human genome. *Nature 2012 489:7414*, *489*(7414), 57–74. https://doi.org/10.1038/nature11247

Eberhardt, C. S., Kissick, H. T., Patel, M. R., Cardenas, M. A., Prokhnevska, N., Obeng, R. C., Nasti, T. H., Griffith, C. C., Im, S. J., Wang, X., Shin, D. M., Carrington, M., Chen, Z. G., Sidney, J., Sette, A., Saba, N. F., Wieland, A., & Ahmed, R. (2021). Functional HPV-specific PD-1+ stem-like CD8 T cells in head and neck cancer. *Nature 2021 597:7875*, *597*(7875), 279–284. https://doi.org/10.1038/s41586-021-03862-z

Elamm, C., Fairweather, D. L., & Cooper, L. T. (2012). Pathogenesis and diagnosis of myocarditis. *Heart*, *98*(11), 835–840. https://doi.org/10.1136/HEARTJNL-2012-301686

Escudier, M., Cautela, J., Malissen, N., Ancedy, Y., Orabona, M., Pinto, J., Monestier, S., Grob, J. J., Scemama, U., Jacquier, A., Lalevee, N., Barraud, J., Peyrol, M., Laine, M., Bonello, L., Paganelli, F., Cohen, A., Barlesi, F., Ederhy, S., & Thuny, F. (2017). Clinical features, management, and outcomes of immune checkpoint inhibitor-related cardiotoxicity. *Circulation*, *136*(21), 2085–2087. https://doi.org/10.1161/CIRCULATIONAHA.117.030571

Falk, K., Rotzschke, O., Stevanovic, S., Jung, G., & Rammenseet, H.-G. (1991). *Allele-specific motifs revealed by sequencing of self-peptides eluted from MHC molecules*.

Foulds, G. A., Vadakekolathu, J., Abdel-Fatah, T. M. A., Nagarajan, D., Reeder, S., Johnson, C., Hood, S., Moseley, P. M., Chan, S. Y. T., Graham Pockley, A., Rutella, S., & McArdle, S. E. B. (2018). Immune-phenotyping and transcriptomic profiling of peripheral blood mononuclear cells from patients with breast cancer: Identification of a 3 gene signature which predicts relapse of triple negative breast cancer. *Frontiers in Immunology*, *9*(SEP), 2028. https://doi.org/10.3389/FIMMU.2018.02028/BIBTEX

Gabrielsen, I. S. M., Helgeland, H., Akselsen, H., Aass, H. C. D., Sundaram, A. Y. M., Snowhite, I. v., Pugliese, A., Flåm, S. T., & Lie, B. A. (2019). Transcriptomes of antigen presenting cells in human thymus. *PLOS ONE, 14*(7), e0218858. https://doi.org/10.1371/JOURNAL.PONE.0218858

Gil-Cruz, C., Perez-Shibayama, C., de Martin, A., Ronchi, F., van der Borght, K., Niederer, R., Onder, L., Lütge, M., Novkovic, M., Nindl, V., Ramos, G., Arnoldini, M., Slack, E. M. C., Boivin-Jahns, V., Jahns, R., Wyss, M., Mooser, C., Lambrecht, B. N., Maeder, M. T., … Ludewig, B. (2019). Microbiota-derived peptide mimics drive lethal inflammatory cardiomyopathy. *Science*, *366*(6467), 881–886. https://doi.org/10.1126/science.aav3487

Granato, M., Santarelli, R., Farina, A., Gonnella, R., Lotti, L. V., Faggioni, A., & Cirone, M. (2014). Epstein-Barr Virus Blocks the Autophagic Flux and Appropriates the Autophagic Machinery To Enhance Viral Replication. *Journal of Virology*, *88*(21), 12715. https://doi.org/10.1128/JVI.02199-14

Gros, A., Parkhurst, M. R., Tran, E., Pasetto, A., Robbins, P. F., Ilyas, S., Prickett, T. D., Gartner, J. J., Crystal, J. S., Roberts, I. M., Trebska-Mcgowan, K., Wunderlich, J. R., Yang, J. C., & Rosenberg, S. A. (2016). Prospective identification of neoantigen-specific lymphocytes in the peripheral blood of melanoma patients. *Nature Medicine 2016 22:4*, *22*(4), 433–438. https://doi.org/10.1038/nm.4051

Gu, Z., Eils, R., & Schlesner, M. (2016). Complex heatmaps reveal patterns and correlations in multidimensional genomic data. *Bioinformatics*, *32*(18), 2847–2849. https://doi.org/10.1093/bioinformatics/btw313

Han, M., Salamat, A., Zhu, L., Zhang, H., Clark, B. Z., Dabbs, D. J., Carter, G. J., Brufsky, A. M., Jankowitz, R. C., Puhalla, S. L., Johnson, R. R., Soran, A., Steiman, J. G., McAuliffe, P. F., Diego, E. J., & Bhargava, R. (2019). Metaplastic breast carcinoma: a clinical-pathologic study of 97 cases with subset analysis of response to neoadjuvant chemotherapy. *Modern Pathology 2019 32:6*, *32*(6), 807–816. https://doi.org/10.1038/s41379-019-0208-x

Hanna, A., & Balko, J. M. (2021). Breast cancer resistance mechanisms: challenges to immunotherapy. *Breast Cancer Research and Treatment 2021 190:1*, *190*(1), 5–17. https://doi.org/10.1007/S10549-021-06337-X

Heather, J. M., Spindler, M. J., Alonso, M. H., Shui, Y. I., Millar, D. G., Johnson, D. S., Cobbold, M., & Hata, A. N. (2021). Stitchr: stitching coding TCR nucleotide sequences from V/J/CDR3 information. *BioRxiv*, 2021.12.20.473544. https://doi.org/10.1101/2021.12.20.473544

Hendry, S., Salgado, R., Gevaert, T., Russell, P. A., John, T., Thapa, B., Christie, M., van de Vijver, K., Estrada, M. v., Gonzalez-Ericsson, P. I., Sanders, M., Solomon, B., Solinas, C., van den Eynden, G. G. G. M., Allory, Y., Preusser, M., Hainfellner, J., Pruneri, G., Vingiani, A., … Fox, S. B. (2017a). Assessing tumor infiltrating lymphocytes in solid tumors: a practical review for pathologists and proposal for a standardized method from the International Immuno-Oncology Biomarkers Working Group: Part 1: Assessing the host immune response, TILs in invasive breast carcinoma and ductal carcinoma in situ, metastatic tumor deposits and areas for further research. *Advances in Anatomic Pathology*, *24*(5), 235. https://doi.org/10.1097/PAP.0000000000000162

Hendry, S., Salgado, R., Gevaert, T., Russell, P. A., John, T., Thapa, B., Christie, M., van de Vijver, K., Estrada, M. v., Gonzalez-Ericsson, P. I., Sanders, M., Solomon, B., Solinas, C., van den Eynden, G. G. G. M., Allory, Y., Preusser, M., Hainfellner, J., Pruneri, G., Vingiani, A., … Fox, S. B. (2017b). Assessing tumor infiltrating lymphocytes in solid tumors: a practical review for pathologists and proposal for a standardized method from the International Immuno-Oncology Biomarkers Working Group: Part 2: TILs in melanoma, gastrointestinal tract carcinomas, non-small cell lung carcinoma and mesothelioma, endometrial and ovarian carcinomas, squamous cell carcinoma of the head and neck, genitourinary carcinomas, and primary brain tumors. *Advances in Anatomic Pathology*, *24*(6), 311. https://doi.org/10.1097/PAP.0000000000000161

Holzmann, M., Nicko, A., Kühl, U., Noutsias, M., Poller, W., Hoffmann, W., Morguet, A., Witzenbichler, B., Tschöpe, C., Schultheiss, H. P., & Pauschinger, M. (2008). Complication rate of right ventricular endomyocardial biopsy via the femoral approach: A retrospective and prospective study analyzing 3048 diagnostic procedures over an 11-year period. *Circulation*, *118*(17), 1722–1728. https://doi.org/10.1161/CIRCULATIONAHA.107.743427

Hu, J.-R. R., Florido, R., Lipson, E. J., Naidoo, J., Ardehali, R., Tocchetti, C. G., Lyon, A. R., Padera, R. F., Johnson, D. B., & Moslehi, J. (2019). Cardiovascular toxicities associated with immune checkpoint inhibitors. *Cardiovascular Research*, *115*(5), 854. https://academic.oup.com/cardiovascres/advance-article/doi/10.1093/cvr/cvz026/5304411

Huang, Y. te, Chen, Y. P., Lin, W. C., Su, W. C., & Sun, Y. T. (2020). Immune Checkpoint Inhibitor-Induced Myasthenia Gravis. *Frontiers in Neurology*, *11*, 634. https://doi.org/10.3389/FNEUR.2020.00634/FULL

Jackson, R., Kroehling, L., Khitun, A., Bailis, W., Jarret, A., York, A. G., Khan, O. M., Brewer, J. R., Skadow, M. H., Duizer, C., Harman, C. C. D., Chang, L., Bielecki, P., Solis, A. G., Steach, H. R., Slavoff, S., & Flavell, R. A. (2018). The translation of non-

canonical open reading frames controls mucosal immunity. *Nature*, *564*(7736), 434–438. https://doi.org/10.1038/s41586-018-0794-7

Ji, C., Roy, M. D., Golas, J., Vitsky, A., Ram, S., Kumpf, S. W., Martin, M., Barletta, F., Meier, W. A., Hooper, A. T., Sapra, P., Khan, N. K., Finkelstein, M., Guffroy, M., & Buetow, B. S. (2019). Myocarditis in cynomolgus monkeys following treatment with immune checkpoint inhibitors. *Clinical Cancer Research*, *25*(15), 4735–4748. https://doi.org/10.1158/1078-0432.CCR-18-4083/74931/AM/MYOCARDITIS-IN-CYNOMOLGUS-MONKEYS-FOLLOWING

Johnson, D. B., Balko, J. M., Compton, M. L., Chalkias, S., Gorham, J., Xu, Y., Hicks, M., Puzanov, I., Alexander, M. R., Bloomer, T. L., Becker, J. R., Slosky, D. A., Phillips, E. J., Pilkinton, M. A., Craig-Owens, L., Kola, N., Plautz, G., Reshef, D. S., Deutsch, J. S., … Moslehi, J. J. (2016). Fulminant myocarditis with combination immune checkpoint blockade. *New England Journal of Medicine*, *375*(18), 1749–1755. https://doi.org/10.1056/NEJMoa1609214

Johnson, D. B., Nixon, M. J., Wang, Y., Wang, D. Y., Castellanos, E., Estrada, M. v., Ericsson-Gonzalez, P. I., Cote, C. H., Salgado, R., Sanchez, V., Dean, P. T., Opalenik, S. R., Schreeder, D. M., Rimm, D. L., Kim, J. Y., Bordeaux, J., Loi, S., Horn, L., Sanders, M. E., … Balko, J. M. (2018). Tumor-specific MHC-II expression drives a unique pattern of resistance to immunotherapy via LAG-3/FCRL6 engagement. *JCI Insight*, *3*(24). http://www.ncbi.nlm.nih.gov/pubmed/30568030

Jutz, S., Leitner, J., Schmetterer, K., Doel-Perez, I., Majdic, O., Grabmeier-Pfistershammer, K., Paster, W., Huppa, J. B., & Steinberger, P. (2016). Assessment of costimulation and coinhibition in a triple parameter T cell reporter line: Simultaneous measurement of NF-κB, NFAT and AP-1. *Journal of Immunological Methods*, *430*, 10–20. https://doi.org/10.1016/j.jim.2016.01.007

Kallikourdis, M., Martini, E., Carullo, P., Sardi, C., Roselli, G., Greco, C. M., Vignali, D., Riva, F., Ormbostad Berre, A. M., Stølen, T. O., Fumero, A., Faggian, G., di Pasquale, E., Elia, L., Rumio, C., Catalucci, D., Papait, R., & Condorelli, G. (2017). T cell costimulation blockade blunts pressure overload-induced heart failure. *Nature Communications 2017 8:1*, *8*(1), 1–14. https://doi.org/10.1038/ncomms14680

Kaminsky, A. (2012). Single-institution experience with neoadjuvant chemotherapy for metaplastic breast cancer (MBC). *Https://Doi.Org/10.1200/Jco.2012.30.27_suppl.140*, *30*(27_suppl), 140–140. https://doi.org/10.1200/JCO.2012.30.27_SUPPL.140

Kamphorst, A. O., Wieland, A., Nasti, T., Yang, S., Zhang, R., Barber, D. L., Konieczny, B. T., Daugherty, C. Z., Koenig, L., Yu, K., Sica, G. L., Sharpe, A. H., Freeman, G. J., Blazar, B. R., Turka, L. A., Owonikoko, T. K., Pillai, R. N., Ramalingam, S. S., Araki, K., & Ahmed, R. (2017). Rescue of exhausted CD8 T cells by PD-1-targeted therapies is CD28-dependent. *Science*, *355*(6332), 1423–1427. https://doi.org/10.1126/SCIENCE.AAF0683/SUPPL_FILE/KLAMPHORST-SM.PDF

Keir, M. E., Freeman, G. J., & Sharpe, A. H. (2007). PD-1 Regulates Self-Reactive CD8+ T Cell Responses to Antigen in Lymph Nodes and Tissues. *The Journal of Immunology*, *179*(8), 5064–5070. https://doi.org/10.4049/JIMMUNOL.179.8.5064

Kiamanesh, O., & Toma, M. (2021). The State of the Heart Biopsy: A Clinical Review. *CJC Open*, *3*(4), 524–531. https://doi.org/10.1016/J.CJCO.2020.11.017/ATTACHMENT/AE83F893-501E-4D18-9E7A-782C9A1369BD/MMC4.MP4

Kim, R., Kawai, A., Wakisaka, M., Sawada, S., Shimoyama, M., Yasuda, N., Hidaka, M., Morita, Y., Ohtani, S., & Arihiro, K. (2020). Immune correlates of the differing pathological and therapeutic effects of neoadjuvant chemotherapy in breast cancer. *European Journal of Surgical Oncology*, *46*(1), 77–84. https://doi.org/10.1016/J.EJSO.2019.09.146

Korotkevich, G., Sukhov, V., Budin, N., Shpak, B., Artyomov, M., & Sergushichev, A. (2016). Fast gene set enrichment analysis. *BioRxiv*, 060012. https://doi.org/10.1101/060012

Korsunsky, I., Millard, N., Fan, J., Slowikowski, K., Zhang, F., Wei, K., Baglaenko, Y., Brenner, M., Loh, P. ru, & Raychaudhuri, S. (2019). Fast, sensitive and accurate integration of single-cell data with Harmony. *Nature Methods 2019 16:12*, *16*(12), 1289–1296. https://doi.org/10.1038/s41592-019-0619-0

Kuehn, H. S., Ouyang, W., Lo, B., Deenick, E. K., Niemela, J. E., Avery, D. T., Schickel, J. N., Tran, D. Q., Stoddard, J., Zhang, Y., Frucht, D. M., Dumitriu, B., Scheinberg, P., Folio, L. R., Frein, C. A., Price, S., Koh, C., Heller, T., Seroogy, C. M., … Uzel, G. (2014). Immune dysregulation in human subjects with heterozygous germline mutations in CTLA4. *Science*, *345*(6204), 1623–1627. https://doi.org/10.1126/SCIENCE.1255904/SUPPL_FILE/KUEHN.SM.PDF

Larkin, J., Chiarion-Sileni, V., Gonzalez, R., Grob, J. J., Cowey, C. L., Lao, C. D., Schadendorf, D., Dummer, R., Smylie, M., Rutkowski, P., Ferrucci, P. F., Hill, A., Wagstaff, J., Carlino, M. S., Haanen, J. B., Maio, M., Marquez-Rodas, I., McArthur, G. A., Ascierto, P. A., … Wolchok, J. D. (2015). Combined Nivolumab and Ipilimumab or Monotherapy in Untreated Melanoma. *New England Journal of Medicine*, *373*(1), 23–34. https://doi.org/10.1056/NEJMOA1504030/SUPPL_FILE/NEJMOA1504030_DISCLOSURES.PDF

Ledderose, C., Heyn, J., Limbeck, E., & Kreth, S. (2011). Selection of reliable reference genes for quantitative real-time PCR in human T cells and neutrophils. *BMC Research Notes*, *4*(1), 1–11. https://doi.org/10.1186/1756-0500-4-427/FIGURES/4

Lehmann, L. H., Cautela, J., Palaskas, N., Baik, A. H., Meijers, W. C., Allenbach, Y., Alexandre, J., Rassaf, T., Müller, O. J., Aras, M., Asnani, A. H., Deswal, A., Laufer-Perl, M., Thuny, F., Kerneis, M., Hayek, S. S., Ederhy, S., Salem, J. E., & Moslehi, J. J. (2021). Clinical Strategy for the Diagnosis and Treatment of Immune Checkpoint Inhibitor–Associated Myocarditis: A Narrative Review. *JAMA Cardiology*, *6*(11), 1329–1337. https://doi.org/10.1001/JAMACARDIO.2021.2241

Li, X., Warren, S., Pelekanou, V., Wali, V., Cesano, A., Liu, M., Danaher, P., Elliott, N., Nahleh, Z. A., Hayes, D. F., Hortobagyi, G. N., Barlow, W. E., Hatzis, C., & Pusztai, L. (2019). Immune profiling of pre- and post-treatment breast cancer tissues from the SWOG S0800 neoadjuvant trial. *Journal for ImmunoTherapy of Cancer*, *7*(1), 1–9. https://doi.org/10.1186/S40425-019-0563-7/FIGURES/6

Liberzon, A., Birger, C., Thorvaldsdóttir, H., Ghandi, M., Mesirov, J. P., & Tamayo, P. (2015). The Molecular Signatures Database Hallmark Gene Set Collection. *Cell Systems*, *1*(6), 417–425. https://doi.org/10.1016/j.cels.2015.12.004

Liedtke, C., Mazouni, C., Hess, K. R., André, F., Tordai, A., Mejia, J. A., Symmans, W. F., Gonzalez-Angulo, A. M., Hennessy, B., Green, M., Cristofanilli, M., Hortobagyi, G. N., & Pusztai, L. (2008). Response to neoadjuvant therapy and long-term survival in patients with triple-negative breast cancer. *Journal of Clinical Oncology*, *26*(8), 1275–1281. https://doi.org/10.1200/JCO.2007.14.4147

Lin, A., & Yan, W. H. (2018). Heterogeneity of HLA-G Expression in Cancers: Facing the Challenges. *Frontiers in Immunology*, *9*, 2164. https://doi.org/10.3389/FIMMU.2018.02164/BIBTEX

Linderman, G. C., Zhao, J., & Kluger, Y. (2018). Zero-preserving imputation of scRNA-seq data using low-rank approximation. *BioRxiv*, *C*, 397588. https://doi.org/10.1101/397588

Liu, L., Yang, L., Yan, W., Zhai, J., Pizzo, D. P., Chu, P., Chin, A. R., Shen, M., Dong, C., Ruan, X., Ren, X., Somlo, G., & Wang, S. E. (2018). Chemotherapy induces breast

cancer stemness in association with dysregulated monocytosis. *Clinical Cancer Research*, *24*(10), 2370–2382. https://doi.org/10.1158/1078-0432.CCR-17-2545/87479/AM/CHEMOTHERAPY-INDUCES-BREAST-CANCER-STEMNESS-IN

Loi, S., Drubay, D., Adams, S., Pruneri, G., Francis, P. A., Lacroix-Triki, M., Joensuu, H., Dieci, M. V., Badve, S., Demaria, S., Gray, R., Munzone, E., Lemonnier, J., Sotiriou, C., Piccart, M. J., Kellokumpu-Lehtinen, P. L., Vingiani, A., Gray, K., Andre, F., … Michiels, S. (2019). Tumor-Infiltrating Lymphocytes and Prognosis: A Pooled Individual Patient Analysis of Early-Stage Triple-Negative Breast Cancers. *Journal of Clinical Oncology*, *37*(7), 559. https://doi.org/10.1200/JCO.18.01010

Loi, S., Dushyanthen, S., Beavis, P. A., Salgado, R., Denkert, C., Savas, P., Combs, S., Rimm, D. L., Giltnane, J. M., Estrada, M. v., Sánchez, V., Sanders, M. E., Cook, R. S., Pilkinton, M. A., Mallal, S. A., Wang, K., Miller, V. A., Stephens, P. J., Yelensky, R., … Balko, J. M. (2016). RAS/MAPK Activation Is Associated with Reduced Tumor-Infiltrating Lymphocytes in Triple-Negative Breast Cancer: Therapeutic Cooperation Between MEK and PD-1/PD-L1 Immune Checkpoint Inhibitors. *Clinical Cancer Research*, *22*(6), 1499–1509. https://doi.org/10.1158/1078-0432.CCR-15-1125

Lozano, A. X., Chaudhuri, A. A., Nene, A., Bacchiocchi, A., Earland, N., Vesely, M. D., Usmani, A., Turner, B. E., Steen, C. B., Luca, B. A., Badri, T., Gulati, G. S., Vahid, M. R., Khameneh, F., Harris, P. K., Chen, D. Y., Dhodapkar, K., Sznol, M., Halaban, R., & Newman, A. M. (2022). T cell characteristics associated with toxicity to immune checkpoint blockade in patients with melanoma. *Nature Medicine 2022*, 1–10. https://doi.org/10.1038/s41591-021-01623-z

Lu, Y., Xue, Q., Eisele, M. R., Sulistijo, E. S., Brower, K., Han, L., Amir, E. A. D., Pe'er, D., Miller-Jensen, K., & Fan, R. (2015). Highly multiplexed profiling of single-cell effector functions reveals deep functional heterogeneity in response to pathogenic ligands. *Proceedings of the National Academy of Sciences of the United States of America*, *112*(7), E607–E615. https://doi.org/10.1073/PNAS.1416756112/-/DCSUPPLEMENTAL

Luen, S. J., Salgado, R., Dieci, M. v., Vingiani, A., Curigliano, G., Gould, R. E., Castaneda, C., D'Alfonso, T., Sanchez, J., Cheng, E., Andreopoulou, E., Castillo, M., Adams, S., Demaria, S., Symmans, W. F., Michiels, S., & Loi, S. (2019). Prognostic implications of residual disease tumor-infiltrating lymphocytes and residual cancer burden in triple-negative breast cancer patients after neoadjuvant chemotherapy. *Annals of Oncology*, *30*(2), 236–242. https://doi.org/10.1093/ANNONC/MDY547

Lv, H., Havari, E., Pinto, S., Gottumukkala, R. V. S. R. K., Cornivelli, L., Raddassi, K., Matsui, T., Rosenzweig, A., Bronson, R. T., Smith, R., Fletcher, A. L., Turley, S. J., Wucherpfennig, K., Kyewski, B., & Lipes, M. A. (2011). Impaired thymic tolerance to α-myosin directs autoimmunity to the heart in mice and humans. *The Journal of Clinical Investigation*, *121*(4), 1561–1573. https://doi.org/10.1172/JCI44583

Ma, C., Cheung, A. F., Chodon, T., Koya, R. C., Wu, Z., Ng, C., Avramis, E., Cochran, A. J., Witte, O. N., Baltimore, D., Chmielowski, B., Economou, J. S., Comin-Anduix, B., Ribas, A., & Heath, J. R. (2013). Multifunctional T-cell Analyses to Study Response and Progression in Adoptive Cell Transfer Immunotherapy. *Cancer Discovery*, *3*(4), 418–429. https://doi.org/10.1158/2159-8290.CD-12-0383

Ma, C., Fan, R., Ahmad, H., Shi, Q., Comin-Anduix, B., Chodon, T., Koya, R. C., Liu, C. C., Kwong, G. A., Radu, C. G., Ribas, A., & Heath, J. R. (2011). A clinical microchip for evaluation of single immune cells reveals high functional heterogeneity in phenotypically similar T cells. *Nature Medicine 2011 17:6*, *17*(6), 738–743. https://doi.org/10.1038/nm.2375

Mahmood, S. S., Fradley, M. G., Cohen, J. v., Nohria, A., Reynolds, K. L., Heinzerling, L. M., Sullivan, R. J., Damrongwatanasuk, R., Chen, C. L., Gupta, D., Kirchberger, M. C.,

Awadalla, M., Hassan, M. Z. O., Moslehi, J. J., Shah, S. P., Ganatra, S., Thavendiranathan, P., Lawrence, D. P., Groarke, J. D., & Neilan, T. G. (2018). Myocarditis in Patients Treated With Immune Checkpoint Inhibitors. *Journal of the American College of Cardiology*, *71*(16), 1755–1764. https://doi.org/10.1016/J.JACC.2018.02.037

Martens, A., Wistuba-Hamprecht, K., Foppen, M. G., Yuan, J., Postow, M. A., Wong, P., Romano, E., Khammari, A., Dreno, B., Capone, M., Ascierto, P. A., di Giacomo, A. M., Maio, M., Schilling, B., Sucker, A., Schadendorf, D., Hassel, J. C., Eigentler, T. K., Martus, P., … Weide, B. (2016). Baseline peripheral blood biomarkers associated with clinical outcome of advanced melanoma patients treated with ipilimumab. *Clinical Cancer Research*, *22*(12), 2908–2918. https://doi.org/10.1158/1078-0432.CCR-15-2412/128449/AM/BASELINE-PERIPHERAL-BLOOD-BIOMARKERS-ASSOCIATED

Martens, J. H. A., & Stunnenberg, H. G. (2013). BLUEPRINT: mapping human blood cell epigenomes. *Haematologica*, *98*(10), 1487. https://doi.org/10.3324/HAEMATOL.2013.094243

Martini, E., Kunderfranco, P., Peano, C., Carullo, P., Cremonesi, M., Schorn, T., Carriero, R., Termanini, A., Colombo, F. S., Jachetti, E., Panico, C., Faggian, G., Fumero, A., Torracca, L., Molgora, M., Cibella, J., Pagiatakis, C., Brummelman, J., Alvisi, G., … Kallikourdis, M. (2019). Single-Cell Sequencing of Mouse Heart Immune Infiltrate in Pressure Overload-Driven Heart Failure Reveals Extent of Immune Activation. *Circulation*, *140*(25), 2089–2107. https://doi.org/10.1161/CIRCULATIONAHA.119.041694

Martins, F., Sofiya, L., Sykiotis, G. P., Lamine, F., Maillard, M., Fraga, M., Shabafrouz, K., Ribi, C., Cairoli, A., Guex-Crosier, Y., Kuntzer, T., Michielin, O., Peters, S., Coukos, G., Spertini, F., Thompson, J. A., & Obeid, M. (2019). Adverse effects of immune-checkpoint inhibitors: epidemiology, management and surveillance. *Nature Reviews Clinical Oncology 2019 16:9*, *16*(9), 563–580. https://doi.org/10.1038/s41571-019-0218-0

Massa, C., Karn, T., Denkert, C., Schneeweiss, A., Hanusch, C., Blohmer, J. U., Zahm, D. M., Jackisch, C., van Mackelenbergh, M., Thomalla, J., Marme, F., Huober, J., Müller, V., Schem, C., Mueller, A., Stickeler, E., Biehl, K., Fasching, P. A., Untch, M., … Seliger, B. (2020). Differential effect on different immune subsets of neoadjuvant chemotherapy in patients with TNBC. *Journal for ImmunoTherapy of Cancer*, *8*(2), 1261. https://doi.org/10.1136/jitc-2020-001261

Massilamany, C., Gangaplara, A., Steffen, D., & Reddy, J. (2011). Identification of novel mimicry epitopes for cardiac myosin heavy chain-α that induce autoimmune myocarditis in A/J mice. *Cellular Immunology*, *271*(2), 438–449. https://doi.org/10.1016/J.CELLIMM.2011.08.013

McNew, K. L., Abraham, A., Sack, D. E., Smart, C. D., Pettway, Y. D., Falk, A., Lister, R. L., Faucon, A. B., Bejan, C. A., Capra, J. A., Aronoff, D. M., Boyd, K. L., & Moore, D. J. (2022). Vascular Alterations Impede Fragile Tolerance to Pregnancy in Type 1 Diabetes. *F&S Science*, *0*(0). https://doi.org/10.1016/J.XFSS.2022.02.001

Meggyes, M., Nagy, D. U., & Szereday, L. (2020). Investigation of the PD-1 and PD-L1 Immune Checkpoint Molecules Throughout Healthy Human Pregnancy and in Nonpregnant Women. *Journal of Clinical Medicine*, *9*(8), 1–16. https://doi.org/10.3390/JCM9082536

Meyer, C., Cagnon, L., Costa-Nunes, C. M., Baumgaertner, P., Montandon, N., Leyvraz, L., Michielin, O., Romano, E., & Speiser, D. E. (2014). Frequencies of circulating MDSC correlate with clinical outcome of melanoma patients treated with ipilimumab. *Cancer Immunology, Immunotherapy*, *63*(3), 247–257. https://doi.org/10.1007/S00262-013-1508-5/FIGURES/4

Mombaerts, P., Iacomini, J., Johnson, R. S., Herrup, K., Tonegawa, S., & Papaioannou, V. E. (1992). RAG-1-deficient mice have no mature B and T lymphocytes. *Cell*, *68*(5), 869–877. https://doi.org/10.1016/0092-8674(92)90030-G

Moslehi, J. J., Salem, J. E., Sosman, J. A., Lebrun-Vignes, B., & Johnson, D. B. (2018). Increased reporting of fatal immune checkpoint inhibitor-associated myocarditis. *The Lancet*, *391*(10124), 933. https://doi.org/10.1016/S0140-6736(18)30533-6

Moslehi, J., Lichtman, A. H., Sharpe, A. H., Galluzzi, L., & Kitsis, R. N. (2021). Immune checkpoint inhibitor–associated myocarditis: manifestations and mechanisms. *The Journal of Clinical Investigation*, *131*(5). https://doi.org/10.1172/JCI145186

Motzer, R. J., Tannir, N. M., McDermott, D. F., Arén Frontera, O., Melichar, B., Choueiri, T. K., Plimack, E. R., Barthélémy, P., Porta, C., George, S., Powles, T., Donskov, F., Neiman, V., Kollmannsberger, C. K., Salman, P., Gurney, H., Hawkins, R., Ravaud, A., Grimm, M.-O., … Escudier, B. (2018). Nivolumab plus Ipilimumab versus Sunitinib in Advanced Renal-Cell Carcinoma. *New England Journal of Medicine*, *378*(14), 1277–1290. https://doi.org/10.1056/NEJMOA1712126/SUPPL_FILE/NEJMOA1712126_DISCLOSURES.PDF

Nazarov, V., immunarch.bot, & Rumynskiy, E. (2020). *immunarch: An R Package for Painless Bioinformatics Analysis of T-Cell and B-Cell Immune Repertoires.* https://doi.org/10.5281/ZENODO.3893991

Newman, A. M., Steen, C. B., Liu, C. L., Gentles, A. J., Chaudhuri, A. A., Scherer, F., Khodadoust, M. S., Esfahani, M. S., Luca, B. A., Steiner, D., Diehn, M., & Alizadeh, A. A. (2019). Determining cell type abundance and expression from bulk tissues with digital cytometry. *Nature Biotechnology*, *37*(7), 773–782. https://doi.org/10.1038/s41587-019-0114-2

Nguyen, L. S., Cooper, L. T., Kerneis, M., Funck-Brentano, C., Silvain, J., Brechot, N., Hekimian, G., Ammirati, E., ben M'Barek, B., Redheuil, A., Gandjbakhch, E., Bihan, K., Lebrun-Vignes, B., Ederhy, S., Dolladille, C., Moslehi, J. J., & Salem, J.-E. E. (2022). Systematic analysis of drug-associated myocarditis reported in the World Health Organization pharmacovigilance database. *Nature Communications*, *13*(1), 25. https://doi.org/10.1038/S41467-021-27631-8

Nishimura, H., Nose, M., Hiai, H., Minato, N., & Honjo, T. (1999). Development of Lupus-like Autoimmune Diseases by Disruption of the PD-1 Gene Encoding an ITIM Motif-Carrying Immunoreceptor. *Immunity*, *11*(2), 141–151. https://doi.org/10.1016/S1074-7613(00)80089-8

Nishimura, H., Okazaki, T., Tanaka, Y., Nakatani, K., Hara, M., Matsumori, A., Sasayama, S., Mizoguchi, A., Hiai, H., Minato, N., & Honjo, T. (2001). Autoimmune dilated cardiomyopathy in PD-1 receptor-deficient mice. *Science*, *291*(5502), 319–322. https://doi.org/10.1126/SCIENCE.291.5502.319/ASSET/5B1133EB-F4DF-451B-969A-C9E739F99C83/ASSETS/GRAPHIC/SE0119110004.JPEG

Oh, H. M., Oh, J. M., Choi, S. C., Kim, S. W., Han, W. C., Kim, T. H., Park, D. S., & Jun, C. D. (2003). An efficient method for the rapid establishment of Epstein-Barr virus immortalization of human B lymphocytes. *Cell Proliferation*, *36*(4), 191–197. https://doi.org/10.1046/J.1365-2184.2003.00276.X

Okazaki, T., Okazaki, I. M., Wang, J., Sugiura, D., Nakaki, F., Yoshida, T., Kato, Y., Fagarasan, S., Muramatsu, M., Eto, T., Hioki, K., & Honjo, T. (2011). PD-1 and LAG-3 inhibitory co-receptors act synergistically to prevent autoimmunity in mice. *The Journal of Experimental Medicine*, *208*(2), 395. https://doi.org/10.1084/JEM.20100466

Okazaki, T., Tanaka, Y., Nishio, R., Mitsuiye, T., Mizoguchi, A., Wang, J., Ishida, M., Hiai, H., Matsumori, A., Minato, N., & Honjo, T. (2003). Autoantibodies against cardiac

troponin I are responsible for dilated cardiomyopathy in PD-1-deficient mice. *Nature Medicine 2003 9:12*, *9*(12), 1477–1483. https://doi.org/10.1038/nm955

Oksanen, J., Blanchet, F. G., Friendly, M., Kindt, R., Legendre, P., Mcglinn, D., Minchin, P. R., O'hara, R. B., Simpson, G. L., Solymos, P., Henry, M., Stevens, H., Szoecs, E., & Maintainer, H. W. (2020). *Package "vegan" Title Community Ecology Package Version 2.5-7.*

Olingy, C. E., Dinh, H. Q., & Hedrick, C. C. (2019). Monocyte heterogeneity and functions in cancer. *Journal of Leukocyte Biology*, *106*(2), 309. https://doi.org/10.1002/JLB.4RI0818-311R

Overman, M. J., Lonardi, S., Wong, K. Y. M., Lenz, H. J., Gelsomino, F., Aglietta, M., Morse, M. A., van Cutsem, E., McDermott, R., Hill, A., Sawyer, M. B., Hendlisz, A., Neyns, B., Svrcek, M., Moss, R. A., Ledeine, J. M., Cao, Z. A., Kamble, S., Kopetz, S., & André, T. (2018). Durable clinical benefit with nivolumab plus ipilimumab in DNA mismatch repair-deficient/microsatellite instability-high metastatic colorectal cancer. *Journal of Clinical Oncology*, *36*(8), 773–779. https://doi.org/10.1200/JCO.2017.76.9901

Parisi, G., Saco, J. D., Salazar, F. B., Tsoi, J., Krystofinski, P., Puig-Saus, C., Zhang, R., Zhou, J., Cheung-Lau, G. C., Garcia, A. J., Grasso, C. S., Tavaré, R., Hu-Lieskovan, S., Mackay, S., Zalevsky, J., Bernatchez, C., Diab, A., Wu, A. M., Comin-Anduix, B., … Ribas, A. (2020). Persistence of adoptively transferred T cells with a kinetically engineered IL-2 receptor agonist. *Nature Communications 2020 11:1*, *11*(1), 1–12. https://doi.org/10.1038/s41467-019-12901-3

Parra, E. R., Villalobos, P., Behrens, C., Jiang, M., Pataer, A., Swisher, S. G., William, W. N., Zhang, J., Lee, J., Cascone, T., Heymach, J. v., Forget, M. A., Haymaker, C., Bernatchez, C., Kalhor, N., Weissferdt, A., Moran, C., Zhang, J., Vaporciyan, A., … Wistuba, I. I. (2018). Effect of neoadjuvant chemotherapy on the immune microenvironment in non-small cell lung carcinomas as determined by multiplex immunofluorescence and image analysis approaches. *Journal for Immunotherapy of Cancer*, *6*(1). https://doi.org/10.1186/S40425-018-0368-0

Parry, R. v., Chemnitz, J. M., Frauwirth, K. A., Lanfranco, A. R., Braunstein, I., Kobayashi, S. v., Linsley, P. S., Thompson, C. B., & Riley, J. L. (2005). CTLA-4 and PD-1 Receptors Inhibit T-Cell Activation by Distinct Mechanisms. *Molecular and Cellular Biology*, *25*(21), 9543–9553. https://doi.org/10.1128/MCB.25.21.9543-9553.2005/SUPPL_FILE/SUPPLEMENTARY_TABLE_1_FINAL.ZIP

Paul, S., Sidney, J., Sette, A., & Peters, B. (2016). TepiTool: A pipeline for computational prediction of T cell epitope candidates. *Current Protocols in Immunology*, *2016*, 18.19.1-18.19.24. https://doi.org/10.1002/cpim.12

Pogoda, K., Niwińska, A., Murawska, M., & Pieńkowski, T. (2013). Analysis of pattern, time and risk factors influencing recurrence in triple-negative breast cancer patients. *Medical Oncology (Northwood, London, England)*, *30*(1). https://doi.org/10.1007/S12032-012-0388-4

Postow, M. A., Chesney, J., Pavlick, A. C., Robert, C., Grossmann, K., McDermott, D., Linette, G. P., Meyer, N., Giguere, J. K., Agarwala, S. S., Shaheen, M., Ernstoff, M. S., Minor, D., Salama, A. K., Taylor, M., Ott, P. A., Rollin, L. M., Horak, C., Gagnier, P., … Hodi, F. S. (2015). Nivolumab and Ipilimumab versus Ipilimumab in Untreated Melanoma. *New England Journal of Medicine*, *372*(21), 2006–2017. https://doi.org/10.1056/NEJMOA1414428/SUPPL_FILE/NEJMOA1414428_DISCLOSURES.PDF

Ribelles, N., Perez-Villa, L., Jerez, J. M., Pajares, B., Vicioso, L., Jimenez, B., de Luque, V., Franco, L., Gallego, E., Marquez, A., Alvarez, M., Sanchez-Muñoz, A., Perez-Rivas, L., & Alba, E. (2013). Pattern of recurrence of early breast cancer is different

according to intrinsic subtype and proliferation index. *Breast Cancer Research : BCR*, *15*(5), R98. https://doi.org/10.1186/BCR3559

Rosshart, S., Hofmann, M., Schweier, O., Pfaff, A. K., Yoshimoto, K., Takeuchi, T., Molnar, E., Schamel, W. W., & Pircher, H. (2008). Interaction of KLRG1 with E-cadherin: New functional and structural insights. *European Journal of Immunology*, *38*(12), 3354–3364. https://doi.org/10.1002/EJI.200838690

Rossi, J., Paczkowski, P., Shen, Y. W., Morse, K., Flynn, B., Kaiser, A., Ng, C., Gallatin, K., Cain, T., Fan, R., Mackay, S., Heath, J. R., Rosenberg, S. A., Kochenderfer, J. N., Zhou, J., & Bot, A. (2018). Preinfusion polyfunctional anti-CD19 chimeric antigen receptor T cells are associated with clinical outcomes in NHL. *Blood*, *132*(8), 804–814. https://doi.org/10.1182/BLOOD-2018-01-828343

Rosskopf, S., Leitner, J., Paster, W., Morton, L. T., Hagedoorn, R. S., Steinberger, P., & Heemskerk, M. H. M. (2018). A Jurkat 76 based triple parameter reporter system to evaluate TCR functions and adoptive T cell strategies. *Oncotarget*, *9*(25), 17608–17619. https://doi.org/10.18632/oncotarget.24807

Safa, H., Johnson, D. H., Trinh, V. A., Rodgers, T. E., Lin, H., Suarez-Almazor, M. E., Fa'Ak, F., Saberian, C., Yee, C., Davies, M. A., Tummala, S., Woodman, K., Abdel-Wahab, N., & Diab, A. (2019). Immune checkpoint inhibitor related myasthenia gravis: Single center experience and systematic review of the literature. *Journal for ImmunoTherapy of Cancer*, *7*(1), 1–11. https://doi.org/10.1186/S40425-019-0774-Y/TABLES/3

Saito, T., & Rehmsmeier, M. (2017). Precrec: Fast and accurate precision-recall and ROC curve calculations in R. *Bioinformatics*, *33*(1), 145–147. https://doi.org/10.1093/bioinformatics/btw570

Salem, J. E., Manouchehri, A., Moey, M., Lebrun-Vignes, B., Bastarache, L., Pariente, A., Gobert, A., Spano, J. P., Balko, J. M., Bonaca, M. P., Roden, D. M., Johnson, D. B., & Moslehi, J. J. (2018). Spectrum of cardiovascular toxicities of immune checkpoint inhibitors: A pharmacovigilance study. *The Lancet. Oncology*, *19*(12), 1579. https://doi.org/10.1016/S1470-2045(18)30608-9

Salem, J.-E., Allenbach, Y., Vozy, A., Brechot, N., Johnson, D. B., Moslehi, J. J., & Kerneis, M. (2019). Abatacept for Severe Immune Checkpoint Inhibitor–Associated Myocarditis. *New England Journal of Medicine*, *380*(24), 2377–2379. https://doi.org/10.1056/NEJMc1901677

Salgado, R., Denkert, C., Demaria, S., Sirtaine, N., Klauschen, F., Pruneri, G., Wienert, S., van den Eynden, G., Baehner, F. L., Penault-Llorca, F., Perez, E. A., Thompson, E. A., Symmans, W. F., Richardson, A. L., Brock, J., Criscitiello, C., Bailey, H., Ignatiadis, M., Floris, G., … Loi, S. (2015). The evaluation of tumor-infiltrating lymphocytes (TILs) in breast cancer: recommendations by an International TILs Working Group 2014. *Annals of Oncology*, *26*(2), 259–271. https://doi.org/10.1093/ANNONC/MDU450

Satija, R., Farrell, J. A., Gennert, D., Schier, A. F., & Regev, A. (2015). *Spatial reconstruction of single-cell gene expression data*. *33*(5), 495–502. https://doi.org/10.1038/nbt.3192

Schadendorf, D., Hodi, F. S., Robert, C., Weber, J. S., Margolin, K., Hamid, O., Patt, D., Chen, T. T., Berman, D. M., & Wolchok, J. D. (2015). Pooled Analysis of Long-Term Survival Data From Phase II and Phase III Trials of Ipilimumab in Unresectable or Metastatic Melanoma. *Journal of Clinical Oncology : Official Journal of the American Society of Clinical Oncology*, *33*(17), 1889–1894. https://doi.org/10.1200/JCO.2014.56.2736

Schauer, D., Starlinger, P., Alidzanovic, L., Zajc, P., Maier, T., Feldman, A., Padickakudy, R., Buchberger, E., Elleder, V., Spittler, A., Stift, J., Pop, L., Gruenberger, B., Gruenberger, T., & Brostjan, C. (2016). Chemotherapy of colorectal liver metastases

induces a rapid rise in intermediate blood monocytes which predicts treatment response. *Oncoimmunology*, *5*(6). https://doi.org/10.1080/2162402X.2016.1160185

Schmid, P., Adams, S., Rugo, H. S., Schneeweiss, A., Barrios, C. H., Iwata, H., Diéras, V., Hegg, R., Im, S.-A., Shaw Wright, G., Henschel, V., Molinero, L., Chui, S. Y., Funke, R., Husain, A., Winer, E. P., Loi, S., & Emens, L. A. (2018). Atezolizumab and Nab-Paclitaxel in Advanced Triple-Negative Breast Cancer. *New England Journal of Medicine*, *379*(22), 2108–2121. https://doi.org/10.1056/NEJMOA1809615/SUPPL_FILE/NEJMOA1809615_DATA-SHARING.PDF

Schmid, P., Cortes, J., Dent, R., Pusztai, L., McArthur, H., Kümmel, S., Bergh, J., Denkert, C., Park, Y. H., Hui, R., Harbeck, N., Takahashi, M., Untch, M., Fasching, P. A., Cardoso, F., Andersen, J., Patt, D., Danso, M., Ferreira, M., … O'Shaughnessy, J. (2022). Event-free Survival with Pembrolizumab in Early Triple-Negative Breast Cancer. *Https://Doi.Org/10.1056/NEJMoa2112651*, *386*(6), 556–567. https://doi.org/10.1056/NEJMOA2112651

Schmid, P., Cortés, J., Dent, R., Pusztai, L., McArthur, H. L., Kuemmel, S., Bergh, J., Denkert, C., Park, Y. H., Hui, R., Harbeck, N., Takahashi, M., Foukakis, T., Fasching, P. A., Cardoso, F., Jia, L., Karantza, V., Zhao, J., Aktan, G., & O'Shaughnessy, J. (2019). KEYNOTE-522: Phase III study of pembrolizumab (pembro) + chemotherapy (chemo) vs placebo (pbo) + chemo as neoadjuvant treatment, followed by pembro vs pbo as adjuvant treatment for early triple-negative breast cancer (TNBC). *Annals of Oncology*, *30*, v853–v854. https://doi.org/10.1093/ANNONC/MDZ394.003

Schubert, D., Bode, C., Kenefeck, R., Hou, T. Z., Wing, J. B., Kennedy, A., Bulashevska, A., Petersen, B. S., Schäffer, A. A., Grüning, B. A., Unger, S., Frede, N., Baumann, U., Witte, T., Schmidt, R. E., Dueckers, G., Niehues, T., Seneviratne, S., Kanariou, M., … Grimbacher, B. (2014). Autosomal dominant immune dysregulation syndrome in humans with CTLA4 mutations. *Nature Medicine 2014 20:12*, *20*(12), 1410–1416. https://doi.org/10.1038/nm.3746

Schwab, C., Gabrysch, A., Olbrich, P., Patiño, V., Warnatz, K., Wolff, D., Hoshino, A., Kobayashi, M., Imai, K., Takagi, M., Dybedal, I., Haddock, J. A., Sansom, D. M., Lucena, J. M., Seidl, M., Schmitt-Graeff, A., Reiser, V., Emmerich, F., Frede, N., … Grimbacher, B. (2018). Phenotype, penetrance, and treatment of 133 cytotoxic T-lymphocyte antigen 4–insufficient subjects. *Journal of Allergy and Clinical Immunology*, *142*(6), 1932–1946. https://doi.org/10.1016/J.JACI.2018.02.055

Shah, Z., Vuddanda, V., Rali, A. S., Pamulapati, H., Masoomi, R., & Gupta, K. (2018). National Trends and Procedural Complications from Endomyocardial Biopsy: Results from the National Inpatient Sample, 2007–2014. *Cardiology*, *141*(3), 125–131. https://doi.org/10.1159/000493786

Stuart, T., Butler, A., Hoffman, P., Hafemeister, C., Papalexi, E., Mauck, W. M., Hao, Y., Stoeckius, M., Smibert, P., & Satija, R. (2019). Comprehensive Integration of Single-Cell Data. *Cell*, *177*(7), 1888-1902.e21. https://doi.org/10.1016/j.cell.2019.05.031

Sung, H., Ferlay, J., Siegel, R. L., Laversanne, M., Soerjomataram, I., Jemal, A., & Bray, F. (2021). Global Cancer Statistics 2020: GLOBOCAN Estimates of Incidence and Mortality Worldwide for 36 Cancers in 185 Countries. *CA: A Cancer Journal for Clinicians*, *71*(3), 209–249. https://doi.org/10.3322/CAAC.21660

Sznol, M., Ferrucci, P. F., Hogg, D., Atkins, M. B., Wolter, P., Guidoboni, M., Lebbé, C., Kirkwood, J. M., Schachter, J., Daniels, G. A., Hassel, J., Cebon, J., Gerritsen, W., Atkinson, V., Thomas, L., McCaffrey, J., Power, D., Walker, D., Bhore, R., … Wolchok, J. D. (2017). Pooled analysis safety profile of nivolumab and ipilimumab combination therapy in patients with advanced melanoma. *Journal of Clinical Oncology*, *35*(34), 3815–3822. https://doi.org/10.1200/JCO.2016.72.1167

Tawbi, H. A., Schadendorf, D., Lipson, E. J., Ascierto, P. A., Matamala, L., Castillo Gutiérrez, E., Rutkowski, P., Gogas, H. J., Lao, C. D., de Menezes, J. J., Dalle, S., Arance, A., Grob, J.-J., Srivastava, S., Abaskharoun, M., Hamilton, M., Keidel, S., Simonsen, K. L., Sobiesk, A. M., … Long, G. v. (2022). Relatlimab and Nivolumab versus Nivolumab in Untreated Advanced Melanoma. *New England Journal of Medicine*, *386*(1), 24–34. https://doi.org/10.1056/NEJMOA2109970/SUPPL_FILE/NEJMOA2109970_DATA-SHARING.PDF

Taylor, B. C., & Balko, J. M. (2022). Mechanisms of MHC-I Downregulation and Role in Immunotherapy Response. *Frontiers in Immunology*, *0*, 771. https://doi.org/10.3389/FIMMU.2022.844866

Tivol, E. A., Borriello, F., Schweitzer, A. N., Lynch, W. P., Bluestone, J. A., & Sharpe, A. H. (1995). Loss of CTLA-4 leads to massive lymphoproliferation and fatal multiorgan tissue destruction, revealing a critical negative regulatory role of CTLA-4. *Immunity*, *3*(5), 541–547. https://doi.org/10.1016/1074-7613(95)90125-6

Tolaney, S. M., Boucher, Y., Duda, D. G., Martin, J. D., Seano, G., Ancukiewicz, M., Barry, W. T., Goel, S., Lahdenrata, J., Isakoff, S. J., Yeh, E. D., Jain, S. R., Golshan, M., Brock, J., Snuderl, M., Winer, E. P., Krop, I. E., & Jain, R. K. (2015). Role of vascular density and normalization in response to neoadjuvant bevacizumab and chemotherapy in breast cancer patients. *Proceedings of the National Academy of Sciences of the United States of America*, *112*(46), 14325–14330. https://doi.org/10.1073/PNAS.1518808112/-/DCSUPPLEMENTAL

Twomey, J. D., & Zhang, B. (2021). Cancer Immunotherapy Update: FDA-Approved Checkpoint Inhibitors and Companion Diagnostics. *AAPS Journal*, *23*(2), 1–11. https://doi.org/10.1208/S12248-021-00574-0/FIGURES/2

Valdés-Ferrada, J., Muñoz-Durango, N., Pérez-Sepulveda, A., Muñiz, S., Coronado-Arrázola, I., Acevedo, F., Soto, J. A., Bueno, S. M., Sánchez, C., & Kalergis, A. M. (2020). Peripheral Blood Classical Monocytes and Plasma Interleukin 10 Are Associated to Neoadjuvant Chemotherapy Response in Breast Cancer Patients. *Frontiers in Immunology*, *11*, 1413. https://doi.org/10.3389/FIMMU.2020.01413/BIBTEX

Valpione, S., Pasquali, S., Campana, L. G., Piccin, L., Mocellin, S., Pigozzo, J., & Chiarion-Sileni, V. (2018). Sex and interleukin-6 are prognostic factors for autoimmune toxicity following treatment with anti-CTLA4 blockade. *Journal of Translational Medicine*, *16*(1), 1–10. https://doi.org/10.1186/S12967-018-1467-X/FIGURES/3

van Maaren, M. C., de Munck, L., Strobbe, L. J. A., Sonke, G. S., Westenend, P. J., Smidt, M. L., Poortmans, P. M. P., & Siesling, S. (2019). Ten-year recurrence rates for breast cancer subtypes in the Netherlands: A large population-based study. *International Journal of Cancer*, *144*(2), 263–272. https://doi.org/10.1002/IJC.31914

Wang, D. Y., Salem, J.-E. E., Cohen, J. v., Chandra, S., Menzer, C., Ye, F., Zhao, S., Das, S., Beckermann, K. E., Ha, L., Rathmell, W. K., Ancell, K. K., Balko, J. M., Bowman, C., Davis, E. J., Chism, D. D., Horn, L., Long, G. v., Carlino, M. S., … Johnson, D. B. (2018). Fatal Toxic Effects Associated With Immune Checkpoint Inhibitors: A Systematic Review and Meta-analysis. *JAMA Oncology*, *4*(12), 1721–1728. http://www.embase.com/search/results?subaction=viewrecord&from=export&id=L624011231

Wang, L., Simons, D. L., Lu, X., Tu, T. Y., Avalos, C., Chang, A. Y., Dirbas, F. M., Yim, J. H., Waisman, J., & Lee, P. P. (2020). Breast cancer induces systemic immune changes on cytokine signaling in peripheral blood monocytes and lymphocytes. *EBioMedicine*, *52*, 102631. https://doi.org/10.1016/J.EBIOM.2020.102631

Waterhouse, P., Penninger, J. M., Timms, E., Wakeham, A., Shahinian, A., Lee, K. P., Thompson, C. B., Griesser, H., & Mak, T. W. (1995). Lymphoproliferative Disorders

with Early Lethality in Mice Deficient in Ctla-4. *Science, 270*(5238), 985–988. https://doi.org/10.1126/SCIENCE.270.5238.985

Wei, S. C., Duffy, C. R., & Allison, J. P. (2018a). Fundamental Mechanisms of Immune Checkpoint Blockade Therapy. *Cancer Discovery, 8*(9), 1069–1086. https://aacrjournals.org/cancerdiscovery/article/8/9/1069/10253/Fundamental-Mechanisms-of-Immune-Checkpoint

Wei, S. C., Duffy, C. R., & Allison, J. P. (2018b). Fundamental mechanisms of immune checkpoint blockade therapy. *Cancer Discovery*, *8*(9), 1069–1086. https://doi.org/10.1158/2159-8290.CD-18-0367/333724/P/FUNDAMENTAL-MECHANISMS-OF-IMMUNE-CHECKPOINT

Wei, S. C., Meijers, W. C., Axelrod, M. L., Anang, N.-A. A. S., Screever, E. M., Wescott, E. C., Johnson, D. B., Whitley, E., Lehmann, L., Courand, P.-Y., Mancuso, J. J., Himmel, L. E., Lebrun-Vignes, B., Wleklinski, M. J., Knollmann, B. C., Srinivasan, J., Li, Y., Atolagbe, O. T., Rao, X., … Allison, J. P. (2020). A Genetic Mouse Model Recapitulates Immune Checkpoint Inhibitor–Associated Myocarditis and Supports a Mechanism-Based Therapeutic Intervention. *Cancer Discovery*, *11*(3), 614–639. https://doi.org/10.1158/2159-8290.cd-20-0856

Wei, S. C., Sharma, R., Anang, N. A. A. S., Levine, J. H., Zhao, Y., Mancuso, J. J., Setty, M., Sharma, P., Wang, J., Pe'er, D., & Allison, J. P. (2019). Negative Co-stimulation Constrains T Cell Differentiation by Imposing Boundaries on Possible Cell States. *Immunity*, *50*(4), 1084-1098.e10. https://doi.org/10.1016/J.IMMUNI.2019.03.004

Wolchok, J. D., Kluger, H., Callahan, M. K., Postow, M. A., Rizvi, N. A., Lesokhin, A. M., Segal, N. H., Ariyan, C. E., Gordon, R.-A., Reed, K., Burke, M. M., Caldwell, A., Kronenberg, S. A., Agunwamba, B. U., Zhang, X., Lowy, I., Inzunza, H. D., Feely, W., Horak, C. E., … Sznol, M. (2013). Nivolumab plus Ipilimumab in Advanced Melanoma. *New England Journal of Medicine*, *369*(2), 122–133. https://doi.org/10.1056/NEJMOA1302369/SUPPL_FILE/NEJMOA1302369_DISCLOSURES.PDF

Wölfl, M., & Greenberg, P. D. (2014). Antigen-specific activation and cytokine-facilitated expansion of naive, human CD8+ T cells. *Nature Protocols 2014 9:4*, *9*(4), 950–966. https://doi.org/10.1038/nprot.2014.064

Wong, K. L., Yeap, W. H., Tai, J. J. Y., Ong, S. M., Dang, T. M., & Wong, S. C. (2012). The three human monocyte subsets: implications for health and disease. *Immunologic Research*, *53*(1–3), 41–57. https://doi.org/10.1007/S12026-012-8297-3

Woo, S. R., Turnis, M. E., Goldberg, M. v, Bankoti, J., Selby, M., Nirschl, C. J., Bettini, M. L., Gravano, D. M., Vogel, P., Liu, C. L., Tangsombatvisit, S., Grosso, J. F., Netto, G., Smeltzer, M. P., Chaux, A., Utz, P. J., Workman, C. J., Pardoll, D. M., Korman, A. J., … Vignali, D. A. A. (2012). Immune inhibitory molecules LAG-3 and PD-1 synergistically regulate T-cell function to promote tumoral immune escape. *Cancer Research*, *72*(4), 917–927. https://doi.org/10.1158/0008-5472.CAN-11-1620

Wu, Y., Borde, M., Heissmeyer, V., Feuerer, M., Lapan, A. D., Stroud, J. C., Bates, D. L., Guo, L., Han, A., Ziegler, S. F., Mathis, D., Benoist, C., Chen, L., & Rao, A. (2006). FOXP3 controls regulatory T cell function through cooperation with NFAT. *Cell*, *126*(2), 375–387. https://doi.org/10.1016/J.CELL.2006.05.042

Xu, C., Chen, Y. P., Du, X. J., Liu, J. Q., Huang, C. L., Chen, L., Zhou, G. Q., Li, W. F., Mao, Y. P., Hsu, C., Liu, Q., Lin, A. H., Tang, L. L., Sun, Y., & Ma, J. (2018). Comparative safety of immune checkpoint inhibitors in cancer: systematic review and network meta-analysis. *BMJ (Clinical Research Ed.)*, *363*. https://doi.org/10.1136/BMJ.K4226

Xue, Q., Bettini, E., Paczkowski, P., Ng, C., Kaiser, A., McConnell, T., Kodrasi, O., Quigley, M. F., Heath, J., Fan, R., Mackay, S., Dudley, M. E., Kassim, S. H., & Zhou, J. (2017).

Single-cell multiplexed cytokine profiling of CD19 CAR-T cells reveals a diverse landscape of polyfunctional antigen-specific response. *Journal for ImmunoTherapy of Cancer*, *5*(1), 1–16. https://doi.org/10.1186/S40425-017-0293-7/FIGURES/5

Yang, X., Bam, M., Becker, W., Nagarkatti, P. S., & Nagarkatti, M. (2020). Long Noncoding RNA AW112010 Promotes the Differentiation of Inflammatory T Cells by Suppressing IL-10 Expression through Histone Demethylation. *The Journal of Immunology*, *205*(4), 987–993. https://doi.org/10.4049/jimmunol.2000330

Yau, C., Osdoit, M., Noordaa, M. van der, Shad, S., Wei, J., Croze, D. de, Hamy, A.-S., Laé, M., Reyal, F., Sonke, G. S., Steenbruggen, T. G., Seijen, M. van, Wesseling, J., Martín, M., Monte-Millán, M. del, López-Tarruella, S., Adamson, K., Albain, K. S., Asare, A. L., … Symmans, W. F. (2021). Residual cancer burden after neoadjuvant chemotherapy and long-term survival outcomes in breast cancer: a multicentre pooled analysis of 5161 patients. *The Lancet Oncology*, *0*(0). https://doi.org/10.1016/S1470-2045(21)00589-1

Zamami, Y., Niimura, T., Okada, N., Koyama, T., Fukushima, K., Izawa-Ishizawa, Y., & Ishizawa, K. (2019). Factors Associated With Immune Checkpoint Inhibitor–Related Myocarditis. *JAMA Oncology*, *5*(11), 1635–1637. https://doi.org/10.1001/JAMAONCOL.2019.3113

Zeng, W., Qin, S., Wang, R., Zhang, Y., Ma, X., Tian, F., Liu, X. R., Qin, X., Liao, S., Sun, L., & Lin, Y. (2020). PDL1 blockage increases fetal resorption and Tfr cells but does not affect Tfh/Tfr ratio and B-cell maturation during allogeneic pregnancy. *Cell Death & Disease 2020 11:2*, *11*(2), 1–13. https://doi.org/10.1038/s41419-020-2313-7

Zhang, L., Zlotoff, D. A., Awadalla, M., Mahmood, S. S., Nohria, A., Hassan, M. Z. O., Thuny, F., Zubiri, L., Chen, C. L., Sullivan, R. J., Alvi, R. M., Rokicki, A., Murphy, S. P., Jones-O'connor, M., Heinzerling, L. M., Barac, A., Forrestal, B. J., Yang, E. H., Gupta, D., … Neilan, T. G. (2020). Major adverse cardiovascular events and the timing and dose of corticosteroids in immune checkpoint inhibitor-associated myocarditis. *Circulation*, *141*(24), 2031–2034. https://doi.org/10.1161/CIRCULATIONAHA.119.044703

Zhu, A., Ibrahim, J. G., & Love, M. I. (2019). Heavy-Tailed prior distributions for sequence count data: Removing the noise and preserving large differences. *Bioinformatics*, *35*(12), 2084–2092. https://doi.org/10.1093/bioinformatics/bty895

Zitvogel, L., Apetoh, L., Ghiringhelli, F., & Kroemer, G. (2008). Immunological aspects of cancer chemotherapy. *Nature Reviews Immunology 2008 8:1*, *8*(1), 59–73. https://doi.org/10.1038/nri2216

Chapter II Appendix

Supplementary material for chapter II: A genetic mouse model recapitulates immune checkpoint inhibitor–associated myocarditis and supports a mechanism-based therapeutic intervention

	Ctla4$^{+/-}$ Pdcd1$^{-/-}$ mice		Ctla4$^{+/+}$ Pdcd1$^{-/-}$ mice	
Heart				
Number of mice evaluated	54		59	
Percentage male	48%		56%	
Percentage female	52%		44%	
Mean age evaluated	154.5 days		164.4 days	
	Male	Female	Male	Female
Percentage of mice with lymphocytic infiltrate	23%	39%	0.09%	19%
Mean lymphocytic infiltrate histology score	2.46	3.71	0.76	1.23
Percentage of mice with T cell infiltrate	34.6%	42.9%	15.2%	19.2%
Mean T cell infiltrate score	3.04	5.73	1.59	2.36
Pancreas				
Number of mice evaluated	44		42	
Percentage male	48%		45%	
Percentage female	52%		55%	
Mean age evaluated	139.6 days		149.4 days	
	Male	Female	Male	Female
Percentage of mice with lymphocytic infiltrate	71%	87%	11%	30%
Mean lymphocytic infiltrate histology score	4.43	5.13	0.68	1.13
Percentage of mice with T cell infiltrate	62%	77%	39%	43%
Mean T cell infiltrate score	3.15	3.27	1.22	1.52
Percentage of mice with exocrine atrophy	43%	57%	5%	0%

Supplemental Table S2.1. Histological analyses of heart and pancreatic tissues of Ctla4+/- Pdcd1-/- mice and Ctla4+/+ Pdcd1-/- mice. Semi-quantitative histologic scores of cardiac and pancreatic tissues. Mouse characteristics including age, sex, and genotype are denoted. Lymphocytic infiltration was defined by a histologic score of greater or equal to 2 of H&E stained tissue section. T cell infiltrate was defined by a histologic score of greater or equal to 2 for CD3 IHC stained tissue sections.
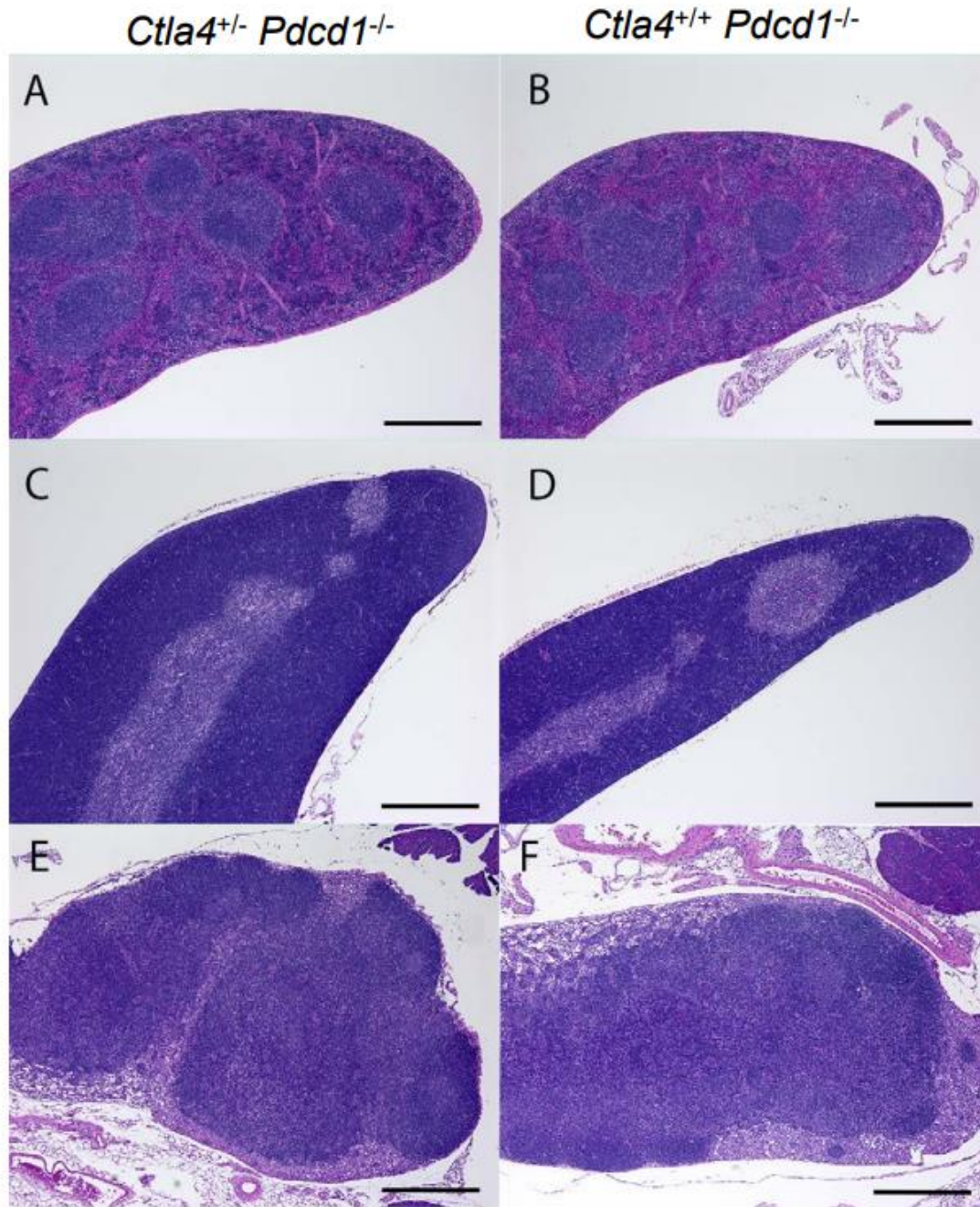
Supplemental Figure S2.1: Absence of lymphoproliferative or abnormal morphology in lymphoid tissues of Ctla4+/- Pdcd1-/- mice. A-B) Representative photomicrograph images of H&E stained spleen tissue from 28-day old *Ctla4+/- Pdcd1-/-* and *Ctla4+/+ Pdcd1-/-* mice. Bar = 500 microns. C-D) Representative photomicrograph images of H&E stained thymus tissue from 28-day old *Ctla4+/- Pdcd1-/-* and *Ctla4+/+ Pdcd1-/-* mice. Bar = 500 microns. E-F) Representative photomicrograph images of H&E stained mesenteric lymph node tissue from 28-day old *Ctla4+/- Pdcd1-/-* and *Ctla4+/+ Pdcd1-/-* mice. Bar = 500 microns.
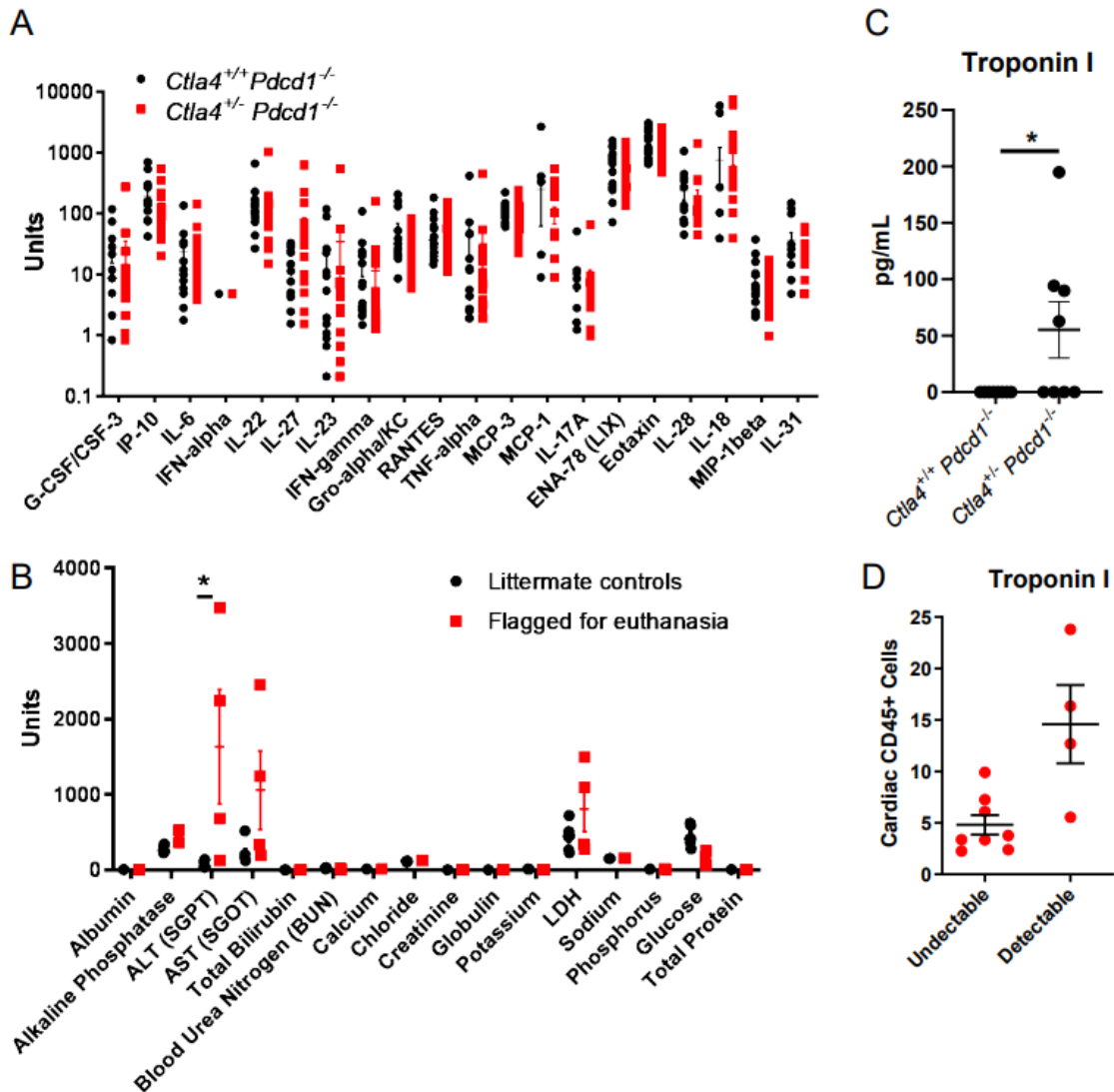
Supplemental Figure S2.2. Characterization of serum properties in Ctla4+/- Pdcd1-/- mice. A) Serum levels of cytokine in *Ctla4+/- Pdcd1-/-* and *Ctla4+/+ Pdcd1-/-* mice. Mice analyzed were 29-362 days old. This combined two cohorts, including a young cohort with *Ctla4+/- Pdcd1-/-* mice that displayed clinical signs as well as aged mice. All comparisons included aged-matched littermate controls. B) Serum chemistry of *Ctla4+/- Pdcd1-/-* mice displaying clinical signs requiring euthanasia and control littermate mice. Mice analyzed were 40-50 days old. C) Serum troponin levels in *Ctla4+/- Pdcd1-/-* and *Ctla4+/+ Pdcd1-/-* mice. Mice analyzed were 40-50 days old. *, P<0.05 T-test. D) CD45+ heart infiltration, by flow cytometry, in *Ctla4+/- Pdcd1-/-* mice where serum troponin levels were detectable via ELISA vs. those where they were not.
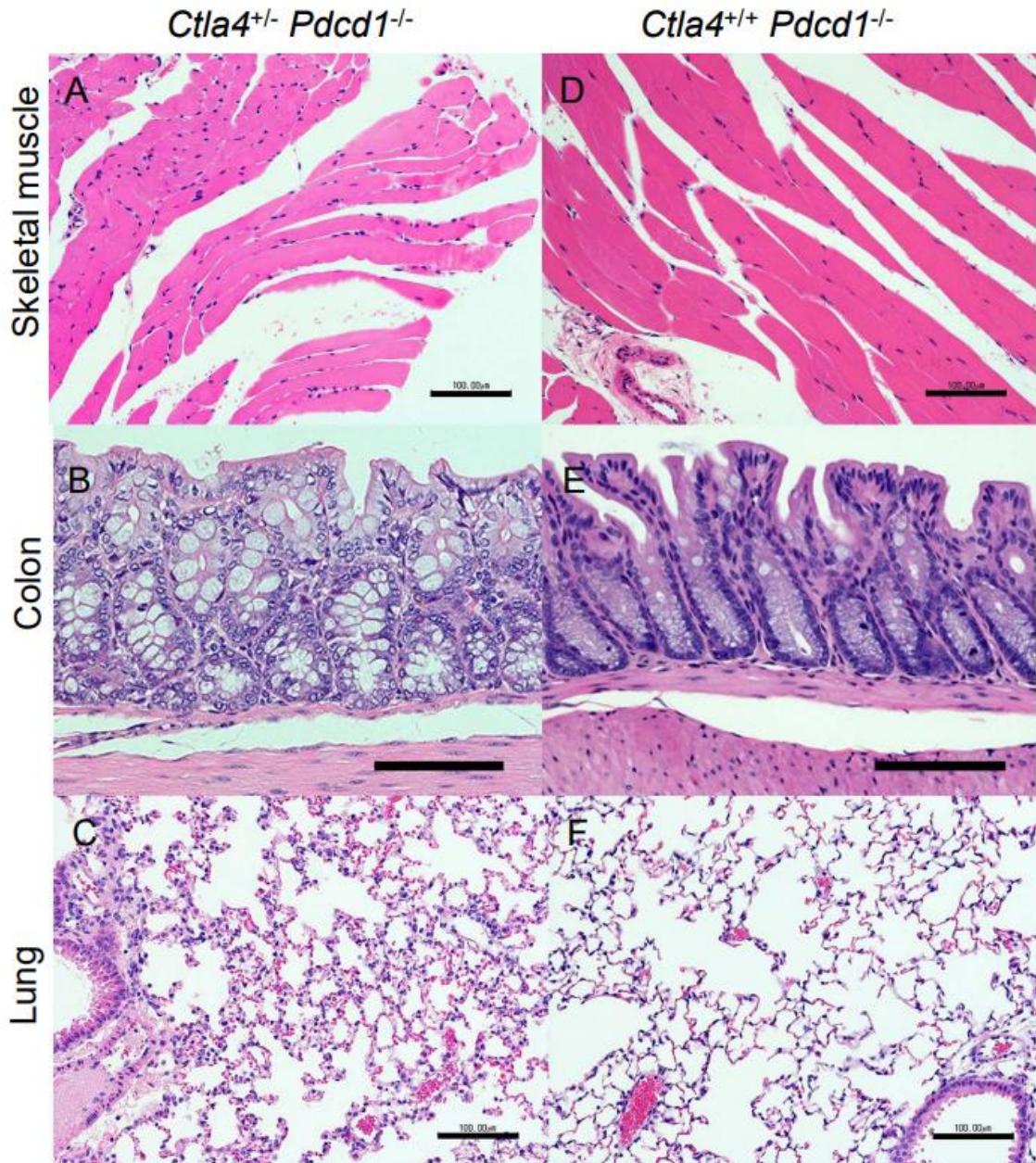
Supplemental Figure S2.3: Histopathology of skeletal muscle, colon and lung tissue in Ctla4+/- Pdcd1-/- mice. Representative photomicrographs of skeletal muscle, colon, and lung from littermate 99-day-old, male heterozygous (A, B, C) and wild-type (D, E, F) Ctla-4 mice. Note the increased cellularity of the interstitium in the lung of the heterozygous mouse. Cellular infiltrates are not increased in skeletal muscle or colon, compared with the wild-type mouse. Hematoxylin and eosin. Bar = 100 microns.
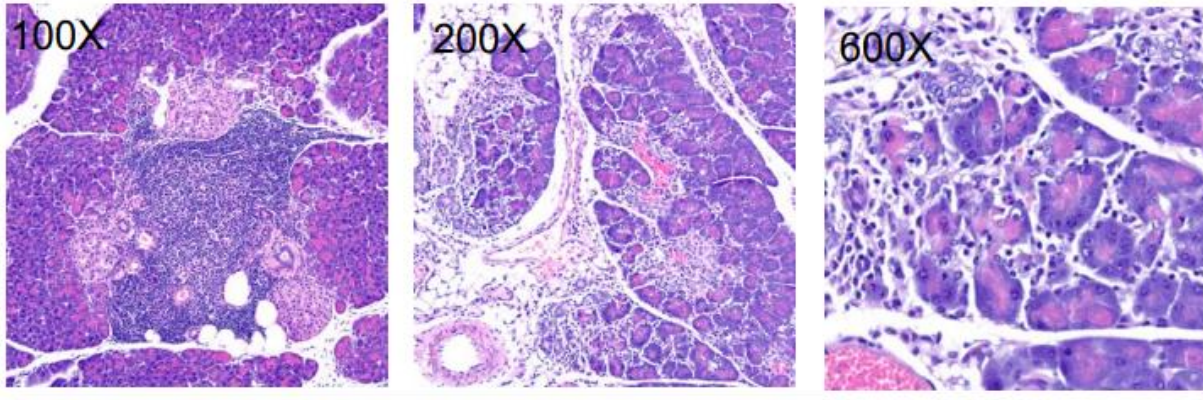
Pancreas

Supplemental Figure S2.4. Pancreatic histopathology in Ctla4+/- Pdcd1-/- mice.
Photomicrograph images of H&E stained pancreatic tissue from Ctla4+/- Pdcd1-/- mice.
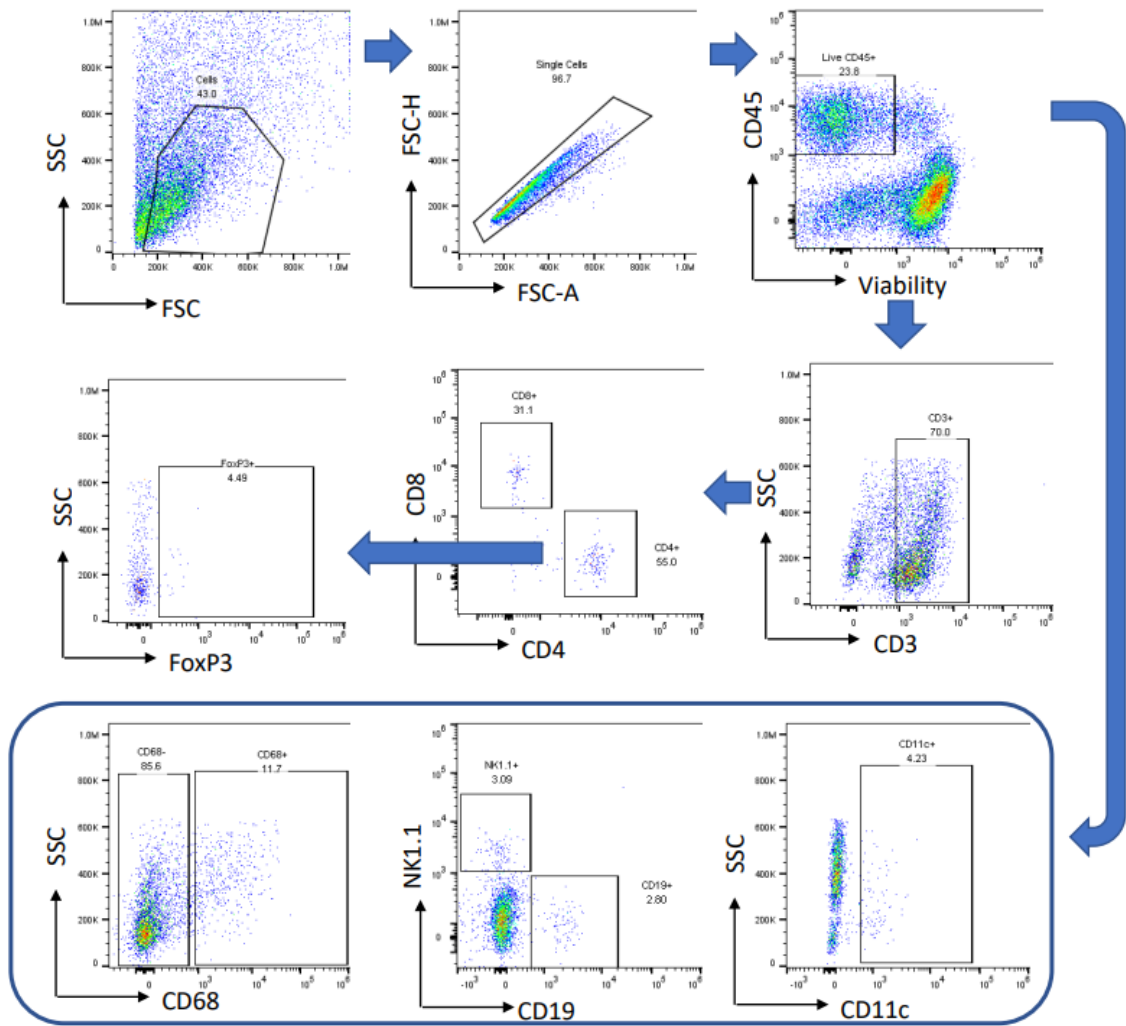
Supplemental Figure S2.5: Gating strategy/example for characterization of cardiac immune infiltrates of Ctla4+/- Pdcd1-/- mice. Dissociated cardiac tissue from mice were gated for singlet status, viability, and CD45 positivity, followed by enumeration of the identified populations.
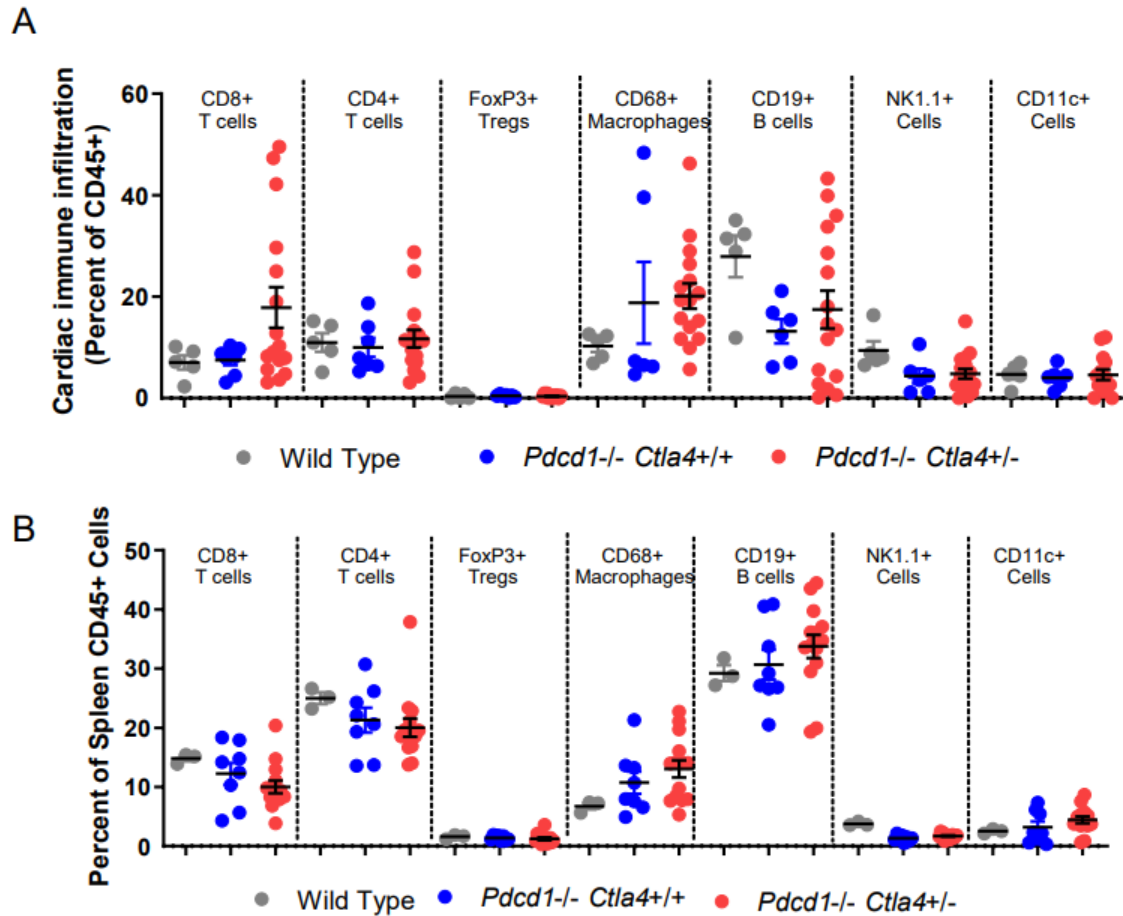
Supplemental Figure S2.6: Characterization of splenic populations among genotypes. A) Flow cytometry analysis of cardiac immune populations expressed as a percent of total CD45+ cells (No statistically significant different between groups by ANOVA) B) Flow cytometry analysis of immune populations in murine spleens, matched from Fig. 2.2E (No statistically significant different between groups by ANOVA).

Chapter III Appendix

Supplementary material for chapter III: Cytotoxic T cells specific for alpha-myosin drive immunotherapy related myocarditis

Supplementary Figure S3.1. Myocarditis is characterized by activated immune cells and clonal T cells. a) Gene expression of key identity genes, showing cell types of clusters. b) Differential
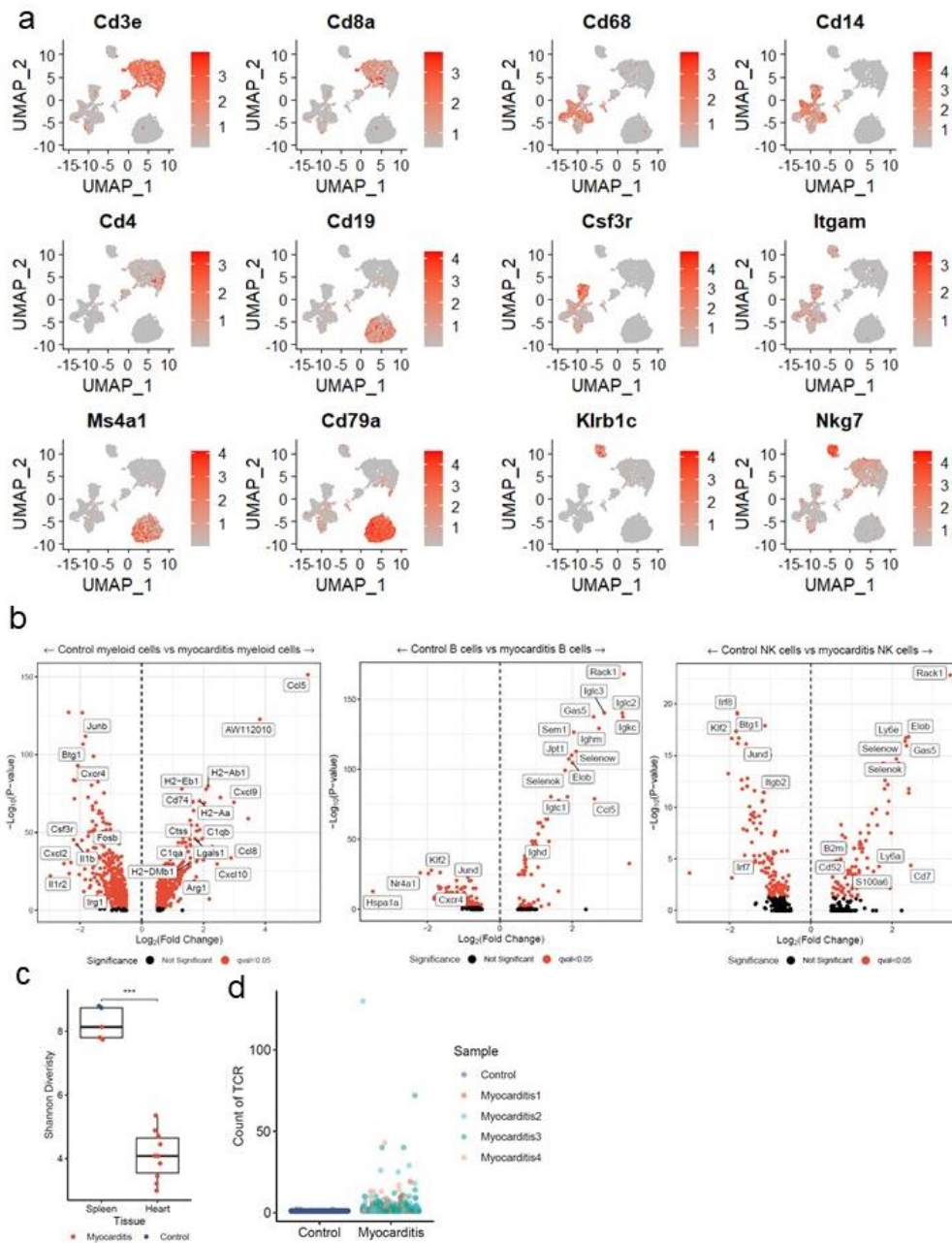
gene expression for myeloid, B and NK cells in myocarditis compared to control cardiac CD45+ cells. Red indicates FDR-corrected p-value (q-value) <0.05. Black indicates not significant. c) Shannon diversity on bulk TCR sequencing beta chain repertoires. Color indicates whether the tissue was derived from a control wild type mouse (blue) or a *Pdcd1-/-Ctla4+/-* mouse with myocarditis (red). P-value represents a Wilcoxon test. d) TCR counts in single cell data. Myocarditis sample is divided by mouse of origin. Clonal TCRs are found in all 4 sequenced hearts.
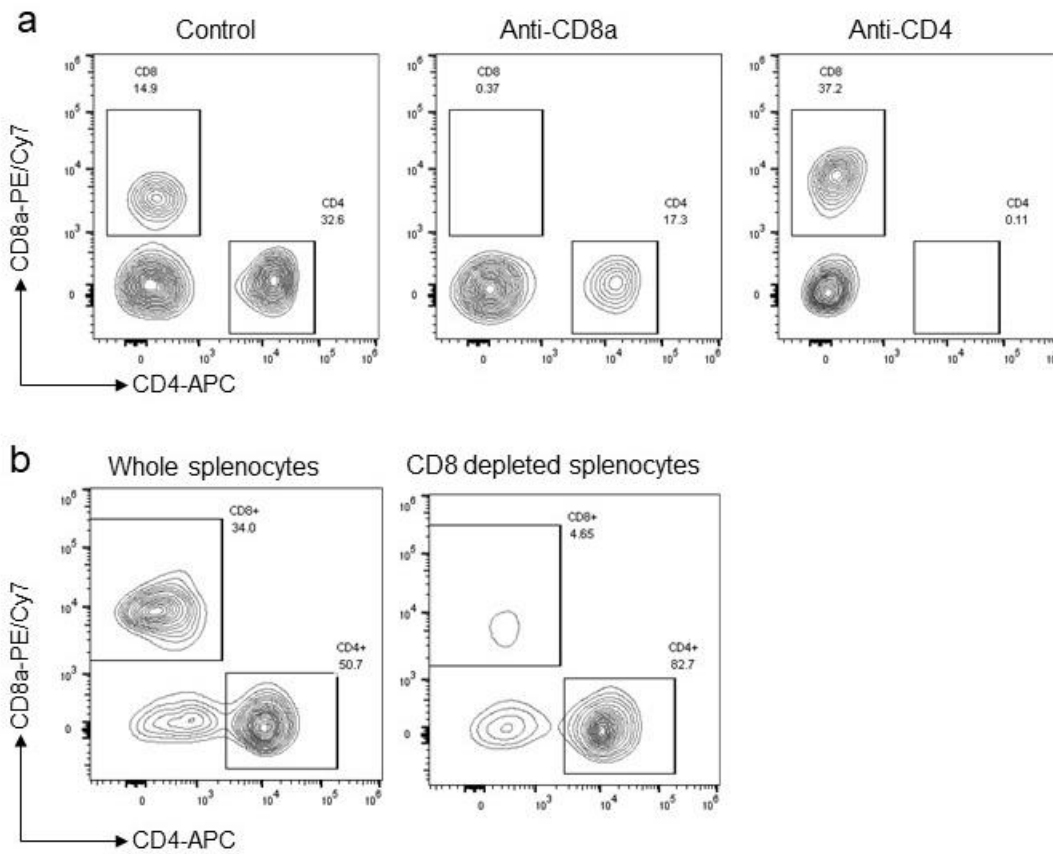
Supplementary Figure S3.2. Confirmation of cell type depletion. a) Representative flow cytometry gated on live CD45+ cells isolated from blood of different treatment groups. b) Representative flow cytometry on CD8 depleted (via magnetic beads) compared to whole splenocytes used for adoptive transfer.
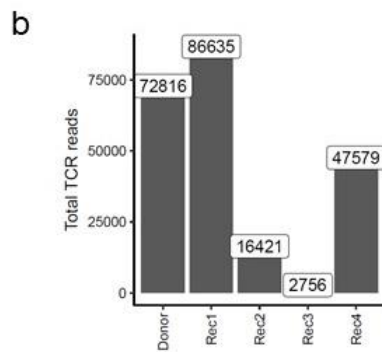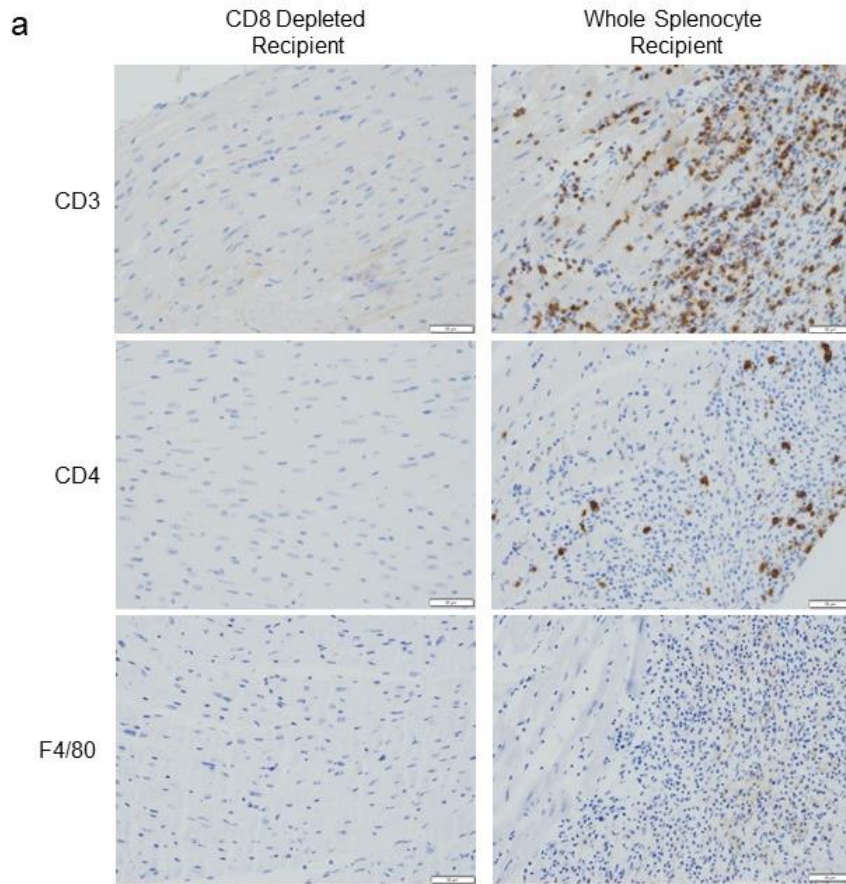
Supplementary Figure S3.3. Adoptive transfer of whole splenocytes recapitulates myocarditis.
a) Representative immunohistochemistry on hearts of a CD8 depleted splenocyte recipient compared to a whole splenocyte recipient. Only cardiac sections are shown. Scale bars show 50μm. b) Total TCR reads for cardiac TCR sequencing on donor and recipient hearts.
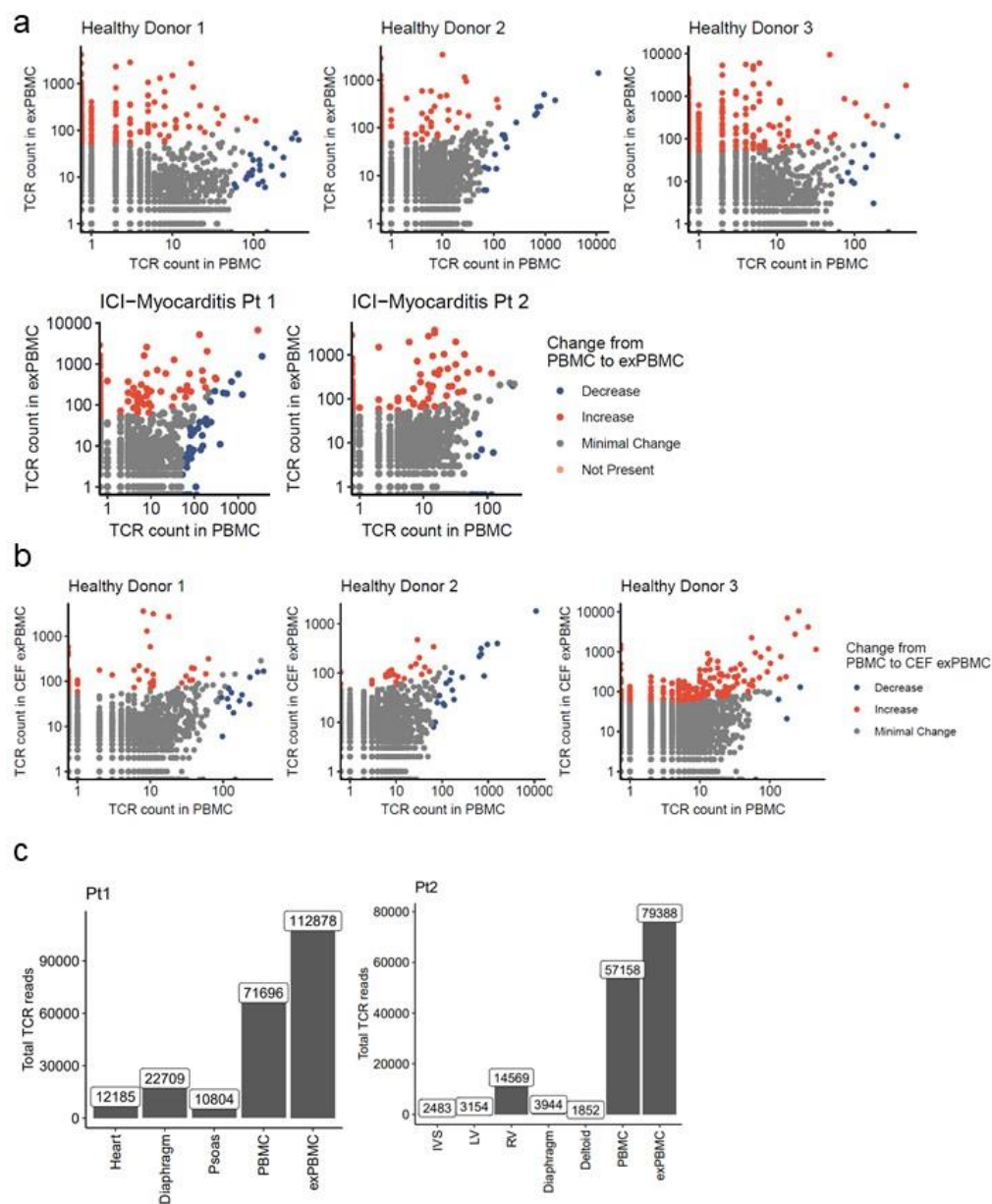
Supplementary Figure S3.4. TCR sequencing on exPBMC shows expansion of alpha-myosin and CEF specific TCRs. a) Comparison of TCR abundance in alpha-myosin exPBMC and pre-expansion PBMC for all patients. Color represents change from PBMC to exPBMC. Minimal change is less than a 50 read count change. b) Comparison of TCR abundance in CEF exPBMC and pre-expansion PBMC for all patients. Color represents change from PBMC to CEF exPBMC. Minimal change is less than a 50 read count change. b) Total TCR reads for biopsy (heart), autopsy, and PBMC samples from patients 1 and 2.
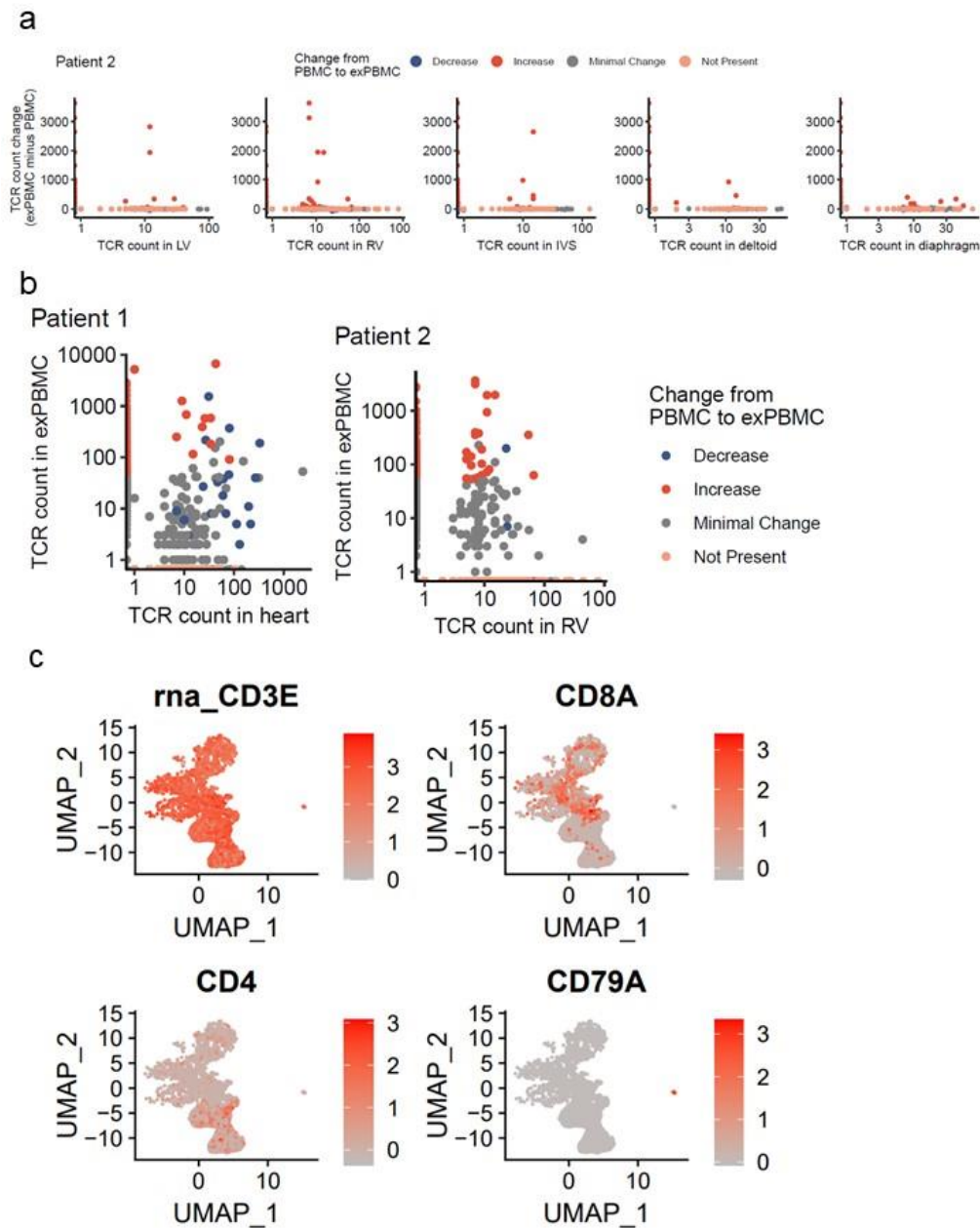
Supplementary Figure S3.5. Alpha-myosin expanded TCRs are found in the hearts and skeletal muscles of patients with ICI-myocarditis. a) Change in TCR counts from PBMC to alpha-myosin exPBMC plotted by abundance in indicated tissues for patient 2. b) Comparison of TCR abundance in alpha-myosin exPBMC and heart (biopsy for patient 1 or right ventricle for patient 2). Color represents change from PBMC to exPBMC. Minimal change is less than a 50 read count change. Not present means not found in either PBMC or exPBMC, but present in indicated tissue. c) Gene expression is shown on single cell sequencing of CD3 sorted exPBMCs from patient 1.

Full TCR sequences

TCR-A

5' GGG – restriction enzyme site for BglII – alpha chain – 2A – Beta Chain- stop codon – restriction site for SalI- GGG 3'

GGGAGATCTATGAAATCCTTGAGTGTTTCCCTAGTGGTCCTGTGGCTCCAGTTAAACTGGG
TGAACAGCCAGCAGAAGGTGCAGCAGAGCCCAGAATCCCTCATTGTCCCAGAGGGAGCCA
TGACCTCTCTCAACTGCACTTTCAGCGACAGTGCTTCTCAGTATTTTGCATGGTACAGACA
GCATTCTGGGAAAGCCCCCAAGGCACTGATGTCCATCTTCTCCAATGGTGAAAAGAAGAA
GGCAGATTCACAATTCACCTCAATAAAGCCAGTCTGCATTTCTCCCTGCACATCAGAGACT
CCCAGCCCAGTGACTCTGCTCTCTACCTCTGTGCAGTGAGCGATAGAGGTTCAGCCTTAG
GGAGGCTGCATTTTGGAGCTGGGACTCAGCTGATTGTCATACCTGACATCCAGAACCCAG
AACCTGCTGTGTACCAGTTAAAAGATCCTCGGTCTCAGGACAGCACCCTCTGCCTGTTCAC
CGACTTTGACTCCCAAATCAATGTGCCGAAAACCATGGAATCTGGAACGTTCATCACTGAC
AAAACTGTGCTGGACATGAAAGCTATGGATTCCAAGAGCAATGGGGCCATTGCCTGGAGC
AACCAGACAAGCTTCACCTGCCAAGATATCTTCAAAGAGACCAACGCCACCTACCCCAGTT
CAGACGTTCCCTGTGATGCCACGTTGACTGAGAAAAGCTTTGAAACAGATATGAACCTAAA
CTTTCAAAACCTGTCAGTTATGGGACTCCGAATCCTCCTGCTGAAAGTAGCCGGATTTAAC
CTGCTCATGACGCTGAGGCTGTGGTCCTCCGGAGAGGGCAGAGGAAGTCTGCTAACATGC
GGTGACGTCGAGGAGAATCCTGGCCCAATGTGGCAGTTTTGCATTCTGTGCCTCTGTGTA
CTCATGGCTTCTGTGGCTACAGACCCCACAGTGACTTTGCTGGAGCAAAACCCAAGGTGG
CGTCTGGTACCACGTGGTCAAGCTGTGAACCTACGCTGCATCTTGAAGAATTCCCAGTATC
CCTGGATGAGCTGGTATCAGCAGGATCTCCAAAAGCAACTACAGTGGCTGTTCACTCTGC
GGAGTCCTGGGGACAAAGAGGTCAAATCTCTTCCCGGTGCTGATTACCTGGCCACACGGG
TCACTGATACGGAGCTGAGGCTGCAAGTGGCCAACATGAGCCAGGGCAGAACCTTGTACT
GCACCTGCAGTGCAGCCTGGGGCGGCAGTGCAGAAACGCTGTATTTTGGCTCAGGAACCA
GACTGACTGTTCTCGAGGATCTGAGAAATGTGACTCCACCCAAGGTCTCCTTGTTTGAGCC
ATCAAAAGCAGAGATTGCAAACAAACAAAAGGCTACCCTCGTGTGCTTGGCCAGGGGCTT
CTTCCCTGACCACGTGGAGCTGAGCTGGTGGGTGAATGGCAAGGAGGTCCACAGTGGGG
TCAGCACGGACCCTCAGGCCTACAAGGAGAGCAATTATAGCTACTGCCTGAGCAGCCGCC
TGAGGGTCTCTGCTACCTTCTGGCACAATCCTCGAAACCACTTCCGCTGCCAAGTGCAGTT
CCATGGGCTTTCAGAGGAGGACAAGTGGCCAGAGGGCTCACCCAAACCTGTCACACAGAA
CATCAGTGCAGAGGCCTGGGGCCGAGCAGACTGTGGAATCACTTCAGCATCCTATCATCA
GGGGGTTCTGTCTGCAACCATCCTCTATGAGATCCTACTGGGGAAGGCCACCCTATATGCT
GTGCTGGTCAGTGGCCTAGTGCTGATGGCCATGGTCAAGAAAAAAAATTCCTAGGTCGAC
GGG

TCR-B

5' GGG – restriction enzyme site for BglII- restriction site for PmeI – Kozak- alpha chain – SG 2A – Beta Chain- stop codon – restriction site for SalI- restriction site for BamHI - GGG 3'

GGGAGATCTGTTTAAACGCCGCCACCATGAACAGGCTGCTGTGCTCTCTGCTGGGGCTTC
TGTGCACCCAGGTTTGCTGGGTGAAAGGACAGCAAGTGCAGCAGAGCCCCGCGTCCTTG
GTTCTGCAGGAGGGGGAGAATGCAGAGCTGCAGTGTAACTTTTCCACATCTTTGAACAGTA
TGCAGTGGTTTTACCAACGTCCTGAGGGAAGTCTCGTCAGCCTGTTCTACAATCCTTCTGG
GACAAAGCAGAGTGGGAGACTGACATCCACAACAGTCATCAAAGAACGTCGCAGCTCTTT
GCACATTTCCTCCTCCCAGATCACAGACTCAGGCACTTATCTCTGTGCTCTGGAGAGGGCC
TCTGGCAGCTGGCAACTCATCTTTGGATCTGGAACCCAACTGACAGTTATGCCTGACATCC
AGAACCCAGAACCTGCTGTGTACCAGTTAAAAGATCCTCGGTCTCAGGACAGCACCCTCTG

141

CCTGTTCACCGACTTTGACTCCCAAATCAATGTGCCGAAAACCATGGAATCTGGAACGTTC
ATCACTGACAAAACTGTGCTGGACATGAAAGCTATGGATTCCAAGAGCAATGGGGCCATTG
CCTGGAGCAACCAGACAAGCTTCACCTGCCAAGATATCTTCAAAGAGACCAACGCCACCTA
CCCCAGTTCAGACGTTCCCTGTGATGCCACGTTGACTGAGAAAAGCTTTGAAACAGATATG
AACCTAAACTTTCAAAACCTGTCAGTTATGGGACTCCGAATCCTCCTGCTGAAAGTAGCCG
GATTTAACCTGCTCATGACGCTGAGGCTGTGGTCCAGTTCCGGAGAGGGCAGAGGAAGTC
TGCTAACATGCGGTGACGTCGAGGAGAATCCTGGCCCAATGGGCATCCAGACCCTCTGTT
GTGTGATCTTTTATGTTCTGATAGCAAATCACACAGATGCTGGAGTTACCCAGACACCCAG
ACATGAGGTGGCAGAGAAAGGACAAACAATAATCCTGAAGTGTGAGCCAGTTTCAGGCCA
CAATGACCTTTTCTGGTACAGACAGACCAAGATACAGGGACTAGAGTTGCTGAGCTACTTC
CGCAGCAAGTCTCTTATGGAAGATGGTGGGGCTTTCAAGGATCGATTCAAAGCTGAGATG
CTAAATTCATCCTTCTCCACTCTGAAGATTCAACCTACAGAACCCAAGGACTCAGCTGTGTA
TCTGTGTGCCAGCAGTCTGAGGAGGGGCGAACAGTACTTCGGTCCCGGCACCAGGCTCA
CGGTTTTAGAGGATCTGAGAAATGTGACTCCACCCAAGGTCTCCTTGTTTGAGCCATCAAA
AGCAGAGATTGCAAACAAACAAAAGGCTACCCTCGTGTGCTTGGCCAGGGGCTTCTTCCC
TGACCACGTGGAGCTGAGCTGGTGGGTGAATGGCAAGGAGGTCCACAGTGGGGTCAGCA
CGGACCCTCAGGCCTACAAGGAGAGCAATTATAGCTACTGCCTGAGCAGCCGCCTGAGGG
TCTCTGCTACCTTCTGGCACAATCCTCGAAACCACTTCCGCTGCCAAGTGCAGTTCCATGG
GCTTTCAGAGGAGGACAAGTGGCCAGAGGGCTCACCCAAACCTGTCACACAGAACATCAG
TGCAGAGGCCTGGGGCCGAGCAGACTGTGGAATCACTTCAGCATCCTATCATCAGGGGGGT
TCTGTCTGCAACCATCCTCTATGAGATCCTACTGGGGAAGGCCACCCTATATGCTGTGCTG
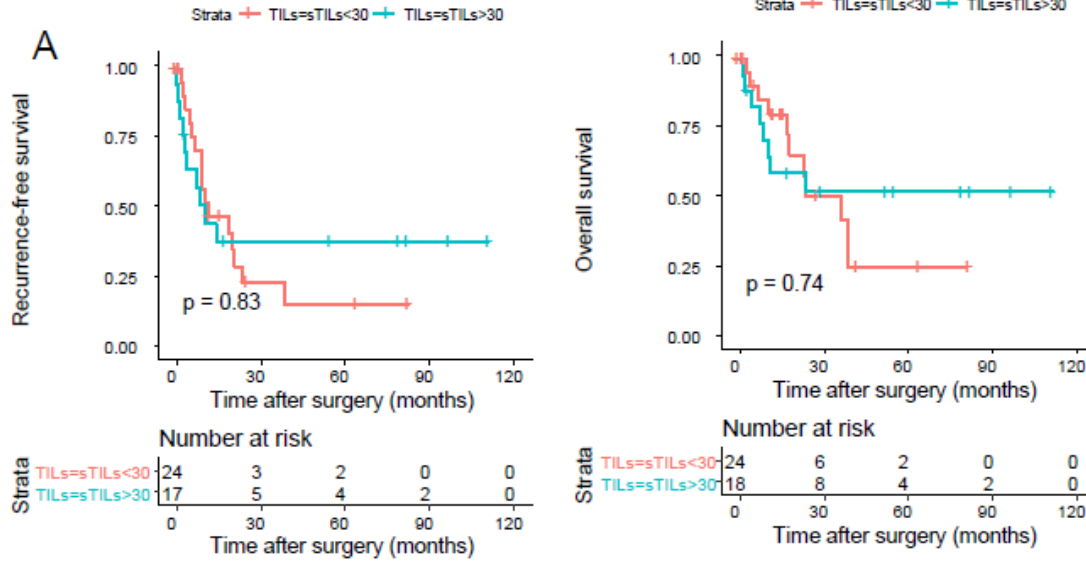GTCAGTGGCCTAGTGCTGATGGCCATGGTCAAGAAAAAAATTCCTAGGTCGACGGATCC
GGG

TCR-C
5' GGG – restriction enzyme site for BglII- restriction site for PmeI – Kozak- alpha chain – SG
2A – Beta Chain- stop codon – restriction site for SalI- restriction site for BamHI - GGG 3'

GGGAGATCTGTTTAAACGCCGCCACCATGGACTTTTCTCCAGGCTTCGTGGCTGTGATACT
TCTCATACTTGGAAGGACCCACGGAGATTCCGTGACTCAAACAGAAGGCCAAGTGACCGT
CTCAGAAAGCAAGTCCCTGATAATAAATTGCACGTATTCAGCCACAAGCATAGCTTACCCTA
ATCTTTTCTGGTATGTTCGATATCCTGGAGAAGGTCTACAACTCCTCCTGAAAGTCATTACG
GCTGGCCAGAAGGGAAGCAGCAGAGGGTTTGAAGCCACATACAATAAAGAAACCACCTCC
TTCCACTTGCAGAAAGCCTCAGTGCAAGAGTCAGACTCGGCTGTGTACTACTGTGCTCTGG
GCGACAGGAATAATGCAGGTGCCAAGCTCACATTCGGAGGGGGAACAAGGTTAACGGTCA
GACCCGACATCCAGAACCCAGAACCTGCTGTGTACCAGTTAAAAGATCCTCGGTCTCAGG
ACAGCACCCTCTGCCTGTTCACCGACTTTGACTCCCAAATCAATGTGCCGAAAACCATGGA
ATCTGGAACGTTCATCACTGACAAAACTGTGCTGGACATGAAAGCTATGGATTCCAAGAGC
AATGGGGCCATTGCCTGGAGCAACCAGACAAGCTTCACCTGCCAAGATATCTTCAAAGAGA
CCAACGCCACCTACCCCAGTTCAGACGTTCCCTGTGATGCCACGTTGACTGAGAAAAGCTT
TGAAACAGATATGAACCTAAACTTTCAAAACCTGTCAGTTATGGGACTCCGAATCCTCCTGC
TGAAAGTAGCCGGATTTAACCTGCTCATGACGCTGAGGCTGTGGTCCAGTTCCGGAGAGG
GCAGAGGAAGTCTGCTAACATGCGGTGACGTCGAGGAGAATCCTGGCCCAATGTCTAACA
CTGCCTTCCCTGACCCCGCCTGGAACACCACCCTGCTATCTTGGGTTGCTCTCTTTCTCCT
GGGAACAAGTTCAGCAAATTCTGGGGTTGTCCAGTCTCCAAGATACATAATCAAAGGAAAG
GGAGAAAGGTCCATTCTAAAATGTATTCCCATCTCTGGACATCTCTCTGTGGCCTGGTATC
AACAGACTCAGGGGCAGGAACTAAAGTTCTTCATTCAGCATTATGATAAAATGGAGAGAGA
TAAAGGAAACCTGCCCAGCAGATTCTCAGTCCAACAGTTTGATGACTATCACTCTGAGATG
AACATGAGTGCCTTGGAGCTAGAGGACTCTGCCGTGTACTTCTGTGCCAGCTCTCTGGGC
GGCACCGTGCAAGACACCCAGTACTTTGGGCCAGGCACTCGGCTCCTCGTGTTAGAGGAT
CTGAGAAATGTGACTCCACCCAAGGTCTCCTTGTTTGAGCCATCAAAAGCAGAGATTGCAA

142

ACAAACAAAAGGCTACCCTCGTGTGCTTGGCCAGGGGCTTCTTCCCTGACCACGTGGAGC
TGAGCTGGTGGGTGAATGGCAAGGAGGTCCACAGTGGGGTCAGCACGGACCCTCAGGCC
TACAAGGAGAGCAATTATAGCTACTGCCTGAGCAGCCGCCTGAGGGTCTCTGCTACCTTCT
GGCACAATCCTCGAAACCACTTCCGCTGCCAAGTGCAGTTCCATGGGCTTTCAGAGGAGG
ACAAGTGGCCAGAGGGCTCACCCAAACCTGTCACACAGAACATCAGTGCAGAGGCCTGGG
GCCGAGCAGACTGTGGAATCACTTCAGCATCCTATCATCAGGGGGTTCTGTCTGCAACCAT
CCTCTATGAGATCCTACTGGGGAAGGCCACCCTATATGCTGTGCTGGTCAGTGGCCTAGT
GCTGATGGCCATGGTCAAGAAAAAAATTCCTAGGTCGACGGATCCGGG

Chapter IV Appendix

Supplementary material for chapter IV: Changes in peripheral and local tumor immunity after neoadjuvant chemotherapy reshape clinical outcomes
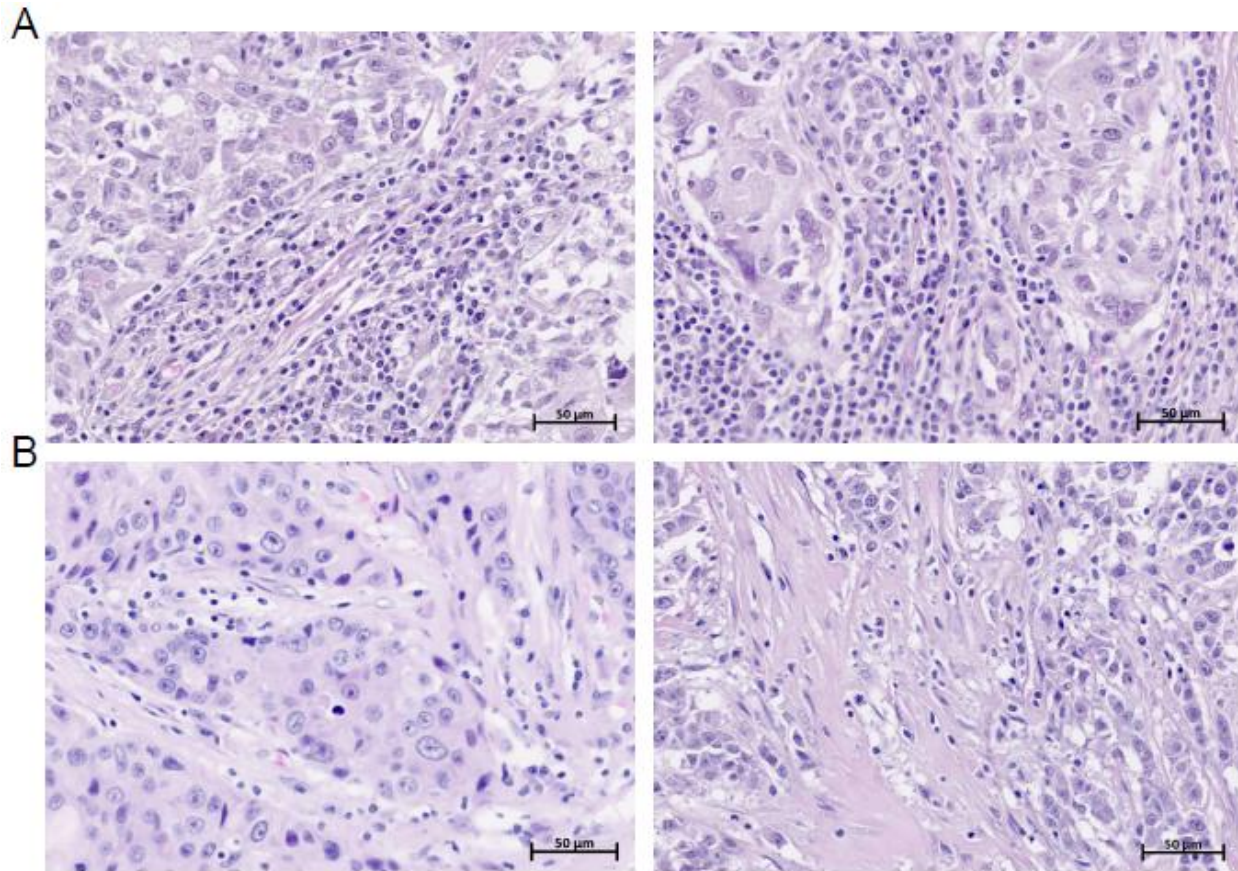
Supplementary Figure S4.1: Representative images of high and low sTILs. A) Representative histology of breast cancer samples with high (>30%) sTILs. Left image has 60% sTILs and right image has 70% sTILs. B) Representative histology of breast cancer samples with low (<30%) sTILs. Left image has 15% sTILs and right image has 5% sTILs.

Supplementary Figure S4.2: Pre-NAC sTILs have minimal prognostic value in breast cancer patients with residual disease. A) Pre-NAC sTILs are not associated with RFS (left) or OS (right) after surgery in TNBC patients with residual disease (n=41 and 42 patients, respectively). Confirmed TNBC patients are stratified based on post-NAC sTILs ≤ 30% or > 30%, scored as recommended by the International TILs Working Group, according to the pre-defined cut point. B) Pre-NAC sTILs are not associated with RFS (left) or OS (right) after surgery in unselected patients with residual disease (n=75 and 81 patients, respectively).

Post-NAC sTILs in all patients

A
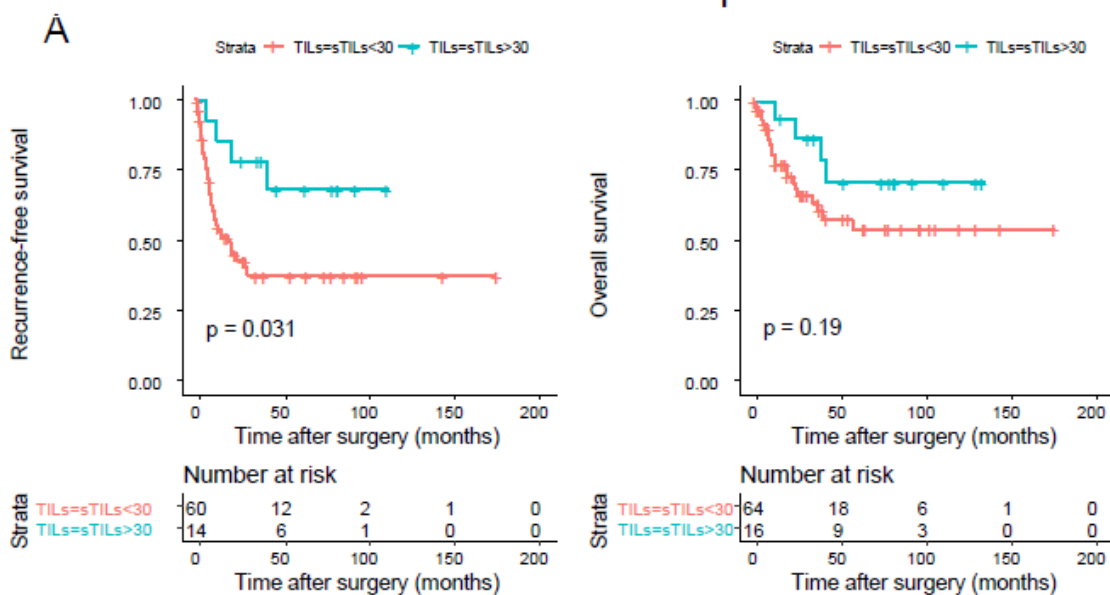
Post-NAC sTILs in non-TNBC patients

B
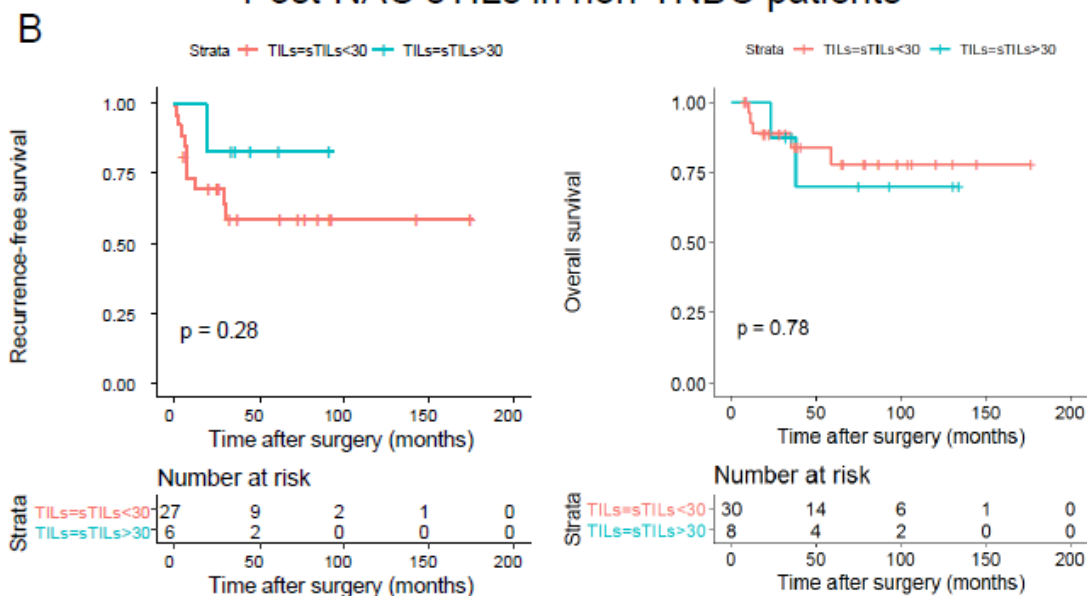
Supplementary Figure S4.3: The prognostic value of sTILs is primarily confined to the post-NAC specimen in TNBC patients with residual disease. A) Post-NAC sTILs are moderately associated with RFS (left), but not OS (right) after surgery in unselected patients with residual disease (n=74 and 80 patients, respectively). B) Post-NAC sTILs are not associated with RFS (left), or OS (right) after surgery in non-TNBC patients with residual disease (n=33 and 38 patients, respectively).
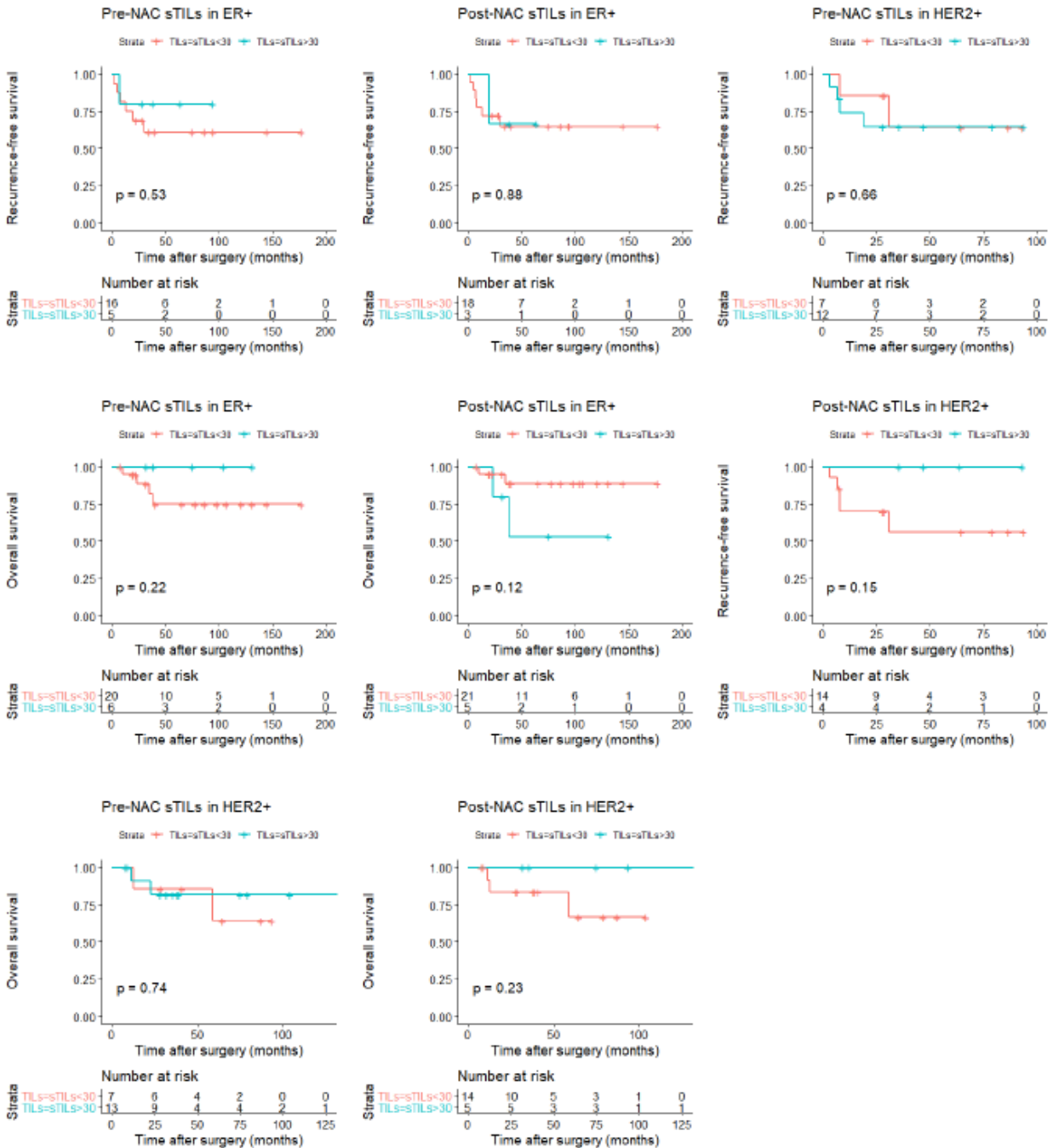
Supplementary Figure S4.4: sTILs are not prognostic in ER+ or HER2+ disease. Kaplan Meier plots of the association of pre- or post- NAC sTILs in either ER+ or HER2+ disease with recurrence-free survival or overall survival.
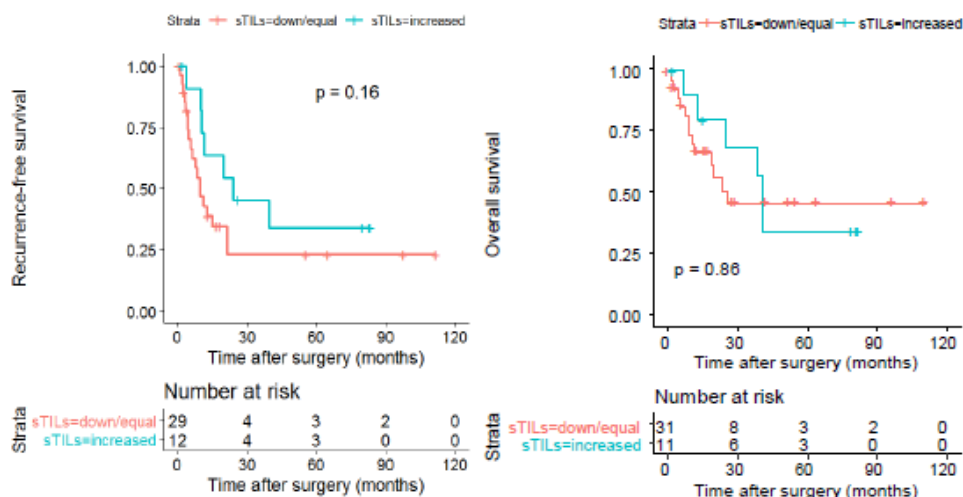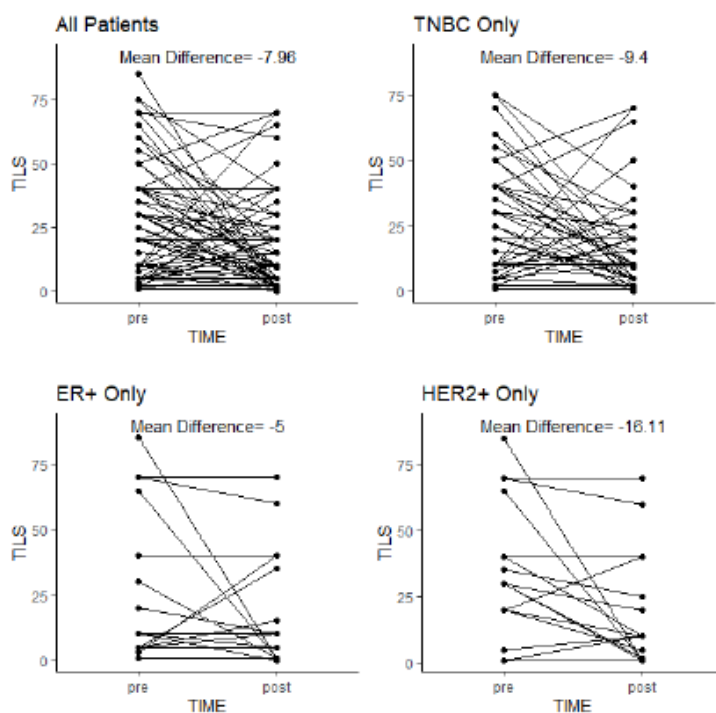
Supplementary Figure S4.5: The change in sTILs during NAC is not prognostic for outcome in TNBC patients with residual disease. A) The change in sTILs from pre- to post-NAC is not associated with RFS (left) or OS (right) after surgery in TNBC patients with residual disease (n=41 and 42 patients, respectively). Strata are defined as whether sTILs was decreased/equivocal (red) or increased (blue). B) Difference in sTILs from pre- to post-NAC is shown for all patients, and by IHC subtype. The mean difference (post - pre) in sTILs for each group is shown on each plot.
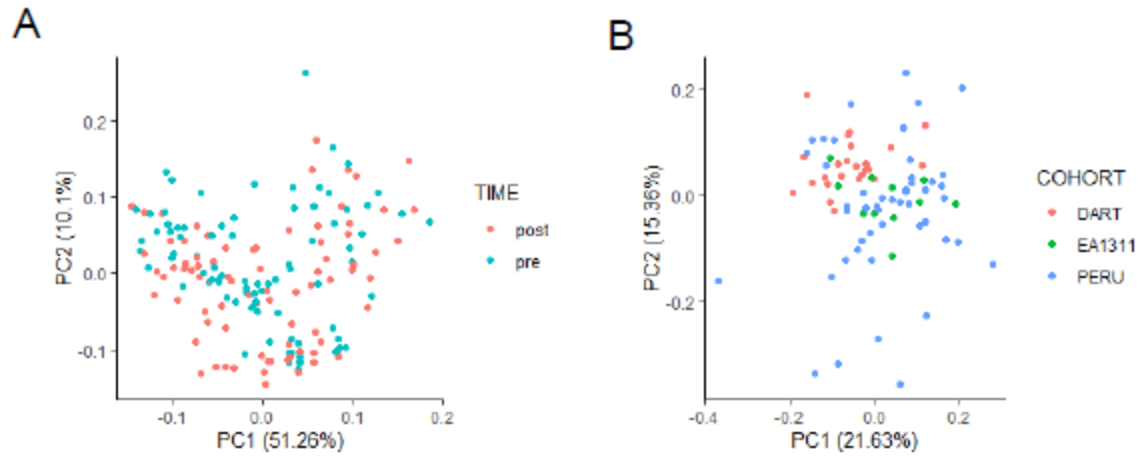
Supplementary Figure S4.6: Neither time of sample nor institution drive significant gene expression changes. A) Principal component analysis of log nanoString data for all samples. Colors represent pre-NAC biopsy or post-NAC surgical resection. B) Principal component analysis of log-delta (post-pre) nanoString data for all samples. Colors represent cohort.
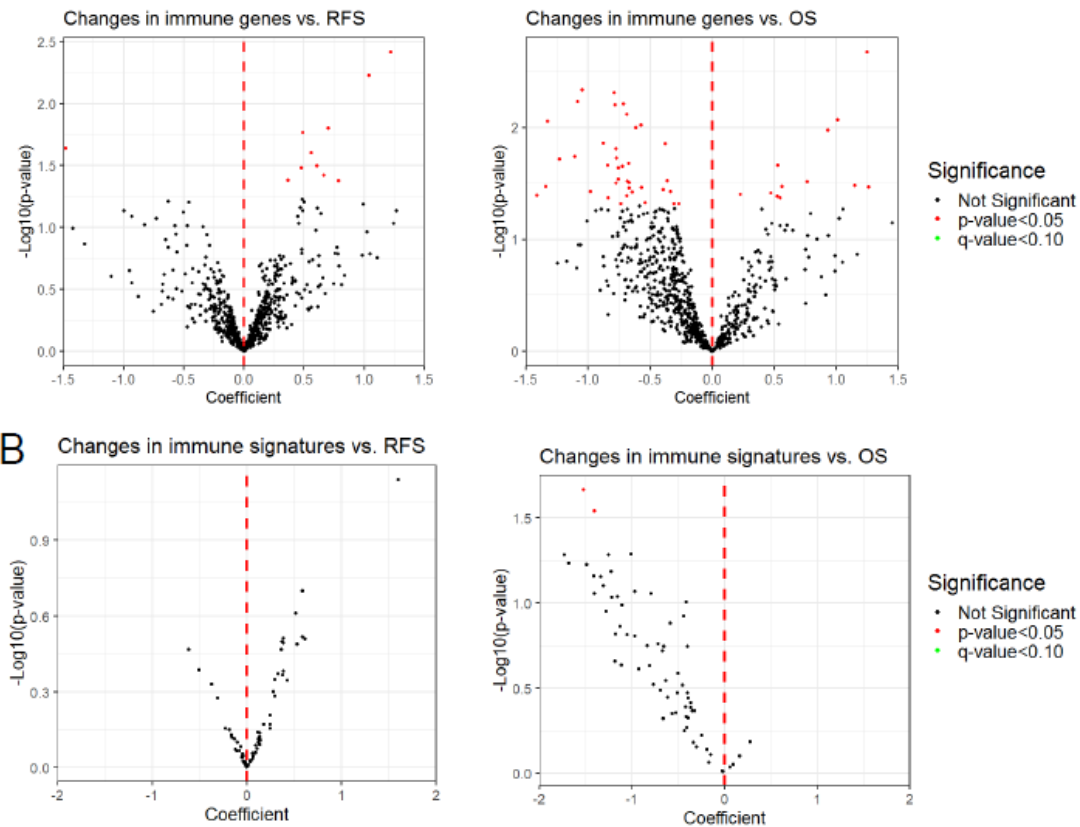
Supplementary Figure S4.7: Changes in immunologic signatures in response to NAC are not associated with outcome in non-TNBC tumors with residual disease. A) Volcano plot of the association of changes in immune genes or B) gene sets (n=70) with RFS or OS in non-TNBC. Genes and sets are colored by statistical significance (red: nominal p-value <0.05; black: not significant). No genes or sets were significantly associated with RFS or OS after correcting for multiple comparisons (q<0.10).
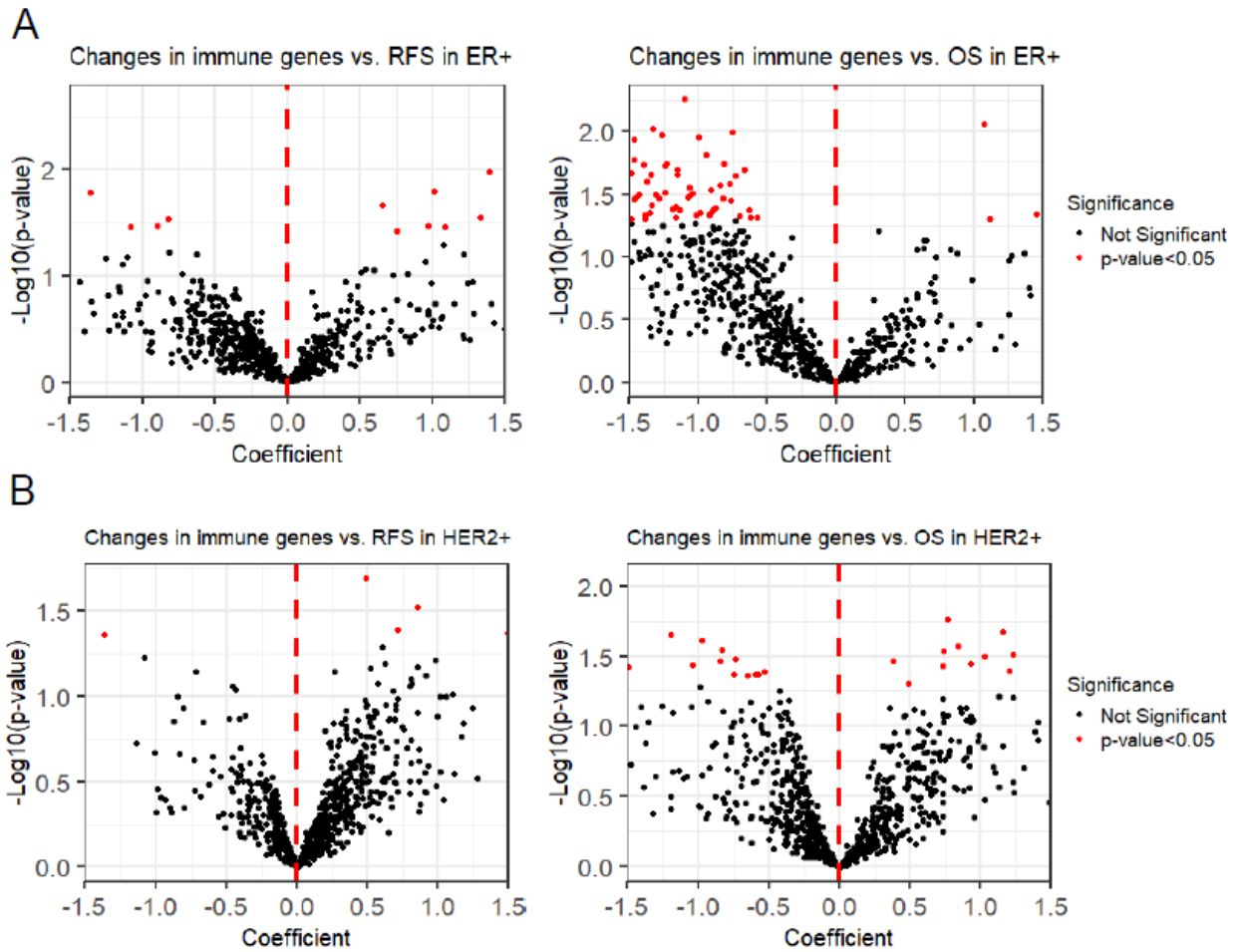
Supplementary Figure S4.8: Changes in immune-related genes in response to NAC are not associated with outcome in ER+ or HER2+ tumors with residual disease. A) Volcano plot of the association of changes in immune genes with RFS or OS in ER+ tumors. B) Volcano plot of the association of changes in immune genes with RFS or OS in HER2+ tumors. Genes are colored by statistical significance (red: nominal p-value <0.05; black: not significant). No genes were significantly associated with RFS or OS after correcting for multiple comparisons (q<0.10).
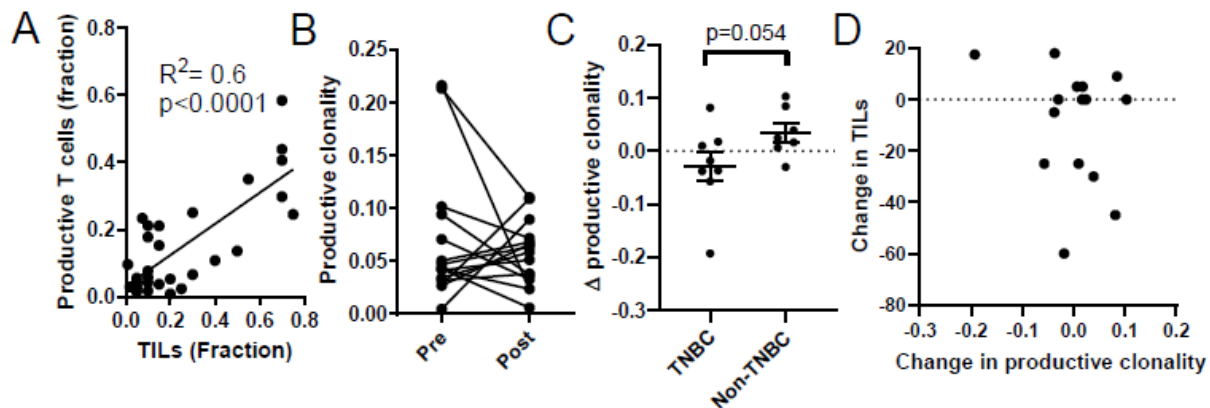
Supplementary Figure S4.9: Changes in sTILs after NAC do not correspond to an observed change in T cell clonality. A) 15 pre- and post-NAC samples (n=30 total) were analyzed by TCRβ chain sequencing (Adaptive ImmunoSEQ). The imputed number of T cells sequenced in each sample correlates strongly to the number of sTILs analyzed by H&E on adjacent sections. B) Changes in intra-tumor T cell clonality before and after NAC is plotted by individual patient. C) Change in intra-tumor T cell clonality before and after NAC (Post-Pre) is plotted according to TNBC status (TNBC n=8; non-TNBC n=7). Error bars represent mean ± sem. P-value represents result of two-sample t-test. D) No correlation was observed between change in sTILs and change in productive TCRβ clonality across individual patients.
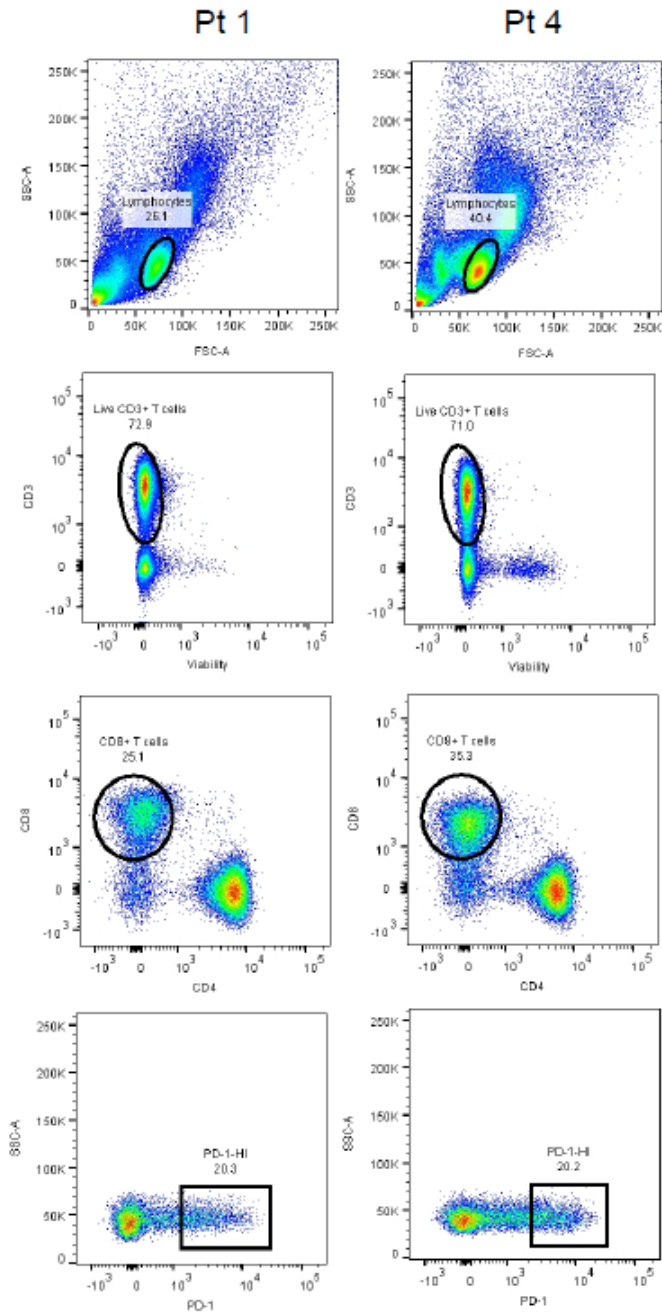
Supplementary Figure S4.10: Example FACS gating to identify PD-1^{HI} CD8+ T cells from peripheral blood. Cells were gated on singlet-lymphocytes, viability-stain negative, CD3+, CD8+, and the top 20% of PD-1 expressing cells were selected for downstream analysis.
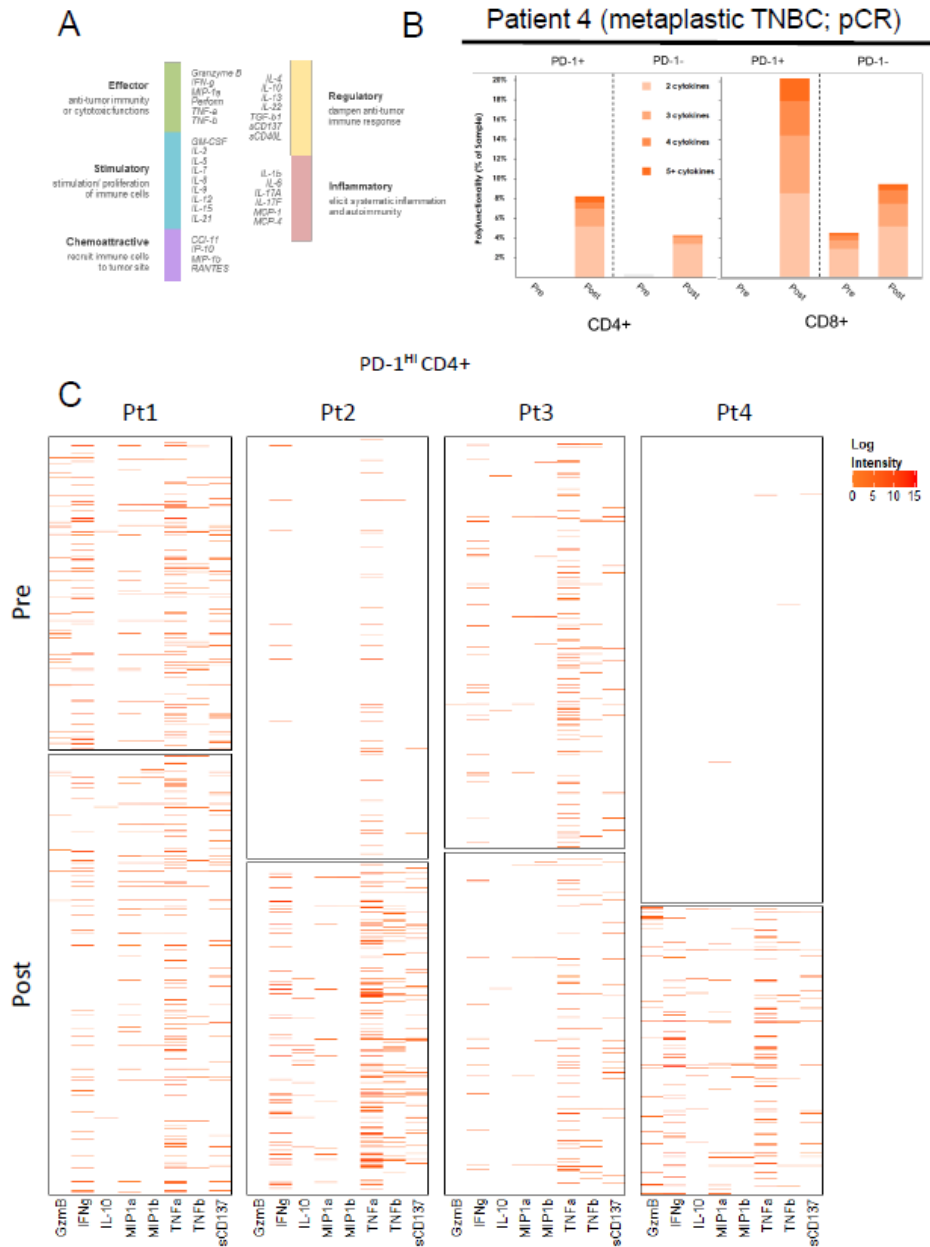
Supplementary Figure S4.11: Cytokine secretion is markedly enriched in PD-1^{HI} T cells after NAC in a patient with pCR to NAC in TNBC. A) Cytokines assayed and functional grouping B) Polyfunctionality of PD-1^{HI} CD4+, PD-1^{NEG} CD4+, PD-1^{HI} CD8+ and PD-1^{NEG} CD8+ T cells isolated from PBMCs in Pt. 4 (TNBC; pCR) prior to and after NAC was determined by Isoplexis single-cell cytokine profiling. Polyfunctionality is defined as the percentage of cells capable of producing ≥ 2 cytokines following CD3/CD28 stimulation. The percentage of cells in each sample capable of secreting 2, 3, 4, or 5+ cytokines are depicting in stacked bars. Greater increases in polyfunctionality in the CD8+ compartment with NAC were observed in PD-1^{HI} cells, consistent with the observation that the PD-1^{HI} CD8+ peripheral T cell compartment is enriched for tumor-specific T cells. C) Heatmap representation of log cytokine signal intensity of each cell in each patient sample, pre and post NAC. Each row represents one PD-1^{Hi}CD4+ T cell. White indicates no cytokine secreted.
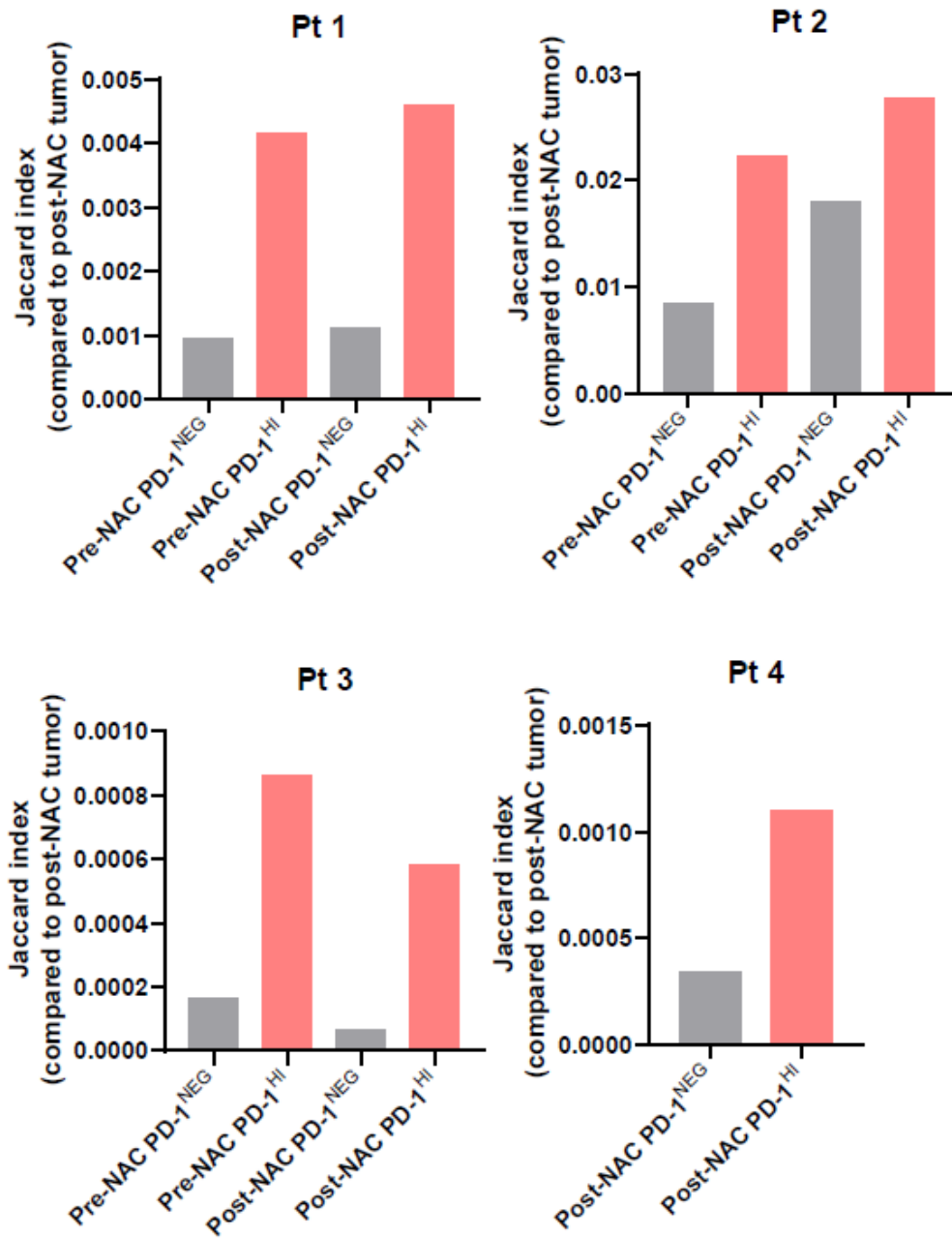
Supplementary Figure S4.12: TCRβ repertoires in the post-NAC residual disease or tumor scar are most like PD-1^{HI} CD8+ peripheral repertoires. For each patient analyzed, the Jaccard index, normalized for individual sample detected TCR repertoire size, is plotted against the TCRβ repertoire detected in the post-NAC tumor (Pts. 1-3) or post-NAC tumor scar (Pt. 4).
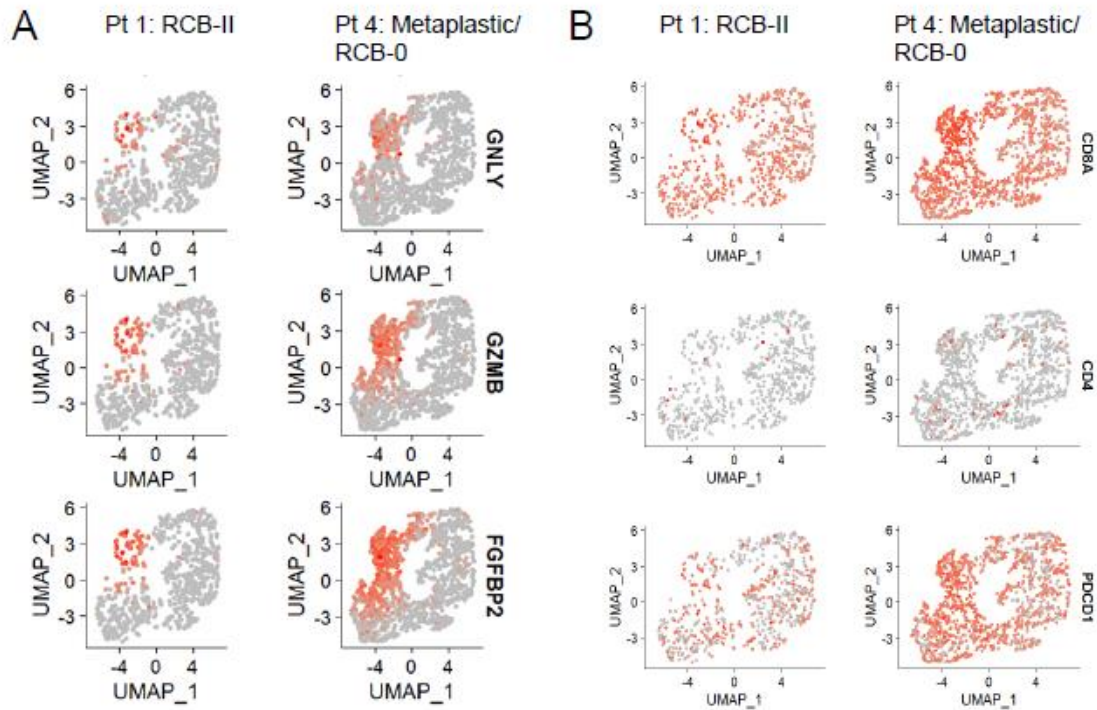
Supplementary Figure S4.13: Purity-of-sort analysis. A) Cluster 0 is selectively enriched for cytolytic transcripts *GNLY, GZMB,* and *FGFBP2*. B) UMAP cluster heatmap analysis of expected RNA markers *CD4* (not expressed), *CD8A* (universally expressed), and *PDCD1* (universally but variably expressed).
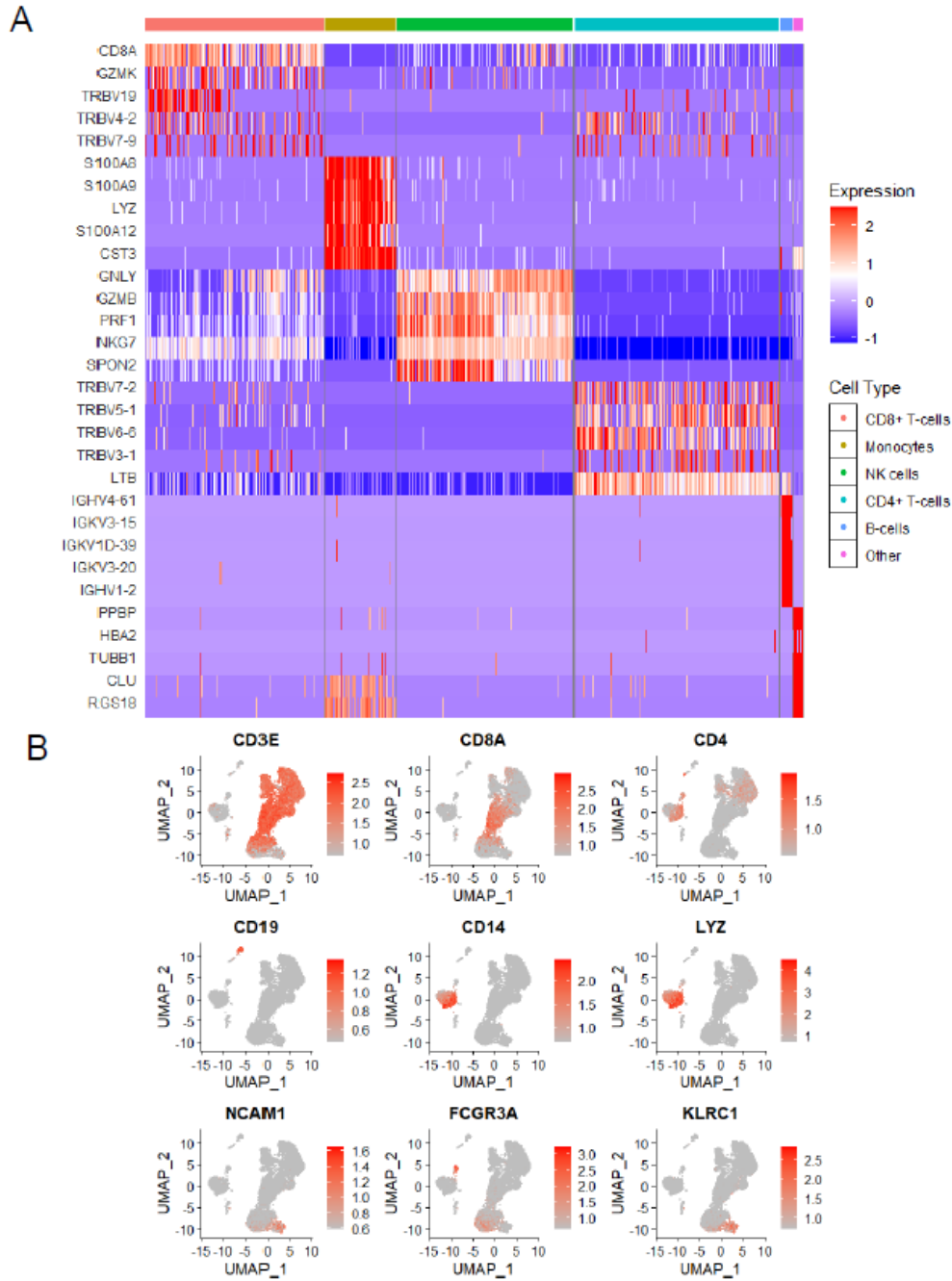
Supplementary Figure S4.14: Differentially expressed genes by cluster in whole blood single cell RNA sequencing. A) Heatmap showing the top 5 differentially expressed transcripts across singleR-defined cell type clusters. B) Feature plots showing expression of key cell type identity genes confirms cell type annotation by singleR.
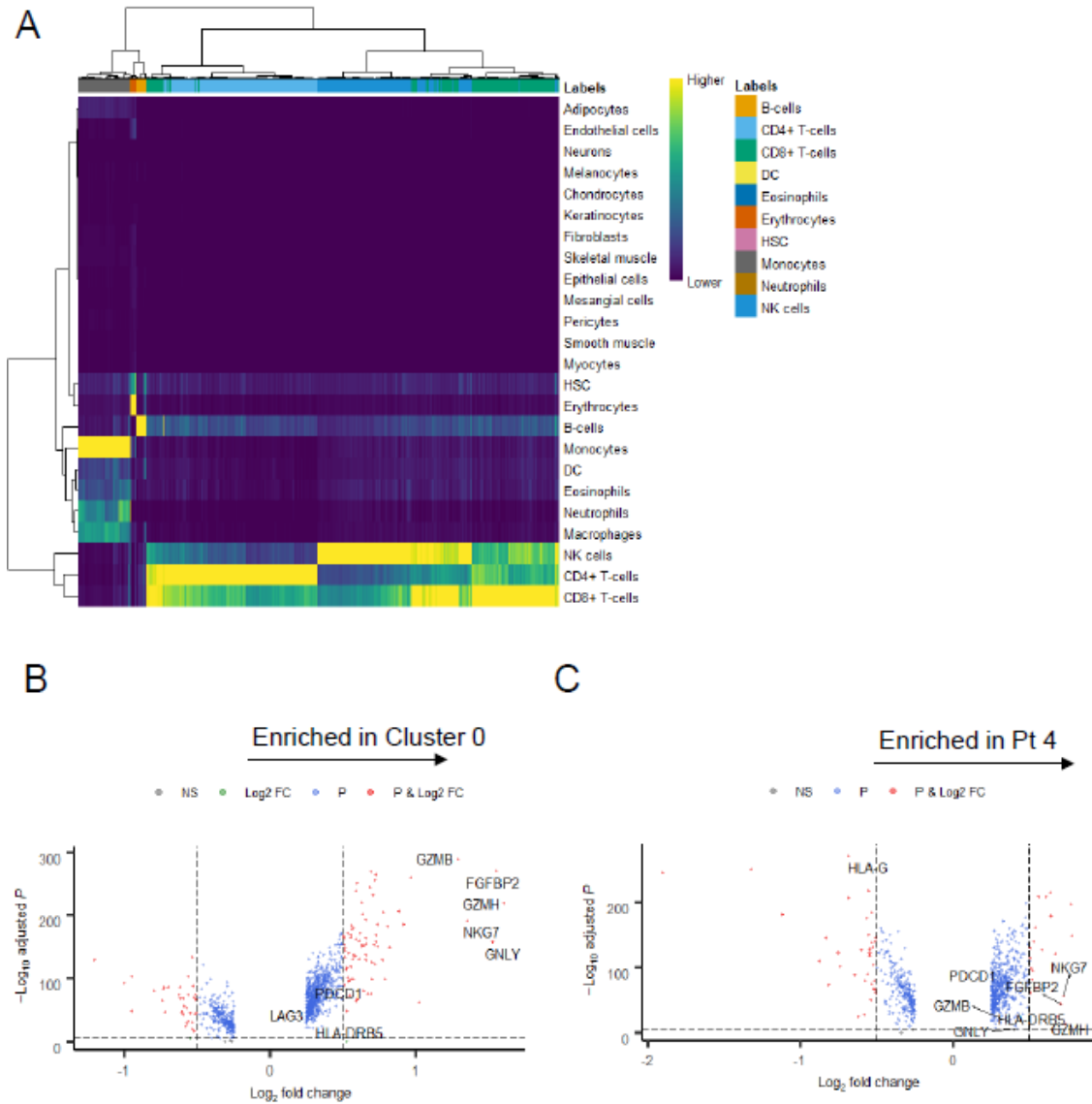
Supplementary Figure S4.15: Differential analysis to identify candidate genes for blood-based detection. A) Heatmap of confidence scores for cell type labels assigned by SingleR using BlueprintEncodeData as a reference. B) Volcano plot for genes enriched in 'cluster 0' versus all others C) Volcano plot for genes enriched in patient 1 versus patient 4. Genes are colored by significance (grey: not significant; green: $\log_2$ fold change> |0.5|; blue: adjusted $p \leq 0.05$; red: adjusted $p < 0.05$ and $\log_2$ fold change > |0.5|).
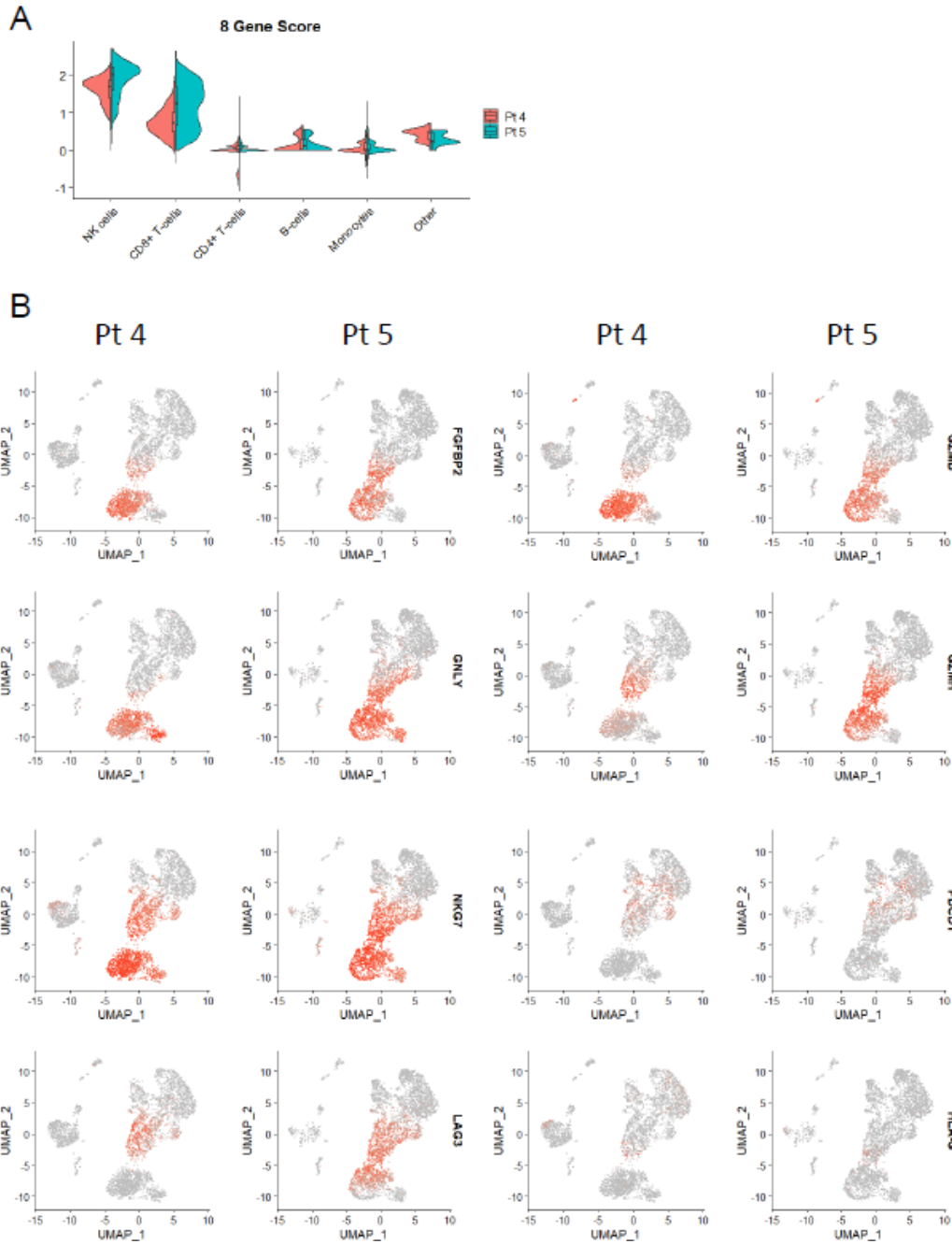
Supplementary Figure S4.16: 8 gene score is predominately expressed by CD8+ T cells and NK cells in both patients. A) Violin plot of 8 gene score (*FGFBP2 + GNLY + GZMB + GZMH + NKG7 + LAG3 + PDCD1 – HLA-G*) by both cell type and patient. Overlaid box plots show mean and interquartile range. B) Feature plots showing expression of each gene in the 8 gene score split by patient.
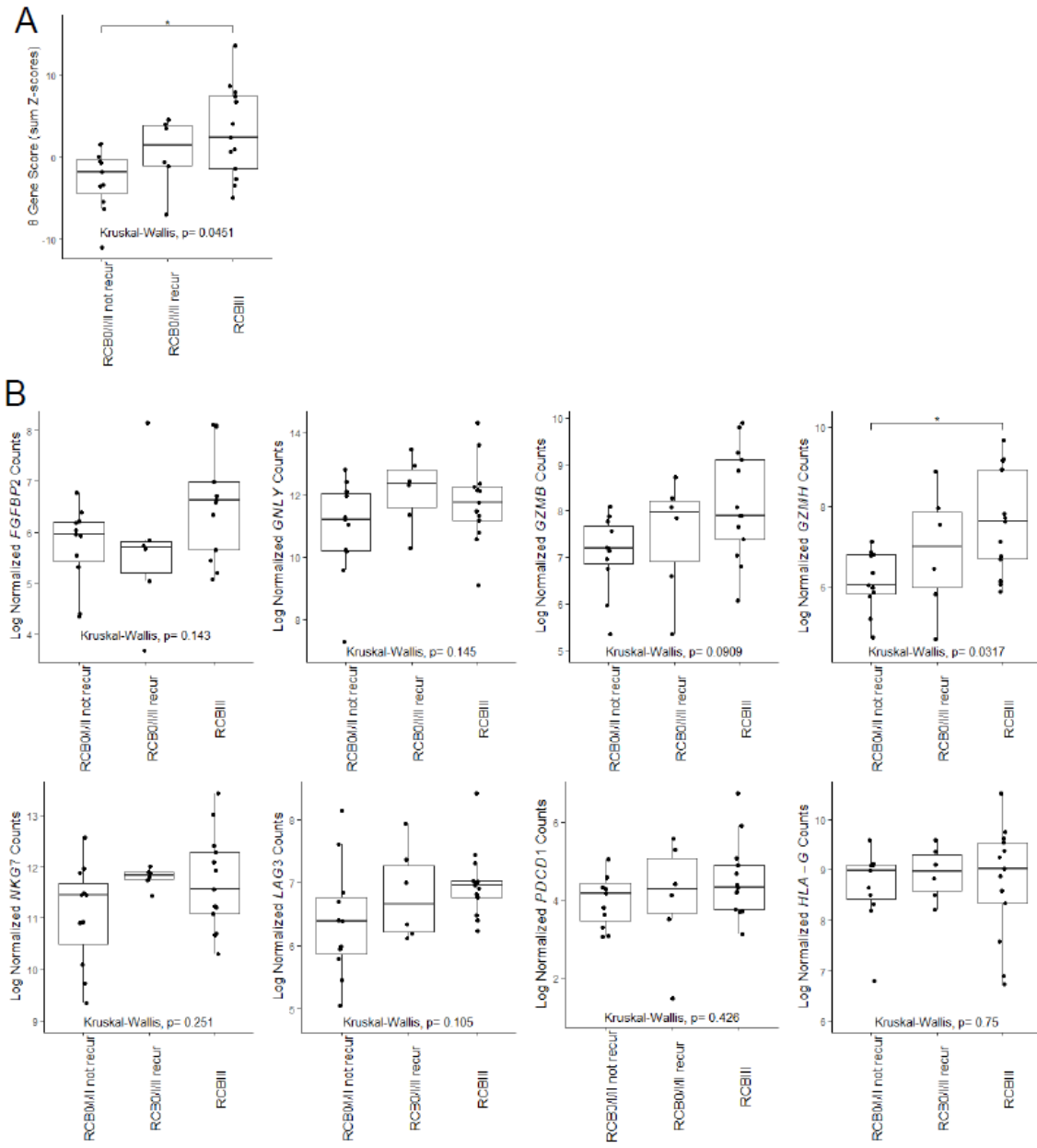
Supplementary Figure S4.17: *An 8-gene activated T cell signature derived from whole blood at surgery is associated with residual disease burden and recurrence.* A) A composite gene signature of 8 analyzed genes by nanoString from RNA derived from whole blood sampled after the completion of neoadjuvant treatment and prior to definitive surgery. The signature is derived as *PDCD1 + NKG7 + LAG3+ GZMH + GZMB + GNLY + FGFBP2 – HLA-G* (sum of z-scores). Datapoints are stratified by RCB0/I/II with or without a recurrence within 3 years after surgery, and RCB III. Box plots represent the interquartile range. P values represent Kruskal-Wallis tests. * indicates p<0.05 by post-hoc Dunn test. B). Individual gene plots for the 8 genes comprising A.

Chapter V Appendix

Supplementary material for chapter V: Peripheral blood monocyte abundance predicts

outcomes in breast cancer patients
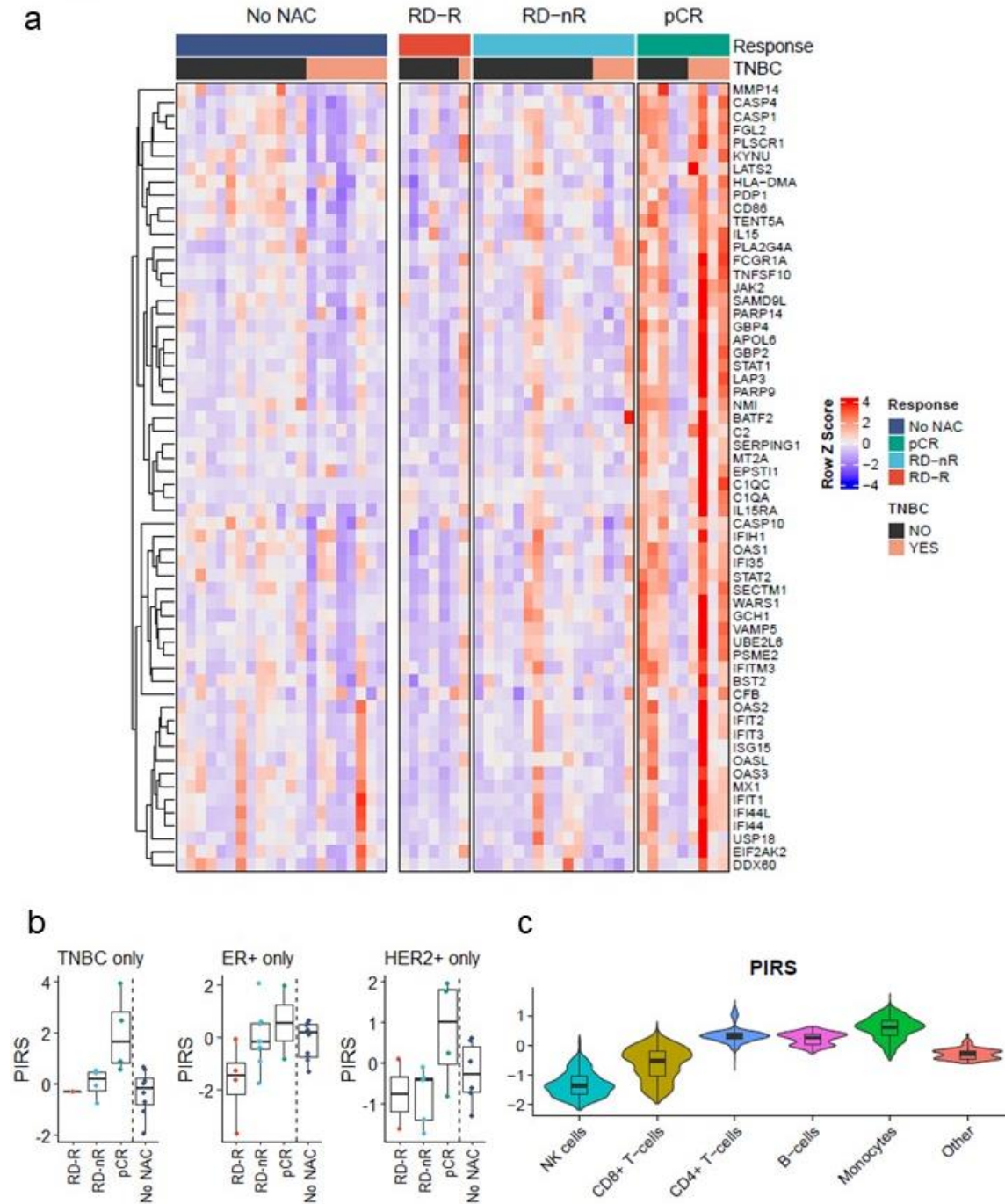
Supplementary Figure S5.1: Expression of immune related genes in the peripheral blood is associated with good outcome following NAC. A) Heatmap showing row standardized (z-score)

gene expression for leading edge IFN/Complement genes (n=60 genes). B) PIRS for TNBC only, ER+ only or HER2+ only patients in the VICC-1 cohort, stratified by outcome. C) Violin plots showing the distribution of PIRS for each cell type in single cell sequencing data. Box plots show the median, first and third quartiles.
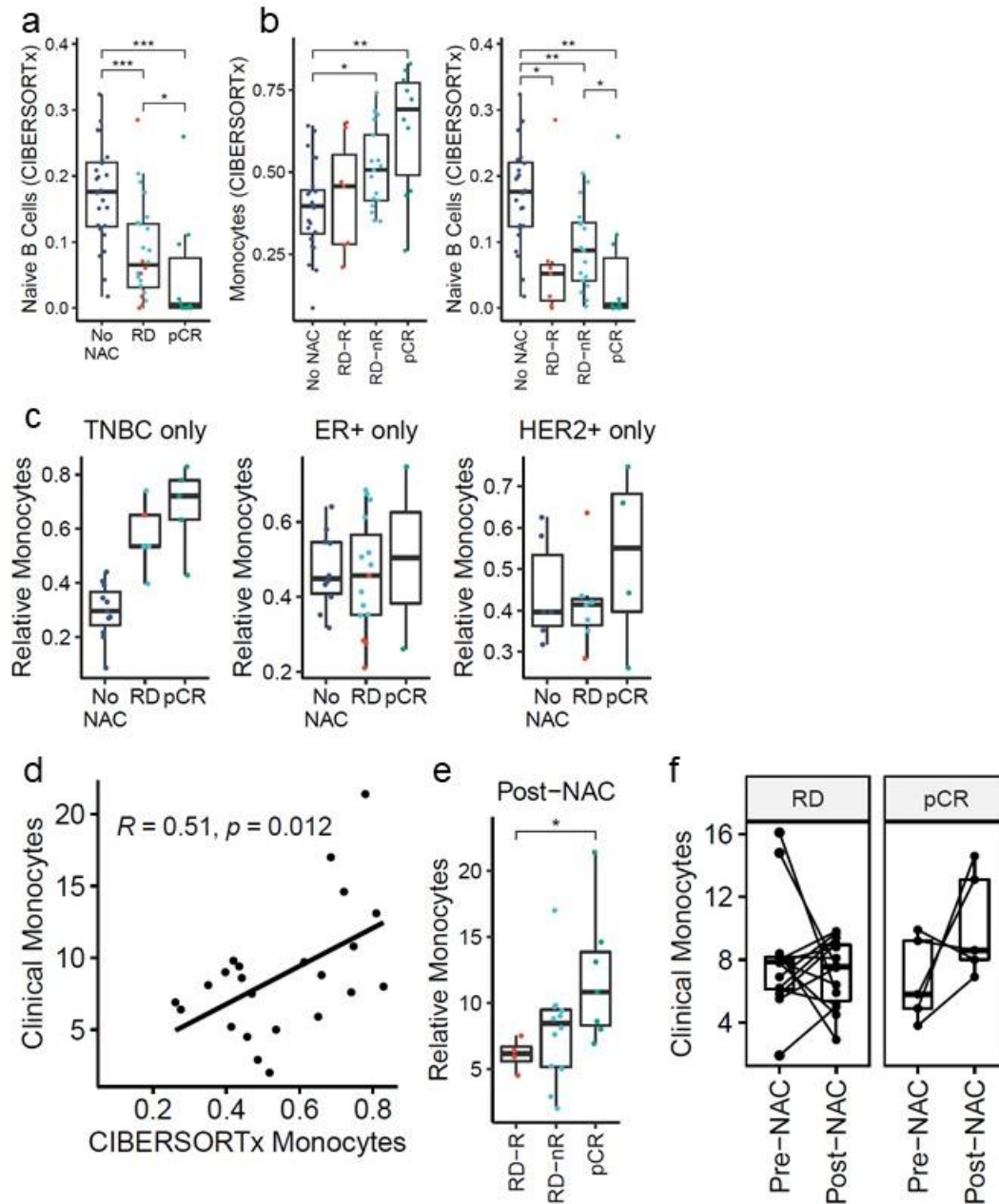
Supplementary Figure S5.2: Monocytes are most abundant in blood of patients with good outcomes following NAC. A) Naïve B cells, as measured by CIBERSORTx, stratified by response to NAC. B) Monocytes and naïve B cells, as measured by CIBERSORTx, stratified by response and recurrence. C) CIBERSORTx monocyte values, stratified by outcome and breast cancer subtype. D) Correlation between clinically measured relative monocytes extracted from the electronic health record and monocytes inferred by CIBERSORTx. E) Post-NAC clinically measured monocytes, stratified by response and recurrence. F) Change in clinically measured relative monocytes from pre- to post-NAC stratified by patients with RD or pCR. Box plots show the median, first and third quartiles. P-values represent one-tailed Wilcox tests (FDR corrected where applicable).
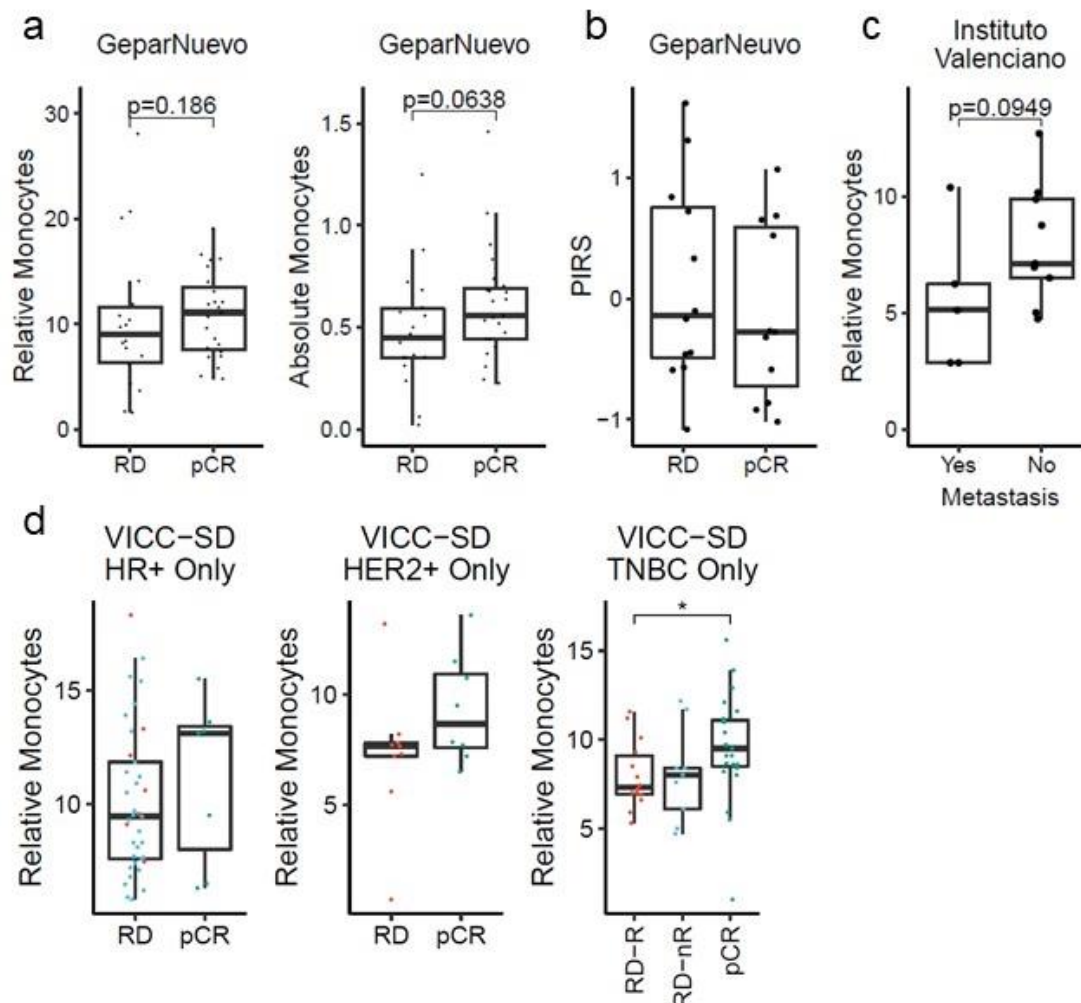
Supplementary Figure S5.3: Monocytes are most abundant in blood of patients with good outcomes following NAC. A) Relative and absolute monocytes in TNBC cohort from GeparNuevo placebo arm, stratified by NAC outcome. B) Peripheral immunologic response score (PIRS) in GeparNuevo TNBC cohort, as measured by NanoString. C) Relative monocytes in the Instituto Valenciano HR+ cohort, stratified by metastasis. D) Relative monocytes in VICC-SD cohort groups, by breast cancer subtype. Box plots show the median, first and third quartiles. P-values represent one-tailed Wilcox tests (FDR corrected where applicable).